

**DISCOVERY, CHARACTERIZATION AND STRUCTURAL STUDIES OF
INHIBITORS AGAINST *MYCOBACTERIUM TUBERCULOSIS* ADENOSINE
KINASE AND BIOTIN PROTEIN LIGASE**

A Dissertation

by

ROBERTO A. CRESPO MORALES

Submitted to the Office of Graduate and Professional Studies of
Texas A&M University
in partial fulfillment of the requirements for the degree of

DOCTOR OF PHILOSOPHY

Chair of Committee,	James C. Sacchetti
Committee Members,	Jean-Philippe Pellois
	David Peterson
	Tadhg Begley
Head of Department,	Gregory Reinhart

December 2017

Major Subject: Biochemistry

Copyright 2017 Roberto A. Crespo Morales

ABSTRACT

The rapid emergence of drug-resistant *Mycobacterium tuberculosis* (Mtb) coupled to the high incidence of HIV-Mtb coinfection is of global concern. Consequently, there is a worldwide necessity to develop new drugs with novel mechanisms of action and new molecular targets. In this dissertation, we describe a crystallographic and high-throughput screening (HTS) approach towards the identification and structural characterization of inhibitors against *Mycobacterium tuberculosis* adenosine kinase (MtbAdoK) and biotin protein ligase (MtbBpL). Parallel studies were also performed to evaluate the *in vitro* potency and antimycobacterial profile of the compounds. Finally, X-ray crystallography was employed to investigate the structural basis of inhibition and to perform structure-guided drug design.

In the first study, we focused on the biochemical, chemical synthesis and structural characterization of adenosine analogs as inhibitors of MtbAdoK. Here, we adopted a bottom-up structural approach towards the discovery, design, and synthesis of a series of compounds that displayed inhibitory constants ranging from 4.3-121.0 nM against the enzyme. Two of these compounds exhibited low micromolar activity against Mtb with 50.0 % minimum inhibitory concentrations of 1.7 and 4.0 μ M. Our selectivity studies showed that the compounds display a higher degree of specificity of MtbAdoK when compared to the human enzyme (hAdoK). Finally, our crystallographic studies revealed

the presence of a potentially therapeutically relevant cavity that is unique to the MtbAdoK homodimer.

Next, we describe the discovery, biochemical and structural characterization of novel dihydro spiro compounds as inhibitors of MtbAdoK. Here, we utilized an HTS approach for the identification of the aforementioned compounds. Our enzymatic assays showed that the compounds are selective inhibitors of MtbAdoK when compared hAdoK. In addition, our antimycobacterial studies revealed that the compounds possess nanomolar potency against Mtb (500.0-810.0 nM). Finally, the crystallographic studies revealed that the inhibitors bind in a previously unknown pocket within the enzyme.

Lastly, we explore the potential of MtbBpL as a drug target. Following identification of the compounds via HTS screening, we demonstrate that the inhibitors lacked any activity against human dermal fibroblast but possess antimycobacterial properties. Finally, steady-state kinetic experiments revealed that the compounds are noncompetitive inhibitors of the enzyme suggesting the presence of a previously uncharacterized allosteric site.

ACKNOWLEDGEMENTS

I would like to express my gratitude to my graduate advisor, Dr. James C. Sacchettini, and my committee members, Dr. Pellois, Dr. Peterson and Dr. Begley, for their guidance and support throughout the course of this research.

I would also like to acknowledge the Sacchettini Lab members (past and present) from which I collectively learned everything I know today. Thanks also go to my friends and colleagues and the department faculty and staff for making my time at Texas A&M University a great experience.

Finally, and most importantly thanks to my mother, father and siblings for their unconditional support and encouragement throughout graduate school and for always pushing me forward to strive for success.

CONTRIBUTORS AND FUNDING SOURCES

Contributors

Part 1, faculty committee recognition

This work was supervised by a dissertation committee consisting of graduate advisor Professor James C. Sacchettini, Professors Jean-Philippe Pellois and David Peterson of the Department of Biochemistry and Biophysics and Professor Tadhg Begley of the Department of Chemistry.

Part 2, student/collaborator contributions

The work described in section 2 is the product of a collaboration between Merck Research Laboratories (MRL) and the Sacchettini Research Group (TAMU). Synthesis of the nucleoside analogs of was carried out by Merck Research Laboratories and WuXi AppTec. Dr. Qun Dang, a former employee of MRL (now Lilly) and Dr. Takao Suzuki of WuXi AppTec wrote the medicinal chemistry aspects of the paper and supplementary information. All other work not related to medicinal chemistry including enzymatic characterization, antimycobacterial profiling, co-crystallization, crystallographic data acquisition and analysis, manuscript and supplementary information preparation was carried out by the student.

All of the work performed on sections 3, and 4 was conducted by the student, including enzymatic characterization, antimycobacterial testing, co-crystallization of compounds, crystallographic data acquisition and analysis, manuscript and supplementary

information preparation. Finally, in all cases, X-ray crystallographic data for sections 2, 3 and 4 were collected at the Argonne National Laboratory, beamlines 19ID, 19BM, and 23ID and whole cell testing of compounds against human dermal fibroblast cells were carried out by Dr. Kim Loesch and Ms. Wen Dong from the Sacchettini Research Group.

Funding Sources

All the work performed in the Sacchettini Lab was made possible by funding from the Welch Foundation (A0015), NIH (P01AI095208) and the Bill and Melinda Gates Foundation (OPP1024055). The work carried out by Merck Research Laboratories and WuXi AppTec was privately funded by Merck Research Laboratories.

TABLE OF CONTENTS

	Page
ABSTRACT	ii
ACKNOWLEDGEMENTS	iv
CONTRIBUTORS AND FUNDING SOURCES.....	v
TABLE OF CONTENTS	vii
LIST OF FIGURES.....	x
LIST OF TABLES	xiv
1. INTRODUCTION.....	1
1.1 History of tuberculosis	1
1.2 Global burden of tuberculosis	5
1.2.1 Rise of drug-resistant Mtb.....	7
1.2.2 Multidrug-resistant and extensively drug-resistant Mtb	10
1.2.3 Totally drug-resistant Mtb.....	13
1.3 Tuberculosis control and treatment: first-line, second-line, and add-on drugs.....	13
1.3.1 Drug-susceptible Mtb treatment: first-line drugs	15
1.3.2 MDR, XDR and TDR Mtb treatment: second-line and add-on drugs.....	29
1.4 Strategies for drug discovery against drug-resistant bacteria.....	46
1.4.1 The ideal Mtb drug target.....	46
1.4.2 Target-based drug discovery approaches to identify new drugs	49
1.4.3 Phenotypic-based drug discovery approaches to identify new drug targets ...	52
1.4.4 Repurposing and screening of previously approved drugs	54
1.4.5 Tuberculosis structural genomics consortium: a worldwide collaboration towards the identification and characterization of new drug targets for Mtb drug development	55
2. STRUCTURE-GUIDED DESIGN OF 6-SUBSTITUTED ADENOSINE ANALOGS AS POTENT INHIBITORS OF <i>MYCOBACTERIUM TUBERCULOSIS</i> ADENOSINE KINASE	58

2.1 Background and significance	58
2.2 Materials and methods	62
2.2.1 Cloning, expression and purification of recombinant MtbAdoK and hAdoK	62
2.2.2 Enzymatic assay, IC ₅₀ determination, steady-state kinetics and K _i determination.....	63
2.2.3 Crystallization, data collection, and crystal structure determination	65
2.2.4 Antimycobacterial assay.....	66
2.2.5 Human dermal fibroblast cytotoxicity assay	67
2.3 Results and discussion.....	67
2.4 Conclusions and future work.....	102
3. DISCOVERY, BIOCHEMICAL AND STRUCTURAL CHARACTERIZATION OF NOVEL UNCOMPETITIVE INHIBITORS AGAINST <i>MYCOBACTERIUM TUBERCULOSIS</i> ADENOSINE KINASE	104
3.1 Background and significance	104
3.2 Material and methods	106
3.2.1 Cloning, expression and purification of recombinant MtbAdoK, MtbAdoK mutants, and hAdoK.....	106
3.2.2 Dynamic scanning fluorimetry (DSF) high-throughput screening assay	108
3.2.3 IC ₅₀ , steady-state kinetics, and K _i determination	108
3.2.4 Crystallization, crystal dehydration, data collection and crystal structure determination.....	110
3.2.5 Antitubercular assay	111
3.2.6 Human dermal fibroblast cytotoxicity assay	112
3.3 Results	112
3.3.1 Discovery and enzymatic testing of dihydro spiro compounds	112
3.3.2 Antimycobacterial and cytotoxic evaluation of dihydro spiro compounds...	116
3.3.3 Structural characterization of the MtbAdoK-dihydro spiro complex	118
3.3.4 Mutagenesis studies of the dihydro spiro binding pocket	125
3.4 Discussion	127
3.5 Conclusions and future work.....	132
4. DISCOVERY, ENZYMATIC AND <i>IN CELLULO</i> CHARACTERIZATION OF NOVEL ALLOSTERIC INHIBITORS OF <i>MYCOBACTERIUM TUBERCULOSIS</i> BIOTIN PROTEIN LIGASE	133
4.1 Background and significance	133
4.2 Material and methods	139
4.2.1 Cloning, expression and purification of MtbBpL	139
4.2.2 DSF high-throughput screening assay.....	139
4.2.3 IC ₅₀ and steady-state kinetics determination	140
4.2.4 Antitubercular assay	141
4.2.5 Human dermal fibroblast cytotoxicity assay	142

4.3 Results and discussion.....	143
4.4 Conclusions and future work.....	155
5. CONCLUSIONS.....	156
REFERENCES.....	159
APPENDIX A.....	196
APPENDIX B.....	215

LIST OF FIGURES

	Page
Figure 1.1: Tuberculosis transmission cycle.	5
Figure 1.2: Tuberculosis is the leading cause of death due to a single infectious agent in recorded history.	6
Figure 1.3: Estimated TB incidence rates, 2015.	7
Figure 1.4: Percentage of new TB cases with MDR-Mtb, 2015.	11
Figure 1.5: Number of patients with laboratory-confirmed XDR-Mtb, 2015.	12
Figure 1.6: Activation of isoniazid by KatG.	17
Figure 1.7: Isoniazid-NAD adduct.	18
Figure 1.8: <i>Mycobacterium tuberculosis</i> KatG active site.	19
Figure 1.9: Crystal structure of <i>Mycobacterium tuberculosis</i> InhA bound to the isoniazid-NAD adduct (PDB ID 2NV6).	20
Figure 1.10: Frequently associated aminoacid substitutions at the RRDR region of RpoB that confer rifampicin resistance.	22
Figure 1.11: Rifampicin bound to the active site of <i>Mycobacterium tuberculosis</i> RNA polymerase.	23
Figure 1.12: Reaction catalyzed by PncA.	25
Figure 1.13: <i>Mycobacterium tuberculosis</i> PncA.	26
Figure 1.14: Chemical structures of third-generation fluoroquinolones moxifloxacin and levofloxacin.	32
Figure 1.15: Chemical structures of the second-line injectable drugs kanamycin, amikacin and capreomycin.	33

Figure 1.16: Chemical structures of prodrugs ethionamide and prothionamide.	35
Figure 1.17: Crystal structure of InhA bound to the ethionamide-NAD adduct (PDB ID 2HI9).	37
Figure 1.18: Chemical structures of cycloserine and terizidone.	38
Figure 1.19: Chemical structure of linezolid.	39
Figure 1.20: Chemical structure of clofazimine.	40
Figure 1.21: Chemical structure of bedaquiline.	41
Figure 1.22: Chemical structure of delamanid.	43
Figure 1.23: Chemical structure of the prodrug PAS and the natural DHFR substrate PABA.	44
Figure 1.24: Chemical structure of thiacetazone.	46
Figure 1.25: Evolution of drug screening and discovery	51
Figure 1.26: Phenotypic vs. target-based drug discovery	52
Figure 2.1: MtbAdoK closed and open conformations.	60
Figure 2.2: Active site pocket of MtbAdoK.	68
Figure 2.3: Tool compounds for crystallography studies.	69
Figure 2.4: Compound 2 bound to the active site of MtbAdoK.	70
Figure 2.5: Compound 3 bound to the active site of MtbAdoK.	71
Figure 2.6: The iodine of 2 is physically occluded by chain B (magenta).	73
Figure 2.7: The amide of 3 is physically occluded by chain B (magenta).	73
Figure 2.8: “Chimney-like” cavity observed above position N6- of the adenine ring. Chain B is colored magenta.	75
Figure 2.9: Compound 4 bound to the active site of MtbAdoK.	76
Figure 2.10: The methylmercapto group of 4 is accommodated in a new compound-induced pocket formed by Arg176 (red).	77

Figure 2.11: The “chimney-like” cavity we observed in the crystal structure of 2 is observed to be closed in the MtbAdoK- 4 complex due to the conformational movement of Arg176.....	78
Figure 2.12: hAdoK in complex with compound 2 (PDB ID 2i6a).....	80
Figure 2.13: MtbAdoK- 2 structure showing the relative position of the iodotubercidin bound to the active site (orange) to that bound to the ATP site (magenta).	82
Figure 2.14: Compound 5 bound to the active site of MtbAdoK.....	82
Figure 2.15: (a) Chemical structure of 6 , (b) compound 6 bound to the active site of MtbAdoK and (c) superimposition of the crystal structures of 4 and 6	84
Figure 2.16: The thiophene of 6 is buried in the compound-induced cavity formed by Arg176 and residues from chain B (magenta).....	86
Figure 2.17: Superimposition of the cocrystal structures of 4 (blue) and 6 (gray) showed that Arg176 moves to accommodate the larger thiophene group of 6	86
Figure 2.18: Reagents and conditions for chemical synthesis.	90
Figure 2.19: Adenosine scaffold showing the positions where medicinal chemistry was performed (R, R ⁶ , Y, Z).....	91
Figure 2.20: R and R ⁶ groups of synthesized adenosine analogs.	92
Figure 2.21: Crystal structure complex of 7 bound to the active site of MtbAdoK.....	94
Figure 2.22: Chemical structures of synthesized adenosine analogs with substitutions at the 5'-position.	96
Figure 2.23: Summary of SAR results for compounds 8-17	98
Figure 2.24: Crystal structure complex of compound 17 bound to the active site of MtbAdoK.....	99
Figure 3.1: Structure of lead dihydro spiro compound 1 and analogs (2-4).	114
Figure 3.2: Lineweaver-Burk plot of compound 2 vs. adenosine.	116
Figure 3.3: Comparison of the potency of compound 2 when mc ² 7000 is grown on a dextrose-supplemented 7H9 or acetate-supplement M9 media.....	117
Figure 3.4: Cytotoxicity profiles of dihydro spiro compounds when tested against HDF cells.	118

Figure 3.5: Superimposition of the MtbAdoK-adenosine, MtbAdoK-apo and MtbAdoK-dihydro spiro structures.....	121
Figure 3.6: Surface representation of the dihydro spiro binding pocket.	122
Figure 3.7: Residues involved in close contacts with the dihydro spiro compound.	123
Figure 3.8: Cation- π and π -stacking interactions of Arg176 and Phe116 with the benzopyrrole-like ring of compound 3	125
Figure 3.9: Orientation of Arg176 and Gln172 in the spiro binding pocket when compared to the adenosine bound MtbAdoK structure (PDB ID 2PKM).....	126
Figure 3.10: Dose response curves for MtbAdoK mutants.	127
Figure 4.1: Enzymatic reaction catalyzed by MtbBpL.	136
Figure 4.2: MtbBpL structure.....	137
Figure 4.3: Structure and numbering convention of lead compound (1) and analogs (2-4).	144
Figure 4.4: Lineweaver-Burk plot of compound 4 vs. biotin.....	150

LIST OF TABLES

	Page
Table 1.1: Current first-line antimycobacterial drugs	16
Table 1.2: Current second-line antimycobacterial drugs.	31
Table 2.1: SAR data for synthesized adenosine analogs with substitutions at position 6.	92
Table 2.2: SAR data for synthesized adenosine analogs with substitutions at the 5'- position.	97
Table 3.1: DSF data for lead compound 1	113
Table 3.2: Enzymatic assay parameters of dihydro spiro compounds.	115
Table 3.3: Kinetic parameters for compound 2	115
Table 3.4: Antimycobacterial and cytotoxic profile of dihydro spiro compounds.	117
Table 3.5: Crystal data collection and refinement statistics.	119
Table 4.1: DSF data for lead compound 1	143
Table 4.2: Enzymatic characterization of compounds.	146
Table 4.3: Antimycobacterial and cytotoxic profile of compounds	148
Table 4.4: Steady-state kinetic parameters for compound 4	149
Table 4.5: Binding and enzymatic characterization of analogs of compound 4	151

1. INTRODUCTION

1.1 History of tuberculosis

It has been hypothesized that the *Mycobacterium* genus itself is over 150 million years old. This is based on the fact that the current distribution and specific habitat requirements of *Mycobacterium ulcerans* were last contiguous when they formed part of the supercontinent of Gondwana.¹ Tuberculosis (TB) is also an ancient disease that has survived throughout millennia. Genetic evidence suggests that an early ancestor of *Mycobacterium tuberculosis* (Mtb) inflicted early hominids of East Africa and around 20,000-15,000 years ago a common ancestor of Mtb appeared.²⁻³ The first written description of tb dates back to 3,300 and 2,300 years ago from Indian and Chinese documents.⁴⁻⁵ Although there is no written evidence of tb in ancient Egyptian papyri, evidence for Pott's disease, also known as tb of the bone; has been observed in Egyptian mummies dating back to 2,400 BC.⁶ Other ancient references to tb are found in Ancient Greece where pulmonary tb was known as "phthisis" (Greek for wasting away). During this time, Hippocrates described the disease accurately by defining its symptoms and characteristic lung lesions, Isocrates made early observations proposing that tb was an infectious disease while Aristotle suggested the contagious nature of it.⁷

In the Middle Ages, a new form of tb referred as "scrofula" which affected the cervical lymph nodes was described.⁸ Along the same time, French surgeon Guy de Chauliac (1363), proposed a healing surgical intervention for scrofula which involved

removal of the affected lymph nodes.⁹ In the 12th century, England and France referred to the disease as “Kings Evil,” thought to be only cured by newly crowned kings who were believed to have special healing powers.⁸ This practice of healing by the “King’s Touch” continued in England until 1714 and in France until 1826.⁸ In 1679, Franciscus Sylvius gave the exact anatomical and pathological description of the disease in his work “*Opera Medica*”.¹⁰ He describes the characteristic lung nodules as “*tubercula*” that progress into abscesses, cavities (ulcers) and empyema in lungs and other sites of tb inflicted patients.¹⁰ The first observations describing the infectious nature of tb were made by Benjamin Marten in 1722 in his work “*A new theory of Consumption.*” He proposed that tb was “*animaliculae or their seed...inimicable to our nature*” and that can be transmitted by “*a breath emits from his lungs...that may be caught by a sound person*”.¹¹ During the 18th and 19th century, tb had become an epidemic with an annual mortality rate of 800 to 1,000 people per 100,000 individuals.¹² For this reason, tb was associated with many names including, “the robber of youth” due to the high mortality rate amongst young adults, “white plague” or “white death” given the characteristic extreme anemic pallor observed in afflicted individuals and the “Captain of All These Men of Death” because of its epidemic dispersion in North America and Europe.¹²⁻¹⁵ In 1834 the German naturalist and physician Johann Lukas Schönlein used the term “*tuberculosis*” in relation to the characteristic tubercles while in 1853 Hermann Brehmer used the word “*tuberculosis*” in his doctoral dissertation to describe pulmonary tb.¹⁶ The first formal demonstration that tb was contagious was made by Jean-Antoine Villemin in 1865 in his work “*Cause et nature de la tuberculose: son inoculation de l’homme au lapin*”.¹⁷⁻¹⁸ Here, he describes the

successful transfer of pus and fluid from human and bovine lesions to rabbits that later developed tb. Almost twenty years later in 1882, Robert Koch astonished the world by successfully isolating and culturing the tubercle bacillus. Cultured bacteria, from cases of pulmonary, extrapulmonary and meningeal tubercular disease were utilized to inoculate and infect animals. The findings from these studies coupled with his previous work with anthrax lead to the formation of a general set of postulates referred as Koch's Postulates. These postulates state that I) the microorganism must be present in all organisms inflicted by the disease and not in healthy subject, II) the microorganism must be isolated from a host and grown in pure culture, III) the cultured microorganism must cause the disease when inoculated into a healthy organism and IV) the microorganism must be isolated from the inoculated host and identified as the original causative agent when compared to the original diseased host. Koch utilized his technique to unequivocally prove that all forms of human and animal tuberculosis were many manifestations of the same bacterial entity. Koch delivered his findings on March 24th, 1882 during a lecture at the Charité Hospital in Berlin under the title "*Die Ätiologie der Tuberkulose, "The Etiology of Tuberculosis."*" For his seminal work, he was awarded the Nobel Prize in Physiology or Medicine in 1905.^{12, 17, 19-21}

Mtb is an obligate human pathogen. The Mtb complex, comprised of a genetically related group of *Mycobacterium* species are known to cause tb in humans. These include *Mycobacterium tuberculosis*, *Mycobacterium africanum*, *Mycobacterium orygis*, *Mycobacterium bovis*, *Mycobacterium canetti*, *Mycobacterium microti*, *Mycobacterium caprae*, *Mycobacterium suricattae*, *Mycobacterium pinnipedii* and *Mycobacterium*

*mun*gi.²²⁻²³ The physiology of Mtb is aerobic, propagating vigorously in highly oxygenated tissues such as the lungs. Once Mtb-bearing particles are inhaled, the bacilli invade the pulmonary alveoli where its phagocytized by alveolar macrophages. Through the action of the initial immune response, Mtb is encapsulated in pulmonary granulomas (tubercula). Granulomas are predominantly composed of a mass of dead and live immune cells that prevent Mtb from spreading. Here, the dormant Mtb can survive for many years (latent tb). In immunocompromised individuals, and through mechanisms not clearly understood, a necrotic expansion and liquefaction of the granuloma can occur allowing a large number of bacteria to proliferate vigorously. The pathophysiological processes aforementioned, lead to the characteristic symptoms of fever, weakness, cough, chest pain, and bloody sputum (Figure 1.1).²⁴⁻²⁹

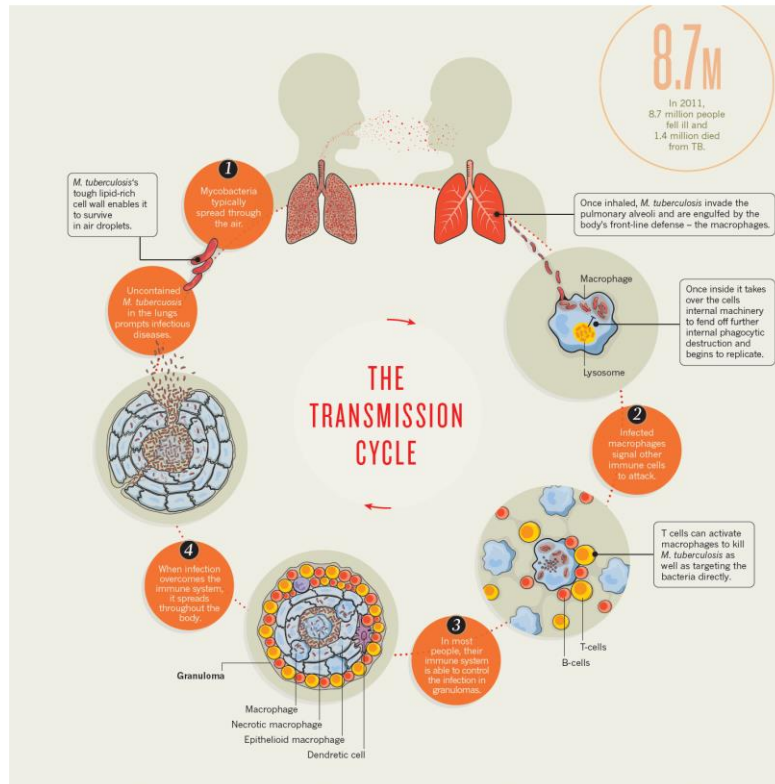


Figure 1.1: Tuberculosis transmission cycle. Reprinted with permission.²⁹

1.2 Global burden of tuberculosis

Tuberculosis is the leading cause of death worldwide due to a single infectious agent (Figure 1.2-1.3).²⁹ As of 2015, 10.4 million people, including an estimate of 1 million children; fell ill to the disease and approximately 1.4 million of these infected individuals died from it. Worldwide, around 2 billion people are living with latent tuberculosis. If untreated, around 5-10 % of these infected people will develop active tuberculosis sometime during their lifetime. This problem is only exacerbated by the rapid emergence

of multidrug-resistant (MDR), extensively drug-resistant (XDR) and totally drug-resistant (TDR) Mtb coupled to the high incidence of HIV-Mtb coinfection.³⁰

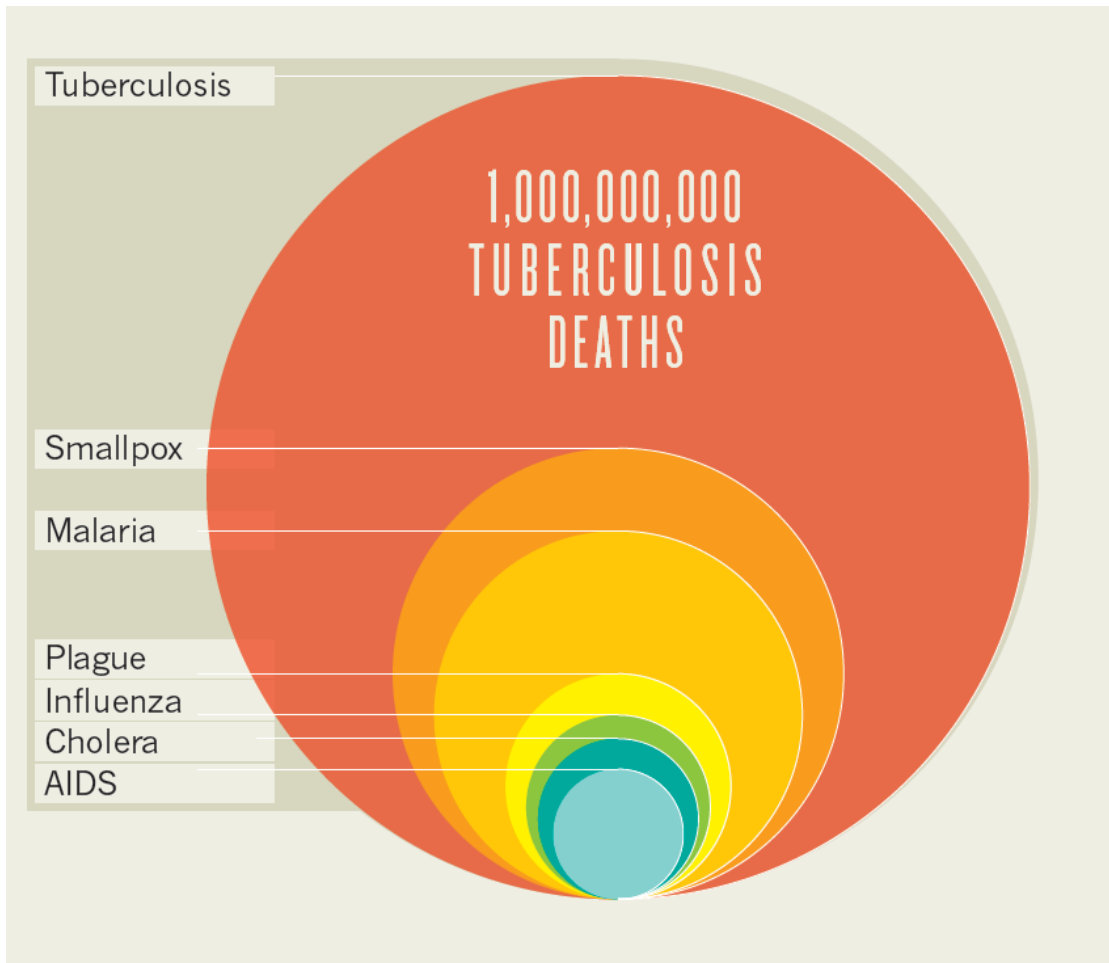


Figure 1.2: Tuberculosis is the leading cause of death due to a single infectious agent in recorded history. Tb is responsible for over one billion deaths in the past 200 years. Reprinted with permission.²⁹

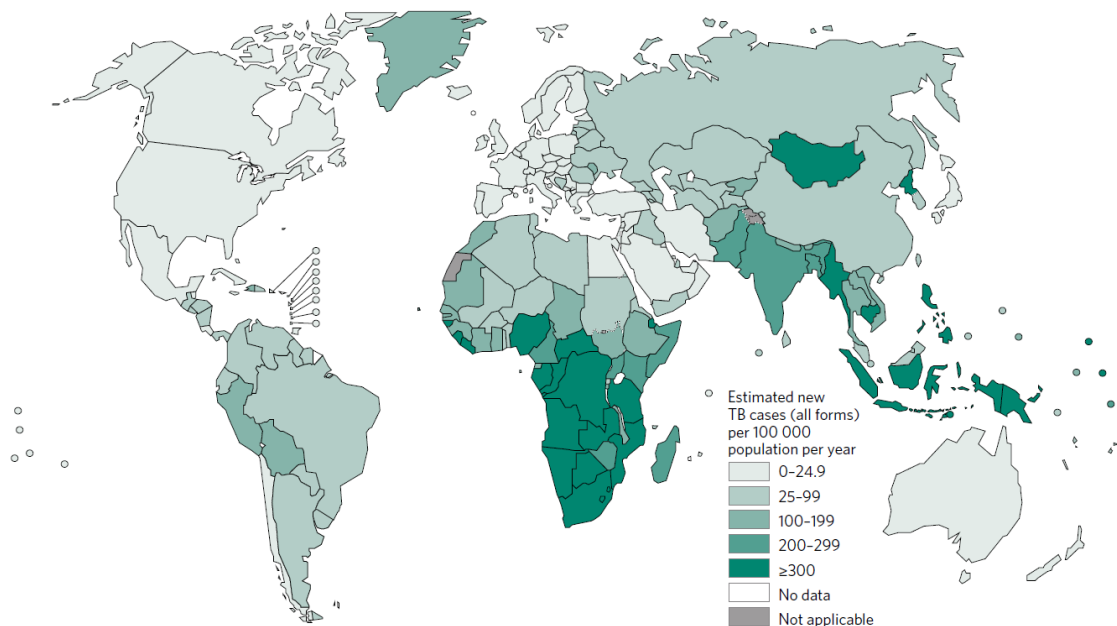


Figure 1.3: Estimated TB incidence rates, 2015. Reprinted with permission.³⁰

1.2.1 Rise of drug-resistant *Mtb*

The increase in *Mtb* drug resistance can be traced back to the 1940s, right after the discovery of streptomycin in 1943.¹¹ Although many patients benefited from a streptomycin-based anti-tb treatment, in 1948 streptomycin resistant strains were isolated from patients afflicted by pulmonary tb.³¹ Fortunately, in 1948 as well, two newly discovered anti-tb agents, thioacetazone, and para-aminosalicylic acid, were launched. When either of these drugs was co-administered with streptomycin, the acquired resistance of *Mtb* went down with a concomitant rise in patient healing rates.³² The 1950s and 1960s was a golden era for anti-tb drugs. In 1951 isoniazid was added to the regimen, this was followed by the addition of pyrazinamide (1952), ethionamide (1956), ethambutol (1961)

and rifampin (1966).³³ In addition to isoniazid, rifampin was another drug that revolutionized tb treatment due to its ease of administration and high level of efficacy.³⁴ However, as in the case of the drugs above, resistance to rifampin came shortly after its discovery.³⁵ Just like streptomycin, when isoniazid was utilized to treat tb as a standalone drug; rapid onset of resistance to isoniazid occurred. However, if it was coadministered with streptomycin or para-aminosalicylic acid, suppression of resistance was observed.³⁶ These early observational experiments laid the foundation to the multidrug treatment regimen utilized for tb and other complex diseases such as cancer and HIV.

Unlike other bacteria which could acquire resistance through horizontal gene transfer, Mtb drug resistance is almost entirely due to chromosomal mutations; many of which are single-nucleotide polymorphisms (SNPs), gene insertions and rarely gene deletions.³⁷ Another key feature of Mtb is the low mutation and replication rates when compared to other bacteria. However, several critical experiments have suggested that *in vivo*, Mtb enters a hypermutable state leading to a rapid rise in drug resistance. For example, a study that employed highly sensitive whole-genome sequencing in sputum samples from three patients undergoing anti-tb treatment; identified that there was a high degree of mutation diversity in the samples. The group identified between 8 and 41 SNPs that occurred during active treatment and as many as 34 unique SNPs from a single sample.³⁸

One of the possible reasons behind the observed hypermutability might be due to transient mutagenesis. This refers to a temporary rise in mutation rate which can be attributed to several factors including mistranslation of proteins like those involved in

DNA replication and repair, transcriptional mutagenesis and upregulation of error-prone DNA polymerases.³⁹⁻⁴⁰ Transcriptional mutagenesis arises when RNA polymerases bypass DNA lesions leading to the incorrect insertions of nucleotides into the mRNA. If the resultant mutant is viable, then this could select for the fixation of the mutation and give rise to a drug-resistant Mtb population. Alternatively, the mRNA that contains the error might code for a protein involved in DNA replication or repair, leading to a mutator phenotype.⁴¹ Mistranslation occurs when there is an error that affects the translation of mRNA into protein. One possible mechanism that might yield such an event could be the mischarging of tRNAs, which can occur if the tRNA gene itself is mutated. Although there is little to no data regarding mistranslation-led hypermutation in Mtb, this phenomenon has been noted to be a mechanism of elevated mutation rates in *E. coli*, *C. albicans*, and *A. baylyi*.⁴²⁻⁴³ Recently, a non-homologous end joining system was identified in *Mycobacterium smegmatis*. This system plays a key role in DNA repair, thus being a potential transient mutator system if up-regulated under certain conditions.⁴³

Antibiotics can also act as mutagens. It has been shown that at sub-inhibitory concentrations, antibiotics can serve as the driving force behind the rise of resistance for many bacteria.⁴⁴ Mtb might encounter such a scenario when the patient has a poor compliance with the regimen or when Mtb is deep within pulmonary cavities, solid caseous material, and empyema pus.⁴⁵ Another source of suboptimal concentrations is when the patient who might have tb is being treated for another infection. For example, it has been noted that sub-lethal concentrations of the fluoroquinolone ciprofloxacin, which invokes the mycobacterial SOS response, lead to elevated mutation rates in several

mycobacterial species *in vitro*.⁴⁶ Indeed, genome-wide studies have shown that fluoroquinolones upregulate the SOS response in Mtb, whereas inhibitors of translation (i.e., ribosome inhibitors) do not.⁴⁷ Another general mechanism that has been noted to induce the SOS response and the non-homologous end joining system is the generation of reactive oxygen species (ROS). Evidence suggests that the production of ROS is a common denominator amongst many antibiotic classes such as fluoroquinolones, aminoglycosides, and β -lactams.⁴³ Moreover, isoniazid has also been implicated in the generation of ROS and studies have observed that following its administration there is a direct upregulation of the SOS response and the non-homologous end joining system. It should be noted that a complete systematic and empirical approach has not been adequately performed to establish the possible link between sub-lethal concentrations of antimycobacterial drugs and Mtb mutation rate.

1.2.2 Multidrug-resistant and extensively drug-resistant Mtb

Retrospectively, one of the earliest documented cases of polydrug-resistant Mtb (i.e., multidrug-resistant) can be traced back to a school outbreak caused by an isoniazid, streptomycin and para-aminosalicylic acid resistant strain during the 1960s and 1970s.⁴⁸ The World Health Organization defines MDR-Mtb as bacilli that are resistant to isoniazid and rifampicin, the most powerful anti-tuberculosis drugs.^{30, 49} Historically, data on drug-resistant Mtb have been scarce, mainly limited by the lack of reliable sources from the countries of high tb incidence and prevalence. In 1994, the WHO and the International Union Against Tuberculosis and Lung Disease (IUATLD) pioneered a global surveillance program to standardize data collection methods.³⁰ In fact, this is still to date the world's

oldest and largest initiative regarding the monitoring of antimicrobial resistance. Worldwide in 2015, an estimated 480,000 individuals were diagnosed with MDR-Mtb, and around 190,000 of them died from the disease.³⁰ The percentage of MDR cases is higher in Central Asian and Eastern European countries. In 2015, China, Russia, and India showed the largest amount of MDR-Mtb cases, accounting for over 50.0 % of all the reported cases worldwide (Figure 1.4). The burden of MDR-Mtb has been relatively constant from 2008 to 2013. However, from 2009-2015, there has been a rapid increase in rifampicin-resistant (RR-Mtb) in several countries including India, Pakistan, China, Bangladesh, South Africa, Nigeria, Indonesia, and the Democratic Republic of Congo.³⁰

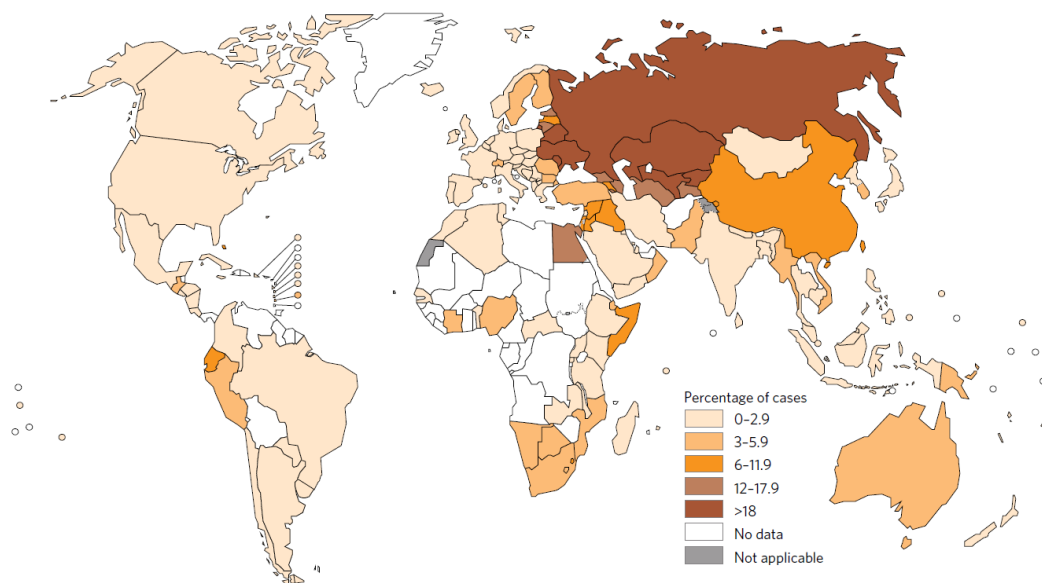


Figure 1.4: Percentage of new TB cases with MDR-Mtb, 2015. Reprinted with permission.³⁰

The first time the “*XDR-tb*” term was utilized was in March 2006 in a joint report by the CDC and the WHO.⁵⁰ Recently in 2015, a pre-XDR strain of Mtb was identified to be the causative agent of an outbreak that occurred in Argentina around 1979. Thereby representing the first documented transmission of XDR-Mtb.⁵¹ XDR-Mtb is a form of MDR-Mtb with additional resistance to other drugs including fluoroquinolones and at least one of the three injectable second-line drugs namely kanamycin, capreomycin, and amikacin. By the end of 2015, XDR-Mtb was reported in 117 countries worldwide (Figure-1.5).³⁰ In addition, 36.0 % of the reported MDR/RR-Mtb patients in 2015 had a positive drug susceptibility (DST) testing results to fluoroquinolones and second-line injectable agents. Thus indicating that these MDR/RR-Mtb cases were misclassified cases of XDR-Mtb.³⁰

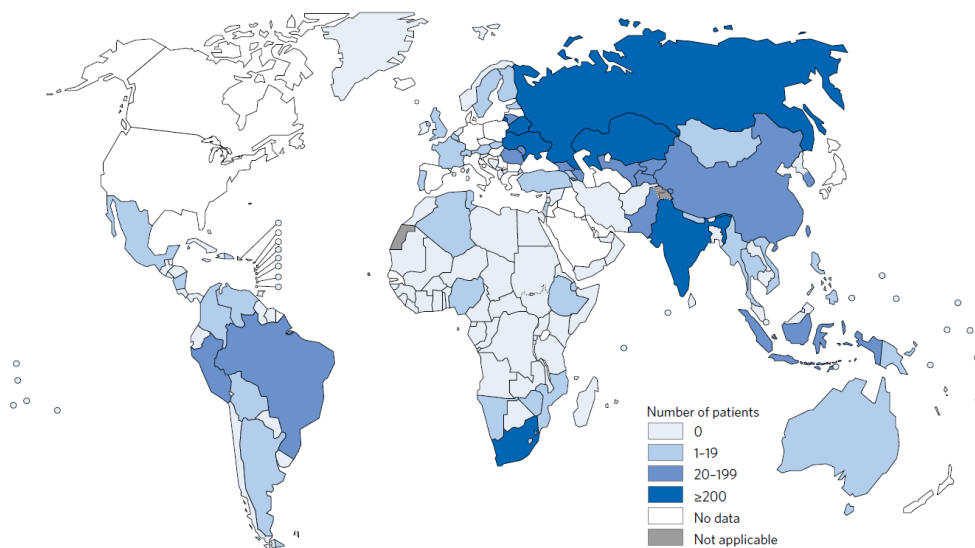


Figure 1.5: Number of patients with laboratory-confirmed XDR-Mtb, 2015. Reprinted with permission.³⁰

1.2.3 Totally drug-resistant Mtb

Totally drug-resistant Mtb (TDR-Mtb), refers to Mtb strains that display *in vitro* resistance to all known anti-tb drugs.⁵² TDR-Mtb was first reported in 2007, detailing two cases that occurred in Italy in 2003. The cases were both related to two young Italian women that were treated by several-first line, second-line and “add-on” drugs (see section 1.3) over the course of 2 years.⁵³ Following their death, DST was performed on the Mtb strains isolated from the patients and yielded positive results to all the drugs tested.⁵³ Since then, TDR-Mtb cases have also been reported in Iran, India and South Africa.⁵³⁻⁵⁷

Officially, TDR-Mtb has not been recognized by the WHO. Only the MDR and XDR Mtb strains have been thoroughly studied and a consensus regarding data gathering, quantification and reproducibility have been well established. Data concerning the reliability and reproducibility of DST for second-line drugs are either non-existent or extremely limited. Therefore, the WHO treats the reported “TDR-Mtb” cases as XDR-Mtb.⁵⁸

1.3 Tuberculosis control and treatment: first-line, second-line, and add-on drugs

Based on historical data as well as scientific literature, the single most effective way to treat drug-resistant bacteria is through drug-combination approaches.⁵⁹⁻⁶¹ Drug combination strategies are almost entirely utilized for the treatment of drug-resistant bacteria. Even in the case of drug-susceptible Mtb, the bacilli are treated with a combination of at least four drugs (see section 1.3.1). The ongoing rise of drug-resistant bacteria, especially Gram-negative bacteria, is shifting the paradigm of monotherapy to an entirely drug-combination approach.⁵⁹ Regardless of the drug combination cocktail, the

strategies behind the therapy can be divided into three categories based on the drug target(s), I) inhibition of targets in different pathways, II) inhibition of various targets in the same pathway and III) inhibition of the same target via different mechanisms.⁶² Drugs that act on several unique targets, exemplified by the treatment of all forms of Mtb, has been the most productive and fruitful therapeutic approach for the treatment of drug-resistant bacteria.

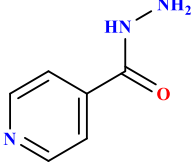
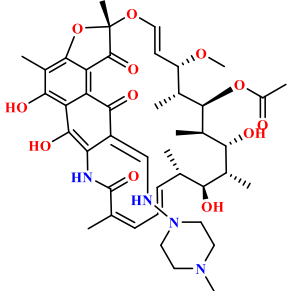
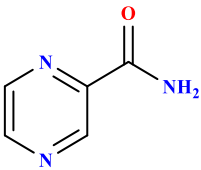
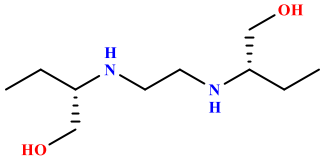
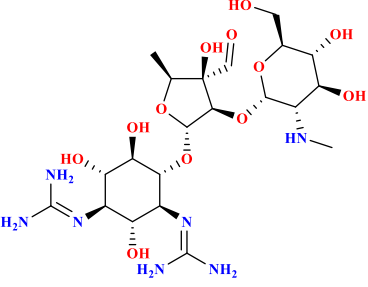
Often a combination of drugs with other molecules (adjuvants) that by themselves do not have bactericidal properties have resulted in favorable outcomes for the treatment of drug-resistant bacteria. The classical example of an antibiotic-adjuvant combination is Augmentin, which combines a β -lactam inhibitor (amoxicillin) with a β -lactamase inhibitor (clavulanic acid). Alternatively, molecules that act upon drug-efflux pumps can maintain the therapeutic concentration of the drug(s) optimal for the desired effect. Such is the case of reserpine which is utilized concomitantly with ciprofloxacin and serves to suppress resistance in *S. aureus* and *S. pneumoniae*.⁶² Another example is the co-administration of the non-steroidal anti-inflammatory (NSAID) celecoxib which has been noted to enhance the bactericidal activity of several antibiotics including chloramphenicol, ampicillin, ciprofloxacin, and kanamycin.⁶³ Targeting different macromolecules in the same pathway has also been utilized as an approach in the treatment against drug-resistant bacteria. Although this represents a less diversified approach, if a carefully selected druggable pathway is chosen then it can prove to be a highly effective strategy. An essential aspect of a potential pathway is that it must be required for the pathogen's survival. In addition, said pathway must be non-redundant the reason being that pathway

redundancy will potentially lead to the rise of resistance.⁶⁴ An example of this strategy is the targeting of cell wall biosynthetic pathways by isoniazid, ethambutol, thioacetazone, and cycloserine. Finally, drug combinations that target the same macromolecule have also been utilized. This is typically employed on multidomain or large biological machinery such as the proteasome and ribosome. An example of this is the utilization of Synercid, a semi-synthetic dual-drug combination that binds in distinct but adjacent sites of the 50S ribosome.⁶⁴ Ultimately the primary advantage drug a combination approach is that it can extend the lifetime of a drug. That is, the likelihood of an organism to develop resistant to a cocktail of drugs is several orders of magnitude less than that of a single drug treatment.⁴³

1.3.1 Drug-susceptible Mtb treatment: first-line drugs

The recommended treatment for drug-susceptible Mtb requires a combination of several drugs administered over a period of 6 months. In 2015, the total cost regarding the treatment for drug-susceptible Mtb was around \$18,000.⁶⁵⁻⁶⁶ According to the latest guidelines by the WHO and the CDC, the regimen consists of an intensive phase of 2 months of rifampicin, isoniazid, pyrazinamide, and ethambutol. This is then followed by another period lasting four months of isoniazid and rifampicin. In previous regimens, streptomycin and thioacetazone were also included as part of the first-line course. However, the WHO recommends replacement by ethambutol due to the severe cytotoxicity of the drugs (Table 1.1).^{49, 67-69}

Table 1.1: Current first-line antimycobacterial drugs.⁴⁹

Compound	Structure	Gene(s) commonly associated with rise of resistance	Role of gene product
isoniazid		<i>katG</i> <i>inhA</i>	catalase/oxidase enoyl reductase
rifampicin		<i>rpoB</i>	β -subunit of RNA polymerase
pyrazinamide		<i>pncA</i>	pyrazinamidase
ethambutol		<i>embB</i>	arabinosyl transferase
streptomycin		<i>rpsL</i> <i>rrs</i> <i>gidB</i>	S12 ribosomal protein 16S RNA 7-methylguanosin methyltransferase

1.3.1.1 Isoniazid

Isoniazid (INH) was originally synthesized in 1912 but introduced as an antimycobacterial in 1951. Isoniazid's structure is simple, containing a pyridine ring with a hydrazide group; both moieties being essential for its bactericidal activity.⁷⁰ Despite INH's simple structure, the mode of action of the molecule is highly complex and to some extent, not completely understood.⁷⁰ When administered, the drug passively diffuses through the cell wall and selectively kills actively growing Mtb. Once inside the cell, INH is activated by the catalase/peroxidase encoded by the *katG* gene (Figure 1.6). In Mtb, the role of KatG is to protect the bacterium against the reactive oxygen species and reactive nitrogen species that are utilized by the human phagosome as a way to control infection.⁷¹

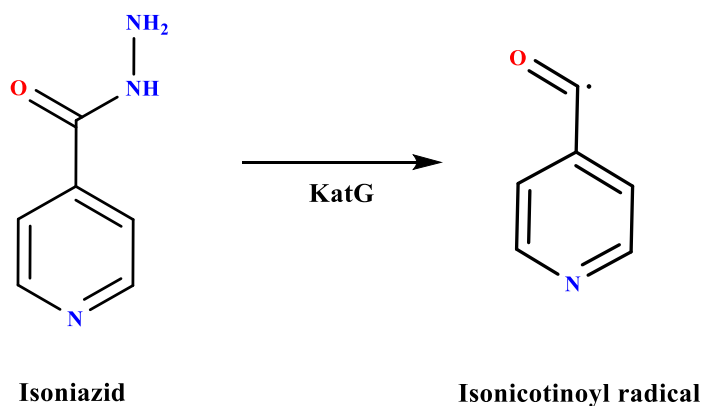


Figure 1.6: Activation of isoniazid by KatG.

Resistance to INH is complex and several genes have been associated with its resistance including *inhA*, *ahpC*, *ndh*, *kasA* and *katG*. However, the most common and prevalent mutations are those that occur in the *katG* and *inhA* genes. There are over one hundred *katG*-associated mutations that have been reported to be related to isoniazid resistance.⁷² Nonetheless, the most common mutation is the S315T mutation in the *katG* gene. This results in a highly deficient INH product that lacks the formation of the INH-NAD adduct which is directly related to the activity of the compound (Figure 1.7).⁷³

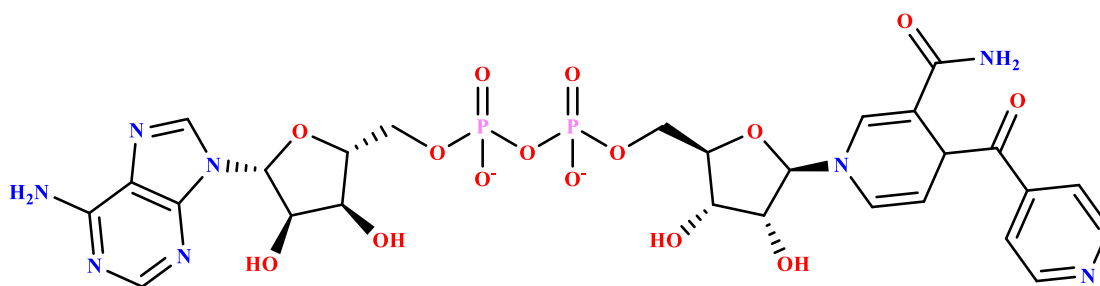


Figure 1.7: Isoniazid-NAD adduct.

In vitro studies have shown that the S315T mutant had a 6-fold reduction in INH metabolizing activity.⁷⁴ In addition, crystallographic and molecular models have suggested that the S315T, a residue located at the entrance of the substrate's access channel, might change the binding site of the hydrazide moiety or that it might alter the electron transfer to the heme moiety of KatG (Figure 1.8).⁷⁵

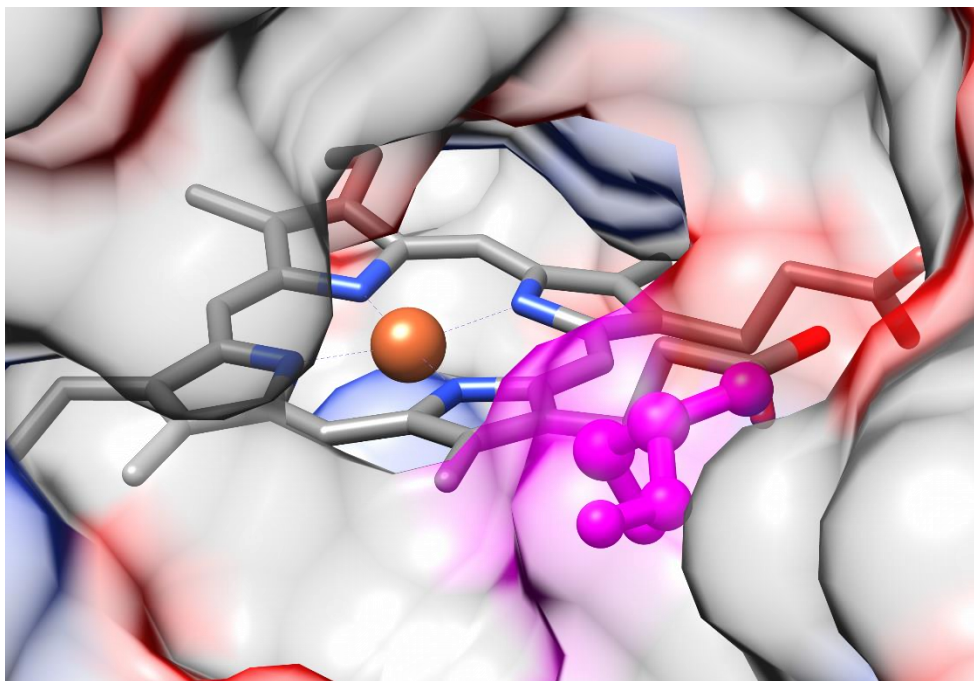


Figure 1.8: *Mycobacterium tuberculosis* KatG active site. Serine 315 is located at the entrance of the substrate's access channel. Active site heme group and serine 315 (magenta) shown as sticks (PDB ID 2CCA).

The enoyl reductase (InhA) encoded by the gene *inhA* is a member of the type 2 fatty acid biosynthesis (FASII) pathway in Mtb. The enzyme catalyzes the NADH-dependent reduction of the trans-2-enoyl-acyl carrier protein which is an essential step in mycolic acid biosynthesis.⁷³ Mutations in the *inhA* gene not only confers resistance to isoniazid but also to the structurally similar second-line drug ethionamide.⁷⁰ INH inhibits InhA via the activated isonicotinyl radical and through the formation of a covalent adduct which results in the ternary complex InhA-isonicotinyl-NADH (Figure 1.9). Genetic, crystallographic and biochemical studies have shown that a mutation in the 94th codon of the *inhA* gene results in a single point mutation from serine to alanine (S94A). In addition,

it has been shown that this single mutation was sufficient to confer clinically relevant resistance to INH bactericidal activity; suggesting that InhA might be isoniazid's true target. Biochemical experiments have shown that the S94A substitution was 17X more resistant to inhibition by the INH-NAD adduct ($IC_{50} \sim 323$ nM) when compared to WT ($IC_{50} \sim 19$ nM). Further crystallographic studies showed that the resistance was primarily due to the decrease in binding of the isoniazid-NAD adduct which was attributed to the displacement of several ordered water molecules that disrupted H-bonding interactions between the protein and the adduct.⁷⁶

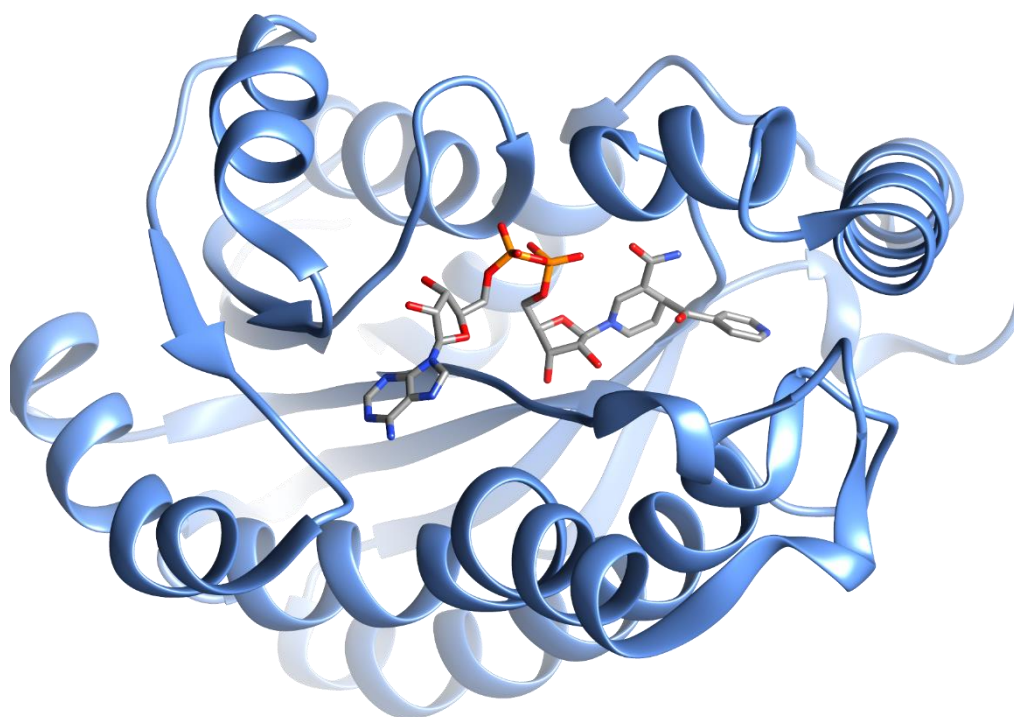


Figure 1.9: Crystal structure of *Mycobacterium tuberculosis* InhA bound to the isoniazid-NAD adduct (PDB ID 2NV6).

1.3.1.2 Rifampicin

Rifampicin (RIF) is a semisynthetic lipophilic ansamycin derived from the natural compound rifamycin and was introduced as an antimycobacterial drug in 1972.⁷⁷ The drug displays early bactericidal activity against actively growing Mtb as well as late sterilizing activity on semi-dormant bacilli. The recognition of the late semi-dormant activity and the addition of pyrazinamide (see section 1.3.1.3) has allowed the treatment of drug-susceptible Mtb to decrease from one year to six months.⁷⁸ Rifampicin inhibits mycobacterial transcription by targeting the DNA-dependent RNA polymerase (RNAP).⁷⁹ Here, the drug binds near the DNA/RNA channel thereby physically blocking the elongation of the growing mRNA chain after 2-3 bases have been polymerized.⁸⁰

Resistance to rifampicin has been mapped to three distinct loci namely RIF-cluster I (codons 512-534), RIF-cluster II (codons 563-574) and RIF-cluster III (codons 563-574) of the RNA polymerase.⁷⁷ Over 96.0 % of Mtb clinical isolates that display resistance to rifampicin have mutations in the so-called “hot-spot region” spanning 81 base pairs. This region is also known as the rifampicin resistance-determining region (RRDR) and is located in RIF-cluster I.⁸¹ Most commonly associated mutations are those that yield single amino acid substitutions and rarely deletions or insertions. Most predominant mutations within the Mtb genome occurs at codons 440, 445, 450 and 452 corresponding to codons 521, 526, 531 and 533 in *E.coli*, respectively. Most notably are substitutions at codons 526 and 531 (445 and 450 in Mtb) which are generally associated with a high degree of resistance to rifampicin. In contrast, substitutions at positions 514 or 533 (433 or 452 in Mtb) results in a lower-degree of resistance (Figure 1.10).⁷⁷ In general, it has been

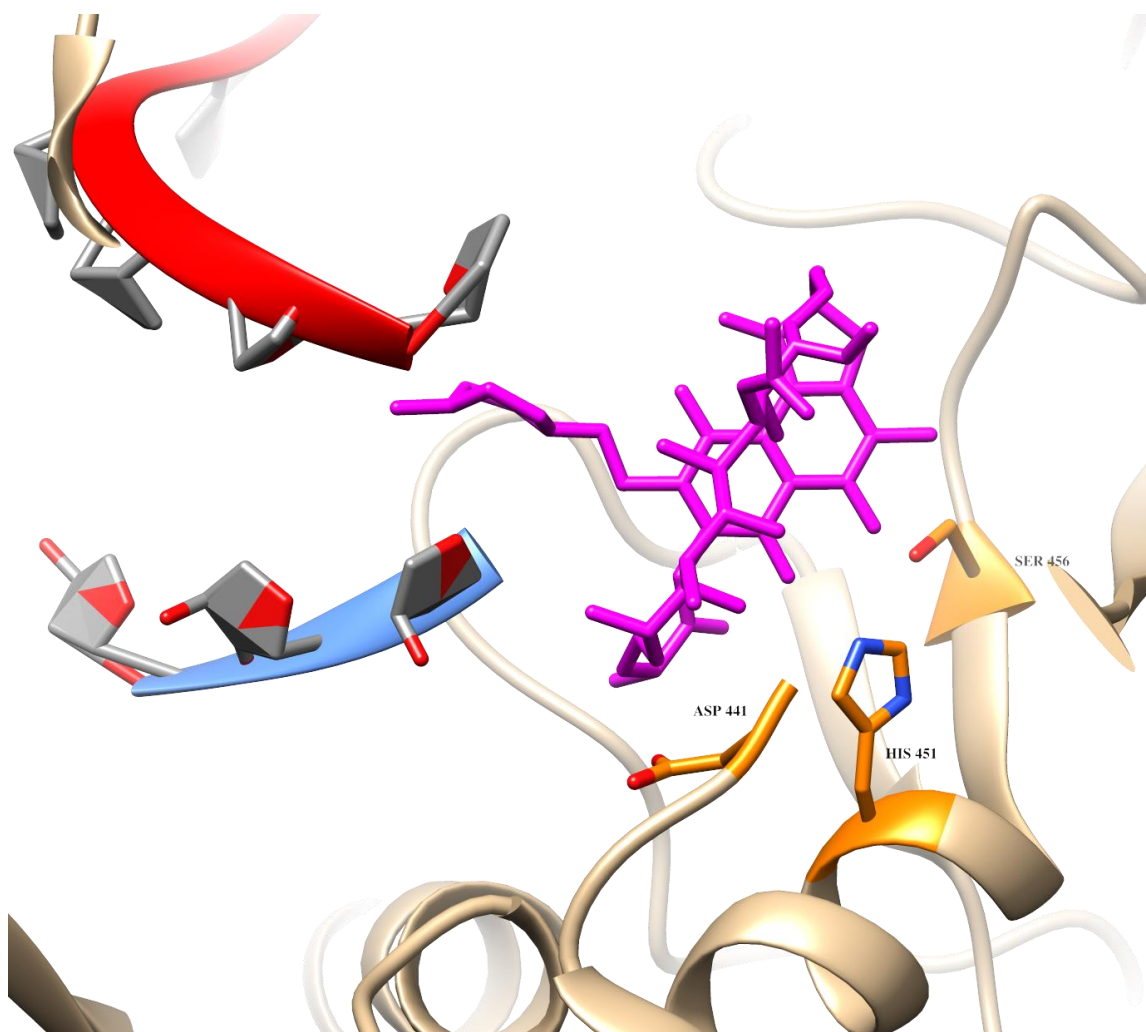


Figure 1.11: Rifampicin bound to the active site of *Mycobacterium tuberculosis* RNA polymerase. Template strand shown in red, 3-nucleotide RNA shown in blue, rifampicin shown in magenta and clinically relevant residues that when mutated confer rifampicin resistance are colored orange (PDB ID 5UHC).

1.3.1.3 Pyrazinamide

Pyrazinamide (PZA) is a nicotinamide analog that was initially synthesized in 1936 but utilized as an antimycobacterial drug in 1952.⁸³ The discovery of PZA was serendipitous, and it was based on the observation that nicotinamide analogs displayed

activity against mycobacteria in animal models. In 1956, it was shown that PZA had a high degree of sterilizing activity when it was utilized alongside isoniazid in infected mouse models.⁸⁴ Moreover, it was later found that PZA was almost as effective as rifampicin in sterilizing semi-dormant Mtb isolates. It was also observed that the tb treatment could be shortened from one year to 9 months if rifampicin or pyrazinamide were used, and from one year to six months if both drugs were added to the regimen alongside isoniazid and ethambutol.^{36, 83} Pyrazinamide's mechanism of action has puzzled scientists ever since its clinical use. One of the most unusual characteristics of pyrazinamide is that it has little to no activity against actively growing bacteria, but it is highly efficient at clearing dormant bacilli.⁸⁵ Although this drug has been used for the last 70 years, the therapeutic mode of action of PZA is the least understood of all anti-tb drugs.⁸⁶

Like isoniazid, pyrazinamide is a prodrug, and it enters the bacilli through passive diffusion.⁸⁷ The current working model of PZA's mechanism of action is that once the drug enters Mtb, it is enzymatically converted to pyrazinoic acid (POA) by the pyrazinamidase/nicotinamidase (PncA) encoded by the *pncA* gene (Figure 1.12).

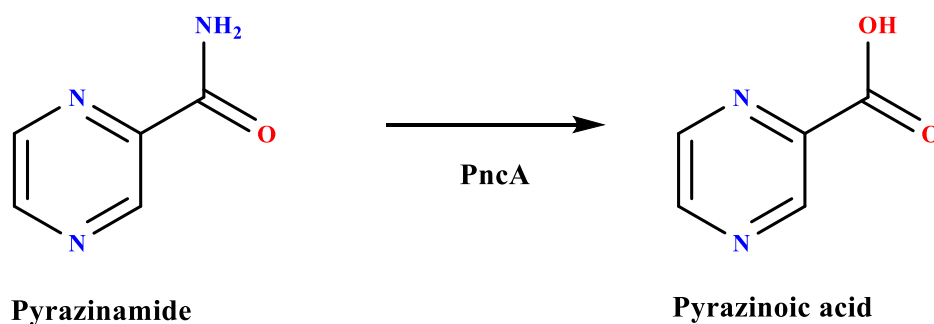


Figure 1.12: Reaction catalyzed by PncA.

POA is then expelled out of the cell through passive diffusion or via an inefficient efflux pump. Once outside the cell, and under acidic conditions, pyrazinoic acid becomes protonated (HPOA) and reabsorbed. Reabsorption of protonated pyrazinoic acid is thought to be more efficient than the excretion of POA which in turn leads to a time-dependent accumulation of HPOA under acidic conditions. The accumulation of protons inside the cell, brought by HPOA, causes cytoplasmic acidification which can act as a general and non-specific mechanism of inhibition of many enzymes. In addition, the accumulation of intracellular POA is thought to de-energize the membrane potential causing a collapse of the proton motive force.⁸⁸⁻⁸⁹

Mutations in the *pncA* gene are frequently associated with the main mechanism of pyrazinamide resistance. In addition, it has been shown that pyrazinamide-resistant clinical isolates are deficient in PncA activity.⁹⁰ The mutations in PncA are diverse and spread along the entirety of the gene. These are commonly missense mutations leading to residue substitutions or nonsense mutations in the promoter region of the *pncA* gene.⁹¹ Despite the high degree of variation, it has been noted that there is a high-level clustering

of mutations in three regions namely residues 3-17, 61-85 and 132-142. These have been observed to correlate with regions that contain the catalytic sites and metal binding sites of the MtbPncA enzyme (Figure 1.13).⁹¹

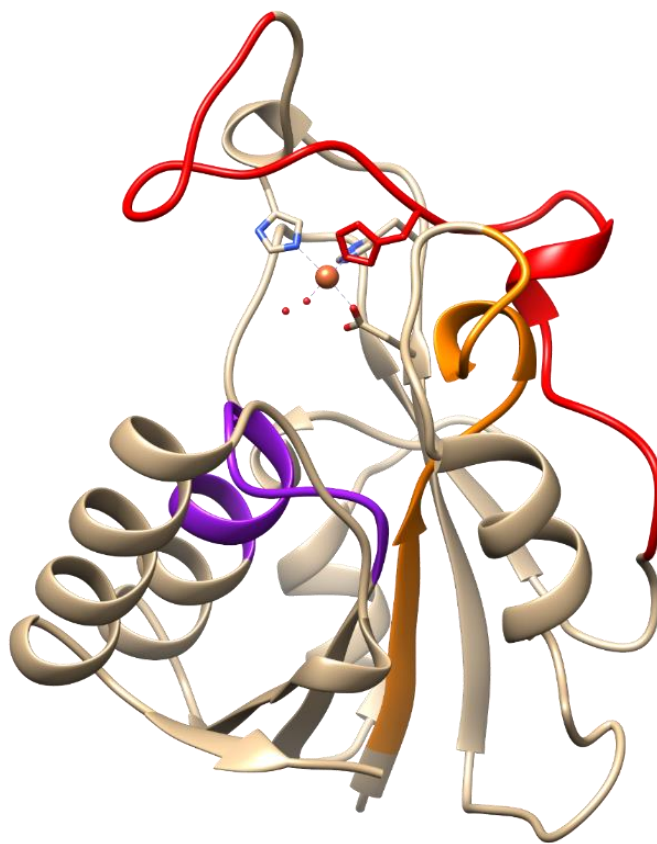


Figure 1.13: *Mycobacterium tuberculosis* PncA. a) Region corresponding to residues 3-17 is colored orange, region corresponding to residues 61-85 is colored red and region corresponding to residues 132-142 is colored purple (PDB ID 3PL1).

1.3.1.4 Ethambutol

Ethambutol (EMB) was introduced as an antimycobacterial drug in 1966, and alongside rifampicin, isoniazid, and pyrazinamide complete the current first-line anti-tb drug regimen.⁶⁷ EMB acts as a bacteriostatic agent that inhibits the machinery involved in the biosynthesis of the arabinogalactan component of the Mtb cell wall.⁹² Within Mtb, the 10 kbp operon containing the genes *embCAB* code for an arabinosyl transferase. Inhibition of the enzyme leads to the accumulation of the intermediate D-arabiofuranosyl-P-decaprenol.⁹³

Laboratory and epidemiological evidence suggest that mutations in the *embCAB* operon are the leading cause of ethambutol resistance in Mtb.⁹⁴ Specifically, the most recognized mechanism of ethambutol-resistance are mutations that occur in codon 306 of the *embB* gene. A German study utilizing 34 ethambutol-resistant strains identified that greater than 10.0 % of the Mtb resistant strains contained mutations in the *embB306* codon.⁹⁵ In addition, an Indian study utilizing 37 isolates from different parts of India, identified that 30 isolates were EMB resistant with the most common mutation occurring at codon 306.⁹⁶ Besides the *embB306* codon mutation, it has been shown that mutations in codons 406 and 497 of *embB* also confer ethambutol resistance, collectively accounting for ~ 60 % of clinically relevant ethambutol resistance. However, studies have shown that the mutations in the codons mentioned above confer low-level EMB resistance with MIC ranges between 6 and 14 µg/mL, inconsistent with the high-level resistance observed in other clinically relevant isolates.⁹⁷ Follow up resistant mutant isolation experiments by the same group identified that mutations in the decaprenylphosphoryl-B-D-arabinose (DPA)

biosynthetic and utilization pathway genes including *Rv3806c*, *Rv3792*, *embB* and *embC* where accumulative and produced a wide range of EMB MIC's. For example, the authors observed that mutations in *Rv3806c* increased the production of DPA which resulted in a MIC increase of 2-4 µg/mL in WT Mtb and 16-32 µg/mL in an *embB306* mutant. In addition, they observed that mutations in the *Rv3792* increased the downstream expression of *embC* which also resulted in an increase of MIC. Taken together the studies suggest that Mtb might accumulate a pre-resistant state characterized by EMB MIC's below the threshold of drug resistance and that the high-level EMB resistance might occur in a stepwise manner.⁹⁸

1.3.1.5 Streptomycin

Although streptomycin is not part of the current first-line anti-tb regimen, it was the first drug to be successfully used to treat tb. Streptomycin is an aminocyclitol glycoside originally isolated in 1943 from the soil microorganism *Streptomyces griseus*. By 1948, streptomycin resistant isolates were identified due to the monotherapeutic administration of the drug.⁸¹

Its mode of action is attributed to the inhibition of the initiation step in protein translation. Specifically, by acting on the 30S subunit of the ribosome with the ribosomal S12 protein and the 16S rRNA which are encoded by the *rpsL* and *rrs* genes, respectively.⁹⁹ In about 60-70 % of clinically relevant isolates, the aforementioned mutations are observed. The most common mutation that produces a high-level of streptomycin resistance is the K43R mutation located in the S12 ribosomal protein. On the other hand, the most common mutation that occurs in the *rrs* gene is located around

nucleotides 530 and 915.⁹⁹ Another mutation that has been associated with low-level streptomycin resistance, that accounts for ~ 27 % streptomycin resistant isolates, occurs in the *gidB* gene. The gene encodes a putative 7-methylguanosine methyltransferase that is specific to the 16S rRNA.¹⁰⁰

1.3.2 MDR, XDR and TDR Mtb treatment: second-line and add-on drugs

MDR-Mtb and XDR-Mtb have an estimated mortality rate of 40.0 and 60.0 %, respectively.³⁰ Treatment of these drug-resistant strains can be very time-consuming and expensive. In the USA, the average costs for inpatient treatment can be as high as \$81,000 for MDR-Mtb and \$285,000 for XDR-Mtb.⁶⁵⁻⁶⁶ Many factors influence the selection and formulation of therapy regarding drug-resistant Mtb. These include the presence of extrapulmonary-Mtb, HIV-Mtb coinfection, age, disease severity, history of usage of first-line and second-line drugs and availability and accessibility to reliable DST.^{49, 101} As of 2016, the updated recommendations by the WHO regarding the treatment of MDR-Mtb should consist of at least five drugs. The regimen must include at least four standard second-line drugs including one fluoroquinolone, one injectable agent and at least two of the following drugs: ethionamide or prothionamide, cycloserine or terizidone, linezolid, and clofazimine. Additional drugs (add-on drugs) that are not currently part of the core MDR-Mtb treatment may be employed when appropriate. These include pyrazinamide, ethambutol, high-dose isoniazid, bedaquiline, delamanid, para-aminosalicylic acid and thioacetazone (Table 1.2).^{49, 67-69} Although multidrug combination approaches have increased favorable outcomes, they have serious drawbacks. Mainly stemming from the high toxicity of the drugs, heavy pill uptake, lack of adherence by patients and at least 6-

8 months of painful injections. In 2016, a shorter course of treatment for MDR-Mtb was standardized for patients with primary resistance.⁴⁹ The short course consists of a 9-12 month long regimen that is successful in ~ 90.0 % of cases. During the short course, prothionamide, kanamycin, and high-dose isoniazid are administered for 4-6 months. This is followed by the addition of moxifloxacin, clofazimine, pyrazinamide, and ethambutol given throughout the rest of the regimen. Eligibility to the short course mainly depends if the patient has or suspected to have resistance to any of the short course drugs (except isoniazid). Also, the patient must not have any prior exposure to the second-line drugs used during the short-course for more than one month. Otherwise, patients not eligible for the short course will have to adhere to the 20-month 5-drug standard regimen for MDR-Mtb treatment.^{49, 102-103}

XDR-Mtb treatment regimens are constructed with similar guidelines when compared to the MDR-Mtb treatment principles and can last up to 30 months. Here, administration of four or more drugs is likely to be effective. A backbone of bedaquiline or delamanid are recommended in addition to linezolid, new generation fluoroquinolones and inclusion of add-on drugs such as para-aminosalicylic acid, high-dose isoniazid, pyrazinamide are also recommended (Table-1.2).⁶⁸

Table 1.2: Current second-line antimycobacterial drugs.⁴⁹

Compound	Gene(s) commonly associated with rise of resistance	Role of gene product
moxifloxacin, levofloxacin	<i>gyrA, gyrB</i>	topoisomerase II (DNA gyrase)
kanamycin, amikacin capreomycin	<i>rrs, eis</i> <i>tlyA</i>	16S RNA, promoter region of aminoglycoside acetyltransferase rRNA methyltransferase
prothionamide, ethionamide	<i>ethA, inhA</i>	monooxygenase, enoyl-ACP-reductase
cycloserine, terizidone	<i>ddlA, alrA, cycA</i>	D-alanine:D-alanine ligase, alanine racemase, alanine permease
linezolid	<i>rrl, rplC</i>	23S rRNA, 50S L3 protein
clofazimine	<i>Rv0678</i>	transcriptional repressor of MmpL5
bedaquiline	<i>atpE</i>	subunit of ATP synthase
delamanid	<i>ddn</i>	deazaflavin-dependent nitroreductase
para-aminosalicylic-acid	<i>thyA, folC, dfrA, ribD</i>	thymidylate synthase, folylpolyglutamate synthase, dihydrofolate reductase, probable riboflavin-specific deaminase
thiacetazone	<i>hadAB, mmA4</i>	subunits of hydroxyacyl-ACP dehydratase, methyltransferase
high-dose isoniazid	see table 1.1	see table 1.1
pyrazinamide	see table 1.1	see table 1.1
ethambutol	see table 1.1	see table 1.1

1.3.2.1 Moxifloxacin, levofloxacin

Moxifloxacin and levofloxacin are third-generation fluoroquinolones currently utilized for the treatment of drug-resistant Mtb. (Figure 1.14).¹⁰⁴ Third generation fluoroquinolones have a higher degree of activity against gram-positive organisms including penicillin-resistant *S. pneumoniae*, and other atypical pathogens such *Chlamydia pneumoniae*, *Mycoplasma pneumoniae* and Mtb.¹⁰⁵

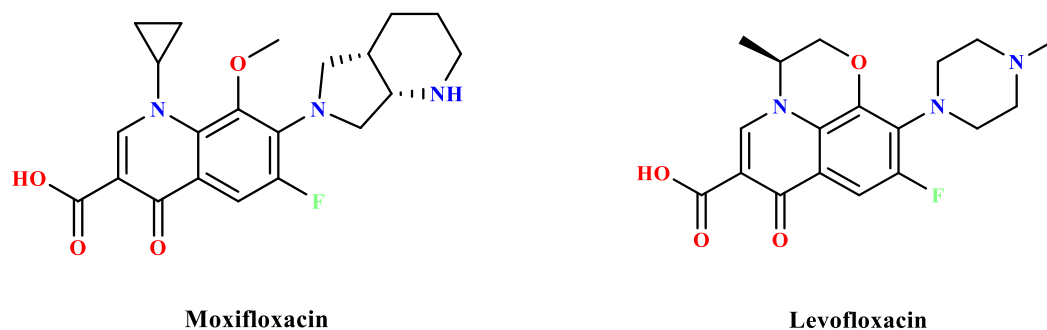


Figure 1.14: Chemical structures of third-generation fluoroquinolones moxifloxacin and levofloxacin.

The mode of action of fluoroquinolones is to inhibit the type II topoisomerase and type IV topoisomerase. Both enzymes being involved in the control of DNA supercoiling and entanglement.¹⁰⁶ Mtb only possess a type II topoisomerase (DNA gyrase) thereby being the only target of the fluoroquinolone antibiotics.¹⁰⁷ DNA gyrase is a tetramer composed of two α -subunits and two β -subunits encoded by the *gyrA* and *gyrB* genes. Studies performed in *M. smegmatis* and Mtb showed that resistance to fluoroquinolones was mainly due to chromosomal mutations in the putative fluoroquinolone binding regions of *gyrA* or *gyrB*. The most prevalent mutations occurred at codons 90 (Ala90) and 94 (Asp94) of the *gyrA* gene and to a lesser extent codon 74 (Ala74), 88 (Gly88) and 91 (Ser91).¹⁰⁸

Cross-resistance to fluoroquinolones were thought to be expected since they are believed to bind in the same general region. Despite this, a group reported a Mtb strain with a mutation that confers resistance to moxifloxacin and gatifloxacin but retained activity to ofloxacin.¹⁰⁹ Suggesting that fluoroquinolone resistance in Mtb might be much

more complex than initially thought. On the other hand, several bacterial species have shown that the main mechanism of fluoroquinolone resistance is mediated by efflux pumps.¹¹⁰ Several studies with Mtb suggest that efflux pumps might also play a role in fluoroquinolone resistance as well as other antimycobacterial drugs.¹¹⁰

1.3.2.2 Kanamycin, capreomycin, amikacin

Kanamycin, capreomycin, and amikacin are the injectable agents currently utilized as a second-line of defense against drug-resistant Mtb (Figure 1.15).

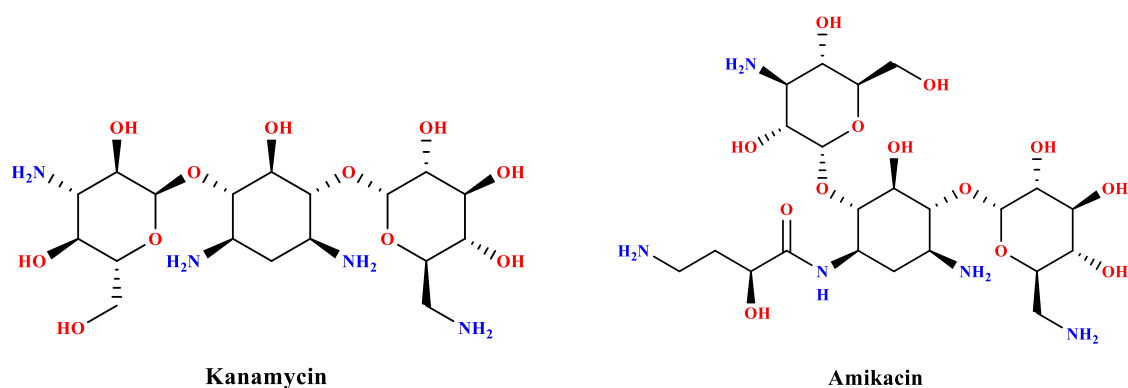
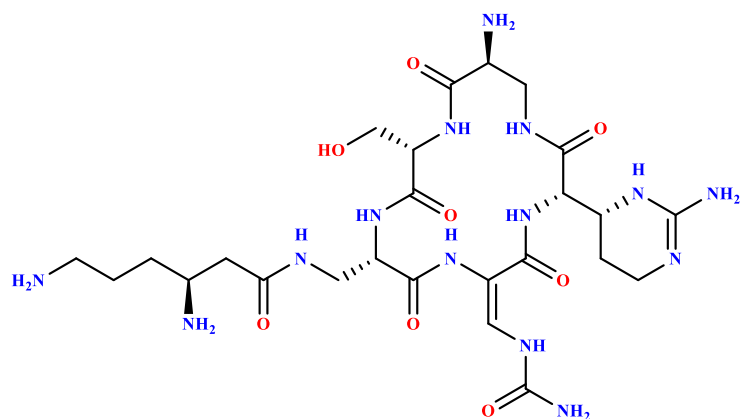


Figure 1.15: Chemical structures of the second-line injectable drugs kanamycin, amikacin and capreomycin.



Capreomycin

Figure 1.15: Continued

Although kanamycin and amikacin are aminoglycosides and capreomycin is a cyclic peptide; they have the same mode of action. That is, they exert their inhibitory activity at the protein translation level. Kanamycin and amikacin inhibit protein translation by interacting with the 16S rRNA. The most prevalent mutation that confers resistance to the aforementioned aminoglycosides is located at codons 1400 and 1401 of the *rrs* gene. Mutations at these positions have been associated with high-level kanamycin and amikacin resistance.¹¹¹ Cross-resistance between the two aminoglycosides is not absolute. That is, studies have shown that there are variable levels of resistance with each of the antibiotics suggesting the possibility of an alternative mode of resistance for different aminoglycosides.¹¹² Along this line, a study that utilized 42 *Mtb* clinical isolates with kanamycin resistance, identified that up to 79.0 % of the isolates have mutations in the promoter region of the *eis* gene. Mutations in this gene caused overexpression of the

encoded aminoglycoside acetyltransferase conferring resistance to kanamycin but not amikacin.¹¹³

Cyclic peptides such as capreomycin have been implicated to bind at the interface of the small and large subunits of the ribosome.¹¹⁴ The most common mutation related to cyclic peptide resistance occurs in the *tlyA* gene which encodes a rRNA methyltransferase that specifically methylates the 2'-oxygen of ribose in rRNA. Mutations in the TlyA enzyme lack methylation activity, suggesting that methylation of the drug might be necessary for its inhibitory activity.¹¹⁵

1.3.2.3 Ethionamide, prothionamide

Just like isoniazid and pyrazinamide, ethionamide and prothionamide are prodrugs. Ethionamide and prothionamide are structurally similar derivatives of isonicotinic acid; the only difference is that the latter has an ethyl group and the former has a propyl group at the same position (Figure 1.16).

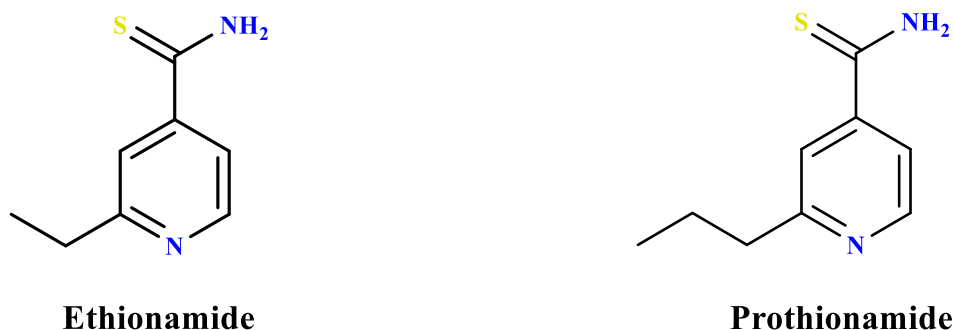


Figure 1.16: Chemical structures of prodrugs ethionamide and prothionamide.

The critical role of these drugs is that they are active against KatG isoniazid-resistant mutants. Activation of the drugs occurs through the action of the *ethA* encoded monooxygenase.¹¹⁶ Following activation and subsequent reaction with NADH yields an ethionamide or prothionamide-NAD adduct. The adduct then inhibits the NADH-dependent InhA enzyme which in turn inhibits mycolic acid biosynthesis leading to mycobacterial cell death (Figure 1.17).¹¹⁷ The most common mutations that confer monoresistance to prothionamide or ethionamide occur in the *ethA* and *inhA* genes. Although variations in the genes mentioned above account for greater than 75.0 % of clinically relevant isolates, other mutations have been reported to occur in the regulatory region of EthA (*ethR*). To date, around 85 *ethA* mutations have been identified scattered along the entirety of the gene.¹¹⁸ Around 60.0 % of the mutations are missense resulting in single amino acid substitutions, other mutations are due to insertions, deletions or nonsense mutations. Unlike the canonical S315T mutation in KatG, which is present in over 94.0 % of clinically isolated resistance mutants, there is no prevalent mutation in the *ethA* gene. This might be due to the presence of other monooxygenase's in Mtb that could take over when EthA activity is lost.¹¹⁹

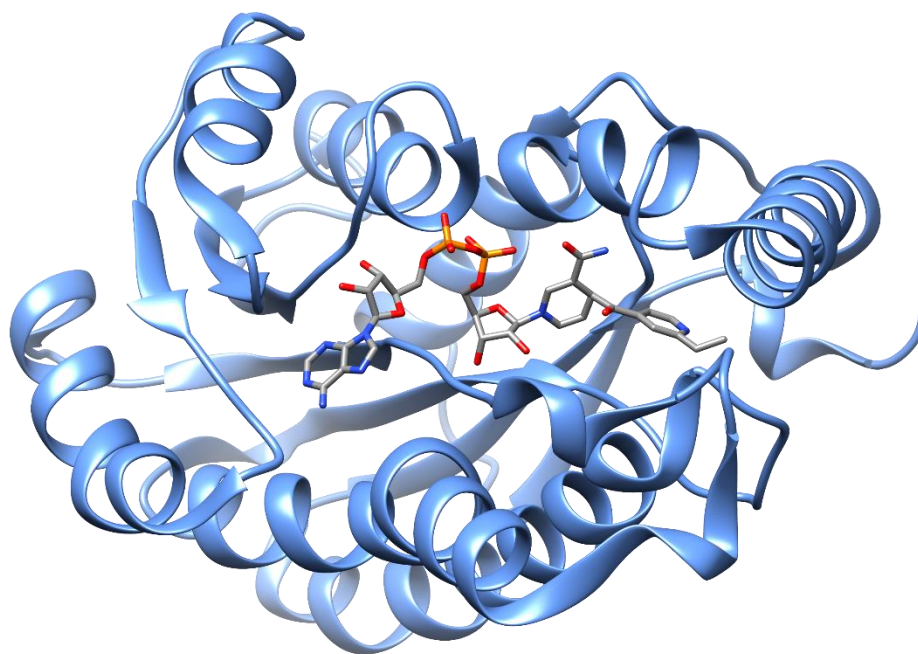
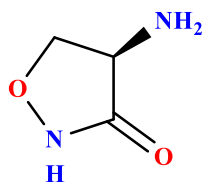


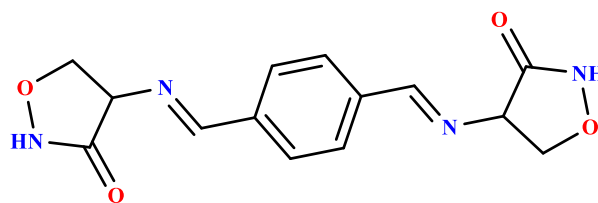
Figure 1.17: Crystal structure of InhA bound to the ethionamide-NAD adduct (PDB ID 2HI9).

1.3.2.4 Cycloserine, terizidone

Cycloserine is a structural analog of D-alanine which is a component of the bacterial cell wall. Terizidone is a derivative of cycloserine and consists of two cycloserines flanking a central benzene core (Figure 1.18).¹²⁰



Cycloserine



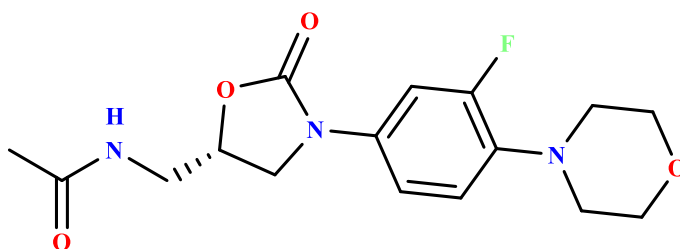
Terizidone

Figure 1.18: Chemical structures of cycloserine and terizidone.

The mechanism of inhibition of cycloserine and terizidone is mainly attributed to the inhibition of several enzymes. These include the D-alanine:D-alanine ligase (DdlA), the D-alanine racemase (Alr) enzyme which is involved in the interconversion of L-alanine to D-alanine and the alanine permease CycA. The pharmacologically relevant target(s) and mechanism of resistance within Mtb are currently unknown. Despite this, preliminary studies with *M. smegmatis* have shown that overexpression of the AlrA racemase leads to resistance of cycloserine. In addition, studies in *M. bovis* revealed that the CycA permease confers a low-level resistance to cycloserine.¹²¹

1.3.2.5 Linezolid

Linezolid is a synthetic oxazolidinone antibacterial originally utilized for the treatment of skin and respiratory tract infections.¹²² In addition, *in vitro* and *in vivo* studies have shown that the drug possesses antimycobacterial properties (Figure 1.19).¹²³



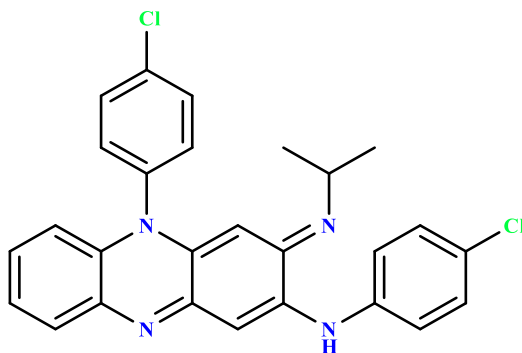
Linezolid

Figure 1.19: Chemical structure of linezolid.

Linezolid acts by inhibiting the early steps of protein synthesis through interactions with the 50S subunit of the ribosome.¹²² Resistance to the drug in Mtb is rare; however, a study performed with 210 MDR-Mtb isolates identified that around 2.0 % were resistant to linezolid. Indicating that resistance against the drug is already on the rise. *In vitro* resistant mutant isolation experiments with linezolid identified that mutations in the G2061T and G2576T of the 23S rRNA lead to an increase in resistance.⁴⁷ Another study utilizing next-generation whole-genome sequencing of *in vitro* selected mutants identified the T460C in the *rplC* gene which encodes the 50S L3 protein of the ribosome.¹²⁴

1.3.2.6 Clofazimine

Clofazimine is a riminophenazine compound whose antimycobacterial properties were known since 1957. However, like many of the second-line drugs; clofazimine has serious side effects including skin discoloration and QT prolongation (Figure 1.20).⁶⁶ Clofazimine is a slow-acting bactericidal agent that might exert its primary inhibitory action as a prodrug.



Clofazimine

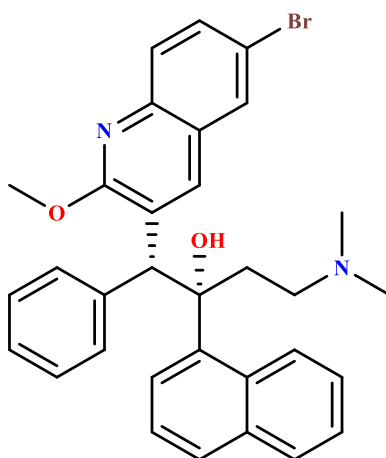
Figure 1.20: Chemical structure of clofazimine.

Studies in *M. smegmatis* showed that clofazimine is reduced by the Type II NADH dehydrogenase-quinone oxidoreductase and after reoxidation liberates reactive oxygen species causing the observed bactericidal effects.¹²⁵ Clofazimine is thought to compete with menaquinone (vitamin K₂), the only quinone present in mycobacteria and key electron transport chain acceptor.¹²⁵ Although the exact resistance mechanism and true

drug target is not known, studies have found that spontaneous mutations that cause upregulation of the Mycobacterial Membrane Protein Large 5 (MmpL5) lead to resistance of clofazimine and other drugs.¹²⁶ MmpL5 has been recently classified as a secondary multidrug transporter from the Resistance-Nodulation-Division (RND) superfamily indicating that one of its functions might be acting as a drug efflux pump.¹²⁶

1.3.2.7 Bedaquiline

Bedaquiline was FDA approved in 2012, representing the first FDA-approved drug in over 40 years for the treatment of tuberculosis (Figure 1.21).⁶⁶ The drug belongs to the diarylquinoline class of drugs and was discovered through a phenotypical screen on *M. smegmatis*.¹²⁷



Bedaquiline

Figure 1.21: Chemical structure of bedaquiline.

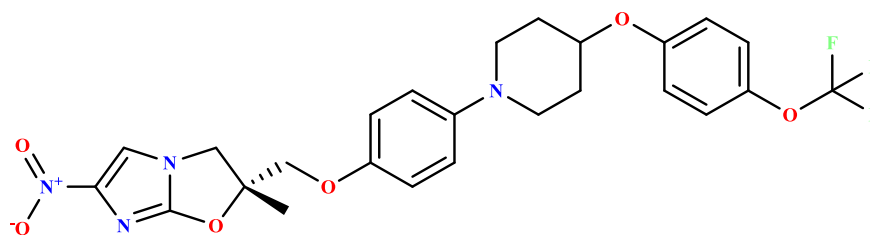
The drug carries a “black-box” warning due to the unexplained deaths that occurred during clinical trials. Bedaquiline’s undesirable effects are mainly attributed to the drug’s interference with the heart’s electrical activity which causes prolongation of the QT interval.¹²⁸ Consequently, the FDA granted accelerated approval for patients afflicted with drug-resistant Mtb when no other alternatives are available.

Bedaquiline possesses a novel mode of action and acts by inhibiting the proton pump of the mycobacterial ATP synthase. The mode of action was identified by resistant mutant isolation experiments coupled to whole-genome sequencing. The studies identified that a mutation occurring in the *atpE* gene which encodes the proteolipid subunit-c part of the Fo subunit of the ATP synthase.¹²⁹ The most common mutations that confer bedaquiline monoresistance is the A63P and I66M amino acid substitution. However, a study in 53 bedaquiline-resistant Mtb strains showed that 15 out of 53 mutants had mutations in the *atpE* gene. The rest of the isolates lacked mutation in the aforementioned gene nor the F0 or F1 operons suggesting alternative mechanisms for bedaquiline resistance within Mtb.¹³⁰

1.3.2.8 Delamanid

Delamanid is a derivative of nitroimidazo-oxazole that has been shown to possess bactericidal activity against drug-susceptible and drug-resistant Mtb (Figure 1.22).¹³¹ Delamanid’s mode of action was elucidated by tracing radiolabeled fatty acids and subsequent incorporation into the mycobacterial cell wall. The authors showed that unlike isoniazid, which inhibits α -mycolic acids, delamanid specifically inhibits methoxy- and keto- mycolic acids.¹³¹ *In vitro* generated resistant mutants have identified that mutations

in the *Rv3547* gene confer delamanid resistance.¹³¹ The gene encodes a deazaflavin-dependent nitroreductase thereby suggesting that just like many Mtb drugs, delamanid is a prodrug and may act through the generation of reactive nitrogen species.



Delamanid

Figure 1.22: Chemical structure of delamanid.

1.3.2.9 Para-aminosalicylic acid

Para-aminosalicylic-acid (PAS) is a prodrug whose antimycobacterial properties have been known since the early 1950s. In fact, it was the second drug to have been utilized for the treatment of tb, right after streptomycin.¹³² However, given the relative lack of potency and higher cost, when compared with the INH, PZA, RIF, and ETH, it is currently used as a second-line anti-tb drug.⁶⁶ Although the drug has been used for over 50 years, the mechanism of inhibition is still not completely understood. Transposon directed mutagenesis studies have identified mutations in the *thyA* gene, and *thyA* gene mutations have been identified in clinically relevant PAS-resistant isolates.¹³³ However, since PAS

is a structural analog of para-amino-benzoic-acid (PABA) it is thought that one of its targets might also be the dihydrofolate reductase (DHFR) (Figure 1.23).

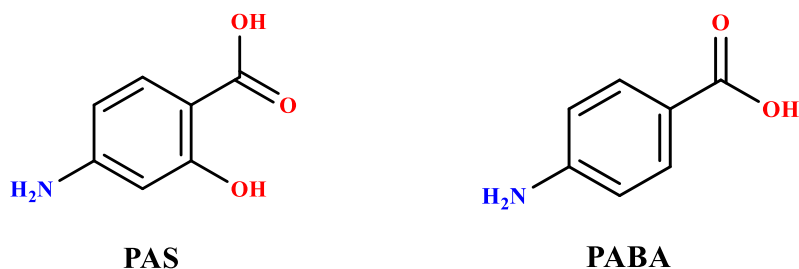
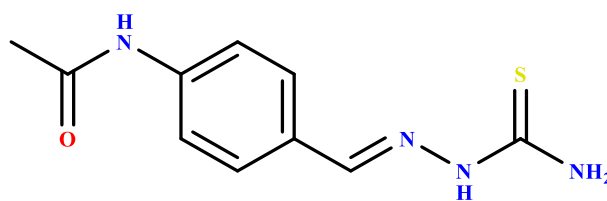


Figure 1.23: Chemical structure of the prodrug PAS and the natural DHFR substrate PABA.

In order to inhibit DHFR, PAS is first activated by dihydropteroate synthase (DHPS) which then leads to the incorporation into the folate pathway, via the generation of a hydroxyl-dihydrofolate antimetabolite; which then inhibits DHFR.¹³⁴ In addition, the same authors show that overexpression of the *dfrA* gene, which encodes for DHFR, leads to a resistant phenotype of Mtb.¹³⁴ On the other hand, it has also been shown that mutations in the *ribD* gene which encodes a putative riboflavin-specific deaminase, lead to a PAS-resistant Mtb phenotype. Other studies in PAS-resistant Mtb isolates have identified missense mutations in the *folC* gene which encodes a dihydrofolate synthase.¹³⁵ Taken together, PAS mechanism of inhibition and resistance is still poorly understood, and the studies suggest that PAS metabolism within Mtb is very complex.

1.3.2.10 Thiacetazone

Thiacetazone is a prodrug that previously formed part of the first-line anti-tb drugs for the treatment of drug-susceptible bacilli (Figure 1.24). Thiacetazone is an inexpensive antimycobacterial that is always used in conjunction with other drugs.¹³⁶ In addition, the drug possesses a relatively weak bactericidal activity; its main purpose is to control the rise of resistance to the other more powerful drugs.⁴⁹ The current first-line regimen now utilizes ethambutol as a replacement mainly due to thiacetazone's high toxicity such as accumulation of serum in the brain.¹³⁶ The mechanism of inhibition and resistance has remained elusive throughout the years; although it is generally accepted that its primary bactericidal activity is through the inhibition of mycolic acid biosynthesis.⁹⁵ Recent resistant mutant isolation studies utilizing 10 thiacetazone-resistant Mtb strains found that one strain had mutations in the *mmA4* gene which encodes a methyltransferase that is involved in mycolic acid modifications.¹³⁷ The remaining 9 strains were found to have missense mutations in several genes including *hadA* and *hadC*; both of which are components of the hydroxyacyl-ACP dehydratase and participate in mycolic acid elongation. Taken together the studies strongly suggest that thioacetazone's intracellular target might indeed be involved in mycolic acid biosynthesis.¹³⁷



Thiacetazone

Figure 1.24: Chemical structure of thiacetazone.

1.4 Strategies for drug discovery against drug-resistant bacteria

The tremendous growth of drug-resistant bacteria imposes a significant global health and economic burden. Presently, the WHO recognizes the rise of drug-resistant bacteria as one of the top three most pressing threats to public health. The CDC estimates that in the United States, up to 2 million Americans suffer from infections related to antibiotic-resistant bacteria. Causing the death of up to 23,000 individuals annually; with a cost of up to \$20 billion.¹³⁸ The hope of overcoming this problem is diminished by the decline in identification and development of novel antibiotics and new drug targets. Therefore, there is an urgent need for novel drugs and drug targets for the treatment and eradication of drug-resistant bacteria.¹³⁸

1.4.1 The ideal Mtb drug target

One aspect key aspect of the ideal drug target is vulnerability. Vulnerability refers to the phenotypical response of death of a pathogen once a drug target is minimally inhibited. Here one must consider the target's essentiality and vulnerability for growth and survival under different conditions. Pathophysiologically, tuberculosis is a very complex

disease as it involves critical interactions between the bacteria and the host's immune system.²⁵ Mtb can diminish the bactericidal properties of macrophages and utilize them as a niche for growth and persistence.¹³⁹ Although many experimental settings including animal models and *in vitro* assays can replicate these conditions to some extent; the details and critical interactions that allow Mtb to persist are still poorly understood.¹⁴⁰⁻¹⁴¹

Secondly, the mutability of the gene coding for the drug target must be considered. As explained in section 1.2, with the advent of any new drug a new mutation conferring resistance followed. Therefore, drug targets that possess a low tolerance for mutation would be ideal drug targets. Mutability will largely depend on the number of genes and gene structure that can produce a resistance phenotype. For example, if on a given gene all positions have equal possibilities, then long genes might have a greater chance of mutation than shorter ones. However, it should be noted that gene size is not always a determinant of the likelihood of mutation given that not all mutations will result in drug resistance. Resistance will most likely occur if the mutations are permissive, that is if the phenotype produced is non-lethal.¹⁴² On the other hand, drugs that target the machinery that is responsible for the mutation itself would be ideal as it would ensure the fidelity of the target being targeted by current drugs first and second-line drugs. Along with this line, the pathways and the proteins involved in spontaneous or DNA-damage induced mutations are currently being characterized in Mtb leading to the identification of potential new drug targets such as C-family DNA polymerase, DnaE2, ImuB, and ImuA. C-Family DNA polymerase and DnaE2 have been implicated in the rise of drug resistance *in vivo*

and *in vitro* whereas ImuB and ImuA are known to form a complex of macromolecules that are required for DNA-damage induced mutagenesis.¹⁴³⁻¹⁴⁴

Another desirable characteristic for a potential drug target is that if the target itself participates in a metabolic “crossroad”. Inhibiting such targets might lead to an increase in metabolites that might prove to be toxic and detrimental to the organism. Such potential choke-point pathways in Mtb could be amino acid biosynthesis, cofactor biosynthetic pathways, cell wall biosynthesis and nucleotide biosynthetic pathways including *de novo* and salvage.¹⁴⁵

In addition to the characteristics described above, drug target essentiality either during latency and active growth must be considered. Presently, most of the potent drugs that are available; target actively growing bacilli. Consequently, there is a paramount need for drugs that target the machinery required by Mtb that confers its ability to persist during its latent phase of infection. Although, the pathophysiological details behind the latent phase of infection are not understood; it has been hypothesized that Mtb has little to no growth and that the bacillus utilizes a unique set of pathways that are distinct from those under active growth. A drug target essential for Mtb survival during the latent phase of infection is extremely desirable as it could potentially cure the disease before its clinical and pathophysiological presentation.¹⁴⁶

Finally, the location of the drug target must be considered. Here the cellular niche where the potential drug target is located is critical to the effect of any given drug. In principle, the more barriers a drug candidate has to go through to reach the target, the less concentration of the drug will reach the target. This can be attributed to enzymatic

inactivation, drug pumping mechanisms and sequestration by other non-essential proteins among others. One significant barrier every drug must face is the highly sophisticated and lipid-rich mycobacterial cell wall. Ideal drug candidates must have a way to cross the membrane without losing its activity. The machinery involved in mycobacterial cell wall biosynthesis has always represented an attractive drug target. Indeed, many currently available drugs target this essential step (see Tables 1.1 and 1.2). Consistent with this idea, the location of the drug target (intracellular or extracellular) will significantly influence the potency of the compound.¹⁴⁵

1.4.2 Target-based drug discovery approaches to identify new drugs

Target-based drug discovery is the product of the advancements in medicinal chemistry, pharmacology, molecular genetics, and biochemistry. This is coupled with the extensive knowledge and research throughout the 1950s and 1960s in enzymes and enzyme kinetics which provided the methods utilized nowadays to determine potency and efficacy of drugs against specific targets. Throughout this time, hundreds of proteins were purified and characterized, later becoming the specific drug targets themselves.¹⁴⁷ During the 1970s, protein receptors became the most frequent targets for drug discovery, and during the 1980s, target-based drug discovery became more popular due to the advances in genomic science and molecular biology.¹⁴⁸ Also, recombinant DNA technology led to the cloning and purification of many enzymes that in turn favored screening of proteins against libraries of compounds.¹⁴⁹⁻¹⁵¹ Finally, during the 1990s target-based drug design became the status quo due to the advent and development of miniaturization and

automation of assays which in turn led to high-throughput screening of vast libraries of small molecules against specific proteins or enzymes.¹⁵²⁻¹⁵³

Target-based drug discovery typically starts with a known protein target that is relevant or known to play a fundamental role in a particular disease. Historically, in Mtb, the principal criteria utilized for target selection are essentiality under active growth or latent phase and a lack of homology or sufficient differences with any human protein. These molecular targets are often identified by gene knockout studies in animals or pathogenic bacterial studies, identification of abnormal phenotype or function of specific proteins and identification of mutations or specific proteins within an essential pathway.¹⁵⁴⁻¹⁵⁵ Once a suitable drug target is identified, assay development is pursued with the goal of performing high-throughput screening of compound libraries to identify inhibitors or molecules that bind the target of interest. Lead compounds are then validated for inhibition or binding using a robust secondary technique, e.g., enzyme kinetics for inhibition and isothermal titration calorimetry for binding and affinity studies. The most potent compounds are then optimized against the target either through chemistry based activity relationship studies or structure-guided drug design. In addition, optimized compounds are assessed *in vivo* to understand and further characterized their ADME properties. Finally, if a compound displays favorable potency and efficacy against relevant disease models, then toxicological and preclinical studies are carried out that might eventually lead to clinical trials. This process can take anywhere from 12-15 years and cost over \$ 1 billion.¹⁵⁶ Target-based drug discovery resulted in the identification of the

most common and fruitful drug targets, namely ion channels, G-protein coupled receptors and enzymes.¹⁵⁷

Although target-based drug discovery has many advantages from a scientific and practical point of view, the high attrition rates in clinical trials for compounds identified through target-based methods have been associated with a lack of efficacy and lack of whole-cell activity of the compounds. Additionally, our current level of knowledge and understating of the complex biological processes upon which drugs act is not sufficient to feasibly predict the therapeutic value of a new drug target.

Analysis of first-in-class FDA approved drugs between 1999 and 2008 showed that 28 of the novel drugs were discovered through classical pharmacology (e.g., phenotypic drug discovery). In contrast, 17 of the drugs were found through target-based drug discovery efforts (Figure 1.6).¹⁵⁸ This observation has renewed the interest of pharmaceutical companies and academic centers towards the application of the classical technique of phenotypic drug discovery (Figure 1.7).¹⁵⁹

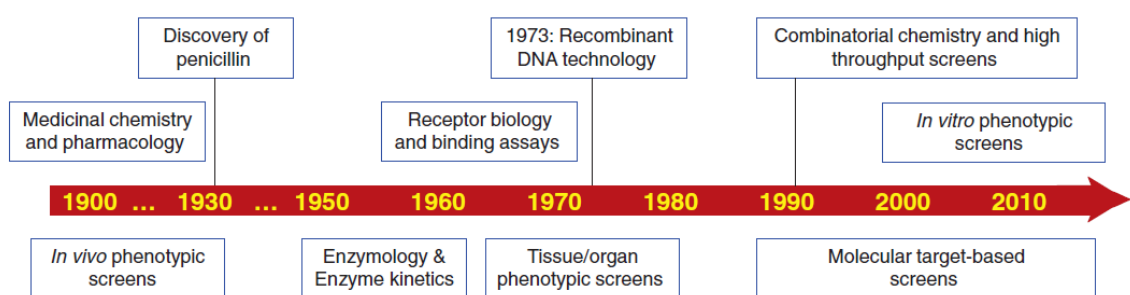


Figure 1.25: Evolution of drug screening and discovery. Reprinted with permission.¹⁶⁰

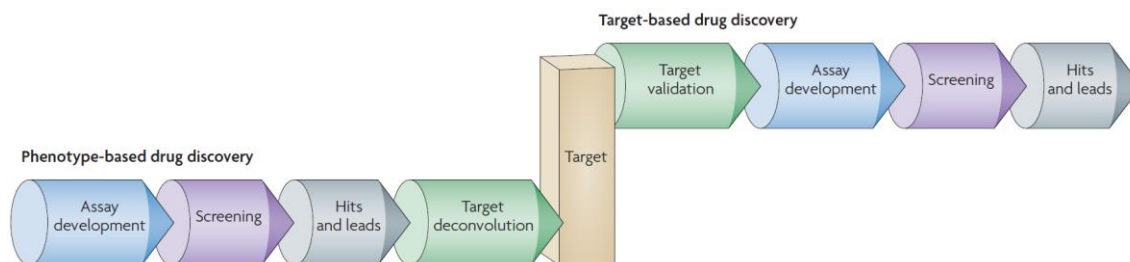


Figure 1.26: Phenotypic vs. target-based drug discovery. In phenotypic drug discovery, active molecules are obtained early during the drug development process. Target-based drug discovery starts with a macromolecule of interest. This is then followed by assay development to find any active compound. Reprinted with permission.¹⁵⁹

1.4.3 Phenotypic-based drug discovery approaches to identify new drug targets

Phenotypic drug discovery and development seeks to identify desirable effects (phenotypes) in disease-relevant biological models (live animals or cell lines).¹⁶¹ Typically, large libraries of compounds (0.2-2 million compounds) are screened in a high-throughput fashion to identify any phenotypic response. Phenotypic drug discovery for Mtb typically requires vast and chemically diverse compound libraries, whole-cell based screening assays that would ideally mimic conditions encountered by Mtb within a host and finally and orthogonal methods to deconvolute the hits.¹⁶² Historically, the golden age of drug discovery was carried out through phenotypic-based drug discovery either by accident or through careful observational studies.¹⁶³ Unlike target-based drug discovery, the particular target, and mode of action can remain unknown even after the compound's activity, and efficacy has been determined. Another advantage of this methodology is that phenotypic screening offers a more physiologically and pharmacologically relevant response given that the screen itself is carried out in a more native cellular environment.

Lead compounds identified can subsequently be chemically optimized to induce a specific/targeted phenotype. One of the major advantages of phenotypic drug discovery is that this technique enables the identification of active compounds that might prove to be useful for rare diseases or development of compounds that are active against diseases with no known molecular targets.¹⁶⁰

Many of the FDA approved drugs in the 1970s have no known molecular target/mode of action.¹⁶⁴ Indeed, many of these drugs were initially identified through phenotypic drug discovery. One key example is acetylsalicylic acid (aspirin) for which almost a century went by before the mechanism of inhibition was determined.¹⁶⁵ Other examples of phenotypically identified drugs include the antihypertensives nicardipine, nifedipine, verapamil and diltiazem.¹⁶⁶⁻¹⁶⁷ Another notable example is the drug Zetia (Ezetimibe), which was discovered by Merck through the screening of compounds in animal models with a high cholesterol diet.¹⁶⁸⁻¹⁶⁹ Presently, drugs that prove to be efficacious and safe for the patient might obtain FDA clearance even if the mode of action is unknown. However, the mode of action and molecular drug target are desirable pieces of information to have given that structure-guided and chemistry efforts can significantly improve potency, selectivity and decrease undesirable side effects.¹⁶⁰ Finally, target identification of the drug producing a desirable phenotype is a daunting and more complicated task than starting with a known target (e.g., target-based). However, it can be performed through a systematic approach and utilizing many techniques such as affinity chromatography, yeast-three hybrid system, phage-display, protein microarrays and resistant mutant isolation.¹⁵⁹

1.4.4 Repurposing and screening of previously approved drugs

Another strategy in the arsenal that is being utilized to combat the rise in drug-resistant bacteria is the screening of previously approved drugs. This technique is mostly applied for the identification of adjuvants to enhance or facilitate the activity of antibiotics. This approach has already identified several non-antibiotic compounds from several drug classes including tranquilizers, antispasmodics, antihistamines, anti-inflammatories and antihypertensive drugs.¹⁷⁰ For example, a screen of 1,057 previously approved drugs, led to the identification of a total of 69 compounds that enhanced the activity of the tetracycline minocycline against *S. aureus* and *E. coli*. The screen identified disulfiram (Antabuse) as having a high bactericidal synergistic effect, whereas loperamide and benserazide (Imodium) showed an increase in the susceptibility of several multidrug resistant strains of *P. aeruginosa*. Also, co-administration of minocycline with loperamide displayed a synergistic effect against *E. coli* and other pathogenic bacteria including *S. enterica*, *K. pneumoniae* and *A. baumannii*.¹⁷¹

Another example of drug repurposing is the non-steroidal anti-inflammatory drug (NSAID) diclofenac. This drug has been identified as having bactericidal enhancement of streptomycin against *E. coli* and *Mycobacterium* spp. and gentamicin activity against *L. monocytogens*. In addition, diclofenac sodium also displayed a synergistic effect in mouse models when co-administered with streptomycin against Mtb and *S. thyphimurium*.¹⁷² Another NSAID that demonstrated a synergistic effect when co-administered with several antibiotics is celecoxib for the treatment of *S. aureus*.

Several phenothiazine derivatives have been shown to possess synergistic and antibacterial activity against several bacteria including mycobacteria. For example, the antipsychotic thioridazine has been noted to have bactericidal activity against Mtb including MDR-Mtb strains. Further investigation has shown that the compound also enhances the effect of rifampicin and streptomycin against several clinical Mtb isolates. Moreover, mouse studies revealed that thioridazine can decrease the number of colony-forming units when it is administered alone and a synergistic effect when co-administered with isoniazid, rifampicin, and pyrazinamide.¹⁷³ In short, repurposing and screening of previously approved drugs offer a fast-track route for the discovery of potential new drugs or molecules that can act as adjuvants. The major advantage of this strategy is that the overall cost of utilizing the potential newly repurposed drug can be up to 40.0 % less than *de novo* identification as well as facilitating a rapid approval for immediate use.

1.4.5 Tuberculosis structural genomics consortium: a worldwide collaboration towards the identification and characterization of new drug targets for Mtb drug development

Structural genomics has played a fundamental role in elucidating, identifying and structurally characterizing potential drug targets for many infectious diseases including Mtb.¹⁷⁴ Structural genomics was conceived through the advancements in high-throughput crystallography, high-throughput molecular cloning and high-throughput protein expression and purification.¹⁷⁵ The consortium seeks to perform large-scale efforts to determine the unique set of protein structures for a given organism; primarily through X-ray crystallography. Presently, high-throughput structural genomics primarily focuses on solving the structures of biologically essential or medically relevant targets for neglected

and recalcitrant to treat infectious diseases. Central to the consortiums ideology is the structural elucidation and characterization of proteins that belong to pathways that are critical to a particular pathogen's survival or virulence.¹⁷⁶ Between 1999 and 2001, several structural genomics consortiums were formed by various agencies worldwide. Including the National Institute of Health (NIH) sponsored Structural Genomics Centers (SGCs), the Northwest Structural Genomics consortium in the United Kingdom, the Protein Structure Factory in Berlin and the RIKEN Structural Genomics and Proteomics Initiative.¹⁷⁷

The Tuberculosis Structural Genomics Consortium (TBSGC) was established in 2000, through the ongoing collaboration of over 100 research laboratories around the world.¹⁷⁸ The TBSGC applies many techniques within the high-throughput pipeline to elucidate, characterize, improve and facilitate the drug discovery progress against the pathogen. As of 2011, the last time the TBSGC reported an update, approximately 250 Mtb protein structures had been deposited in the PDB, accounting for over 33.0 % of the Mtb structures deposited.¹⁷⁹ Most of the 3,989 open reading frames within Mtb have been cloned into the Gateway system (Invitrogen), accelerating the process of recombination into protein expression systems.^{177, 180} Protein expression and purification is achieved in a high-throughput fashion via the Consortium's protein production facility located in Los Alamos National Lab which utilizes robotics, cell-free expression systems, and high-throughput solubility determination assays.¹⁸¹ Protein purification is typically performed through affinity chromatography via the attachment of an N-terminal hexa-histidine tag for subsequent separation and enrichment in a Nickel column. This is in turn followed by crystallization trials which entail the screening of commercially available and proprietary

protein crystallization conditions. Once crystals are obtained, the TBSCG utilizes several high-intensity synchrotron beamlines such as the Advanced Light Source in Stanford or the Advanced Photon Source in Chicago to obtain atomic resolution protein structures.¹⁷⁷

The TBSCG also employs a bioinformatics platform to gather and combine as much relevant data as possible to prioritize targets. Another powerful complementary technique that the TBSCG employs for the elucidation of essential genes is whole-genome sequencing. Whole-genome sequencing can provide valuable insight into gene duplication/loss, gene structure, and conservation amongst species and evolutionary relationships.¹⁸¹ Moreover, when the technique above is coupled to data gathered from Mtb knockout studies (e.g., transposon site hybridization and CRISPR); whole-genome sequencing can potentially accelerate the elucidation of essential genes for Mtb survival *in vivo* and *in vitro*.¹⁸²⁻¹⁸³ Although structural elucidation of Mtb proteins still represents a challenging task, structural data is critical to understand the molecular basis of Mtb drug resistance to a particular drug. The information learned from such structures can then be utilized to perform structure-guided design of compensatory modifications in the drug scaffold to stay ahead of the evolutionary race.¹⁷⁶

2. STRUCTURE-GUIDED DESIGN OF 6-SUBSTITUTED ADENOSINE ANALOGS AS POTENT INHIBITORS OF *MYCOBACTERIUM TUBERCULOSIS* ADENOSINE KINASE

2.1 Background and significance

Mycobacterium tuberculosis (Mtb), the bacterium that causes pulmonary tuberculosis (TB); represents one of the major leading causes of death worldwide by a single infectious agent. One-third of the world's population is thought to harbor latent tb, and around 5-10 % of these infected individuals are expected to develop the active disease sometime during their lifetime.³⁰ The rapid emergence of multi-drug resistant (MDR) and extensively drug-resistant (XDR) tb demands the development of novel chemotherapeutic agents with novel molecular targets.

The purine salvage pathway is an emerging druggable pathway within mycobacteria. In this pathway, preformed nucleobases from the product of nucleic acid breakdown, are converted to their corresponding purine nucleotides by the purine salvage enzymes. Although the *de novo* and purine salvage pathways have not been extensively studied in Mtb, it is known that Mtb possesses all the enzymes required for both pathways. It is currently unknown if there is restrictive regulation of the two pathways. However, by switching to the salvage pathway Mtb can bypass several chemically demanding steps.² This has led to the hypothesis that the salvage pathway might be the most likely source of

nucleotides within the hostile and nutrient-deprived microenvironment encountered by Mtb during its latent phase of infection.¹⁸⁴⁻¹⁸⁵

Mycobacterium tuberculosis adenosine kinase (MtbAdoK) performs a critical step in the purine salvage pathway within mycobacteria. The enzyme catalyzes the conversion of adenosine to adenosine monophosphate in a Mg^{+2} and ATP-dependent manner.¹⁸⁶ The crystal structure of MtbAdoK has been previously solved at high-resolution with the substrate (adenosine), the substrate analog 2-fluoroadenosine, an ATP analog AMP-PCP and without substrate (apo) at resolutions of 1.90 Å, 1.93 Å, 1.90 Å and 1.50 Å, respectively.¹⁸⁷

The crystallographic data showed that the apo and the AMP-PCP structures adopted the opened conformation of the protein. In contrast, the substrate or substrate analog complexes revealed that lid domain of MtbAdoK undergoes a 30° movement upon substrate binding.¹⁸⁸ This conformational change effectively brings lid domain residues Asp12, Phe116, and Phe102 in close contacts with adenosine thereby completing the active site (Figure 2.1a).^{187, 189-191} As previously described, the binding of the ribose and adenine rings are primarily mediated by π -stacking interactions with residues Phe102 and Phe116, respectively (Figure 2.1b). Hydrogen bonding networks with the adenine moiety were described to occur with residues Gln172 (backbone O-N6 distance of 3.26 Å), Gln173 (NE2-N1 distance of 2.99 Å, OE1-N6 distance of 2.96 Å), Ser8 (OG-N3 distance of 2.62 Å) and Ser36' (OG-N7 distance of 2.65 Å, OG-N6 distance of 3.43 Å). The ribose forms extensive hydrogen bonding interactions with residues Gln172 (NE2-O4' distance of 3.26 Å, NE2-O5' distance of 2.62 Å), Asp12 (OD2-O3' distance of 2.70 Å, OD1-O2'

distance of 2.75 Å), Gly48 (backbone N-O3' distance of N 2.99 Å, backbone N-O2' distance of 2.82 Å) Asn52 (ND2-O3' distance of 3.01 Å), and catalytic base Asp257 (OD2-O5' distance of 2.69 Å) (Figure 2.1b).¹⁸⁷

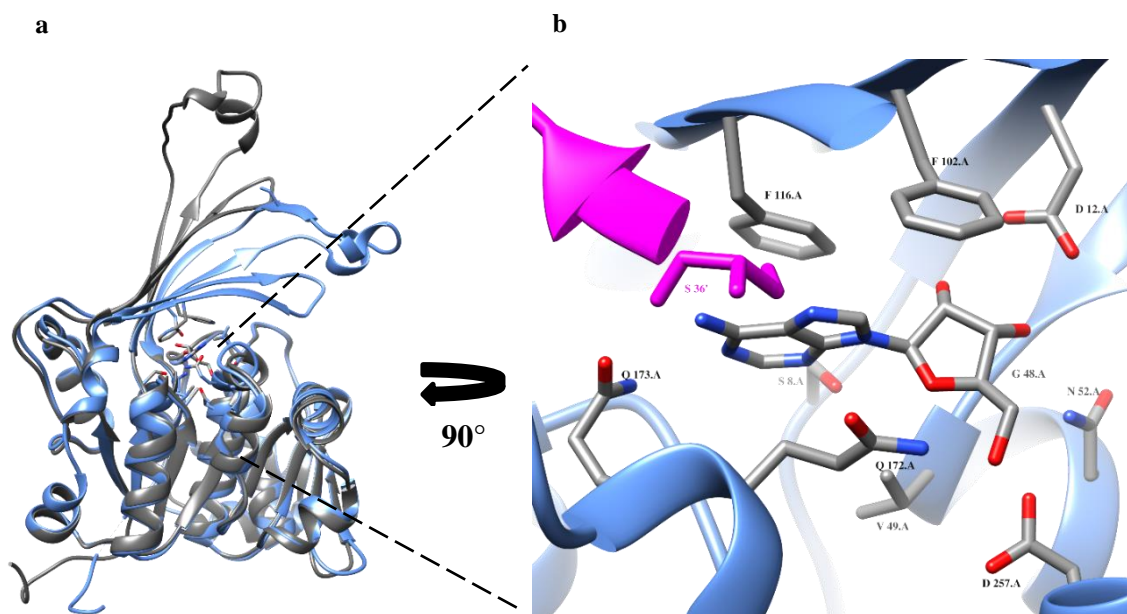


Figure 2.1: MtbAdoK closed and open conformations. (a) Superimposition of the closed (blue, PDB ID 2PKM) and open conformation (gray, PDB ID 2PKF) of MtbAdoK. Only chain A of the dimer is shown. (b) Adenosine bound to the active site of MtbAdoK. Adenosine and residues involved in binding are shown as sticks and labeled with one-letter code and chain identifier. Chain B residues are colored magenta.

MtbAdoK is significantly different when compared to eukaryotic adenosine kinases.¹⁹⁰ Although hAdoK and MtbAdoK are composed of a small-lid like domain and a large domain, hAdoK shares less than 20.0 % sequence identity with MtbAdoK. The human adenosine kinase (hAdoK) structure has been previously solved at 1.4 Å with

substrate bound. The structure was initially solved with two molecules of adenosine embedded within the enzyme, one in the active site and another in cofactor (ATP) site.¹⁹⁰ A critical difference between MtbAdoK and its eukaryotic counterparts is that MtbAdoK is a functional homodimer.¹⁹⁰ In addition, prior to its discovery and characterization by Long et al. in 2003, the *adoK* gene was thought to be unique to eukaryotic organisms and was annotated as a general carbohydrate kinase (*cbhK*) in Mtb.¹⁸⁶ Based on its amino acid sequence, MtbAdoK is more closely related to members of the kinase B family of sugars kinases, which includes ribokinase; a homodimer and the prototypical member of this family.¹⁸⁸

MtbAdoK is essential for the survival of the bacilli when utilizing cholesterol as a carbon source and in infected mouse models.¹⁸²⁻¹⁸³ Even though the precise role of the purine salvage pathway under these conditions is currently unknown, biochemical and structural characterization suggests that MtbAdoK might represent a new class of bacterial adenosine kinases that differs from its eukaryotic counterparts by its unique quaternary structure and regulatory mechanisms. The essentiality and differences with the human adenosine kinase make MtbAdoK an attractive drug target.

To date, most reported inhibitors of MtbAdoK have been designed as substrate surrogates to elicit the production of toxic metabolites.¹⁹²⁻¹⁹⁵ For example, Parker *et al.* showed that the H37Ra Mtb strain was able to uptake the adenosine analog 2-methyl-adenosine and that MtbAdoK was responsible for its activation into the toxic metabolite 2-methyl-AMP.¹⁹⁴ Despite having some advantages, AMP or ATP toxic metabolites could

inadvertently lead to undesirable and cross-species off-target effects exacerbating the identification and diminishing the value of a potential drug target.

In this work, we adopted a structure-guided approach to the design of very potent and safe adenosine analogs. To gain insight into the chemical space surrounding the active site, we have solved the crystal structures of MtbAdoK complexed to several adenosine analogs at resolutions between 1.75-2.36 Å. This initial approach laid the foundation for the structure-guided design and synthesis of several very potent N6-substituted adenosine analogs as selective inhibitors of MtbAdoK. Several of the synthesized compounds displayed low micromolar anti-Mtb activity in a whole-cell assay; which supports the concept that inhibition of MtbAdoK can be used as an approach to treat TB. Finally, the compounds exhibited a higher degree of specificity against MtbAdoK when compared to the human counterpart.

2.2 Materials and methods

2.2.1 Cloning, expression and purification of recombinant MtbAdoK and hAdoK

The WT MtbAdoK gene (*Rv2202c*) was amplified by polymerase chain reaction (PCR) from total genomic DNA of *Mycobacterium tuberculosis* H37Rv. The following oligonucleotides were used: 5'-GGAATTCATATGGTGACGATCGCGGTAACC-3' and 5'-CTTAAGCTTCTAGGCCAGCAC-3', respectively. The amplified DNA fragment was digested with NdeI and HindIII restriction enzymes (New England BioLabs) and sub-cloned into the corresponding restriction sites of the pET28b vector containing an N-terminal TEV cleavable His-tag.¹⁸⁷ The human adenosine kinase gene was PCR amplified from clone HsCD00042641 (DNASU plasmid repository) using the following

oligonucleotides: 5'-GGAATTCCATATGATGACGTCAGTCAGAGAAAATATTC-3' and 5'-CCCAAGCTTCTAGTGGAAGTCTGGC-3' and was cloned into the same pET28b using the same procedures above. In all cases, gene fidelity was confirmed by DNA sequencing, and sequenced plasmids were used to transform *E.coli* BL21 (DE3) cells for protein expression. For protein expression, cell cultures were grown in LB media at 37.0 °C. Cells were induced with 0.5 mM isopropyl β -D-1-thiogalactopyranoside (IPTG) when the cell density reached $A_{600} \sim 0.6$ –1.0. Cell cultures were incubated for 18 h at 18.0 °C before harvesting.

Harvested cells were lysed using a French press, and the lysate was centrifuged at 17,000 rpm for 1 h. Recombinant MtbAdoK and hAdoK were purified by using a HisTrap HP Nickel column (GE Healthcare). Purification buffers A and B contained, 50.0 mM HEPES, pH 7.5, 500.0 mM NaCl, 500.0 mM imidazole (buffer B only), and 5.0 % glycerol. For crystallization studies, MtbAdoK was dialyzed in 20.0 mM HEPES, pH 7.5, 50.0 mM NaCl, 2.0 mM DTT and 5 % glycerol. For enzymatic assays, the proteins were dialyzed in 50.0 mM HEPES, 50.0 mM NaCl, 100.0 mM KCL, 4.0 mM DTT and 20.0 % glycerol. Finally, the proteins were aliquoted and stored in -80.0 °C for subsequent crystallization and enzymatic assays.

2.2.2 Enzymatic assay, IC_{50} determination, steady-state kinetics and K_i determination

Compounds were tested against MtbAdoK using the pyruvate kinase-lactate dehydrogenase coupled assay system in a Cary100 UV-Vis spectrophotometer.¹⁹⁶ The reaction was started by the addition of 60.0 nM of enzyme into a final volume of 200.0 μ L master mix containing 50.0 mM HEPES pH 7.5, 50.0 mM KCl, 6.0 mM MgCl₂ (4.0

mM MgCl₂ for hAdoK), 3.0 mM ATP (2.0 mM ATP for hAdoK), 200.0 μM NADH, 1.0 mM phosphoenolpyruvate, 1.0 mM DTT, 12.0 U/mL pyruvate kinase, 12.0 U/mL lactate dehydrogenase and 15.0 μM adenosine. IC₅₀ values for each compound were determined by varying the concentration of inhibitor at fixed concentrations of enzyme and by fitting the dose-response data into the four-parameter logistic curve (Equation 2.1) model of GraphPad prism 7.02, as follows:

$$Y = Y_{min} + \frac{(Y_{max} - Y_{min})}{(1 + 10^{(\log I C_{50} - I)H})} \quad (2.1)$$

Where I is the logarithm of inhibitor concentration, H is the Hill slope and Y, Y_{max} and Y_{min} are the specific activity, maximum specific activity, and minimum specific activity, respectively. Kinetic assays for MtbAdoK were performed as described above with the following exceptions: the master mix contained 60.0 nM MtbAdoK and the reaction was started by the addition of varying concentrations of adenosine in the presence of constant concentrations of compound (0.0 nM, 20.0 nM, 40.0 nM). Kinetic data were obtained by fitting the initial velocity data into GraphPad Prism 7.02 nonlinear regression function of Michaelis-Menten model (Equation 2.2), as follows:

$$V_o = \frac{(Y_{max})[S]}{(K_m + [S])} \quad (2.2)$$

Where V_o is the initial velocity, Y_{max} is the maximum specific activity, S is the substrate concentration, and K_m is the Michaelis-Menten constant.

Specific activity values for kinetics and IC₅₀ measurements were determined using (Equation 2.3):

$$specific\ activity = \frac{\left(\frac{a}{\varepsilon_{NADH} * b} d\right)}{c} \quad (2.3)$$

Where a is the change in absorbance over time, ϵ_{NADH} is the millimolar extinction coefficient of NADH, b is the pathlength, d is the dilution factor of the enzyme in the assay and c is the concentration of enzyme stock used for the assay.

Finally, the inhibition constant (K_i) was determined by using the Cheng-Prusoff relationship for competitive inhibition (Equation 2.4).¹⁹⁷⁻¹⁹⁸

$$K_i = IC_{50} / \left(\frac{[S]}{K_m + 1} \right) \quad (2.4)$$

In all cases, the compounds were serially diluted in 100.0 % DMSO and added to the respective enzymatic reaction to a final concentration of 2.5 % DMSO.

2.2.3 Crystallization, data collection, and crystal structure determination

Purified MtbAdoK was concentrated to 18.0 mg/mL before crystallization trials. All cocrystals were obtained by vapor diffusion method. MtbAdoK-**2**, **3**, **4** and **NZ637** cocrystals were achieved by mixing 2.0 μL of protein solution, preincubated with 5.0 mM of the compound for 1 h at 25.0 $^{\circ}\text{C}$, with 1.0 μL of 100.0 mM HEPES pH 7.5, 2.0 M ammonium sulfate and 2.0 % PEG 400. MtbAdoK-**5** co-crystals were obtained by mixing 2.0 μL of protein solution, preincubated with 4.0 mM of **5** for 1 h at 25.0 $^{\circ}\text{C}$, with 1.0 μL of 100.0 mM HEPES pH 7.5 and 1.2 M sodium citrate tribasic dihydrate. MtbAdoK-**6** cocrystals were obtained by mixing 2.0 μL of protein solution, preincubated with 4.0 mM of the compound for 1 h at 25.0 $^{\circ}\text{C}$, with 1.0 μL of 5.0 M sodium formate. Finally, MtbAdoK-**17** cocrystals were obtained by mixing 2.0 μL of protein solution, preincubated with 2.0 mM **17** for 1 h at 25.0 $^{\circ}\text{C}$, with 1.0 μL of 100.0 mM Bis-Tris pH 6.5, 2.0 M ammonium sulfate and 2.0 % PEG 400. In all cases, crystals were grown at 20.0 $^{\circ}\text{C}$. Before

data collection; crystals were cryoprotected with Paratone (Hampton Research) and flash frozen in liquid nitrogen. X-ray diffraction data was collected at Argonne's National Lab Advanced Photon Source beamlines 19ID and 23ID. Diffraction data was indexed, scaled and integrated using HKL2000.¹⁹⁹ Initial phases were obtained by molecular replacement in MOLREP using the high-resolution structure of the MtbAdoK-1 complex with PDB accession code 2PKM.²⁰⁰ Refinement was performed in PHENIX followed by iterative runs of inspection and manual modification using coot.²⁰¹⁻²⁰² Ligand model and restraint files were created in ELBOW from the PHENIX suite and fitted into the electron density using COOT. Images and figures were rendered using Molsoft ICM, Chimera and PyMOL.²⁰³⁻²⁰⁵

2.2.4 Antimycobacterial assay

Antitubercular testing and MIC₅₀ determination was performed using the MABA assay in a 96-well format as previously described.²⁰⁶⁻²⁰⁷ Starter culture of Mtb mc²7000 was grown in 7H9 media supplemented with OADC (Middlebrook), 0.5 % dextrose, 0.085 % NaCl, 0.05 % Tyloxapol (Sigma), 0.25 µg/mL malachite green (Sigma) and 25.0 µg/mL pantothenate. Once cells reached an optical density of OD₆₀₀ ~1.5, cells were diluted to an OD₆₀₀ of 0.01 in the same media composition without OADC. Compounds were serially diluted in 100.0 % DMSO and added to the cells to a final concentration of DMSO of 2.5 %. Plates were incubated for ten days before staining with resazurin (Sigma). After staining, plates were incubated for two additional days for developing. Finally, developed plates were read using a POLARstar Omega spectrophotometer (BMG Labtech) and by

monitoring the fluorescence emission of resazurin (excitation = 570 nm, emission = 585 nm). In all cases, rifampicin was used as a negative control.

2.2.5 Human dermal fibroblast cytotoxicity assay

Human dermal fibroblasts (HDF) were purchased from ATCC (Manassas, VA). HDF cells were cultured in DMEM (Lonza) media supplemented with 10.0 % fetal bovine serum albumin (Lonza) and penicillin/streptomycin (Lonza). For the cytotoxicity assay, compound stocks were serially diluted in phosphate buffered saline (PBS) plus 10.0 % DMSO. On the day of assay, HDF cells were trypsinized, counted and resuspended at a concentration of 64,000 cells/ml in media. Cells were plated, overlaid with the compound serial dilutions and incubated at 37.0 °C. After 48 h, resazurin dye was added and the assay plates cultured for another 24 h. The next day the absorbance of the resazurin was measured on a microplate reader to assess cell death. Cytotoxicity was determined as a percent of dead cells versus living.

2.3 Results and discussion

Structural analysis of the MtbAdoK-adenosine (**1**) complex showed a high potential for structure-guided drug design (Figure 2.2).¹⁸⁷ Of particular interest are positions N6 and N7 of the adenine ring and position O5' of the ribose moiety; all of which have been the focal point of several chemistry-based structural activity relationship (SAR) studies.^{192, 208-209} These studies have highlighted that substitutions at the aforementioned positions confer inhibitory activity against MtbAdoK and hAdoK. The chemistry-based efforts have also suggested that there is a higher degree of selectivity against MtbAdoK when substitutions are located at the N6-position when compared to the N7-analogs.

However, the structural and molecular basis for the reported selectivity has remained unexplored. The 5'-position offers a more practical approach towards inhibition given that the critical hydroxyl group is required for catalysis.

To guide our drug discovery efforts and to investigate the molecular basis of selectivity and inhibition we solved the crystal structure complexes of several known AdoK inhibitors. Iodotubercidin (**2**) and sangivamycin (**3**) were selected to investigate the conformational flexibility and the chemical properties surrounding the binding pocket near the N7-position of the adenosine scaffold. Additionally, 6-methylmercaptapurine riboside (**4**) and 5'-aminoadenosine (**5**) cocrystal structures were solved to explore the 6- and 5'-positions of the adenosine scaffold, respectively (Figures 2.2-2.3).

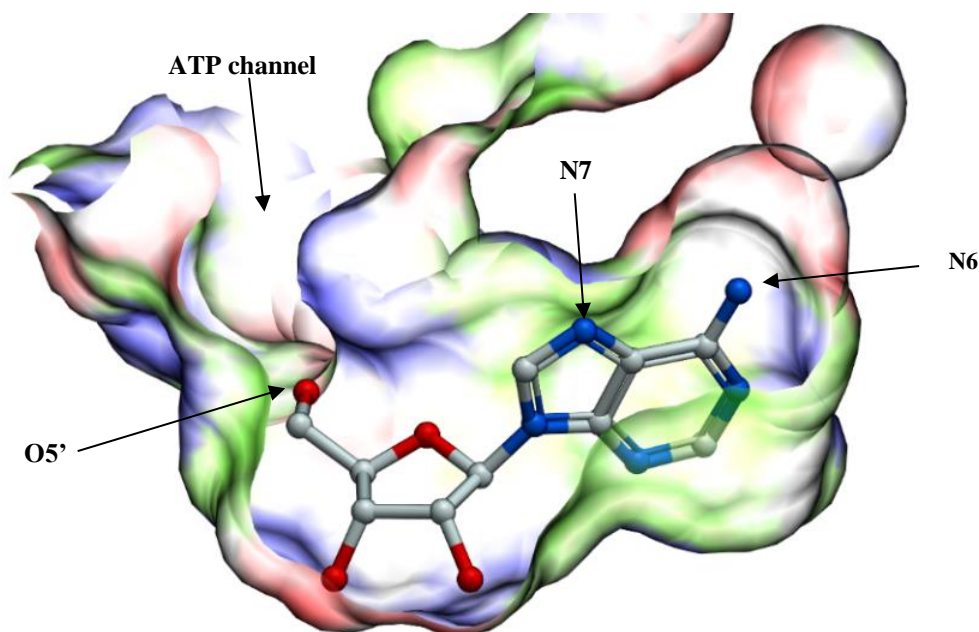


Figure 2.2: Active site pocket of MtbAdoK. Positions of interest for structure-based drug design are highlighted.

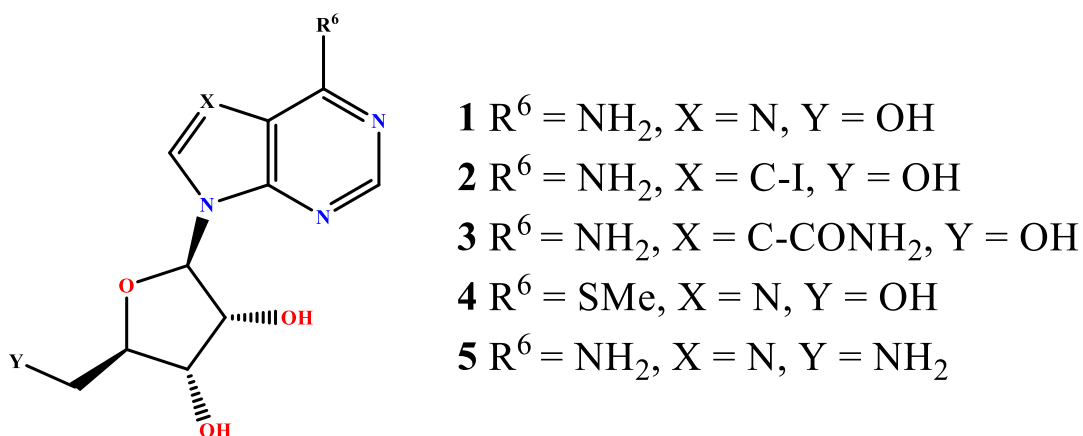


Figure 2.3: Tool compounds for crystallography studies.

Our structural studies commenced with the cocrystallization of the N7-substituted analogs. Iodotubercidin, possesses an iodine group at position 7 and is a semi-synthetic derivative of the natural compound tubercidin whereas sangivamycin is a natural compound derived from *Streptomyces rimosus* and contains an amino group at position 7.^{192, 210-211} Compound **2** has been noted to be a general kinase inhibitor, displaying inhibitory activity against MtbAdoK, hAdoK, MAP kinases, and Ser/Thr kinases while compound **3** has been previously observed to be an inhibitor of protein kinase C, MtbAdoK, and hAdoK.^{192, 212}

Cocrystallization of MtbAdoK with compounds **2** and **3** was produced via vapor diffusion, and the structures were solved using the molecular replacement method (MR) utilizing the previously reported adenosine-bound structure.¹⁸⁷ The crystals of both complexes were determined to be in the $P4_1$ crystal space group with two molecules in the asymmetric unit (ASU). The MtbAdoK-**2** complex was refined to 1.95 Å resolution and

displayed a closed conformation of the enzyme with a backbone rmsd of 1.49 Å amongst all C α atoms when superimposed to the MtbAdoK-adenosine structure (Figure 2.4). The MtbAdoK-**3** complex refined to 1.95 Å resolution displayed a closed conformation of the enzyme with a backbone rmsd of 1.46 Å amongst all C α atoms when superimposed to the MtbAdoK-adenosine structure (Figure 2.5). As in the case of the hAdoK-adenosine structure, both crystal structures showed positive density for the inhibitor bound to the active site in a similar position to adenosine and density in the cofactor (ATP) binding site. However, only compound **2** displayed full electron density in the ATP binding site while compound **3** displayed partial density for the adenine ring only.

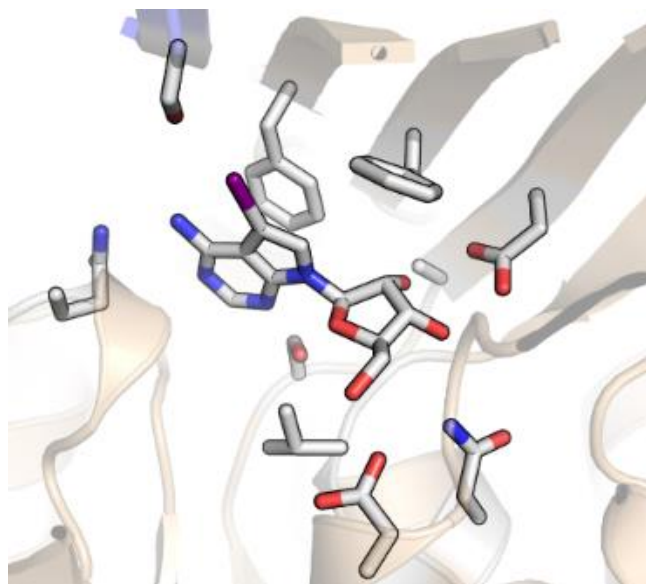


Figure 2.4: Compound **2** bound to the active site of MtbAdoK.

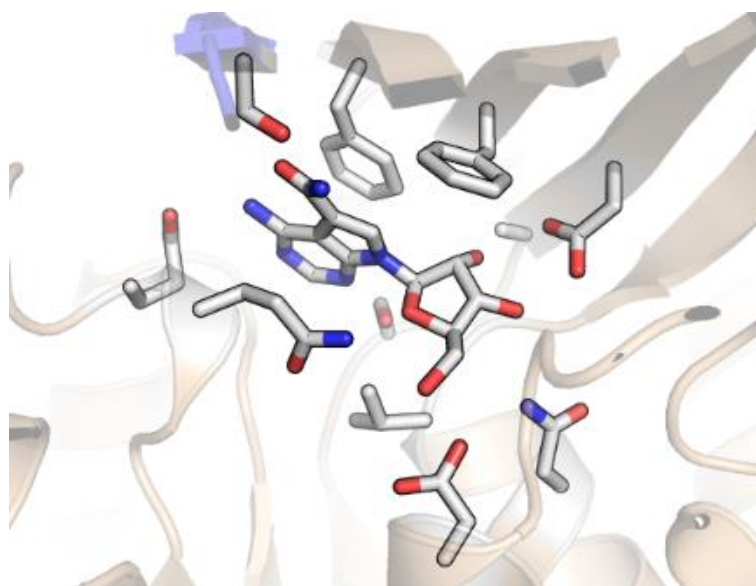


Figure 2.5: Compound **3** bound to the active site of MtbAdoK.

Overall the crystal structures of compounds **2** and **3** displayed many similarities with the previously reported MtbAdoK-adenosine complex. The inhibitors were bound in the same conformation and locations as we observed in the adenosine-bound structure. Residues Phe116 and Phe102 were involved in π -stacking interactions with the adenine and ribose rings, respectively. The ribose moiety was found to be stabilized by hydrogen bonding with several residues. Asp12 oxygen OD1 H-bonds with the O2' and O3' of ribose, OD2 of catalytic base Asp257 H-bonds with O5', ND2 of Asn52 H-bonds with O3', and backbone N of Gly48 H-bonds O2'; all of which are likely to contribute significantly to the binding affinity.

The most notable differences between the cocrystal structures of adenosine, **2** and **3** were observed in the interactions formed by residues Gln172, Gln173, and Ser36'. In

the adenosine bound structure, Gln172 NE2 H-bonds with O5' (2.62 Å) and O4' (3.26 Å) while backbone O of Gln172 H-bonds with N6 (3.26 Å). In contrast, in the MtbAdoK-3 complex, NE2 of Gln172 formed longer H-bonds with O5' (3.03 Å) and O4' (3.10 Å). Unexpectedly, interactions formed by residue Gln172 were not observed in the MtbAdoK-2 complex. A similar scenario was seen for Gln173. In the MtbAdoK-1 structure, NE2 of Gln173 H-bonds with N1 (2.99 Å) while OE1 of Gln173 H-bonds with N6 (2.97 Å) of the adenine scaffold. On the other hand, as observed in the MtbAdoK-3 and MtbAdoK-2 binary complexes, Gln173 only formed H-bonds with N6 with distances of 3.26 Å (OE1-N6) and 2.98 Å (OE1-N6), respectively.

The crystal structures of compounds **2** and **3** showed that the iodine group of **2** and the amide group of **3** was oriented towards Ser36'. One critical aspect of MtbAdoK, being a homodimer, is that residues from one chain complete the active of the other. It has been previously shown that Ser36 from chain B completes the active site of chain A and vice versa by hydrogen bonding with positions N6 (OG-N6 distance of 3.43 Å) and N7 (OG-N7 distance of 2.65 Å) of the adenine ring.¹⁸⁷ Ser36 residue forms part of the lid-domain of MtbAdoK, and as reported before, the dimerization interface of MtbAdoK occurs via extensive van der Waal (VDW) contacts formed by the lid-domain of each chain.¹⁸⁷ The observed orientation of both N7-substituted adenosine analogs (**2-3**) suggests that the N7-position is obstructed by chain B. That is, chain B represents an imposing physical barrier at this position thereby limiting drug discovery efforts to the active site of the enzyme (Figures 2.6-2.7).

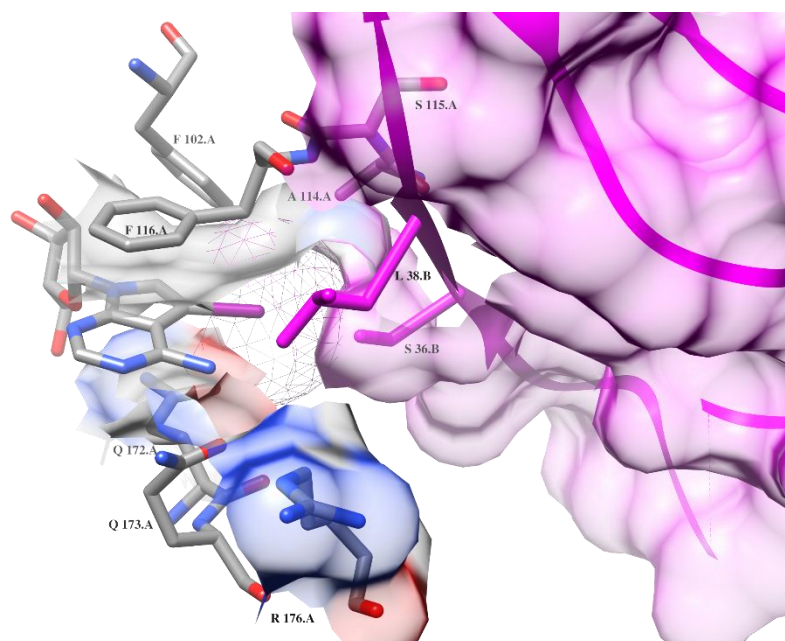


Figure 2.6: The iodine of **2** is physically occluded by chain B (magenta).

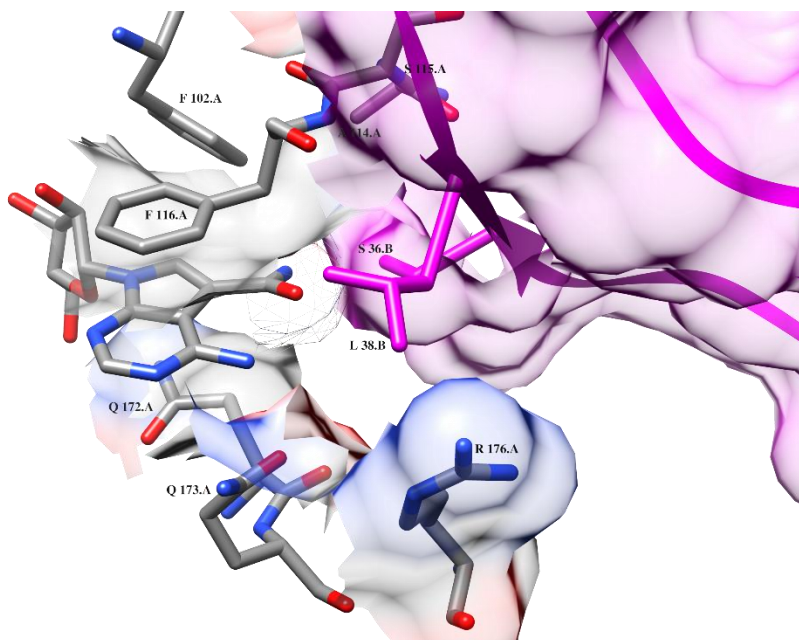


Figure 2.7: The amide of **3** is physically occluded by chain B (magenta).

The MtbAdoK-**3** structure showed that the -NH₂ of the amide group of **3** formed a H-bond with OG of Ser36' (2.82 Å). In contrast, H-bond interactions mediated by Ser36' with compound **2** were not observed in the MtbAdoK-**2** complex. Instead, the interaction is of VDW nature with OG-I distance of 3.00 Å. Finally, the N7-substituents of **2** and **3** were observed to be buried in a pocket formed by several conserved active site residues of MtbAdoK including Phe102 (Cys123 hAdoK) and Phe116 (Phe170 hAdoK).

Overall, structural analysis of the N7-analogs (compounds **2-3**) suggested that bulky substitutions at the N7-position are likely to be favorably accommodated in the active site (Figures 2.6-2.7). Our structural findings go well in accordance with previously reported chemistry-based SAR efforts focused on N7-substituted adenosine analogs; where Snášel et al. reported that several N7-anthracene or N7-phenanthrene derivatives displayed high potency against the enzyme.²⁰⁹ The same group synthesized several N7-chain-extended bulky groups that displayed low potency against the enzyme more than likely due to occlusion by chain B; further validating our structural assessment.²⁰⁹ The bulky iodine group of **2** is observed to be completely buried in a pocket formed by residues Phe116, Phe102, Gln172, Gln173, Ala114, Ser115, Leu38' and Ser36' leading to several polar and VDW interactions (Figure 2.6). In contrast, the amide group of **3** occupies a smaller portion of the pocket (Figure 2.7). We also observed that the amide group of **3** participates in many of the conserved H-bond interactions (Gln172 with O5' and O4', Gln173 with N6 and Ser36' with N6) when compared to the MtbAdoK-adenosine complex. In contrast, the bulky iodine group of **2** sterically hinders many of the conserved interactions described in the MtbAdoK-adenosine complex. Including all the H-bonds

formed by Gln172 and Ser36' (Gln172 with O5', O4' and N6 and Ser36' with N6 and N7) and the H-bond between Gln173 and N1. Our enzymatic assay showed that compound **2** is more potent than compound **3** displaying a 50 % inhibitory concentrations (IC_{50}) of 1.2 μ M and 16.5 μ M, respectively; further validating our structural assessment. Finally, the crystal structure complexes of the N7 analogs revealed the presence of a “chimney-like” cavity above the N6-position that extends towards chain B and that is formed by residues from both chains of the MtbAdoK homodimer thereby representing a unique structural feature of MtbAdoK for structure-guided drug design (Figure 2.8).

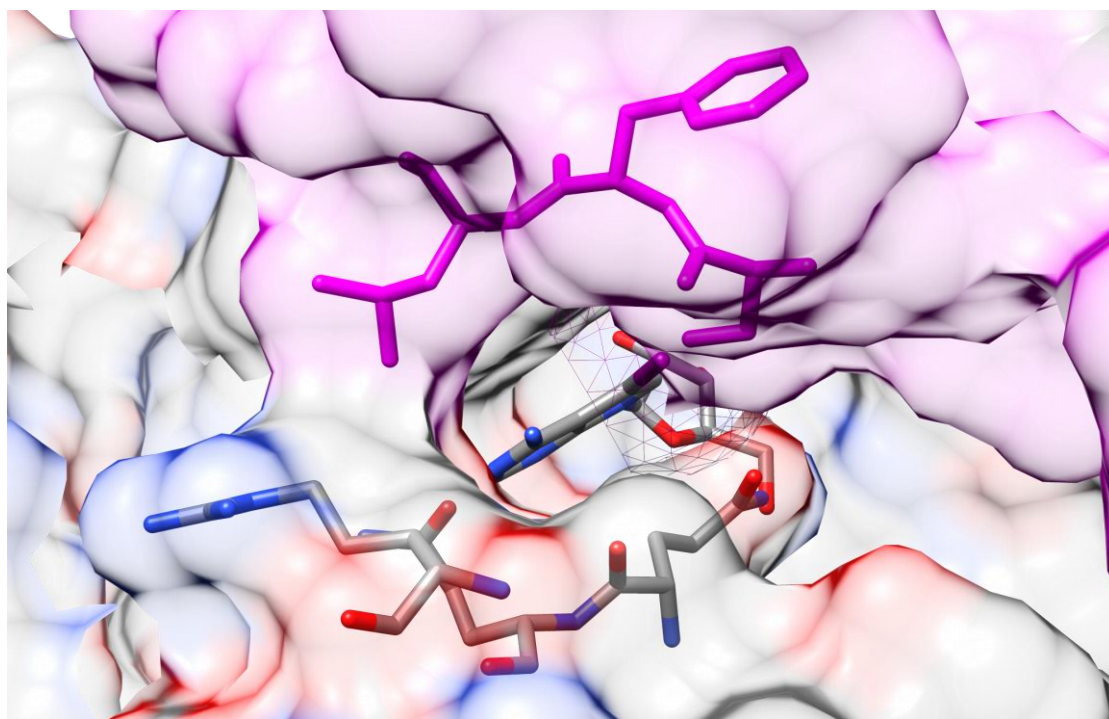


Figure 2.8: “Chimney-like” cavity observed above position N6- of the adenine ring. Chain B is colored magenta.

Next, we decided to explore the chemical space surrounding the binding pocket near the N6-position by cocrystallizing MtbAdoK with 6-methylmercaptapurine riboside. Compound **4** is a derivative of mercaptopurine, a drug used to treat acute lymphatic leukemia and possess a methylmercapto group at the N6-position of the adenosine scaffold. The binary complex of MtbAdoK-**4** was refined to 1.99 Å resolution with two molecules in the ASU in the P4₁ crystal space group (Figure 2.9). Like the cocrystals structures of **2** and **3**, the MtbAdoK-**4** binary complex displayed a closed conformation of the enzyme with a backbone rmsd of 1.65 Å amongst all C α atoms when compared to the MtbAdoK-**1** complex. Positive density was observed as well for a molecule of **4** bound to the ATP site. As in the case of the MtbAdoK-**3** structure, we were only able to model the adenine moiety due to the absence of density of the ribose.

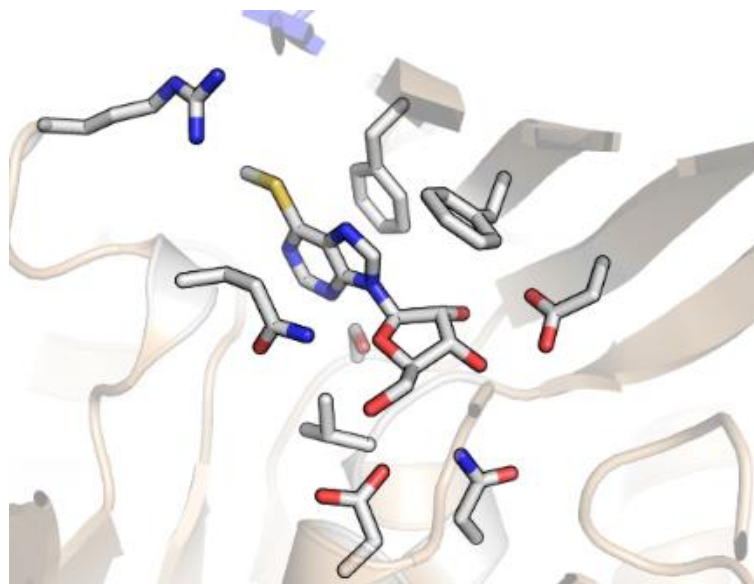


Figure 2.9: Compound **4** bound to the active site of MtbAdoK.

The MtbAdoK-**4** structure was very similar to the structures of compounds **2** and **3** and the MtbAdoK-adenosine structure. The aforementioned binding interactions formed by residues Phe102, Phe116, Asp12, Asp257, Ser8, Asn52, Gly48, and Val49 were maintained. The most notable differences were found with residues Gln173 and Ser36'. Foremost, the critical H-bonds formed by NE2 and OE1 of Gln173 with N1 and N6 of compound **4** were not observed. Also, the H-bonds formed by OG of Ser36' with N6 and N7 of compound **4** were not observed in the cocrystal structure. The lack of interactions with residues Ser36' and Gln173 can be attributed to steric shielding by the methylmercapto group of **4**. Detailed inspection of the binary complex revealed that the thiomethyl group of **4** was oriented towards a pocket formed by residues Gln173, Gln172, Met121, Phe116, Arg176, Leu38' and Ser36' (Figure 2.10).

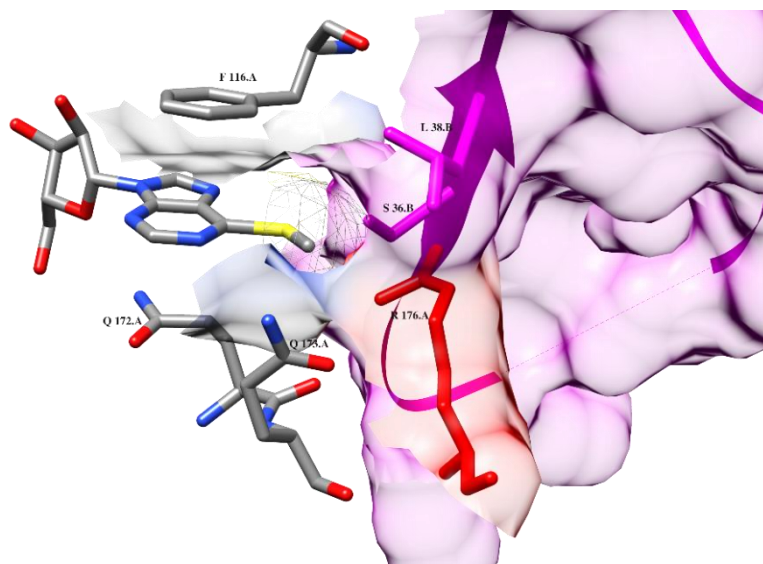


Figure 2.10: The methylmercapto group of **4** is accommodated in a new compound-induced pocket formed by Arg176 (red).

Arg176 was observed to be oriented towards the solvent in the MtbAdoK-adenosine and the crystals structures of compounds **2** and **3** (Figures 2.6-2.7). However, the MtbAdoK-**4** structure revealed that Arg176 had clear electron density for the side chain oriented towards the methylmercapto of **4**. The reorientation of Arg176 led to the formation of a new compound-induced pocket between residues Phe116, Gln172, Gln173, Arg176, Leu38' and Ser36'. Consequently leading to extensive VDW and polar interactions between the aforementioned residues and the methylmercapto group (Figure 2.10). Moreover, the compound-induced movement of Arg176 closed the “chimney-like” cavity we saw in the cocrystal structures of compounds **2** and **3** indicating that residues surrounding the N6-position are flexible (Figure 2.11).

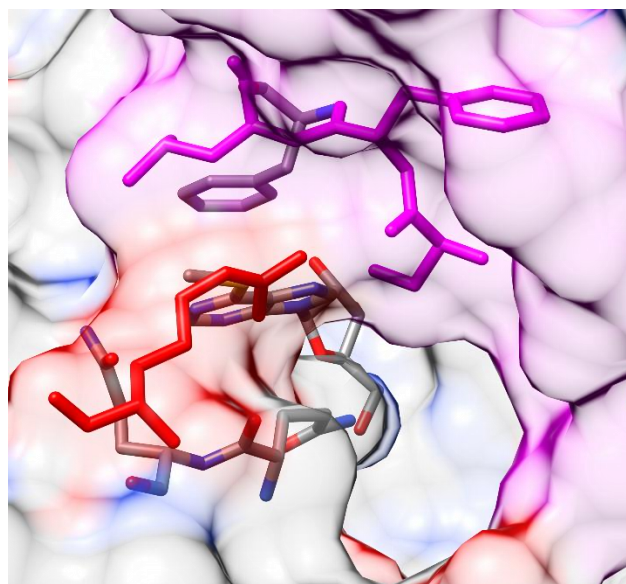


Figure 2.11: The “chimney-like” cavity we observed in the crystal structure of **2** is observed to be closed in the MtbAdoK-**4** complex due to the conformational movement of Arg176.

The orientation and proximity (4.2 Å) of the cationic CZ of Arg176 with respect to the sulfur atom of the methylmercapto group suggests the possibility of cation-polar interactions. Finally, it should be noted that the methylmercapto group seemed to occupy a small portion of the pocket, indicating that bulky groups might be good candidates to further improve contacts at the N6-position.

Just like compound **2**, compound **4** displayed good potency (IC₅₀ of 2.3 μM) in our enzymatic assay. The similar potencies can be attributed to the similar VDW and polar contacts formed by the substituents within their respective pockets. Although these two inhibitors have substitutions at different positions within the adenine ring, their mode of interaction with the protein is similar. That is to say, both substitutions prevented H-bonds with positions N1, N6, and N7 of the adenine moiety. Our structure-guided SAR studies revealed that the iodine group of **2** sterically hinders the interactions with the adenine atoms mentioned above and that are formed by residues Ser36', Gln172, and Gln173. In contrast, the methylmercapto group of **4** not only sterically blocked the aforementioned interactions but also was accommodated in a new compound-induced pocket that comprised in part by residues from both chains of the MtbAdoK homodimer (Gln173, Gln172, Met121, Phe116, Arg176, Leu38' and Ser36'). It should be noted that compound **2** has been reported to be a very potent inhibitor of hAdoK (K_{ihAdoK} ~ 30 nM and K_{iMtbAdoK} ~ 210 nM).¹⁸⁶ The different degrees of potencies can be attributed to the way the **2** interacts with the enzymes. In our MtbAdoK-**2** complex, the compound is shown to be partially solvent exposed due to the presence the “chimney-like” cavity. In contrast, the previously solved hAdoK-**2** structure shows that the compound is completely buried within the

hAdoK monomer due to a unique latch-like region of hAdoK comprised by residues 23-57 of the enzyme's lid-domain (Figure 2.12).²¹³ In addition, the lack of selectivity of compound **2** can be attributed to the fact that the compound is buried within several conserved residues located in the active site. Overall the N7 vs. N6 substituents, exemplified by compounds **2-3** and **4**, seemed to be accommodated in mutually exclusive pockets. The N7 pocket is formed by several conserved active site residues while the N6 pocket is compound-induced and formed by unique MtbAdoK residues Gln172, Gln173, Ser36' Leu38' and flexible Arg176.

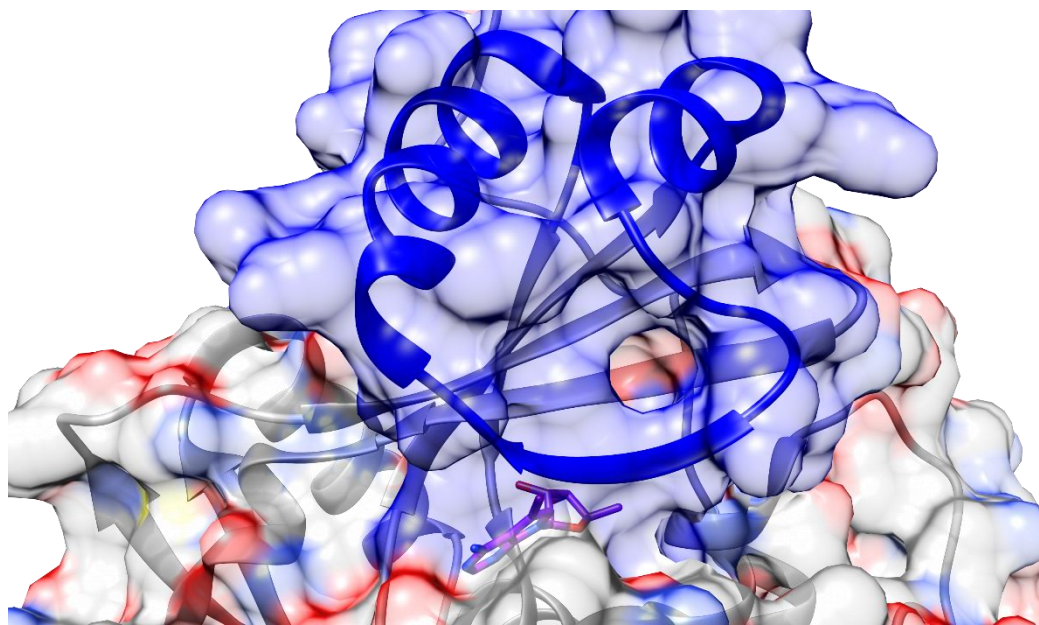


Figure 2.12: hAdoK in complex with compound **2** (PDB ID 2i6a). **2** (purple) is completely buried within hAdoK due to the latch-like region (blue) of the lid domain.

Finally, to explore the potential for modifying the 5'-position and to evaluate if the ATP channel can be utilized as a viable route for drug design, we solved the crystal structure of 5'-aminoadenosine bound to MtbAdoK (Figure 2.13). As in the case of the compounds described above, compound **5** has been previously shown to possess inhibitory activity against AdoKs.²⁰⁸ The MtbAdoK-**5** cocrystal was obtained in the same condition as the reported adenosine-bound structure and was refined to 1.75 Å resolution in the P3₁2₁ crystal space group with one molecule in the ASU. The binary complex displayed a closed conformation of the enzyme with a backbone rmsd of 0.27 Å amongst all C α backbone atoms when compared to the MtbAdoK-adenosine complex, and the inhibitor was bound in a very similar fashion as adenosine (Figure 2.14). Unlike, the cocrystal structures of **2**, **3** and **4**; the MtbAdoK-**5** structure had no density for a molecule of **5** bound to the ATP site. The interactions observed between **5** and MtbAdoK were remarkably similar to those previously described in the adenosine-bound complex.¹⁸⁷ Indeed, the main difference was the interaction formed by the 5'-NH₂; displaying a H-bond with OD2 of Asp257 (2.69 Å). Here, the enzymatic inhibition (IC₅₀ of 8.0 μM) is attributed to the absence of the hydroxyl group that is required for catalysis.

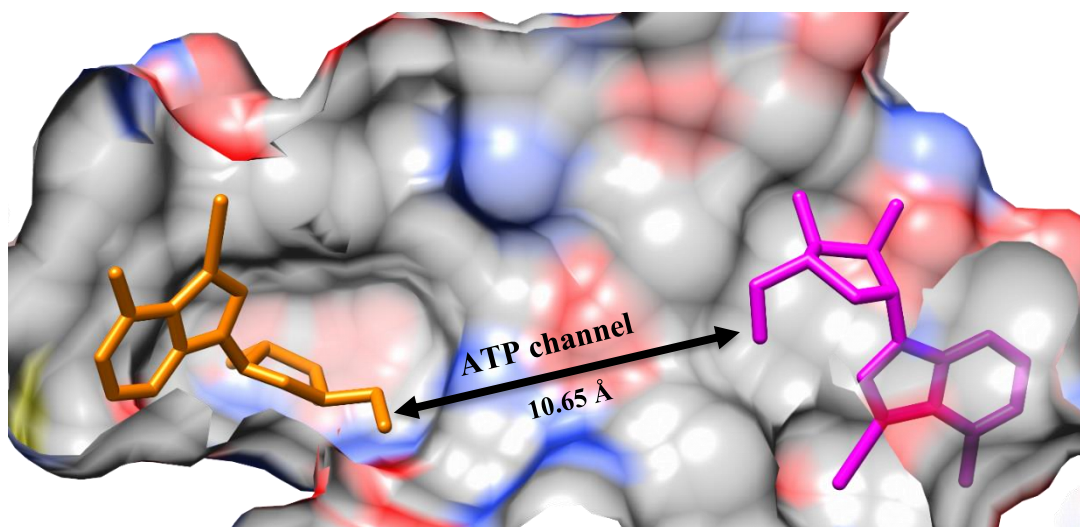


Figure 2.13: MtbAdoK-2 structure showing the relative position of the iodotubercidin bound to the active site (orange) to that bound to the ATP site (magenta). The orientation and proximity of the molecules suggest that bisubstrate-like inhibitors might take advantage of both binding sites.

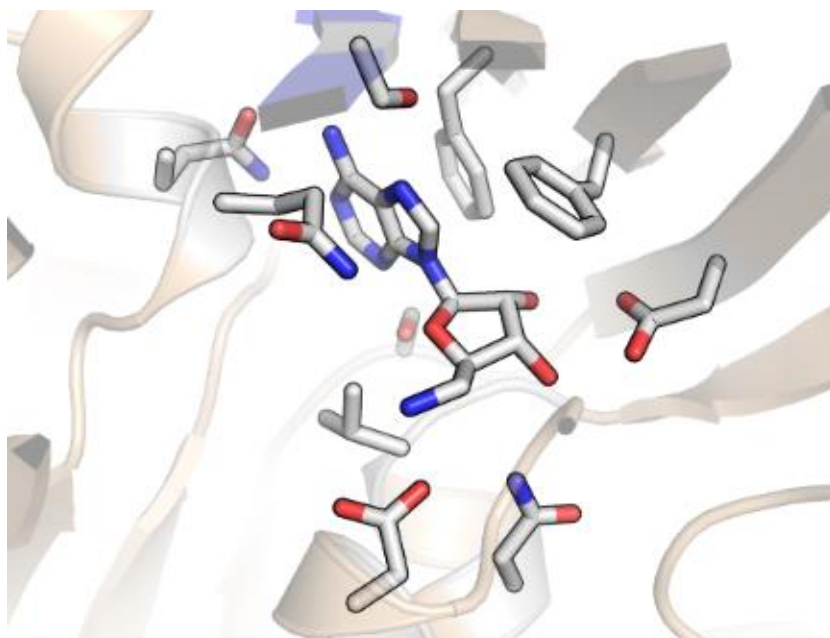


Figure 2.14: Compound 5 bound to the active site of MtbAdoK.

Based on the preliminary structure-guided SAR efforts with compounds **2-5**, we screened Merck's focused library of ~ 140 nucleoside analogs with substitutions at N6, N7 and/or 5' positions. The very potent compound identified in this screen (compound **6**, IC₅₀ of 196.5 ± 20.3 nM) had bulky thiophene group at position N6; validating the pharmacological relevance of N6-substituted analogs (Figure 2.15a). To investigate the structural basis of the ~ 10 X increase in potency when compared to compounds **2** and **4** and to advance our structure-guided drug discovery efforts we crystallized the MtbAdoK-**6** binary complex. The cocrystal structure of compound **6** was solved by MR and refined to a resolution of 2.10 Å in the P2₁2₁2₁ crystal space group with 2 molecules in the ASU (Figure 2.15b). As observed in the structures described above, the MtbAdoK-**6** complex displayed a closed conformation with a backbone of 2.18 Å amongst all C α atoms when compared to the MtbAdoK-**1** structure with the compound. Unlike the structures of compounds **2-5**, the MtbAdoK-**6** complex revealed that the compound binds in a different orientation with respect to adenosine (Figure 2.15c). As in the case of the crystal structure complexes of compounds **2**, **3**, and **4**; the MtbAdoK-**6** structure showed electron density in the active site and the ATP site.

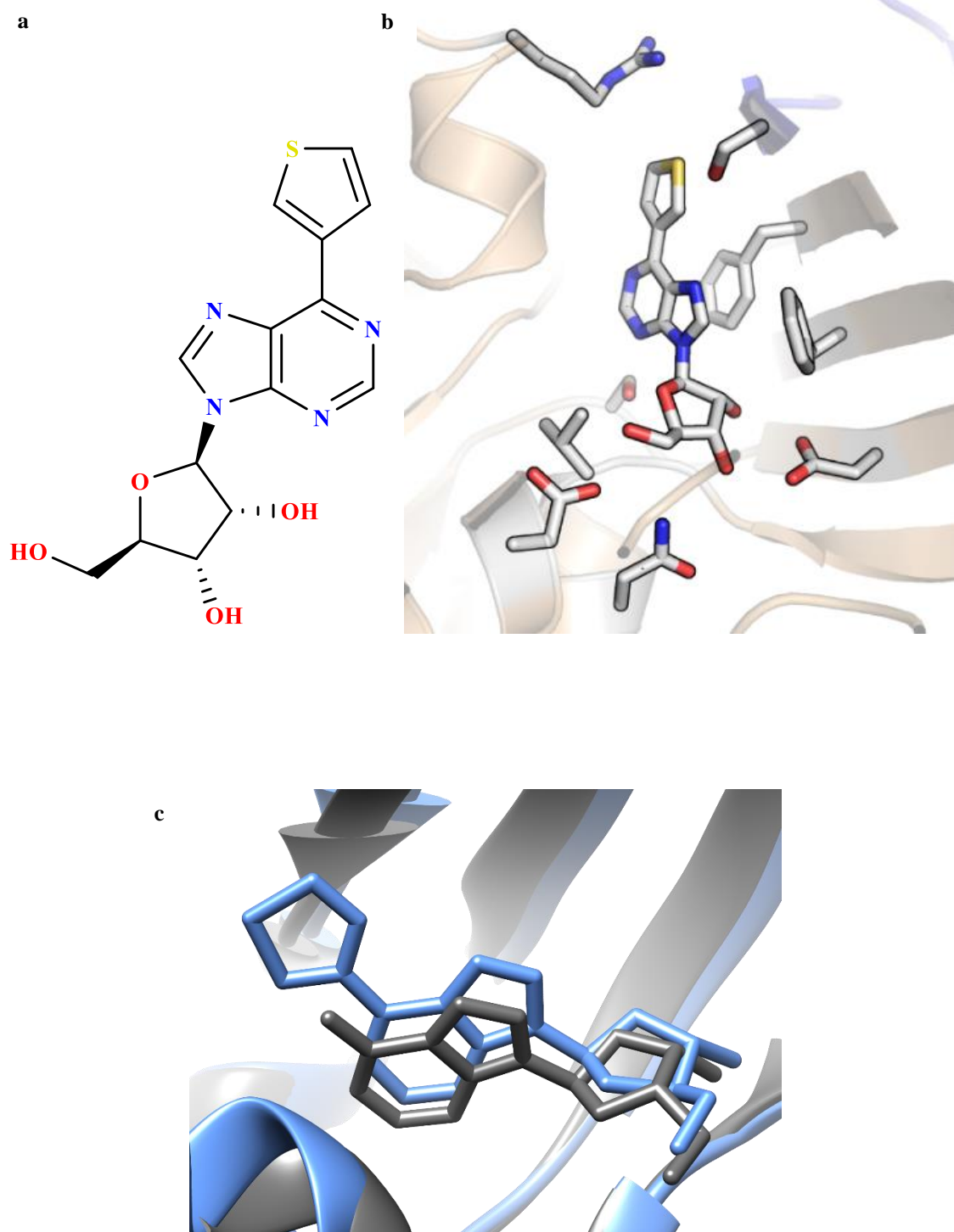


Figure 2.15: (a) Chemical structure of **6**, (b) compound **6** bound to the active site of MtbAdoK and (c) superimposition of the crystal structures of **4** and **6**.

The cocrystal structure of compound **6** showed that the interactions formed by residues Phe116, Phe102, Ser8, Asp12, Asn52, Asp257, Gly48 are maintained. The significant differences were found once more with residues Gln172, Gln173 and Ser36'. In fact, none of the H-bond interactions formed between Gln172 (with O4', O5' and N6), Gln173 (with N1 and N6) and Ser36' (with N6 and N7) were observed. Instead, these residues were involved in weaker VDW interactions with the adenine ring and ribose rings. Unique contacts were formed by the thiophene moiety. This group was observed to be completely buried within the newly identified and compound-induced pocket that is formed by residues Phe102, Phe116, Gln172, Gln173, Arg176, Ser36', Leu38' and Phe37' (Figure 2.16). Closer inspection of the pocket showed that Arg176 reorients once more to accommodate the bulkier thiophene group validating the plasticity of this residue. Furthermore, the orientation of the aromatic thiophene ring with respect to Phe116 suggests the possibility of parallel-displaced π -stacking interactions while the orientation of cationic CZ of Arg176 with respect to the sulfur atom of the thiophene group (CZ-S distance of 4.03 Å) suggests the possibility of T-shaped stacking interactions. In general, the extensive VDW interactions within the pocket coupled to the stacking interactions are the most likely molecular source behind the significant increase in potency of **6** when compared to compounds **2** and **4**. Finally, the orientation of Arg176, when compared the MtbAdoK-4 structure, suggested that the "chimney-like" cavity we observed in the crystal structure complexes might be accessible if larger substitutions are utilized to persuade Arg176 to give access into cavity (Figure 2.17).

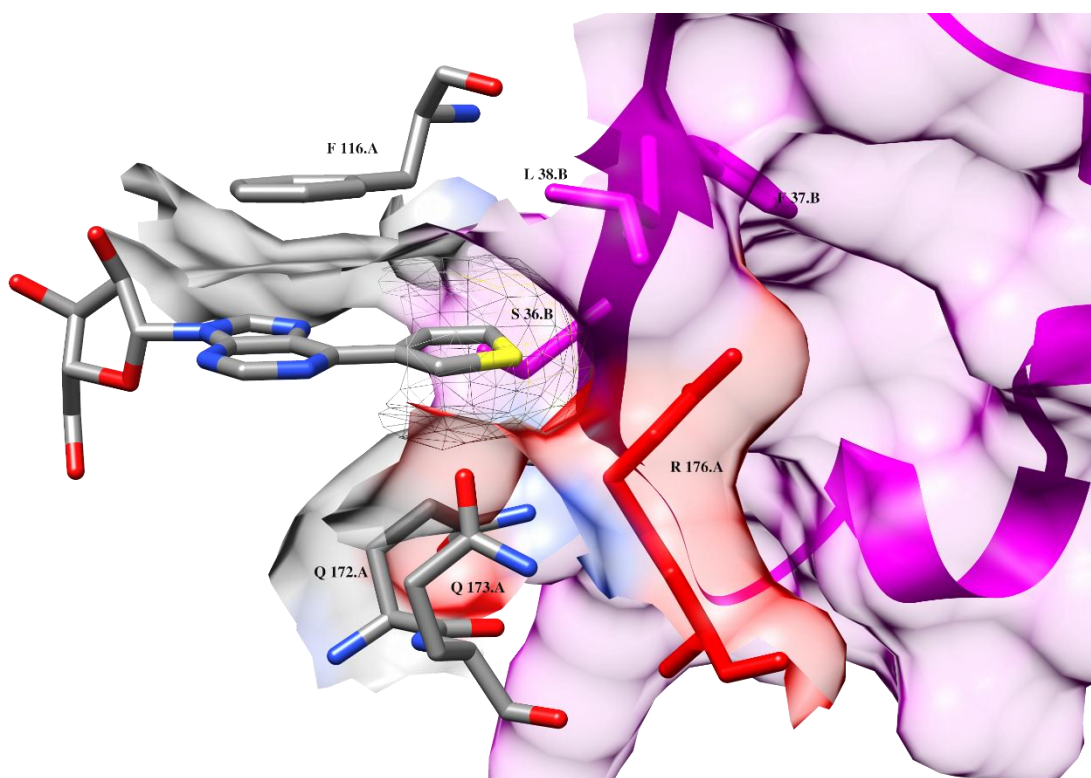


Figure 2.16: The thiophene of **6** is buried in the compound-induced cavity formed by Arg176 and residues from chain B (magenta).

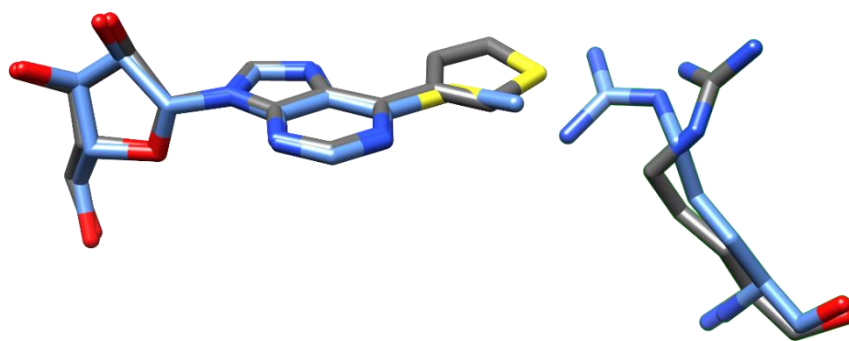


Figure 2.17: Superimposition of the cocrystal structures of **4** (blue) and **6** (gray) showed that Arg176 moves to accommodate the larger thiophene group of **6**.

To further characterize compound **6**, we determined the antimycobacterial and cytotoxic profile of the compound. The antimycobacterial assay with compound **6** showed a 50 % minimum inhibitory concentration (MIC₅₀) of 25.6 ± 2.4 μM with a 50 % cytotoxic concentration (CC₅₀) > 100 μM against HDF cells. Indicating that, in general, N6-substituted adenosine analogs might show selectivity against MtbAdoK over the human counterpart.

Overall, the structure-based SAR efforts showed that the N6, N7, and 5' positions are indeed conducive to inhibition of the MtbAdoK enzyme through different molecular and structural means. The 5'-position provides a mechanistic approach to inhibition by taking advantage of the critical hydroxyl group required for catalysis and provides a platform to design inhibitors that might take advantage of the ATP channel. The crystal structures of the N7 and N6 substituted adenosine analogs showed that the substitutions sterically hindered conserved H-bonds formed by residues Gln172, Gln173 and Ser36' with key positions N1, N6 and N7 of the adenine ring; all of which have been noted to be critical for substrate binding and recognition for human, rabbit and *T. gondii* adenosine kinase.¹⁸⁸ The crystal structures of the N7-substituted analogs (**2-3**) revealed the presence of a “chimney-like” cavity that extends above the N6-position and that is formed by the MtbAdoK homodimer. However, the MtbAdoK-**4** complex showed that the cavity is closed by a conformational movement of Arg176 to interact with the N6-substituent of compound **4** thereby forming a new and compound-induced pocket. Identification of the very potent compound **6** revealed that the bulky aromatic thiophene group is not only

completely buried within the newly identified pocket but also suggested that bulkier substitutions could open back up the “chimney-like” cavity.

Despite offering inhibitory activity against MtbAdoK, the N7-substituents were observed to be buried in a pocket that is formed by several conserved active site residues and that the substituent itself is physically blocked by the dimerization event of MtbAdoK. Consequently, limiting medicinal chemistry efforts to the conserved active site. In contrast, the N6-position offers a better route for structure-guided drug design by providing the possibility of exploiting many contacts formed by the unique oligomerization state of MtbAdoK. In addition, it is possible that the presence of this cavity is the structural basis behind the reported higher degree of specificity conferred by N6-substituted analogs when compared to hAdoK.¹⁹² Taken together, we hypothesized that chain extension via bulky substitutions at the N6-position might trigger a conformational change of Arg176 thereby opening the “chimney-like” thus providing a unique route to increase potency and selectivity.

We next set out to synthesize a series of N6-substituted adenosine analogs. Synthesis of the novel N6-adenosine analogs (**7–18**) are shown in Figure 2.18. Starting from the known 6-chloro-9*H*-purine **A1** and TBS protected **A2**, 4-biphenyl and 4-Br-phenylpiperazinyl moieties were introduced by substitution in EtOH to afford **B1** and **B2** that was converted to variety of 4-arylphenyl (R) piperazine by using different arylboronic acids followed by removal of acetonide with/without TBS group gave the triol adenosines, **7, 9, 10, 12, 13, 14, 16** and **18** respectively.²¹⁴⁻²¹⁵

The cyclopentane **15** was directly synthesized from (*1R,2S,3R,5R*)-3-(6-chloro-9*H*-purin-9-yl)-5-(hydroxymethyl)cyclopentane-1,2-diol **A3** without alcohol protection.²¹⁶ C-C bond at 6-position of purine was formed by Suzuki-Miyaura or Sonogashira cross-coupling to lead to alkyne analogs **11** and **17**. To the tri-acetyl protected 7-Cl-imidazopyridine **A4**, C-N coupling in the presence of 2nd generation RuPhos precatalyst proceeded smoothly and global deprotection of acetyl groups by ammonium hydroxide gave the triol **8** (Figure 2.18).²¹⁷

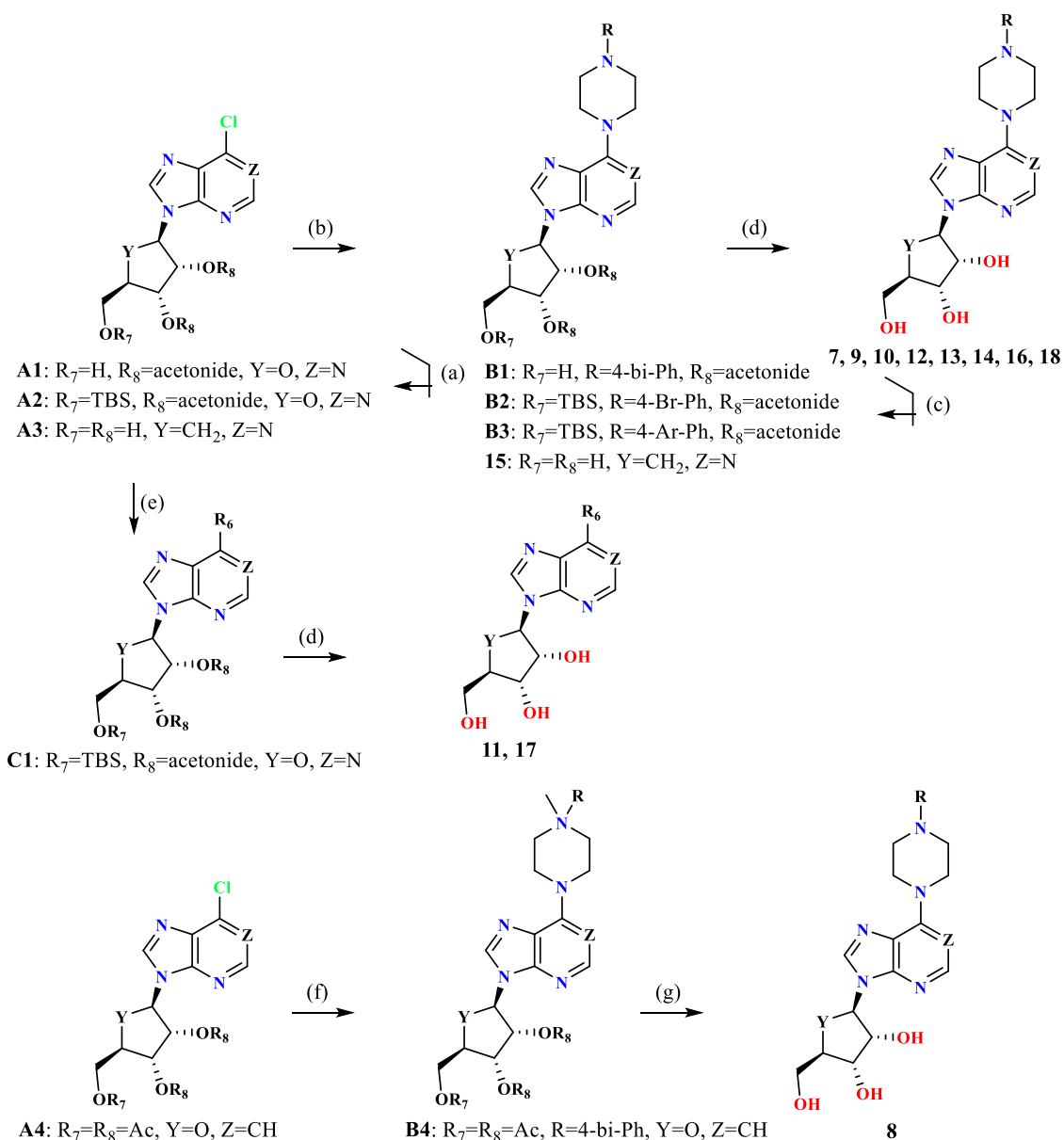


Figure 2.18: Reagents and conditions for chemical synthesis. (a) TBSCl, imidazole, DCM, 15 °C, 17 h, 99% (b) 1-([1,1'-biphenyl]-4-yl)piperazine or 1-(4-bromophenyl)piperazine, DIEA, EtOH, 70–80 °C, 17 h, 13–90% (c) $\text{ArB}(\text{OH})_2$, K_3PO_4 , 2nd generation XPhos precatalyst, THF/ H_2O , 70 °C, 17 h, 49–87% (d) TFA, THF/ H_2O , 15–25 °C, 2–17 h, 13–67% (e) 4,4,5,5-tetramethyl-2-(4-(phenylethynyl)phenyl)-1,3,2-dioxaborolane, K_3PO_4 , XPhos Pd G2, THF, 70 °C, 12 h, 95% or 4-ethynyl-1,1'-biphenyl, Cs_2CO_3 , CuI, 2nd generation XPhos precatalyst, CH_3CN , 90 °C, 17 h, 27% (f) 1-([1,1'-biphenyl]-4-yl)piperazine, Cs_2CO_3 , 1-([1,1'-biphenyl]-4-yl)piperazine, 2nd generation RuPhos precatalyst, *tert*-Amyl-OH, 100 °C, 17 h, 50% (g) NH_4OH , MeOH, 15 °C, 24 h, 21%.

All of the synthesized adenosine analogs were characterized enzymatically against MtbAdoK and hAdoK. The compounds were also tested against Mtb and HDF cells to profile their antimycobacterial and cytotoxic properties, respectively (Figures 2.19, 2.20 and Table 2.1).

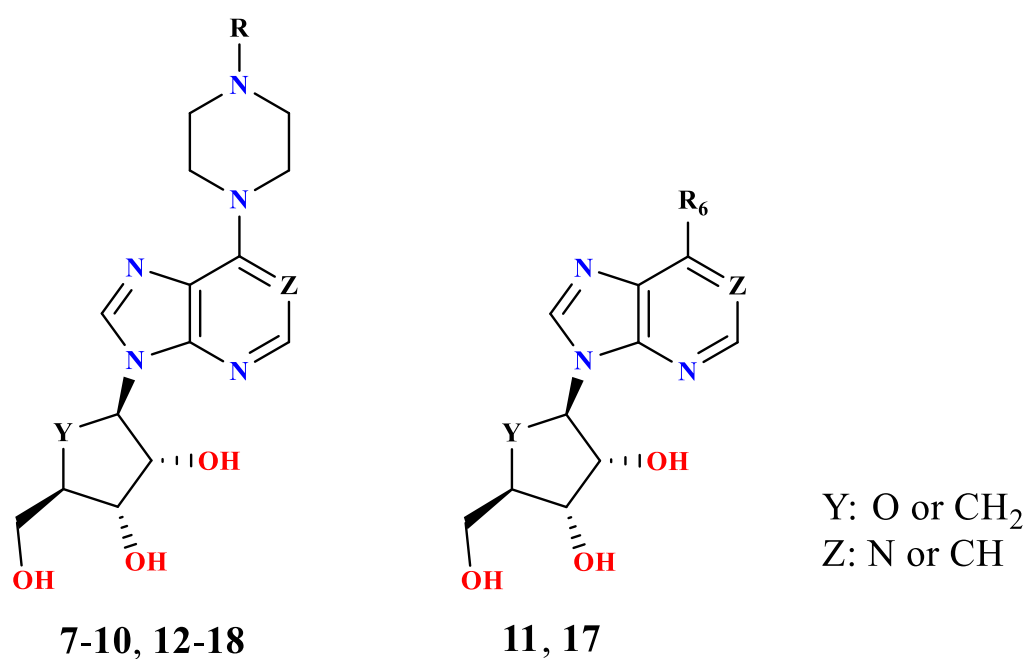


Figure 2.19: Adenosine scaffold showing the positions where medicinal chemistry was performed (R, R⁶, Y, Z).

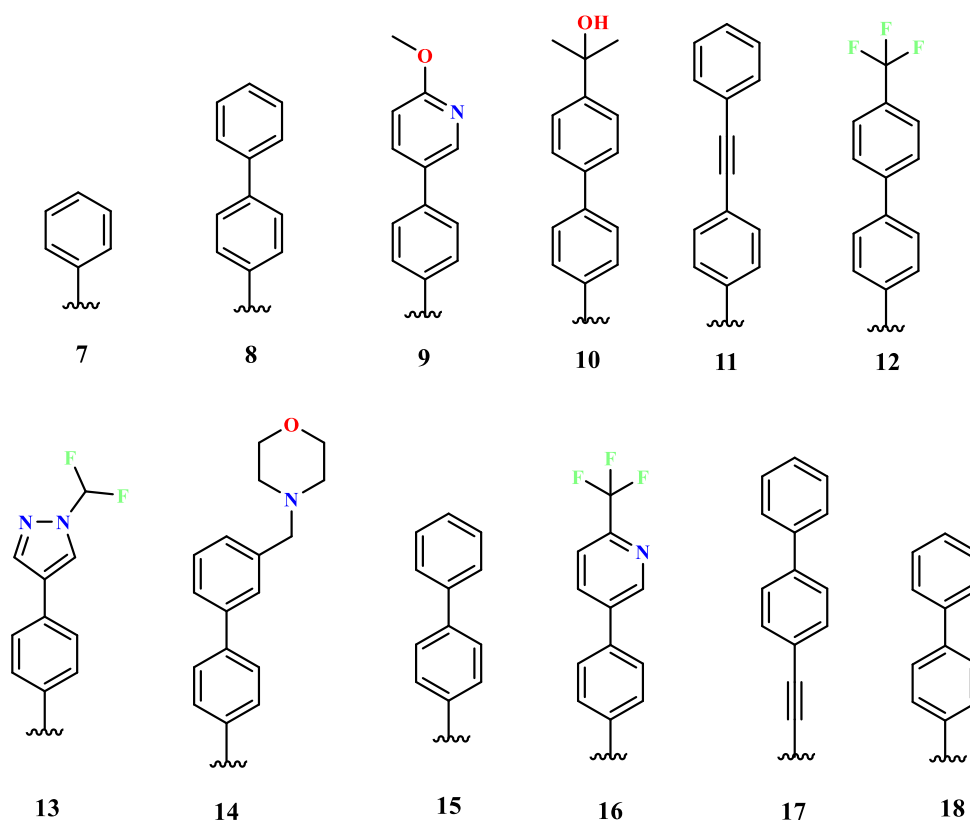


Figure 2.20: R and R⁶ groups of synthesized adenosine analogs.

Table 2.1: SAR data for synthesized adenosine analogs with substitutions at position 6.

ID	R or R ₆	Y	Z	MtbAdoK K _i (nM)	hAdoK K _i (μM)	MtbMIC ₅₀ (μM)	HDF CC ₅₀ (μM)
7	R	O	N	120.2 ± 0.98	n/a	n/a	n/a
8	R	O	CH	16.3 ± 0.1	n/a	n/a	n/a
9	R	O	N	18.5 ± 0.06	n/a	n/a	n/a
10	R	O	N	18.9 ± 0.5	n/a	≥ 30.0	n/a
11	R ₆	O	N	19.9 ± 0.03	n/a	≥ 50.0	n/a
12	R	O	N	21.3 ± 0.2	n/a	n/a	n/a
13	R	O	N	23.0 ± 1.1	≥ 15.1	n/a	n/a
14	R	O	N	25.5 ± 2.8	0.41 ± 0.07	≥ 25.0	n/a
15	R	CH ₂	N	27.5 ± 3.5	n/a	n/a	n/a
16	R	O	N	32.6 ± 0.3	1.6 ± 0.1	n/a	n/a
17	R ₆	O	N	48.0 ± 0.6	n/a	1.7 ± 0.02	3.5 ± 0.4
18	R	O	N	5.3 ± 0.07	^a n/a	4.0 ± 0.2	n/a

^aNot applicable; no inhibition observed.

We began these efforts with compound **7**. This compound showed excellent potency and selectivity against MtbAdoK when compared to hAdoK. We hypothesized that the piperazine group might lead to favorable contacts with flexible residue Arg176 while the benzene ring could extend to the unique cavity thereby conferring selectivity. To investigate the structural basis of inhibition and selectivity of **7**, we cocrystallized the compound with MtbAdoK. The crystal structure of the MtbAdoK-**7** binary complex was solved by MR in the P4₁ crystal space group with two molecules in the ASU and refined to a resolution of 1.65 Å (Figure 2.21a-c). Like the structures described above, the MtbAdoK-**7** complex displayed a closed conformation of the enzyme with a backbone rmsd of 1.68 Å amongst all C α atoms when compared to the MtbAdoK-adenosine structure. Unlike the structures described above, the MtbAdoK-**7** structure had no electron density for a compound bound to the ATP site. Overall, the interactions seen between the adenine ring and the ribose scaffold were very similar to those observed in the MtbAdoK-adenosine complex. Interestingly, the most significant differences were found once more with residues Gln172, Gln173 and Ser36. Here, Gln173 and Ser36 were not observed to make any of the critical H-bonds with positions N1, N6, and N7 while Gln172 retains the H-bonds with O4' of ribose (NE2-O4' distance of 2.97 Å) and O5' (NE2-O5' distance of 3.36 Å) but lacks the H-bond with N6. As in the case of the MtbAdoK-**6** structure, superimposition of the crystal structure complexes of MtbAdoK-adenosine and MtbAdoK-**7** showed that the bulky substitution of **7** causes the compound to bind in a different orientation with respect to adenosine with notable differences in crucial lid domain residues Asp12, Phe102 and Phe116 (Figure 2.21b). Here, the lid domain gap of

with respect to the MtbAdoK-adenosine complex was an average of 4.13 Å. We also observed that the phenylpiperazine forces Arg176 to open the “chimney-like” cavity by reorienting the residue back to the solvent. The crystal structure also showed that the piperazine group redirects the distal benzene group within the enzyme’s active site groove and that there was sufficient space to incorporate additional groups at the distal benzene ring to fully occupy the cavity (Figure 2.21c).

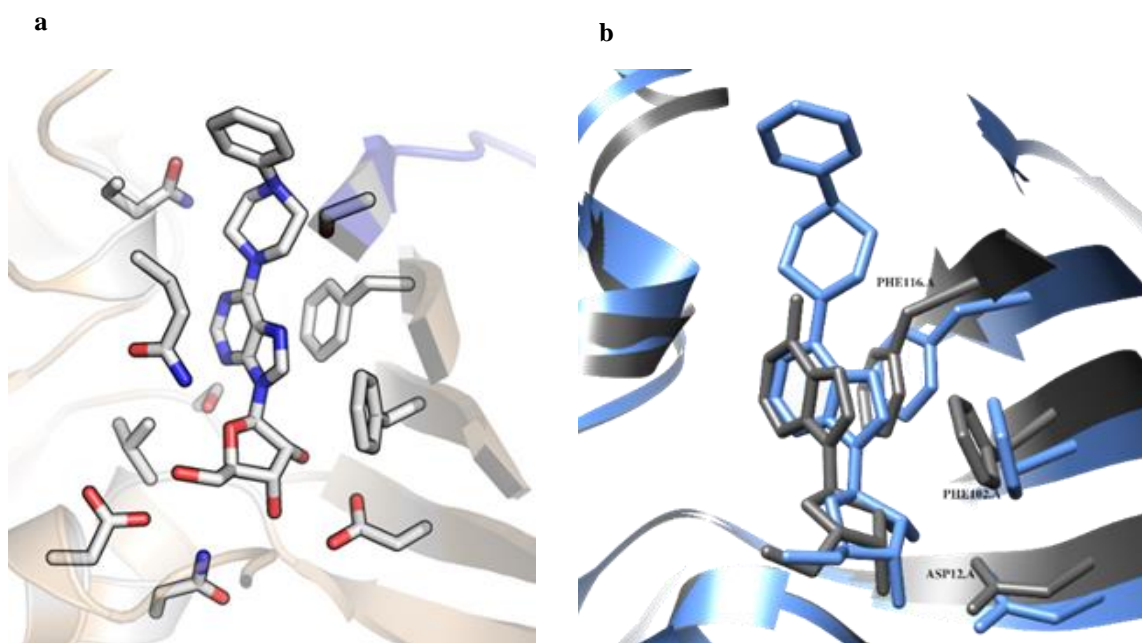


Figure 2.21: Crystal structure complex of **7** bound to the active site of MtbAdoK. (a) Residues involved in close contacts with **7**. Chain A is colored wheat, and chain B is colored blue. (b) The bulky substitution of **7** (blue) forces the compound to bind in a different orientation with respect to adenosine (gray; PDB ID 2PKM). (c) The bulky substituent forces Arg176 open the cavity and the distal benzene ring is reoriented back into the active site groove that is formed by residues of chain A (heteroatom) and chain B (magenta).

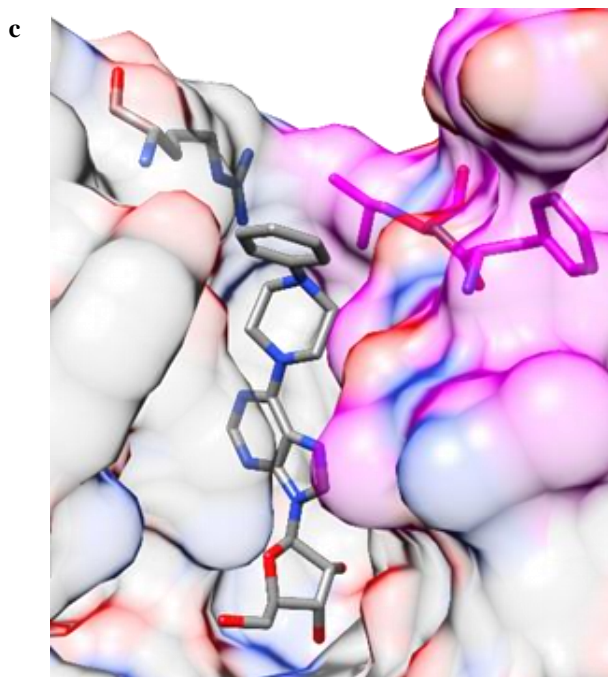


Figure 2.21: Continued

As noted above, another position of interest was the 5'-position of the ribose scaffold. The preliminary structure-based SAR with compound **5** suggested that bisubstrate-like inhibitors might be able to take advantage of the ATP channel. To investigate if the ATP channel is a viable route for drug design, we synthesized several 5'-substituted adenosine analogs (Figure 2.22 and Table 2.2). Despite having sufficient space to accommodate large groups, bulky phenyl substituents the 5'-position resulted in inhibitors with negligible inhibitory activity. Indeed, only one of the synthesized compounds displayed some measurable inhibitory activity against the enzyme with 53.0 % inhibition at 12.5 μ M of the compound (Figure 2.22 and Table 2.2). The lack of

inhibitory activity of these analogs may be due to suboptimal angles adopted by the 5' substituent.

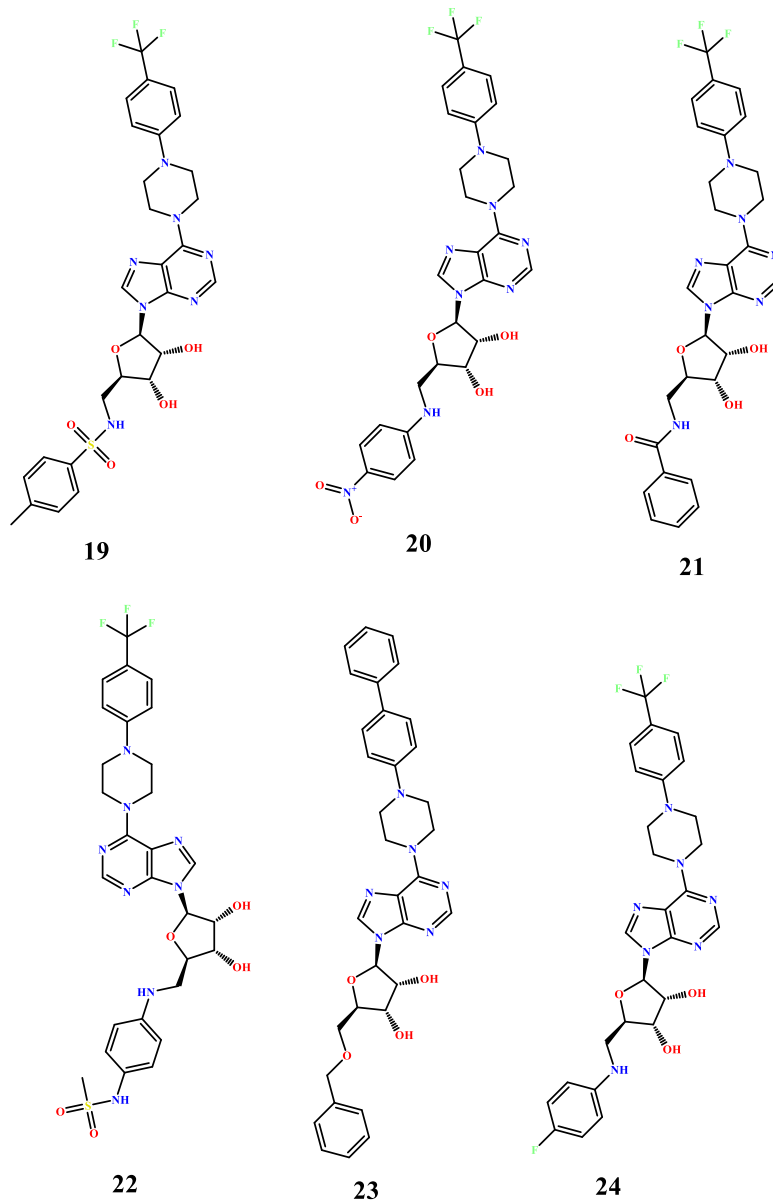


Figure 2.22: Chemical structures of synthesized adenosine analogs with substitutions at the 5'-position.

Table 2.2: SAR data for synthesized adenosine analogs with substitutions at the 5'-position.

ID	MtbAdoK IC₅₀ (μM)	mc²7000 MIC₅₀ (μM)
19	≥ 12.5	^a n/a
20	n/a	≥ 50.0
21	n/a	n/a
22	n/a	n/a
23	n/a	n/a
24	n/a	n/a

^a Not applicable; no inhibition observed.

The MtbAdoK-7 complex suggested that further extension at the distal benzene group could be accommodated in the cavity and that rigid substituents at the N6-position might orient the substituent within the cavity. Based on these observations, we synthesized compounds **8-17**. As shown in Table 2.1, all compounds displayed high potency against MtbAdoK with K_i values ranging from ~ 16 -48 nM. Overall, the SAR results are in accordance previous observations where it was noted that N6-substituted adenosine analogs displayed a higher degree of specificity to MtbAdoK when compared to hAdoK (Figure 2.23).^{192, 218} It is currently unknown how Mtb uptakes and discriminate between these series of compounds.

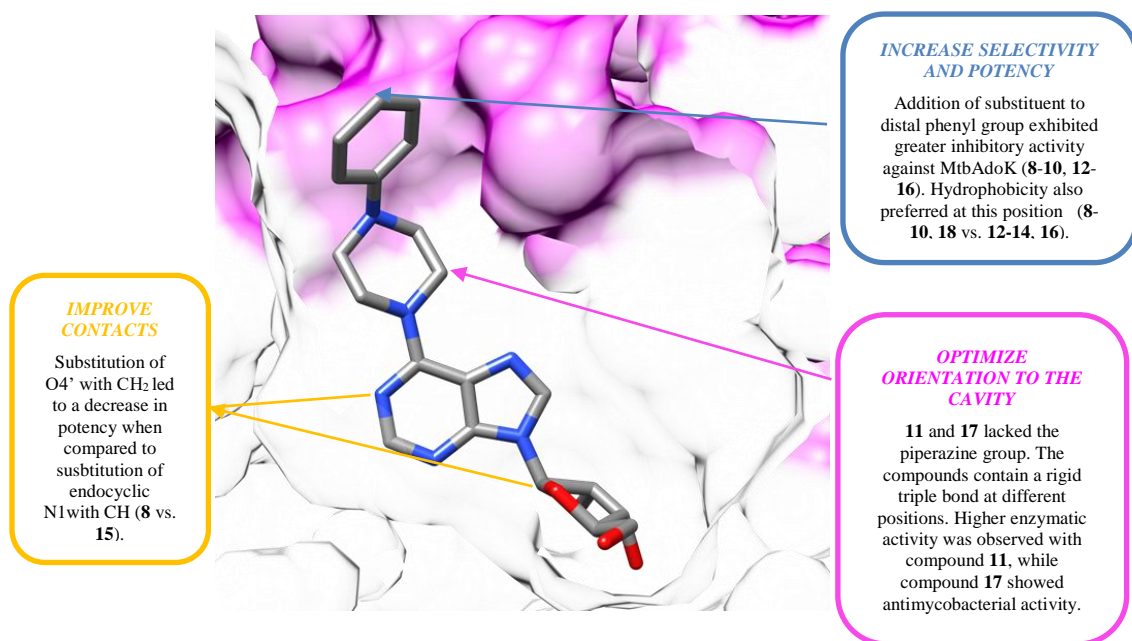


Figure 2.23: Summary of SAR results for compounds **8-17**. Compound **7** bound to the active site of MtbAdoK. Based on the MtbAdoK-**7** complex, compounds **8-17** were synthesized. Chain A is colored white, and chain B is colored magenta.

Compounds **11** and **17** were designed to test different orientations of the N6-substituent within the cavity. These compounds possess a rigid triple bond instead of the flexible piperazine group. Since compound **17** displayed antimycobacterial activity, we decided to determine the cocrystal structure of the MtbAdoK with compound **17**. The crystal structure of the MtbAdoK-**17** complex was solved by MR in the $P4_1$ crystal space group with two molecules in the ASU and refined to a resolution of 2.35 Å (Figures 2.24a-c). The binary complex displayed a closed conformation of the enzyme with a backbone rmsd of 1.63 Å amongst all $C\alpha$ atoms when compared to the MtbAdoK-adenosine structure. Just like the MtbAdoK-**7** structure, the MtbAdoK-**17** binary complex had no electron density for another molecule of **17** bound to the ATP site. Superimposition of the

crystal structure complexes of compounds **17** and adenosine also showed that the bulky N6-substitution of **17** causes the compound to bind in a different orientation with respect to adenosine; leaving lid domain gap of 2.29 Å when compared to the MtbAdoK-adenosine complex (Figure 2.24c).

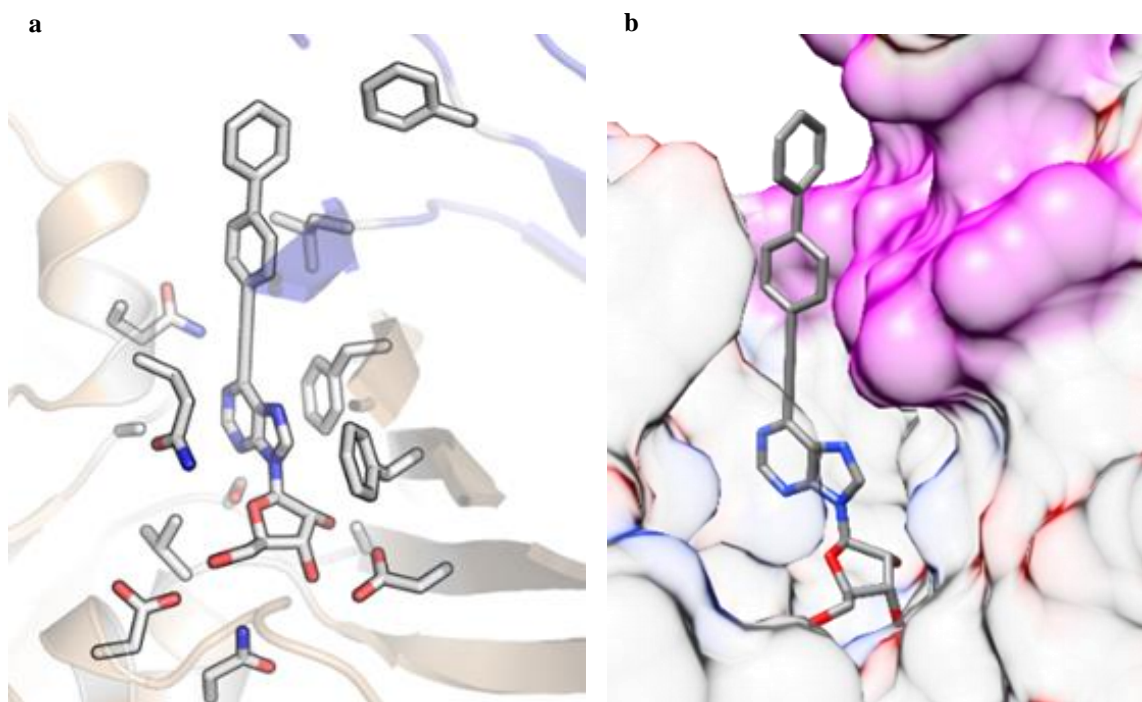


Figure 2.24: Crystal structure complex of compound **17** bound to the active site of MtbAdoK. (a) Residues involved in close contacts with **17**. (b) The large bulky substitution gets accommodated in the “chimney-like” cavity. (c) Compound **17** (blue) binds in a different orientation with respect to adenosine (gray). (d) Superimposition of crystal structure complexes of **17** (blue) and **7** (gray). Chain B residues forming the distal part of the “chimney-like” cavity colored magenta while chain A residues are colored by heteroatom.

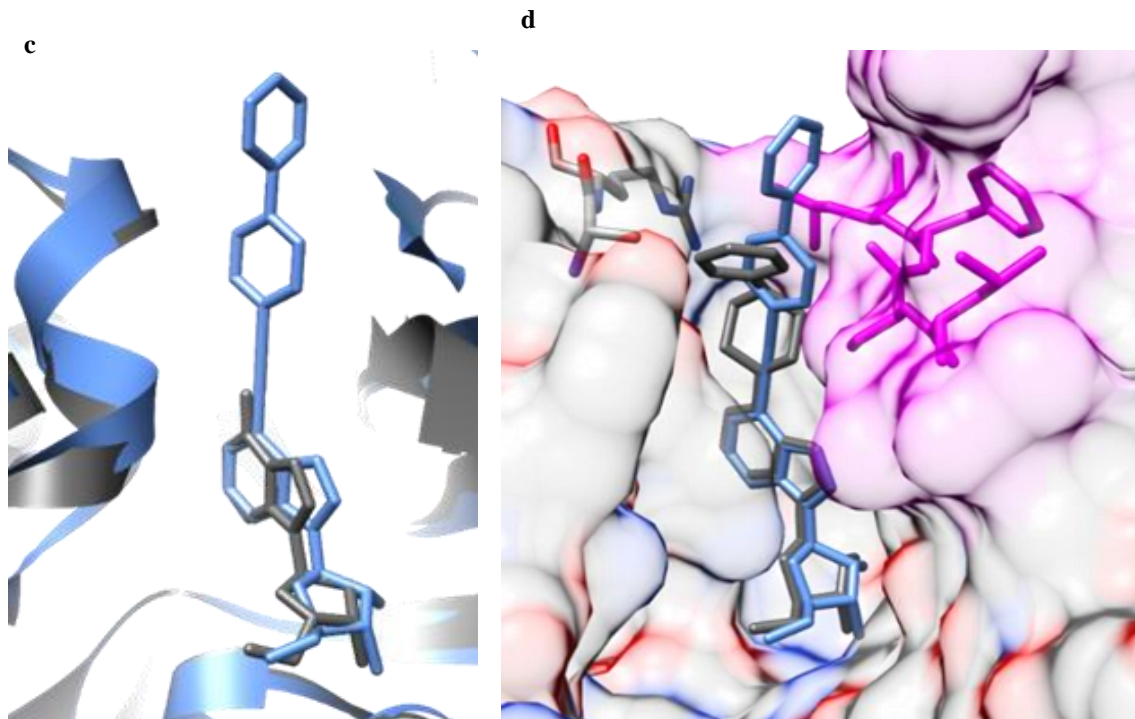


Figure 2.24: Continued

The MtbAdoK-**17** binary complex showed that the compound binds to the active site of the enzyme forming similar contacts with the protein as observed with the adenosine-bound complex (Figure 2.24a). Structural differences were found again with residues Gln172, Gln173 and Ser36'. Gln172 was seen to form a weak H-bond with O4' (NE2-O4' distance of 3.44 Å) while Gln173 formed a weak H-bond with endocyclic N1 of the adenine ring (NE2-N1 distance of 3.11 Å). Key residue Ser36' was not found to make any interactions with compound **17**. The major difference between the MtbAdoK-**7** and the MtbAdoK-**17** structures is the orientation that the N6-substituent adopts as it goes into the “chimney-like” cavity. The cocrystal structure of the MtbAdoK-**7** complex

suggests that the piperazine containing adenosine analogs might reorient to the active site groove that is composed of hydrophobic residues from both chains including Ala175.A, Leu38.B, Leu35.B, Phe37.B and polar residues Ser36.B and Arg176.A. In contrast, the rigidity imparted by the triple bond of compound **17** limits the substitution to adopt a bond angle of 180° with respect to the N6-position. Consequently, one side of the distal benzene ring of **17** was seen to be oriented towards backbone and main chain atoms of Phe37.B while the other side was observed to partially solvent (Figure 2.24d).

Finally, based on the chemistry and structure-guided SAR efforts with compounds **7-17** we synthesized compound **18**. This compound is an analog of compounds **8** and **15**. The major difference is that **18** contains endocyclic atoms N1 and O4' which we observed in the structures described above that they were involved in key H-bond interactions with residues Gln172 and Gln173, and the SAR suggested to be relevant in potency. Indeed, compound **18** was our most potent derivative, exhibiting a K_i of ~ 5 nM against MtbAdoK, no cytotoxicity, no activity against hAdoK and a MIC_{50} of ~ 4.0 μ M against Mtb. To further characterize this very potent compound, and as a representative of the group, we performed steady-state kinetic experiments on compound **18** to determine the mode of inhibition. As expected, we found that increasing the concentration of adenosine in the presence of a fixed inhibitor concentration, led to an increase of the K_m ; consistent with a competitive mode of inhibition. The K_m value for adenosine determined with our enzymatic assay was $1.71 \pm 0.02 \mu$ M, well in agreement with previously reported values of 0.8-3.4 μ M.^{186, 219}

Taken together, the observed differences in binding modalities of reorientation within the enzyme vs. solvent exposed might explain the overall higher potency of the piperazine substituted analogs (Table 2.1). Furthermore, the predominantly hydrophobic character of the “chimney-like” cavity goes in accordance with the SAR studies where hydrophobic substitutions displayed a higher degree of potency when compared to the polar substituted analogs (Table 2.1).

2.4 Conclusions and future work

These studies represent a structure-guided approach to the rational design of very potent MtbAdoK inhibitors with low micromolar activity against MtbAdoK. Furthermore, our studies offer a structural explanation behind the specificity of previously reported N6-substituted adenosine analogs.^{192, 208-209, 218} That is, substitutions at the N6-position of the adenine scaffold might be accommodated in a compound-induced pocket that is formed within the unique oligomerization state of MtbAdoK when compared to hAdoK and other eukaryotic adenosine kinases. Unlike the crystal structures of compounds **2-6**, the crystal structures of **7** and **17** did not display any electron density for a compound bound to the ATP site suggesting that there might be a size threshold conferring specificity to the active site vs. ATP site. Therefore, future strategies to design bisubstrate-like inhibitors should focus on small substituents at the N6-position with bulkier groups at the 5'-position.

The crystal structures of the bulky N6-adenosine analogs suggested that the reorientation conferred by the piperazine group might lead to more favorable contacts with the enzyme thereby leading to a higher degree of potency. The predominantly hydrophobic character of the cavity goes in accordance with the SAR studies demonstrating that

hydrophobic substitutions were preferred at the N6-position. Moreover, the lid domain gaps and different orientation of compounds **6**, **7** and **17** with respect to the MtbAdoK-adenosine structure suggest that bulky substitutions at position N6 might exert its inhibitory effects by sterically preventing full lid domain closure. Overall, we showed that the unique “chimney-like” cavity formed by the unique oligomerization state of MtbAdoK could be utilized as a canvas for future medicinal chemistry efforts to further improve potency and selectivity.

3. DISCOVERY, BIOCHEMICAL AND STRUCTURAL CHARACTERIZATION OF NOVEL UNCOMPETITIVE INHIBITORS AGAINST *MYCOBACTERIUM TUBERCULOSIS* ADENOSINE KINASE

3.1 Background and significance

Mycobacterium tuberculosis, the etiological agent of tuberculosis, continues to represent a significant global burden to human health. As of 2015, 10.4 million people, including an estimated 1 million children; fell ill to the disease and approximately 2 million of these infected persons died from it. Worldwide, around 2 billion people are living with latent tuberculosis. If untreated, around 5-10 % of these infected individuals will develop active tb during their lifetime. This problem is only exacerbated by the rapid emergence of multi-drug resistant and extensively drug resistant tb coupled to the high incidence of HIV-Mtb coinfection. As a result, there is a worldwide necessity to develop new antimicrobial agents with novel mechanisms of action and new molecular targets.³⁰

The purine salvage pathway is a promising pathway for drug development within mycobacteria. Recent evidence suggests that this pathway might play a crucial role in mycobacterial latency. Most of the enzymes involved in this pathway including inosine monophosphate dehydrogenase, adenylate kinase, adenylosuccinate synthase, guanylate kinase, hypoxanthine-guanine phosphoribosyltransferase, guanosine monophosphate synthase, adenylosuccinate lyase, and adenosine kinase have been shown to be essential for the survival of the bacilli *in vivo* and *in vitro*.¹⁸²⁻¹⁸³ Purine nucleotides can be

synthesized from simple anabolites via the *de novo* pathway or can be synthesized by the action of the purine salvage pathway enzymes by turning preformed nucleobases into their corresponding nucleotides.¹⁸⁴

Purine metabolism in Mtb is not completely understood. Nevertheless, it is known that Mtb possesses all the enzymes required for the *de novo* and salvage pathways. Although it is currently unknown what internal or external stimuli triggers Mtb to prefer one route over the other, it is possible that Mtb might prefer the salvage pathways during its latent phase of infection. By switching to the salvage pathway, Mtb can bypass up to eleven chemically demanding steps thus making the salvage pathway the most likely source of purine nucleotides within the hostile and nutrient deprived microenvironment encountered by tb during latency.²²⁰

MtbAdoK belongs to the purine salvage pathway within mycobacteria. In Mtb, AdoK catalyzes the phosphorylation of adenosine to AMP in a Mg^{2+} and ATP dependent manner. The MtbAdoK structure has been solved at high-resolution with the substrate (adenosine) and without substrate (apo) at 1.5 Å and 1.9 Å resolutions respectively. The crystallographic data support what has been previously observed in other AdoKs, which is that upon substrate binding the lid-like domain undergoes a substantial conformational change to form the closed conformation of the enzyme.¹⁸⁷ Human adenosine kinase only shares 16.0 % sequence identity with MtbAdoK. Despite this, their overall structural topology is similar; consisting of a large domain and a smaller lid-like domain.¹⁹⁰ However, as opposed to hAdoK, MtbAdoK is a functional dimer while the former is a monomer in solution. In vitro and in vivo data have shown that MtbAdoK is essential

when tb is grown under cholesterol as a carbon source and that the gene is required for Mtb survival in critically infected mouse models, respectively; making MtbAdoK an attractive target. To the best of our knowledge, all drug discovery efforts to date have focused on adenosine analogs as competitive inhibitors of MtbAdoK or adenosine analogs as substrate surrogates for the production of toxic metabolites.^{192, 208-209, 218, 221}

In this work, we report the discovery, biochemical, biological and structural characterization of a series of dihydro spiro derivatives as novel non-nucleoside inhibitors of MtbAdoK. We also report the crystal structures of MtbAdoK in complex with the novel inhibitors at resolutions of 2.75-2.80 Å. Moreover, kinetic experiments demonstrate that the inhibitors act as uncompetitive inhibitors of the enzyme and our *in cellulo* experiments showed that the compounds have nanomolar potency against Mtb. In addition, selectivity studies showed a higher degree of activity against MtbAdoK when compared to hAdok. Finally, crystallographic and mutagenesis studies were employed to characterize and validate the novel binding site.

3.2 Material and methods

3.2.1 Cloning, expression and purification of recombinant MtbAdoK, MtbAdoK mutants, and hAdoK

The WT MtbAdoK gene (*Rv2202c*) was amplified by polymerase chain reaction from total genomic DNA of *Mycobacterium tuberculosis* H37Rv. The following oligonucleotides were used: 5'-GGAATTCCATATGGTGACGATCGCGGTAACC-3' and 5'-CTTAAGCTTCTAGGCCAGCAC-3', respectively. The amplified DNA fragment was digested with NdeI and HindIII restriction enzymes (New England BioLabs) and sub-

cloned into the corresponding restriction sites of the pET28b vector containing an N-terminal TEV cleavable His-tag. MtbAdoK mutants were generated using Agilent technologies QuickChange site-directed mutagenesis kit and cloned similarly into pET28b vector containing an N-terminal TEV cleavable His-tag. The MtbAdoK mutants were constructed utilizing the following mutagenic oligonucleotides for the polymerase chain reaction: for R176L 5'-CAGCAGCTGGCGCTGCTGTCGGGTGAG-3' and for R176A 5'-CAGCAGCTGGCGCTGTCGGGTGAG-3'. Finally, for the active site mutant Q172P; 5'-GCCGATCCGTCTCCGCAGCTGGCGAGG. Human adenosine kinase (hAdoK) gene was PCR amplified from clone HsCD00042641 (DNASU plasmid repository) utilizing the same procedure and oligonucleotides as explained in section 2.2.1. In all cases, gene fidelity was confirmed by DNA sequencing, and sequenced plasmids were used to transform *E.coli* BL21 (DE3) cells for protein expression. For protein expression, cell cultures were grown in LB medium at 37.0 °C. Cells were induced with 0.5 mM isopropyl β -D-1-thiogalactopyranoside (IPTG) when the cell density reached $A_{600} \sim 0.6$ –1.0. Finally, cell cultures were incubated for 18 h at 18.0 °C before harvesting.

Harvested cells were lysed using a French press, and the lysate was centrifuged at 17,000 rpm for 1 h. Recombinant MtbAdoK, hAdoK and MtbAdoK mutants were purified by using a HisTrap HP nickel column (GE Healthcare). Purification buffers A and B contained, 50.0 mM HEPES, pH 7.5, 500.0 mM NaCl, 500.0 mM imidazole (buffer B only), and 5.0 % glycerol. For crystallization studies, MtbAdoK was dialyzed in 20.0 mM HEPES, pH 7.5, 50.0 mM NaCl, 2.0 mM DTT and 5.0 % glycerol. For enzymatic assays, the proteins were dialyzed in 50.0 mM HEPES, 50.0 mM NaCl, 100.0 mM KCL, 4.0 mM

DTT and 20.0 % glycerol. Finally, the proteins were aliquoted and stored in -80.0 °C for subsequent crystallization and enzymatic assays.

3.2.2 Dynamic scanning fluorimetry (DSF) high-throughput screening assay

A total of 2,534 compounds from our in-house collection of whole cell active compounds was screened in a 96-well format using the DSF assay described by Niesen *et al.*²²² In short, the samples contained a final concentration of MtbAdoK of 3.0 μM, 100.0 mM HEPES pH 7.5, 50.0 μM of compound dissolved in 100.0 % DMSO and a final concentration of 5X of SYPRO® ORANGE dye. Reaction volume across the 96-well PCR plate was 20.0 μL. Positive and negative control reactions were carried out similarly but using adenosine and DMSO, respectively. Following sample preparation, the 96-well plate was covered with an UltraClear film (Axygen Scientific). The assay was performed on Agilent Technologies Mx3005P qPCR system by using a temperature gradient of 25°-99 °C at 0.5 °C per minute and monitoring the fluorescence emission of the SYPRO ORANGE® (excitation = 492.0 nm, emission = 610.0 nm).

3.2.3 IC₅₀, steady-state kinetics, and K_i determination

IC₅₀ and steady-state kinetics studies were performed by monitoring the conversion of NADH to NAD⁺ ($\epsilon_{\text{NADH}} = 6.22 \times 10^3 \text{ M}^{-1} \text{ cm}^{-1}$) using the pyruvate kinase-lactate dehydrogenase coupled assay system in a Varioskan™ Lux multi-mode plate reader. The reaction was started by the addition of 60.0 nM of enzyme into a final volume of 200.0 μL master mix containing 50.0 mM HEPES pH 7.5, 50.0 mM KCl, 6.0 mM MgCl₂ (4.0 mM MgCl₂ for hAdoK), 3.0 mM ATP (2.0 mM ATP for hAdoK), 200.0 μM NADH, 1.0 mM phosphoenolpyruvate, 1.0 mM DTT, 12.0 U/mL pyruvate kinase, 12.0 U/mL lactate

dehydrogenase and 15.0 μM adenosine. IC_{50} values for each compound were determined by varying the concentration of inhibitor at a fixed concentration of enzyme and by fitting the dose response data into the four-parameter logistic curve (Equation 3.1) model of GraphPad prism 7.02, as follows:

$$Y = Y_{min} + \frac{(Y_{max} - Y_{min})}{(1 + 10^{(\log \text{IC}_{50} - I)H})} \quad (3.1)$$

Where I is the logarithm of inhibitor concentration, H is the Hill slope and Y, Y_{max} and Y_{min} are the specific activity, maximum specific activity and minimum specific activity, respectively. Kinetic assays for MtbAdoK were performed essentially as described above with the following exceptions: the master mix contained 60 nM MtbAdoK and the reaction was started by the addition of varying concentrations of adenosine in the presence of constant concentrations of dihydro spiro compound (0.0 μM , 12.0 μM , 24.0 μM). Kinetic data was obtained by fitting the initial velocity data into GraphPad Prism 7.02 nonlinear regression function of Michaelis-Menten model (Equation 3.2), as follows:

$$V_o = \frac{(Y_{max})[S]}{(K_m + [S])} \quad (3.2)$$

Where V_o is the initial velocity, Y_{max} is the maximum specific activity, S is the substrate concentration, and K_m is the Michaelis-Menten constant. Specific activity values for kinetic and IC_{50} measurements were determined using (Equation 3.3):

$$\text{specific activity} = \frac{\left(\frac{a}{\epsilon_{\text{NADH}} * b} d\right)}{c} \quad (3.3)$$

Where a is the change in absorbance over time, ϵ_{NADH} is the millimolar extinction coefficient of NADH, b is the pathlength, d is the dilution factor of the enzyme in the assay and c is the concentration of enzyme stock used for the assay.

Finally, the K_i was determined by using the Cheng-Prusoff relationship for uncompetitive inhibition (Equation 4).¹⁹⁷⁻¹⁹⁸

$$K_i = IC_{50} / \left(\frac{K_m}{[S]+1} \right) \quad (3.4)$$

In all cases, the compounds were serially diluted in 100.0 % DMSO and added to the enzymatic reaction to a final concentration of 2.5 % DMSO. Unless otherwise stated, all assays were performed in duplicates, and the error is reported as plus or minus standard deviation.

3.2.4 Crystallization, crystal dehydration, data collection and crystal structure determination

Purified MtbAdoK was concentrated to 18.0 mg/mL before crystallization trials. MtbAdoK-dihydro spiro cocrystals were obtained by means of the microbatch under oil crystallization technique. The screening was performed in a 96-well format using the MRC under oil 96-well microbatch plates (Swissci) and TTP Labtech's Mosquito Crystal robot system to screen over 800 different crystallization conditions per crystallization attempt. Crystals were obtained at 4.0 °C by mixing 800.0 nL of concentrated protein solution, pre-incubated for 1 h at 25.0 °C with 1.0 mM of the compound, with 400.0 nL of 1.6 M sodium citrate tribasic dihydrate pH 6.5 under Al's oil (Hampton research). Before data collection, crystals were cryoprotected with Paratone (Hampton research) and flash frozen in liquid nitrogen. In some cases, crystal dehydration was necessary to improve X-ray diffraction quality. Dehydration solution was composed of 25.0 µL of 100.0 % glycerol and 75.0 µL of crystallization condition and was performed at 4.0 °C for

2-4 h prior to cryoprotection and data collection. X-ray diffraction data was collected at Argonne's National Lab Advanced Photon Source beamlines 19ID and 19BM. Diffraction data was indexed, scaled and integrated into $P6_2$ space group using HKL2000.¹⁹⁹ Initial phases were obtained by molecular replacement in MOLREP using the high-resolution structure of apo MtbAdoK with PDB accession code 2PKF.²⁰⁰ Refinement was performed in PHENIX followed by iterative runs of inspection and manual modification using coot.²⁰¹⁻²⁰² Ligand model and restraint files were created in ELBOW from the PHENIX suite and fitted into the electron density using COOT. Images and figures were rendered using Molsoft ICM, Chimera and PyMOL.²⁰³⁻²⁰⁵

3.2.5 Antitubercular assay

Antitubercular testing and MIC₅₀ determination was performed using the MABA assay in a 96-well format as previously described.²⁰⁶⁻²⁰⁷ Starter culture of Mtb mc²7000 was grown in 7H9 media supplemented with OADC (Middlebrook), 0.5 % dextrose, 0.085 % NaCl, 0.05 % Tyloxapol (Sigma), 0.25 µg/mL malachite green (Sigma) and 25.0 µg/mL pantothenate. Once cells reached an optical density of OD₆₀₀ ~1.0, cells were diluted to an OD₆₀₀ of 0.01 in the same media composition without OADC. For acetate-supplemented media, once cells reached the aforementioned OD₆₀₀, cells were diluted to an OD₆₀₀ of 0.01 in 0.5 % sodium acetate (Sigma), 2.0 mM MgSO₄ (Sigma), 0.1 mM CaCl₂ (Sigma), 0.05 % Tyloxapol, 0.25 µg/mL malachite green and 25.0 µg/mL pantothenate. Compounds were serially diluted in 100.0 % DMSO and added to the cells to a final concentration of DMSO of 2.5 %. Plates were incubated for 10 days (30 days for acetate-supplemented media) prior to staining with resazurin (Sigma). After staining, plates were incubated for

2 additional days (7 additional days for acetate-supplemented media) for developing. Finally, developed plates were read using a POLARstar Omega spectrophotometer (BMG Labtech) and by monitoring the fluorescence emission of resazurin (excitation = 570.0 nm, emission = 585.0 nm). In all cases, rifampicin was used as a negative control and the experiments were performed in duplicates were the reported error represents plus or minus standard deviation.

3.2.6 Human dermal fibroblast cytotoxicity assay

Human dermal fibroblasts (HDF) were purchased from ATCC (Manassas, VA). HDF cells were cultured in DMEM (Lonza) media supplemented with 10.0 % fetal bovine serum (Lonza) and penicillin/streptomycin (Lonza). For the cytotoxicity assay, compound stocks were serially diluted in phosphate-buffered saline (PBS) and 10.0 % DMSO. On the day of assay, HDF cells were trypsinized, counted and resuspended at a concentration of 64,000 cells/ml in media. Cells were plated, overlaid with the compound serial dilutions and incubated at 37.0 °C. After 48 h, resazurin dye was added and the assay plates cultured for another 24 h. The next day the absorbance of the resazurin was measured on a microplate reader to assess cell death. Cytotoxicity was determined as a percent of dead cells versus living. All assays were performed in triplicates and the error reported represents plus or minus standard deviation.

3.3 Results

3.3.1 Discovery and enzymatic testing of dihydro spiro compounds

Dynamic scanning fluorimetry (DSF) was used as the primary platform to screen in a 96-well format our in-house library of whole-cell active compounds at a single

concentration of 50.0 μM .²²² Hits were identified as compounds that had a thermal shift equal or greater than the positive control (Table 3.1).

Table 3.1: DSF data for lead compound **1**.

Average T_m of negative control ($^{\circ}\text{C}$)	Average T_m of positive control ($^{\circ}\text{C}$)	MtbAdoK-1 T_m ($^{\circ}\text{C}$)	ΔT_m ($^{\circ}\text{C}$)
52.70	55.72	55.0	3.02

Lead compound **1** was the only non-nucleoside-like hit identified. Several analogs (compounds **2-4**) were purchased and tested enzymatically against MtbAdoK and hAdoK (Figure 3.1 and Table 3.2). The compounds exhibited inhibition constants between 5.1-19.6 μM . Compounds **3** and **4**, with electron withdrawing substituents at position 4 of the benzopyrrole-like ring, displayed a 2-fold and 3.8-fold increase in potency when compared to lead compound **1**, respectively.

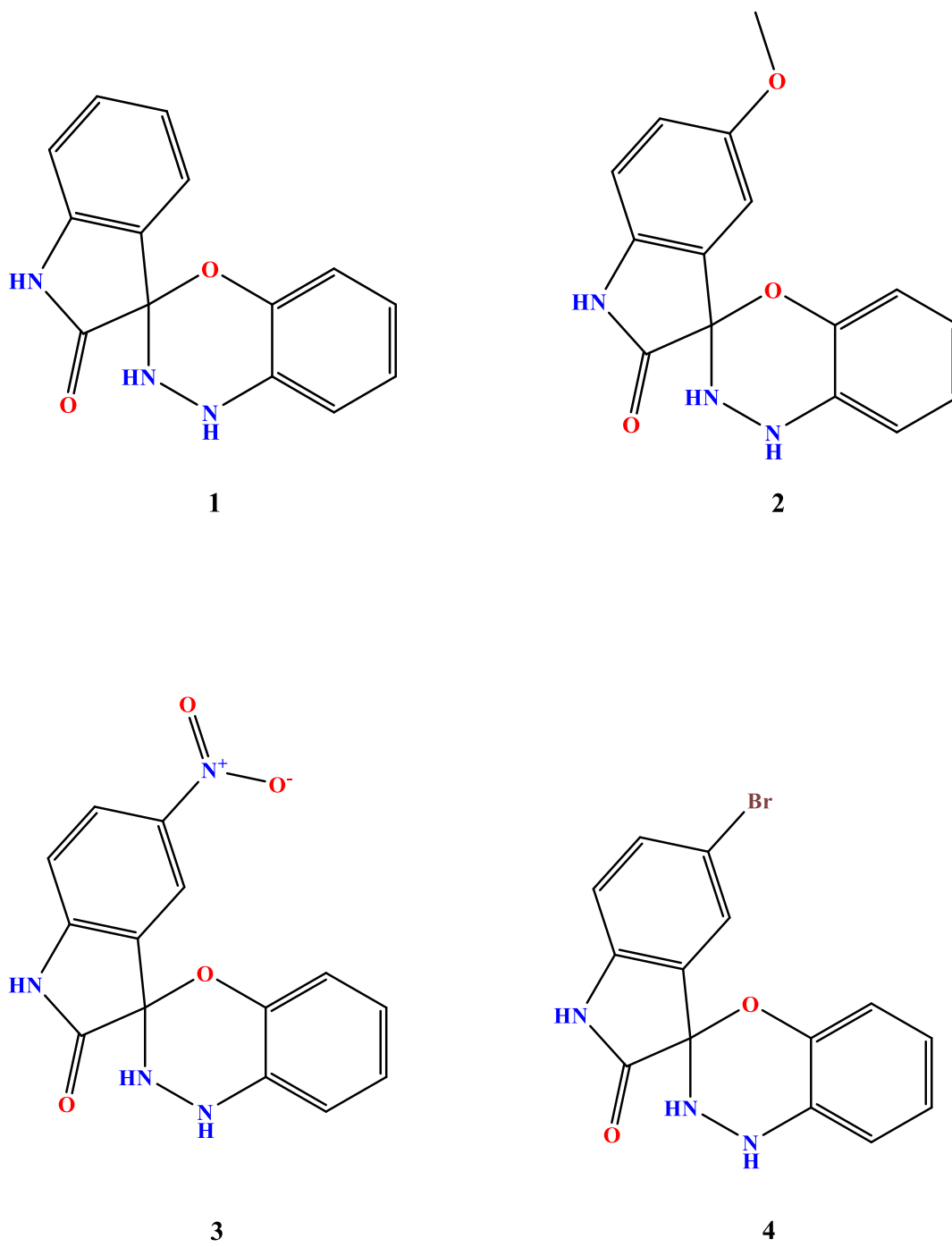


Figure 3.1: Structure of lead dihydro spiro compound **1** and analogs (**2-4**).

Table 3.2: Enzymatic assay parameters of dihydro spiro compounds.

ID	MtbAdoK K_i (μM)	hAdoK K_i (μM)
1	19.6 ± 1.8	n/a
2	16.7 ± 1.9	n/a
3	9.8 ± 1.0	n/a
4	5.1 ± 0.9	n/a

Error is reported as \pm SD of 2 independent experiments.

n/a; no activity detected

As a representative of all the compounds, we evaluated the mechanism of inhibition of compound **2** against MtbAdoK. As observed in Table 3.3 and Figure 3.2, increasing the concentration of substrate in the presence of fixed inhibitor concentrations results in a decrease of the K_m and specific activity values; consistent with uncompetitive inhibition. In addition, the Lineweaver-Burk plot shows a series of parallel lines; consistent with uncompetitive inhibition. Therefore, the compounds bind to and inhibit, the enzyme-substrate complex. The K_m value for adenosine determined with our enzyme coupled assay was $1.66 \mu\text{M}$ with a specific activity of $4.23 \mu\text{mol}/\text{min}/\text{mg}$. This is in good agreement with previously reported values of 0.8 - $3.4 \mu\text{M}$ for K_m and 3.7 - $4.0 \mu\text{mol}/\text{min}/\text{mg}$ for specific activity.¹⁸⁶

Table 3.3: Kinetic parameters for compound **2**.

[2] (μM)	K_m (μM)	Specific activity ($\mu\text{mol}/\text{min}/\text{mg}$)
0.0	1.66 ± 0.19	4.23 ± 0.02
12.0	0.49 ± 0.05	1.79 ± 0.03
24.0	0.35 ± 0.07	1.28 ± 0.17

Error is reported as \pm SD of 3 independent experiments.

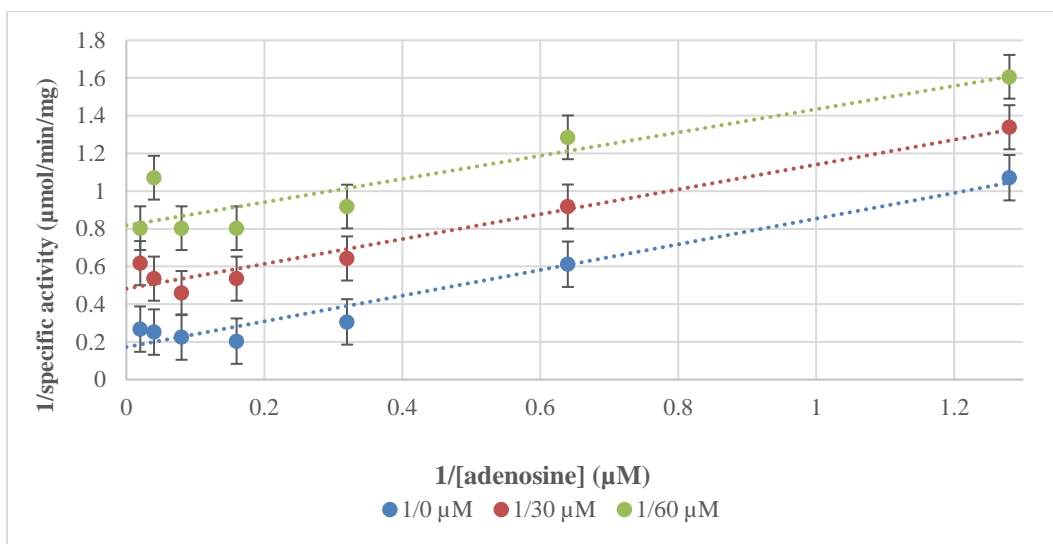


Figure 3.2: Lineweaver-Burk plot of compound **2** vs. adenosine. Initial velocity data was transformed to linear analysis to evaluate inhibitor type. The error bars represent \pm SD of 3 experiments.

3.3.2 Antimycobacterial and cytotoxic evaluation of dihydro spiro compounds

The antimycobacterial activity of the dihydro spiro compounds was evaluated against mc²7000. This Mtb strain is a BL2-approved double deletion mutant (Δ *panCD* and Δ *RDI*) that was created as a potential vaccine strain.²²³ Initial testing was carried out in 0.2 % acetate-supplemented M9 media to mimic a lipid-driven metabolism and in 0.2 % dextrose-supplemented 7H9 media to simulate a carbohydrate-driven metabolism. All compounds were freshly dissolved from solid material before the assays. Preliminary testing with compound **2** indicated a 29.6-fold increase in potency when tested on a dextrose-supplemented media (Figures 3.3a-b). Based on the initial tests, we opted to perform the rest of antimycobacterial assays in a dextrose-supplemented 7H9 media. All compounds exhibited sub-micromolar activity against Mtb mc²7000 with MIC₅₀ ranges of

508.3-829.2 nM indicating high potency for lead compounds (Table 3.4). Since the adenosine kinase gene is mostly found in eukaryotic organisms, we tested the compounds against HDF cells. Only compound **2** displayed cytotoxic activity with a CC_{50} of 10.4 μ M, whereas compounds **1**, **3** and **4** had no effect against HDF cells (Table 3.4 and Figure 3.4a-d).

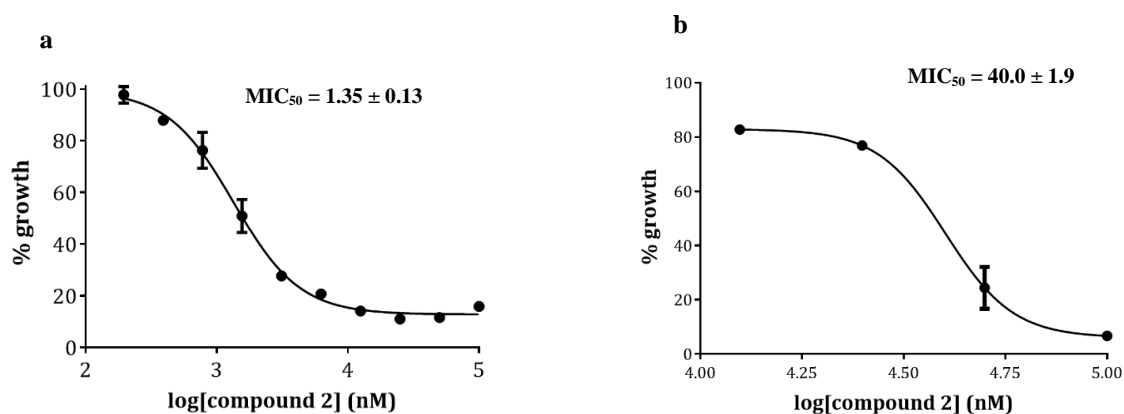


Figure 3.3: Comparison of the potency of compound **2** when mc²⁷⁰⁰⁰ is grown on a dextrose-supplemented 7H9 or acetate-supplement M9 media. (a) Dose response curve of compound **2** when tested in dextrose-supplemented (b) acetate-supplemented media to mimic a carbohydrate, and fatty acid derived catabolism, respectively. In all cases, **2** was tested from 0-100 μ M. The data is normalized to the 0 μ M (DMSO) control, and the error bars represent the SD of 3 independent experiments.

Table 3.4: Antimycobacterial and cytotoxic profile of dihydro spiro compounds.

ID	MIC ₅₀ -mc ²⁷⁰⁰⁰ (nM)	CC ₅₀ -HDF cells (μ M)
1	829.2 ± 121.7	n/a ^a
2	825.5 ± 98.6	10.4 ± 1.5
3	517.5 ± 40.8	n/a
4	508.3 ± 30.8	n/a

Error is reported as ± SD of 3 independent experiments.

^aNot applicable; no cytotoxicity detected.

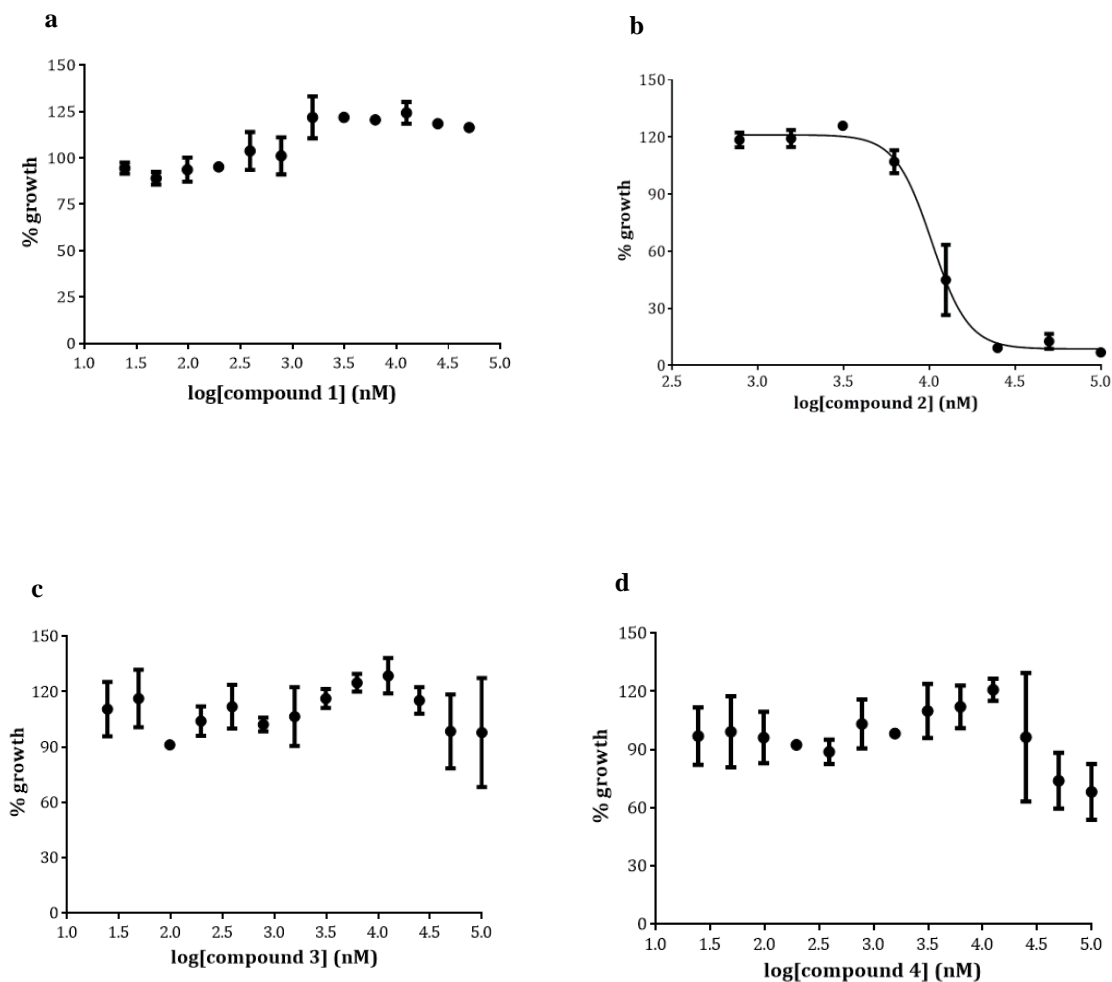


Figure 3.4: Cytotoxicity profiles of dihydro spiro compounds when tested against HDF cells. (a) **1**, (b) **2**, (c) **3**, (d) **4**. Only compound **2** displayed some cytotoxicity against HDF cells. In all cases, the compounds were tested from 0-100 μ M. The data is normalized to the 0 μ M (DMSO) control, and the error bars represent the \pm SD of 3 independent experiments.

3.3.3 Structural characterization of the MtbAdoK-dihydro spiro complex

To further explore the molecular details behind the novel uncompetitive inhibitors, we sought to determine the cocrystal structures of the MtbAdoK-dihydro spiro complex.

Thousands of crystallization trials utilizing conventional vapor diffusion methods were attempted to no avail. Cocrystals of the binary complex were only possible when using the microbatch under-oil crystallization technique, and only cocrystals for compounds **2**, **3** and **4** were obtained.²²⁴ Compound **2** cocrystals diffracted poorly (6-7 Å). In contrast, compounds **3** and **4** readily diffracted to 2.7-3.0 Å (Table 3.5).

Table 3.5: Crystal data collection and refinement statistics.

Statistic	MtbAdoK-2	MtbAdoK-3	MtbAdoK-4
Data collection			
Space Group	P6 ₂	P6 ₂	P6 ₂
Cell Dimensions			
a, b, c (Å)	149.70, 149.70, 66.27	150.39, 150.39, 65.57	150.41, 150.41, 65.88
α, β, γ (°)	90, 90, 120	90, 90, 120	90, 90, 120
Resolution (Å)	36.2 - 2.8 (2.9 - 2.8)	37.6 - 2.75 (2.8 - 2.75)	37.6 - 2.78 (2.88 - 2.78)
R _{merge}	0.080	0.078	0.071
I/ σ I	21.66	29.78	14.49
Completeness %	99.69	99.42	98.66
Redundancy	7.5	7.3	5.0
Refinement			
Resolution	2.80	2.75	2.78
No. of reflections	21114	22218	21358
R _{work} /R _{free}	0.19/0.24	0.18/0.23	0.19/0.24
No. of atoms			
Protein	4956	4982	4957
Ligand	35	46	42
Water	0	27	9
B factors			
Protein	101.1	84.6	100.19
Ligand/ion	77.7	108.4	106.6
Water	n/a	57.5	66.75
rmsd			
Bond lengths (Å)	0.009	0.01	0.008
Bond angles (°)	1.26	1.29	1.16

To circumvent the lack of diffraction of compound **2**, crystal dehydration experiments were employed.²²⁵⁻²²⁷ A 75.0 % mother liquor solution was mixed with 25.0 % glycerol and was used to dehydrate the co-crystals for 2 h at 4.0 °C. Crystals were then cryoprotected, flash frozen and stored for remote data collection. Dehydration experiments were also attempted for compounds **3** and **4** to increase the diffraction power of the crystals. However, dehydration proved to be detrimental to the diffraction quality (data not shown).

All the binary complexes showed a fully opened conformation of MtbAdoK (Figure 3.5) when compared to the apo structure (PDB ID 2PKF) of MtbAdoK (rmsd of α 's 0.51, 0.41 and 0.43 Å for compounds **1**, **2** and **3**, respectively).¹⁸⁷ In addition, only chain A of the MtbAdoK dimer had well-defined density of the compound. On the other hand, and most likely due to the low solubility of the compounds, chain B had significantly less density. Closer inspection of the binary complexes of all cocrystals, reveals that the compounds bind in a narrow cavity formed by residues from chain A and chain B of the MtbAdoK homodimer.



Figure 3.5: Superimposition of the MtbAdoK-adenosine, MtbAdoK-apo and MtbAdoK-dihydro spiro structures. Apo (blue; PDB ID 2PKF), MtbAdoK-2 (green), MtbAdoK-3 (orange), MtbAdoK-4 (purple) and MtbAdoK-adenosine (pink; PDB ID 2PKM). Only one chain of the MtbAdoK homodimer is shown for comparison.

The crystal structure also indicates that this narrow cavity is adjacent to the active site of MtbAdoK and that is distinct from the cofactor binding site (Figure 3.6a-b). One side of this cavity is mostly comprised of hydrophobic residues Met121.A, Leu38.B, Phe116.A, Phe102.A, and polar residues Ser36.B and Ser8.A. On the other hand, the other side of the cavity is solely comprised of polar residues including Arg176.A, Gln172.A and Gln173.A (Figure 3.7).

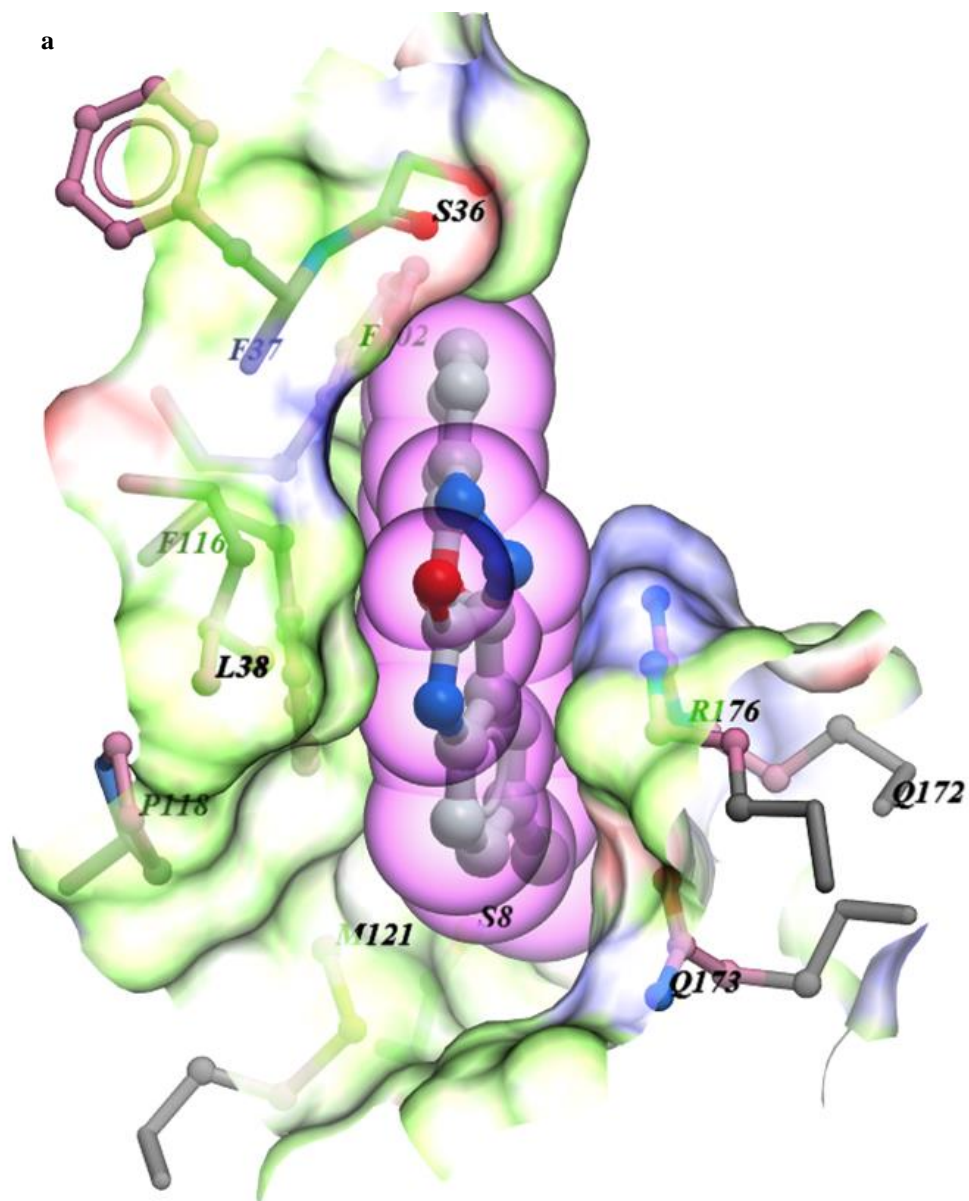


Figure 3.6: Surface representation of the dihydro spiro binding pocket. (a) The dihydro spiro compound binds in a narrow cavity formed by residues from chain A and chain B. (b) The dihydro spiro compound occupies a distinct site adjacent to the active site (iodotubercidin-green), and that is not the cofactor binding site (iodotubercidin-purple).

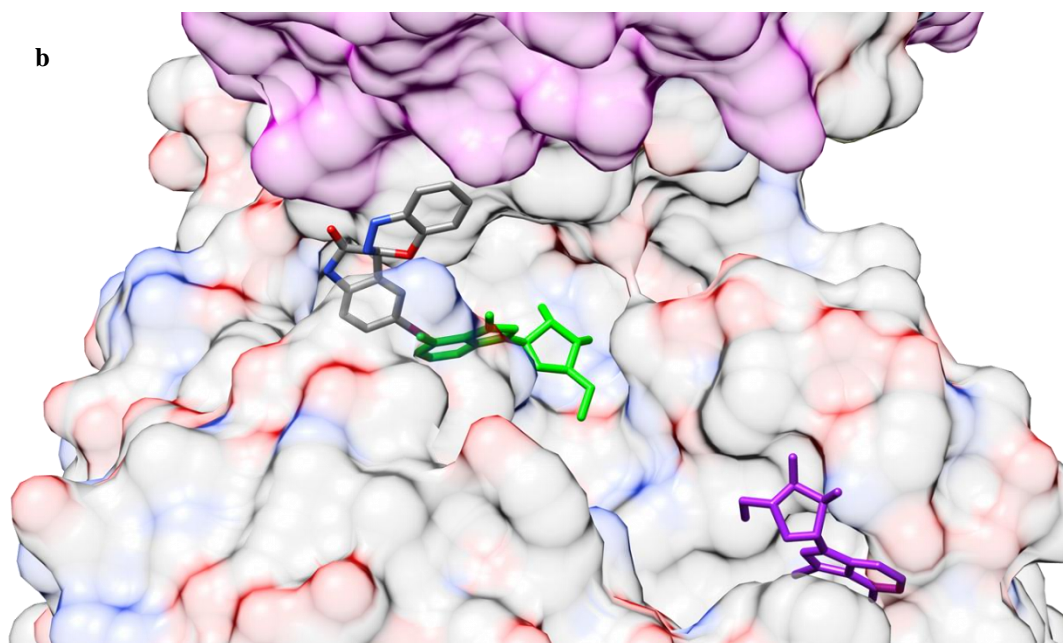


Figure 3.6: Continued

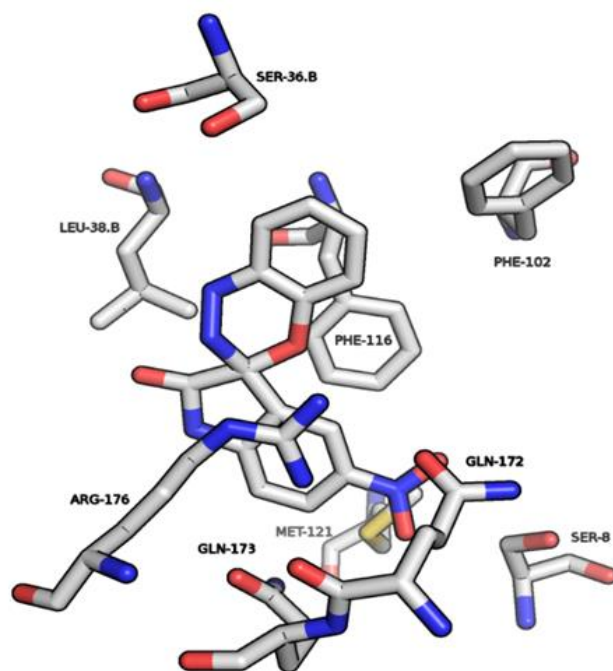


Figure 3.7: Residues involved in close contacts with the dihydro spiro compound.

Residues Leu38.B, Met121.A and Arg176.A are unique to the spiro binding pocket. In contrast, residues Phe102.A, Phe116.A, Ser36.B, Ser8.A, Gln172.A, Gln173.A are known to coordinate the substrate when it's bound to the active site. Phe116 and Phe102 are involved in π -stacking interactions with the adenine and ribose rings, respectively. Ser8 hydrogen bonds with endocyclic N3 of the adenine ring, Gln172 is involved in hydrogen bonding with ribose O5' and O4' atoms, Gln173 hydrogen bonds with N1 and N6 of the adenine ring and Ser36.B completes the active site by hydrogen bonding with N7 of the adenine moiety. It should be noted that residues Asp12, catalytic base Asp257 and hinge region residues Gly47 and Gly48 do not form part of the spiro binding pocket but they are conserved across all members of the phosphofructokinase B family of carbohydrate kinases.¹⁸⁸

Arg176 and Phe116 form key interactions at the dihydro spiro binding pocket. The crystal structure shows that Arg176 orients itself towards the compound with an average distance of 3.5 Å between CZ of Arg176 and the benzopyrrole-like ring. We also observed that Phe116 is located at an average distance of 5.0 Å from the aforementioned ring (Figure 3.8). This suggests that Arg176 and Phe116 are involved in strong cation- π and π -stacking interactions with the dihydro spiro compound, respectively.

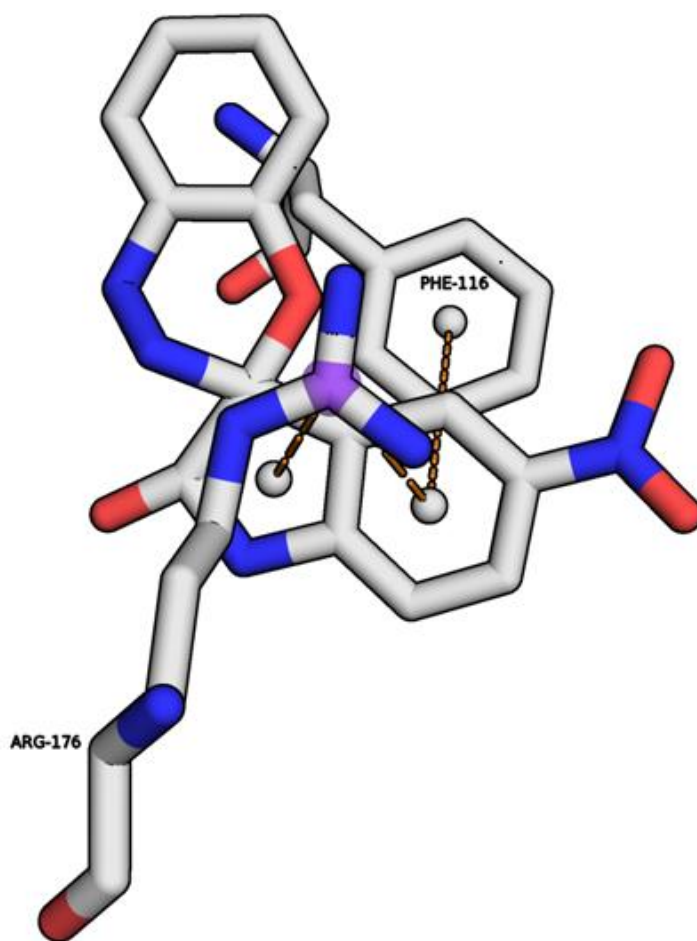


Figure 3.8: Cation- π and π -stacking interactions of Arg176 and Phe116 with the benzopyrrole-like ring of compound **3**. Residues are labeled with the 3-letter code and are colored by heteroatom. Orange dashed lines indicate the average distance between Arg176 (3.5 Å) and Phe116 (5.0 Å) with respect to the benzopyrrole-like ring of compound **3**.

3.3.4 Mutagenesis studies of the dihydro spiro binding pocket

We next performed mutagenesis studies to investigate the role of key residues in the dihydro spiro binding pocket. Superimposition of the adenosine bound structure with the cocrystal structure of compound **3**, shows that Arg176 and Gln172 orient themselves towards the dihydro spiro binding pocket (Figure 3.9). Point mutations of these residues

(Arg176L, Arg176A and Gln172P) were constructed to assess the relevance of these residues within the novel binding site. The Arg176L and Arg176A point mutants were constructed to mimic the corresponding hydrophobic residue in hAdoK while the Gln172P mutant was designed in light of our recent findings that show that this mutation confers resistant to Mtb against iodotubercidin, a well-known inhibitor of hAdoK and MtbAdoK (data not shown; manuscript in progress). As observed in Figure 3.10a-d, all dihydro spiro derivatives displayed a significant decrease in efficacy when compared to WT. In all cases, the MtbAdoK mutants exhibited higher than 40.0 % activity at the highest concentration tested of 200.0 μ M.

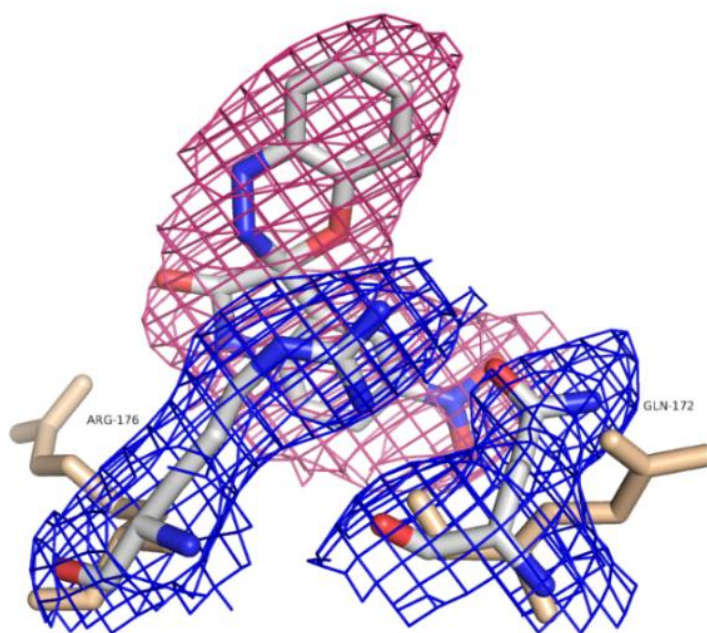


Figure 3.9: Orientation of Arg176 and Gln172 in the spiro binding pocket when compared to the adenosine bound MtbAdoK structure (PDB ID 2PKM). MtbAdoK-**3** residues are colored by heteroatom and MtbAdoK-adenosine residues are colored wheat. $2F_o-F_c$ maps contoured around Arg176, Gln172 and compound **3** are displayed at 1.5σ .

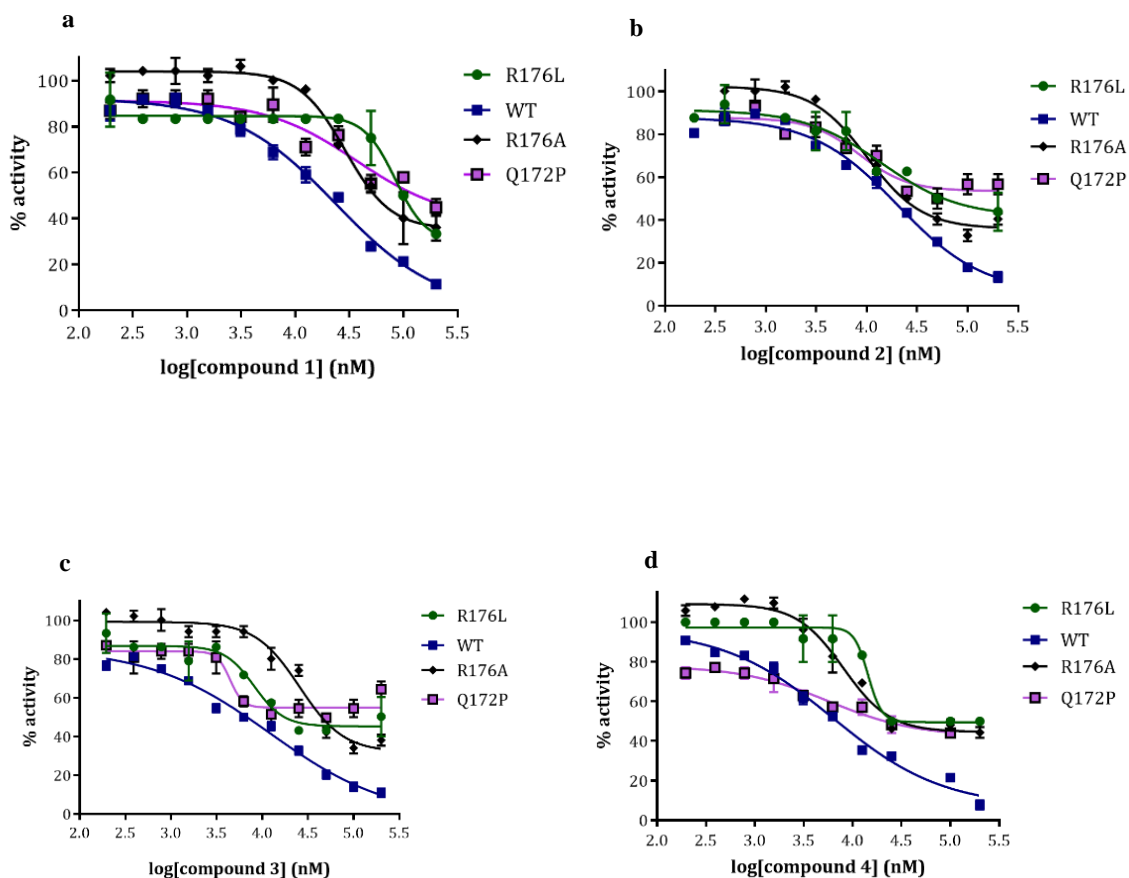


Figure 3.10: Dose response curves for MtbAdoK mutants. (a-d) All compounds were tested from 0-200 μ M. The data is normalized to the 0 μ M (DMSO) control, and the error bars represent the \pm SD of 2 independent experiments.

3.4 Discussion

Non-nucleoside uncompetitive inhibitors that modulate inhibition by exploiting the open conformation of MtbAdoK have never been reported. However, this type of inhibition has been observed for non-nucleoside inhibitors of hAdoK.²¹³ By definition, uncompetitive inhibitors do not compete with the substrate's binding pocket; they bind at

a distinct site.²²⁸ Crystallization attempts of the ternary enzyme-substrate-inhibitor complex have been unsuccessful. However, uncompetitive inhibitors that display no affinity against the free enzyme are very rare.²²⁹ Despite this, our mutagenesis and crystallographic experiments confirmed that the novel pocket where the compound is located is indeed the true binding site of the inhibitor. One of the advantages of uncompetitive inhibition is that high selectivity can be achieved against other enzymes that utilize adenosine as a substrate or share a similar reaction mechanism. When a biological process is inhibited, the first expected effect is an increase in the substrate(s) of the inhibited reaction. However, the downstream implications of this will largely vary depending on the mode of inhibition. If the inhibitor is competitive, increasing the concentration of substrate will eventually bypass inhibition. On the other hand, if the inhibitor is uncompetitive, increasing the concentration of substrate will only serve to potentiate the action of the inhibitor. Thus, increasing the accumulation of substrates, potentially leading to toxic and detrimental effects to the organism.²³⁰⁻²³¹

To our surprise, all inhibitors displayed sub-micromolar activity against Mtb mc²7000 strain. In addition, a trend can be observed when comparing the IC₅₀ and MIC₅₀ values of **1** with **2** and **3** with **4**. The lower activity values correspond to the lead hit compound **1** and compound **2**. In contrast, electron-withdrawing substituents at position 4 of the dihydro spiro compound, exemplified by compounds **2** and **4**; seem to potentiate the *in vivo* and *in vitro* activity. The *in vitro* potency can be rationalized by the extra interactions observed by the Br and NO₂ groups with the residues surrounding the substituents mentioned above. The fact that compound **2** was more potent in a dextrose-

supplemented media suggests that the most relevant molecular target within Mtb is an enzyme involved in carbohydrate metabolism. Purine and carbohydrate metabolism are linked via the pentose phosphate pathway by providing ribose-5-phosphate, one of the key substrates for nucleotide synthesis. Further biochemical and genetic studies will be needed to elucidate the type of mechanism that is utilized by Mtb to uptake this series of compounds and to identify the true molecular target(s) within Mtb. Along this line, Mtb mc²7000 resistant mutant isolation and CRISPR knockdowns of the *Rv2202c* gene are currently underway to shed some light in the true biological target.

Prior to microbatch crystallization, several thousand crystallization experiments were attempted under vapor diffusion methods. We were only able to obtain crystals utilizing the classical method of microbatch crystallization at 4.0 °C. It is very likely that the low temperature coupled with the slower diffusion rates observed under oil led to favorable conditions for nucleation and eventual crystal formation. Only one of the monomers in the asymmetric unit had clear density amenable for fitting the dihydro spiro compound. The occupancy issues can be attributed to the lack of solubility and the relatively low potency against the enzyme. Despite the lack of occupancy observed in chain B, the orientation of Arg176.B and Gln172.B are very similar to those of chain A. Both residues orient themselves towards the spiro binding pocket, suggesting that there is a dihydro spiro molecule, albeit at a lower occupancy. Our crystallization studies were performed utilizing a protein concentration of 18.0 mg/mL (~ 0.52 mM) and a compound concentration of 1.0 mM, corresponding to a 1.9X molar ratio. It has been suggested that to achieve full occupancy for compounds with low micromolar potency, a molar ratio of

5-10X should be used.²³² However, during our preliminary crystallization experiments, we observed that all of the dihydro spiro compounds precipitated at concentrations ≥ 1.25 mM in buffer; significantly hindering our crystallization efforts.

Closer inspection of the interactions at the dihydro spiro binding pocket indicates a high potential for structure-guided drug design. For example, positions C2, C3, and C5 can be modified to polar groups to make favorable hydrogen bonding interactions with Gln172, Gln173 and Arg176. Most notably is position 20 of the dihydro spiro compounds. This position overlaps with the NH₂ at position 6 of adenosine, suggesting that linking the adenine moiety to the compound might lead to a more potent bisubstrate-like inhibitor. One fundamental difference between hAdoK and MtbAdoK is that the latter is a functional dimer whereas the former is a monomer in solution. The dihydro spiro binding pocket is formed by residues from chain B and chain A of the MtbAdoK dimer. These unique interactions can be exploited through structure-guided drug design to achieve a higher degree of specificity and potency.

One of the most significant interactions is observed between Arg176 and the benzopyrrole-like ring of the compounds. This highly entropic and solvent-exposed residue was entirely oriented towards the dihydro spiro pocket. The orientation and proximity of Arg176 with respect to the benzopyrrole-like ring of the dihydro spiro compound suggest the possibility of strong cation- π interactions. It has been shown that cation- π interactions are prevalent in protein structures and that they play a vital role for several clinically relevant drugs such as varenicline (Chantix), ondansetron (Zofran) and granisetron (Kytril). Also, it has been observed that when an aromatic group is near a

cationic residue, the geometry is biased to the formation of favorable cation- π interactions.²³³⁻²³⁵ Our crystal structure suggests that the orientation and proximity of Phe116 with respect to the benzopyrrole-like ring might lead to the participation of π -stacking interactions. In the same fashion that Phe116 participates with π -stacking interactions with the adenine ring when adenosine is bound, and the closed conformation of MtbAdoK is adopted.

Our mutagenesis studies showed that Arg176 and Gln172 are key residues located in the dihydro spiro binding pocket. Unlike our MtbAdoK-dihydro spiro cocrystal structures, Arg176 is observed to be oriented towards the solvent in the MtbAdoK-adenosine structure, and Gln172 is oriented towards the adenine ring. It should be noted that the MtbAdoK mutants and hAdoK displayed a similar activity when tested against the dihydro spiro compounds. In both cases, the enzymes remained more than 40.0 % active at the highest concentrations tested of 200.0 μ M. This phenotype can be attributed to partial inhibition of the compounds against the MtbAdoK mutants and hAdoK. Possible experimental artifacts behind partial inhibition could be a lack of solubility of the compounds or lack of compound fidelity. However, if the lack of solubility would have been the source of the phenotype, then we would have expected to observe the same trend with the WT MtbAdoK. As far as compound fidelity goes, we have confirmed through LC-MS and NMR their integrity (data not shown). Taken together, the mutagenesis and selectivity studies validate the relevance of Arg176 and Gln172 within the novel binding site.

3.5 Conclusions and future work

In summary, our mechanistic, structural and mutagenesis studies show the selective inhibition of MtbAdoK by a series of novel non-nucleoside uncompetitive inhibitors. This type of inhibition has proven to be successful for several other clinically relevant molecular targets including inosine 5'-monophosphate, dihydrofolate reductase, topoisomerase I, and steroid 5 α -reductase.²²⁹ Uncompetitive inhibition offers a unique advantage over the more conventional competitive adenosine analogs and suggests that the discovery of highly specific, therapeutically relevant inhibitors of this enzyme might be achievable. Our crystallographic data provides the template for a structure-guided optimization of the compounds to achieve rationally designed bisubstrate-like inhibitors of MtbAdoK. Finally, further crystallization attempts are currently underway to determine the crystal structure of the enzyme-substrate-inhibitor ternary complex.

4. DISCOVERY, ENZYMATIC AND *IN CELLULO* CHARACTERIZATION OF NOVEL ALLOSTERIC INHIBITORS OF *MYCOBACTERIUM TUBERCULOSIS* BIOTIN PROTEIN LIGASE

4.1 Background and significance

Biotin is a crucial cofactor for lipid biosynthesis and lipid degradation within Mtb. The rise of resistance against current anti-TB drugs accentuates the necessity of new drugs and drug targets. Presently, most antibiotics target actively growing Mtb by inhibiting a metabolic process required for primary and progressive infection.²³⁶ Conversely, latent or dormant Mtb is harder to treat given that it possesses a highly complex mechanism to evade both the host's immune system and antibiotics.²³⁷ A potentially new strategy for tb treatment is to develop novel anti-mycobacterial drugs that are active against the primary and latent stages of Mtb infection.

Mtb possess the most complex and highly regulated lipid metabolism of any bacteria.¹⁸⁰ Mycobacteria contains examples of all known lipids and polyketide biosynthetic machineries including those found in plants, mammals, and other bacterial systems. In fact, whole-genome sequencing of Mtb led to the identification of ~ 250 distinct enzymes solely involved in lipid metabolism. This is in stark contrast with *E. coli*, which have ~ 50 enzymes.²³⁸ The first committed step in fatty acid biosynthesis is initiated through the carboxylation of acetyl-coenzyme A (CoA) to yield malonyl-CoA. This process is catalyzed by the multifunctional and multi-domain acyl CoA carboxylases

(ACCs).²³⁹ To be functionally active, the ACCs must be post-translationally biotinylated at the biotin-carboxylase carrier protein (BCCP) domain by a biotin protein ligase. Within Mtb, the sole enzyme responsible for the post-translational biotinylation of proteins is the biotin protein ligase (MtbBpL).²⁴⁰ Only when the ACC is biotinylated by MtbBpL, the biosynthesis of methyl-malonyl coenzyme A, malonyl-CoA, and the C22-C24 malonyl-CoA derivatives can proceed. These building blocks are then subsequently utilized for the biosynthesis of the complex and diverse lipids that are the hallmark of Mtb, including the C60-C90 mycolic acids.²⁴⁰ In addition to lipid biosynthesis, lipid catabolism is thought to be a critical aspect of Mtb's survival within the host. Several decades of evidence suggest that Mtb is lipolytic *in vivo* and derive most of its nutrients through the breakdown of host fatty acids.²⁴¹⁻²⁴³ Moreover, MtbBpL is involved in the biotinylation of the BCCP domain of pyruvate carboxylase. Pyruvate carboxylase is an enzyme that plays a key anaplerotic role in carbon metabolism. This enzyme channels oxaloacetate to phosphoenolpyruvate carboxykinase, a gluconeogenic enzyme that is essential for Mtb growth when lipids are used as the primary carbon source.²⁴⁴ Taken together, it is possible that MtbBpL is one of the few enzymes that globally regulates lipid metabolism making it an attractive drug target.

MtbBpL is monomeric enzyme encoded by the *birA* gene (*Rv3279c*) and forms part of the class I family of biotin protein ligases. Class I BpLs are characterized by the lack of a 60-residue long N-terminal helix-turn-helix DNA binding domain. Therefore, they can catalyze only post-translational biotin addition. Class II BpLs, like *E.coli* BpL, are bifunctional proteins. These enzymes are not only able to catalyze the post-

translational biotinylation of its protein substrates but can also act as a transcriptional repressor by interacting with the biotin operon through its helix-turn-helix N-terminal segment. Here, transcription regulation is mediated by the levels of intracellular biotin and apo-acyl CoA carboxylase. Several studies have shown that overexpression of BpL in *E.coli* lead to repression of the biotin operon whereas overexpression of apo ACC leads to the derepression of the operon.²⁴⁵⁻²⁴⁶

All biotin protein ligases, catalyze the highly specific ATP-dependent ligation of biotin to the BCCP domain of their protein substrates in two sequential steps. In step one, biotin protein ligase promotes the nucleophilic attack from the biotin carboxylate moiety to the α -phosphate of ATP yielding the reaction intermediate biotinyl-5'-AMP and pyrophosphate. In the second step, the enzyme ligates biotin to a conserved lysine residue located between the 'AMKM' sequence within the BCCP domain of the ACC (Figure-4.1).²⁴⁷

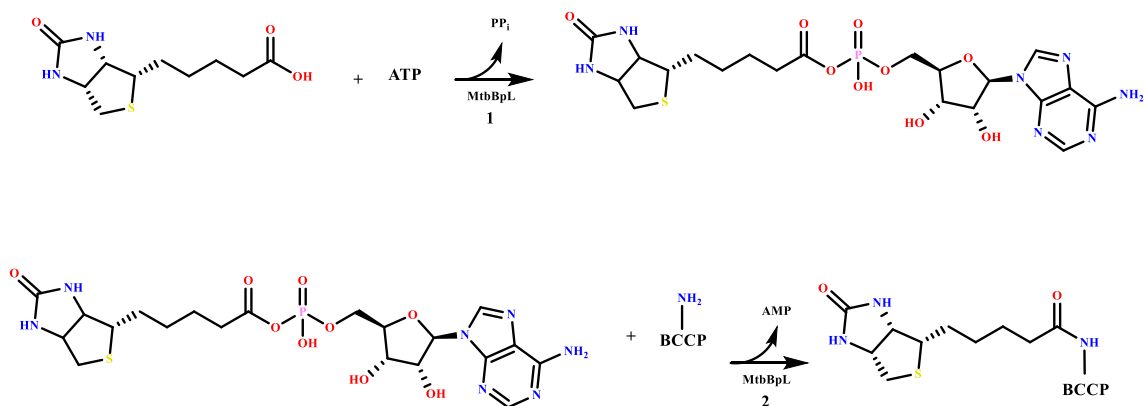


Figure 4.1: Enzymatic reaction catalyzed by MtbBpL. The first half-reaction (1) yields the biotinyl-AMP intermediate. The second half reaction (2) involves the transfer of the biotin moiety to a conserved lysine residue of the acceptor protein located in the BCCP domain.

The structure of MtbBpL has been solved at high-resolution without substrate (Figure 4.2a) and with the reaction intermediate biotinyl-5'-AMP (Figure 4.2b) at 1.8 Å and 1.7 Å resolutions respectively.²⁴⁸⁻²⁴⁹ The protein consists of a large N-terminal domain (residues 1-217) and a smaller SH3-like C-terminal domain (residues 218-266). The core of the protein, located in the N-terminal domain, consists of seven β -strands that are flanked by five α -helices. The ligand-binding pocket is formed by loop residues Gln63, Thr39, Ser38, Arg67, Arg69, Arg72, Ala75 and core region residues Lys138, Asn130, Asn158, and Gln81. Catalytic base lysine 138 promotes the nucleophilic attack of the α -phosphate of ATP from the carboxylate group of biotin moiety. Finally, loop residues 63-77, 162-171 have been noted to transition from disordered to ordered upon substrate or inhibitor binding.¹⁹⁶

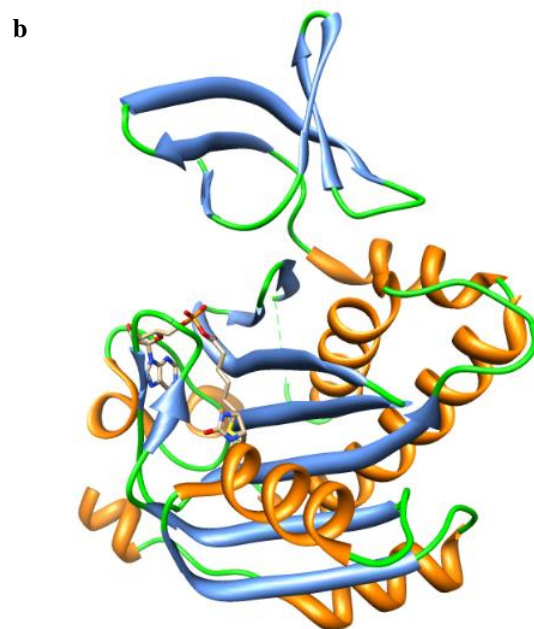
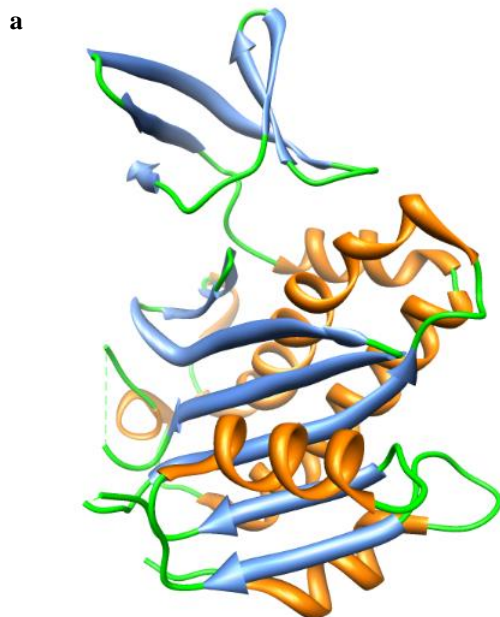


Figure 4.2: MtbBpL structure. (a) Apo MtbBpL (PDB ID 2CGH). (b) MtbBpL complex to biotinyl-AMP (PDB ID 4OP0). In both cases, the structures are colored by secondary structure.

Several biochemical and genetic studies have shown the essentiality on BpLs in known bacterial pathogens such as *Streptococcus pneumoniae*, *Staphylococcus aureus*, *Escherichia coli* and *Mycobacterium tuberculosis*.²⁵⁰ All of these studies have two aspects in common: the lack of an alternative pathway for protein biotinylation within these organisms and the importance of this post-translational modification for lipid metabolism. One of the most potent inhibitors of MtbBpL to date was described by Duckworth *et al.* 2011.²⁴⁷ Several key observations can be made about this work: I) The biotinyl-AMP analog (Bio-AMS) has sub-nanomolar potency against the enzyme displaying a $K_i \sim 530$ pM, II) this inhibitor also displays sub-micromolar potency against several MDR and XDR strains of Mtb, III) that there is a dose-dependent decrease in global biotinylation levels in lysates of Mtb H37Rv when incubated with Bio-AMS, IV) the authors also showed that *Mycobacterium smegmatis* is unable to form colonies when the *birA* gene is deleted and V) that there is an increase in tolerance of Bio-AMS in Mtb strains that overexpressed BpL. It should be noted, however, that the *in vitro* activity of Bio-AMS was not assessed against human BpL (hBpL) and that some cytotoxicity was indeed observed in Vero cells; indicating a potential lack of selectivity for the compound.

In this work, we describe the identification, enzymatic, *in cellulo* and kinetic characterization of a series of bromo-benzylidene-fluorobenzohydrazides. Our enzymatic and *in cellulo* studies showed that the compounds displayed low-micromolar potencies against the enzyme and mc²7000 and no cytotoxicity against HDF cells. Finally, our kinetic studies revealed a novel noncompetitive mechanism of inhibition, suggesting the presence of a previously unknown allosteric site within MtbBpL.

4.2 Material and methods

4.2.1 Cloning, expression and purification of MtbBpL

The MtbBpL gene (*Rv3279c*) was amplified by polymerase chain reaction from total genomic DNA of *Mycobacterium tuberculosis* H37Rv. The following oligonucleotides were used: 5' - TACTTCCAATCCAATGCCGTGACCGACCGC - 3' and 5' - TTATCCACTTCCAATGTTATTAACGCAAATGCACCACGTCG - 3'. The amplified fragment was cloned into the ligation independent vector pmcsg-7 containing an N-terminal cleavable His-tag. Gene fidelity was confirmed by DNA sequencing. Following ligation, the plasmid was transformed into *E.coli* BL21 (DE3) for expression. A nickel affinity column was then utilized to purify recombinant MtbBpL. Purification buffers A and B contained, 50.0 mM HEPES, pH 7.5, containing 500.0 mM NaCl, 500.0 mM imidazole (buffer B only) and 5.0 % glycerol. The His-tag was then removed by dialyzing the protein in 20.0 mM Tris-HCl, pH 8.0, 50.0 mM NaCl, 5.0 % glycerol, and 4.0 mM DTT with tobacco etch virus (TEV) protease. The TEV and tag were then separated from MtbBpL by passing the dialyzed sample through another round of nickel affinity column. Finally, Mtb was dialyzed one more time in 20.0 mM HEPES, pH 7.5, 50.0 mM NaCl, 2.0 mM DTT and 5.0 % glycerol. The protein was then aliquoted and stored in -80.0 °C for subsequent assays and crystallization trials.

4.2.2 DSF high-throughput screening assay

The primary high-throughput screening assay of our in-house compound libraries was the thermal shift assay described by Niesen *et al.* 2007 and was performed in the same fashion as outlined in section 3.2.2 of this dissertation. In short, the samples contained a

final concentration of MtbBpL of 3.0 μM , 100.0 mM HEPES pH 7.5, 50.0 μM of screening compound dissolved in 100.0 % DMSO and a final concentration of 5X of SYPRO ORANGE[®] dye. Reaction volume across the 96-well PCR plate was 20.0 μL . Positive and negative control reactions were carried out similarly but using biotin and buffer respectively. After sample preparation, the 96-well plate was covered with an UltraClear film (Axygen Scientific). The assay was then performed on Agilent Technologies Mx3005P qPCR system by using a temperature gradient of 25.0° - 99.0°C at 0.5 °C / min and monitoring the fluorescence emission of the SYPRO ORANGE[®] (excitation = 492.0 nm, emission = 610.0 nm).

4.2.3 IC_{50} and steady-state kinetics determination

MtbBpL was assayed against the primary screen hits compounds using the 7-methylthioguanosine (MESG)-hydroxamate coupled enzyme assay system as described in Duckworth *et al.* 2011 and Wilson *et al.*²⁵¹ The compounds were preincubated for five minutes in a master mix containing 250.0 nM MtbBpL, 50.0 mM Tris-HCl pH 8.5, 5.0 mM MgCl_2 , 2.5 mM ATP, 200.0 μM MESG, 150.0 mM hydroxylamine 1.0 mM DTT, 1.0 U/mL of purine nucleoside phosphorylase and 0.5 U/mL of pyrophosphatase. The reaction was started by the addition of biotin at a final concentration of 250.0 μM . The reactions were performed in 96-well UVStar plates (Greiner Bio-one), and the formation of MESG was monitored at 360 nm in a Varioskan[™] Lux multi-mode plate reader. IC_{50} values for each compound were determined by varying the concentration of inhibitor at a fixed concentration of enzyme and by fitting the dose response data into the four-parameter logistic curve (Equation 4.1) model of GraphPad prism 7.02, as follows:

$$Y = Y_{min} + (Y_{max} - Y_{min}) / (1 + 10^{(logIC_{50} - I)H}) \quad (4.1)$$

Where I is the logarithm of inhibitor concentration, H is the Hill slope and Y, Y_{max} and Y_{min} are the absorbance, maximum absorbance and minimum absorbance, respectively. Kinetic assays for MtbBpL were performed essentially as described above with the following exception: the reaction was started by the addition of varying concentrations of biotin in the presence of constant concentrations of test compound (0.0 μM, 5.0 μM and 10.0 μM). Kinetic data was obtained by fitting the initial velocity data into GraphPad Prism 7.02 nonlinear regression function of Michaelis-Menten model (Equation 4.2), as follows:

$$V_o = (Y_{max})[S] / (K_m + [S]) \quad (4.2)$$

Where V_o is the initial velocity, Y_{max} is the maximum absorbance, S is the substrate concentration, and K_m is the Michaelis-Menten constant.

4.2.4 Antitubercular assay

Antitubercular testing and MIC₅₀ determination was performed using the MABA assay in a 96-well format as previously described.²⁰⁶⁻²⁰⁷ Starter culture of Mtb mc²7000 was grown in 7H9 media supplemented with OADC (Middlebrook), 0.5 % dextrose, 0.085 % NaCl, 0.05 % Tyloxapol (Sigma), 0.25 μg/mL malachite green (Sigma) and 25.0 μg/mL pantothenate. Once cells reached an optical density of OD₆₀₀ ~1.0, cells were diluted to an OD₆₀₀ of 0.01 in the same media composition without OADC. For acetate-supplemented media, once cells reached the aforementioned OD₆₀₀, cells were diluted to an OD₆₀₀ of 0.01 in 0.5 % sodium acetate (Sigma), 2.0 mM MgSO₄ (Sigma), 0.1 mM CaCl₂ (Sigma),

0.05 % Tyloxapol, 0.25 $\mu\text{g}/\text{mL}$ malachite green and 25.0 $\mu\text{g}/\text{mL}$ pantothenate. Compounds were serially diluted in 100.0 % DMSO and added to the cells to a final concentration of DMSO of 2.5 %. Plates were incubated for 10 days (30 days for acetate-supplemented media) prior to staining with resazurin (Sigma). After staining, plates were incubated for 2 additional days (7 additional days for acetate-supplemented media) for developing. Finally, developed plates were read using a POLARstar Omega spectrophotometer (BMG Labtech) and by monitoring the fluorescence emission of resazurin (excitation = 570.0 nm, emission = 585.0 nm). In all cases, rifampicin was used as a negative control and the experiments were performed in duplicates were the reported error represents plus or minus standard deviation.

4.2.5 Human dermal fibroblast cytotoxicity assay

Human dermal fibroblasts (HDF) were purchased from ATCC (Manassas, VA). HDF cells were cultured in DMEM (Lonza) media supplemented with 10 % fetal bovine serum (Lonza) and penicillin/streptomycin (Lonza). For the cytotoxicity assay, compound stocks were serially diluted in phosphate-buffered saline (PBS) and 10.0 % DMSO. On the day of assay, HDF cells were trypsinized, counted and resuspended at a concentration of 64,000 cells/ml in media. Cells were plated, overlaid with the compound serial dilutions and incubated at 37.0 °C. After 48 h, resazurin dye was added and the assay plates cultured for another 24 h. The next day the absorbance of the resazurin was measured on a microplate reader to assess cell death. Cytotoxicity was determined as a percent of dead cells versus living.

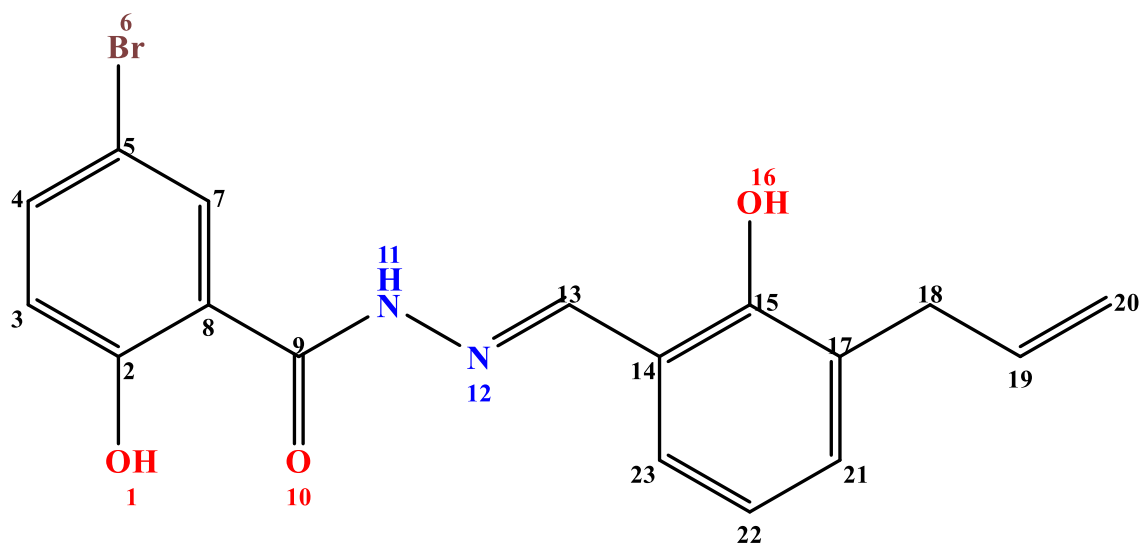
4.3 Results and discussion

As in the case of section 2, a total of 2,534 compounds from our in-house collection of whole cell active compounds was screened by DSF at a single concentration of 50.0 μ M. Hits were identified as compounds that had a thermal shift equal or greater than the positive control.

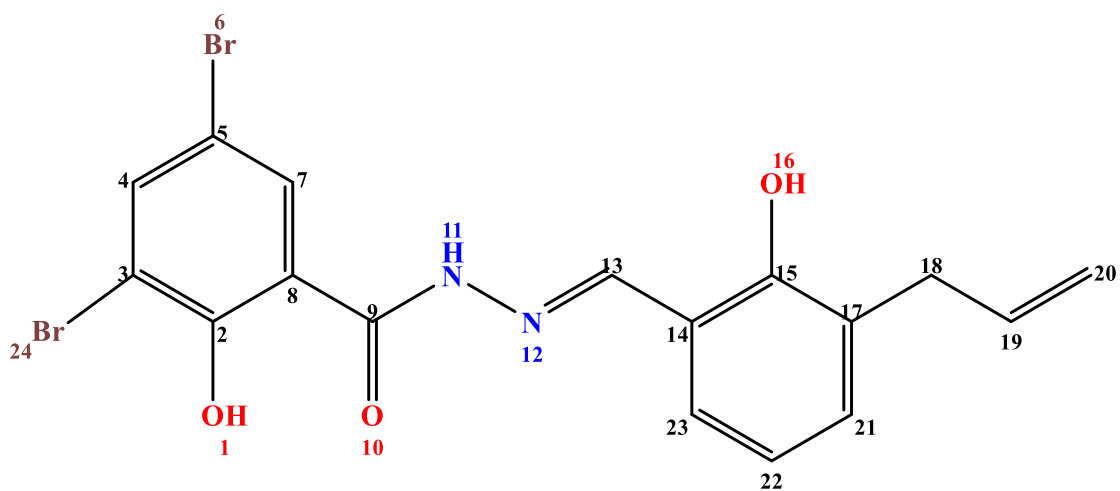
Table 4.1: DSF data for lead compound **1**.

Average T_m of positive control ($^{\circ}$C)	Average T_m of negative control ($^{\circ}$C)	MtbBpL-1 T_m ($^{\circ}$C)	ΔT_m ($^{\circ}$C)
59.00	57.13	59.00	3.02

Lead compound **1** was the only compound identified to have a thermal shift equal to that of the positive control (Figure 4.3 and Table 4.1). Based on the DSF results, we purchased several analogs (**2**, **3** and **4**) to perform structural activity relationship studies (SAR) and tested enzymatically against MtbBpL.



1



2

Figure 4.3: Structure and numbering convention of lead compound (1) and analogs (2-4).

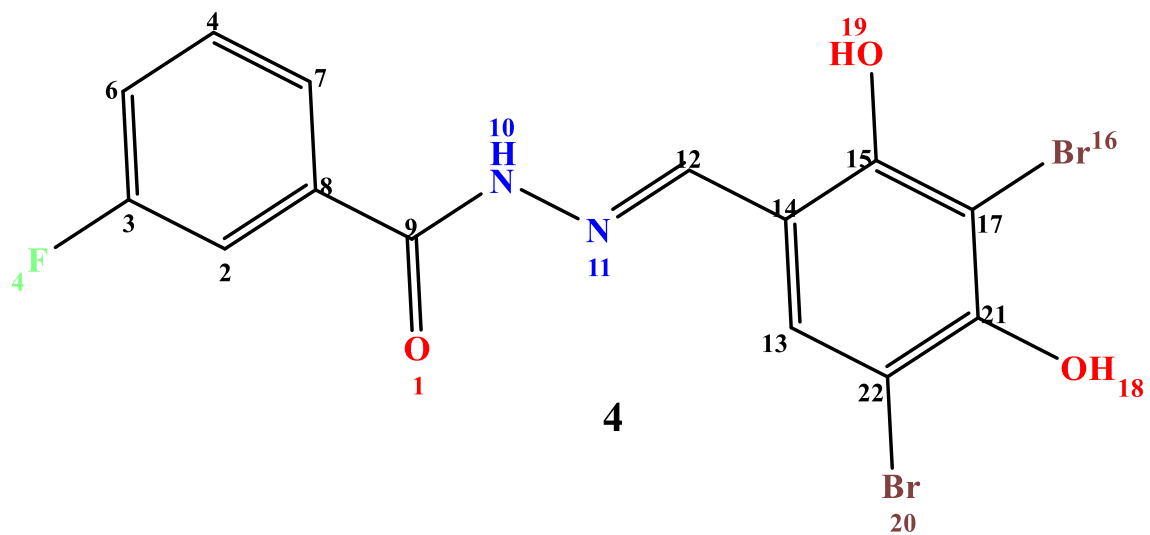
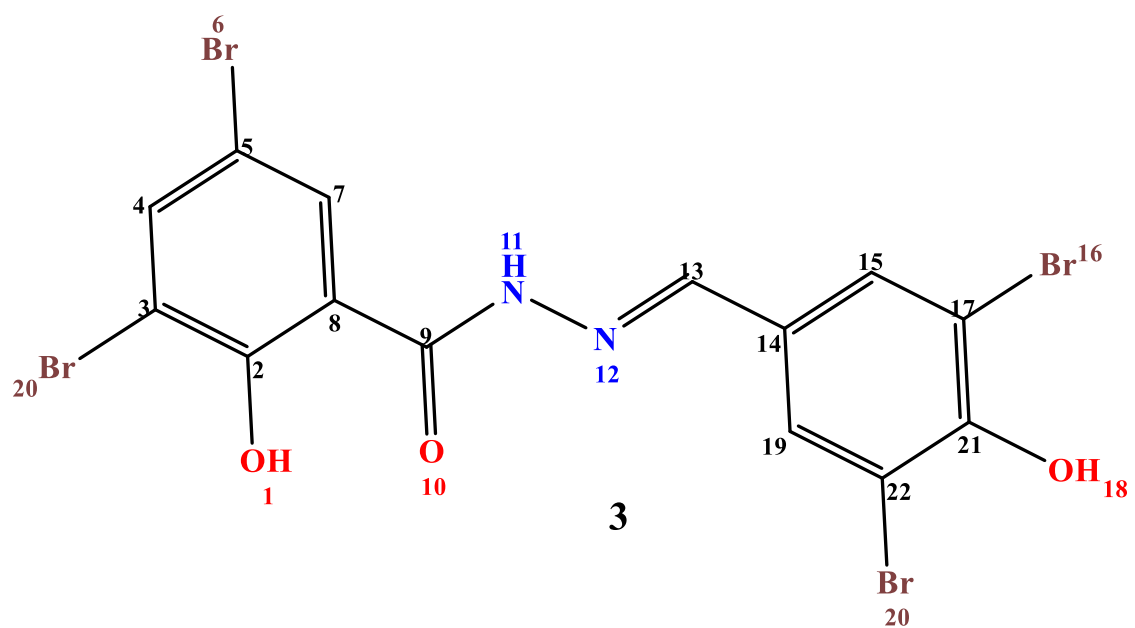


Figure 4.3: Continued

Table 4.2: Enzymatic characterization of compounds.

ID	MtbBpL IC ₅₀ (μ M)
1	≥ 75.0
2	23.0 ± 3.0
3	11.4 ± 2.3
4	9.4 ± 1.6

Error is reported as \pm SD of 2 independent experiments.

The compounds exhibited 50.0 % inhibitory concentrations between 75.0-9.4 μ M (Table 4.2). The only difference between compounds **1** and **2** is the addition of a bromide group at position 3. Surprisingly, this extra substitution was enough to increase potency ~ 3-fold. Thus, indicating that electron withdrawing groups at position 3 might be favorable. Compound **3** has several similarities and some key differences when compared to compound **2**. Compound **3** retains the same 3,5-dibromo-2-hydroxybenzohydrazide moiety. However, the allyl group at position 17 is substituted for bromine, and the hydroxyl group at position 15 is moved to position 21. Also, compound **3** has another bromine group at position 22. Taken together, the chemistry based SAR suggests that increasing the polarity of the hydroxybenzylidene moiety is favorable as indicated by the increase in potency. At this point, it is difficult to rationally explain what substitution (or a combination of substitutions) conferred the increase in potency when comparing compound **2** with **3**. The reason being that several substitutions were made concomitantly as opposed to a more systematic approach. Current medicinal chemistry efforts are underway to discern this issue. Finally, compound **4** possess the same 3,5-dibromo-2-hydroxybenzylidene group as **3** with the addition of the “original” hydroxyl group at

position 15 as observed in compounds **1** and **2**. The main difference is observed with the benzohydrazide. Here, the bromides and the hydroxyl group are absent with the concomitant addition of the more electronegative fluoride group at position 3. The relative increase in potency of **4** when compared to **3**, suggests that the groups mentioned above might not be optimal. In summary, the preliminary chemistry-based SAR suggests that electronegative groups at position 3 might be optimal at this position as observed with **1**, **2** and **3**. In addition, the initial SAR also suggests that a greater degree of polarity regarding substitutions on the benzylidene moiety are favorable as well.

We next sought to determine the antimycobacterial and cytotoxic activity of the compounds against mc²7000 and HDF cells, respectively. Initial testing against Mtb was carried out in 0.2 % acetate-supplemented M9 media to mimic fatty acid-driven metabolism and in 0.2 % dextrose-supplemented 7H9 media to mimic a carbohydrate-driven metabolism. All compounds displayed inhibitory activity against our Mtb strain (Table 4.3). Surprisingly, lead compound **1** displayed nanomolar potency when glucose was utilized as the sole carbon source with a MIC₅₀ of ~ 230 nM. In contrast, when acetate was utilized as the sole carbon source, the MIC₅₀ was significantly higher (3.2 μM). Compound **2** was the second most potent compound with MIC₅₀'s of 1.8 μM and 5.9 μM in dextrose and acetate, respectively. Next in potency was compound **4** with MIC₅₀'s of 10.1 μM and 8.9 μM in dextrose and acetate, respectively. Finally, the least potent was compound **3**, displaying MIC₅₀'s of 30.3 μM and 53.1 μM in dextrose and acetate, respectively.

The only difference between compounds **1** and **2** is the extra bromide group at position 3 of the benzohydrazide moiety. This modification makes compound **2** more polar than compound **1**. In addition to the overall lack of polar and halogenic substituents, another major difference when comparing compounds **1** and **2** with compounds **3** and **4** is the absence of the ally group. It is possible that the allyl group might facilitate uptake or diffusion through the highly hydrophobic mycobacterial cell wall while proving to be a barrier against the more polar compounds **3** and **4**. The fact that all compounds displayed activity in both carbon sources suggest that the molecular targets (s) are active when tb catabolizes carbohydrates and lipids, which could prove to be pharmacologically relevant. Further biochemical and genetic studies will be needed to elucidate the type of mechanism that is utilized by Mtb to uptake this series of compounds and to identify the true molecular target(s). Along this line, Mtb mc²7000 resistant mutant isolation and CRISPR knockdowns of the *Rv3279c* MtbBpL gene are currently underway to shed some light in the biological target. Finally, as observed in Table 4.3, the compounds displayed no cytotoxicity against HDF cells.

Table 4.3: Antimycobacterial and cytotoxic profile of compounds

ID	MIC₅₀-mc²7000 in dextrose (μM)	MIC₅₀-mc²7000 in acetate (μM)	CC₅₀-HDF cells (μM)
1	0.23 ± 0.04	3.2 ± 0.1	n/a
2	1.8 ± 0.3	5.9 ± 0.3	n/a
3	30.3 ± 1.6	53.1 ± 3.3	n/a
4	10.1 ± 0.4	8.9 ± 0.4	n/a

Error is reported as ± SD of 2 independent experiments.

^aNot applicable; no cytotoxicity detected.

Given that the compounds are not structural analogs of MtbBpL's cognate substrates (biotin and ATP), we decided to investigate the mechanism of inhibition of the compounds. As a representative of the group, we evaluated the mechanism of inhibition of compound **4** against MtbBpL. As observed in Table 4.4, increasing the concentration of substrate in the presence of fixed inhibitor concentrations; results in an increase of the K_m with a concomitant decrease of the initial velocity values; consistent with noncompetitive inhibition. Moreover, the Lineweaver-Burk plot shows a series of lines that intersect each other at a point that is not the y-axis but is above the x-axis (Figure 4.4).

Table 4.4: Steady-state kinetic parameters for compound **4**.

[4] μM	K_m (μM)	V_{max} ($\Delta\text{abs}/\text{time}$)
0.0	1.17 ± 0.04	0.21 ± 0.001
5.0	1.87 ± 0.34	0.01 ± 0.006
10.0	5.99 ± 0.06	0.007 ± 0.06

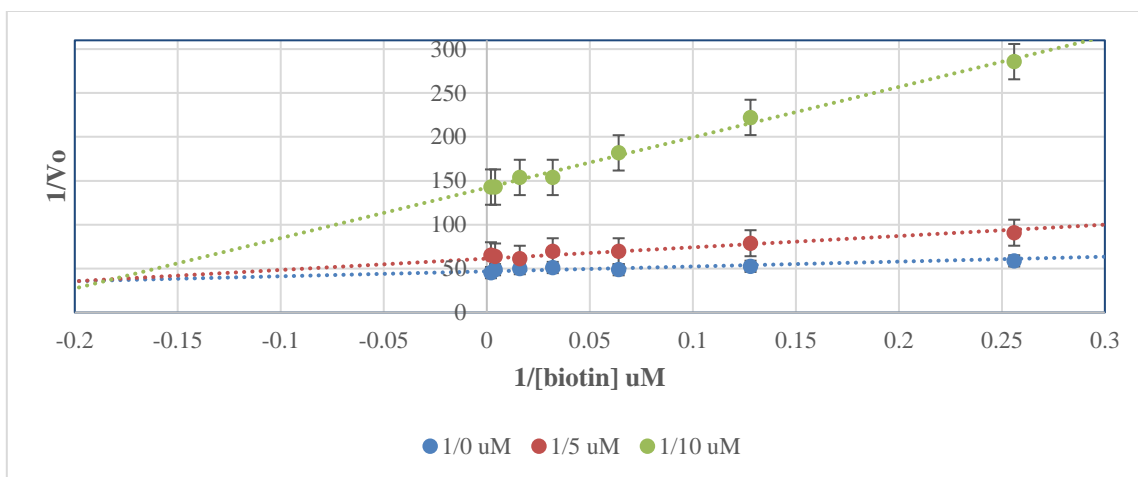


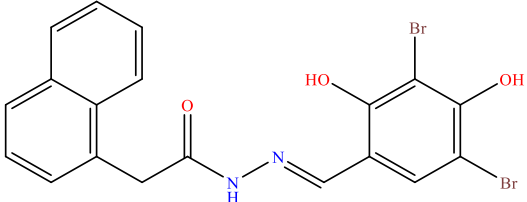
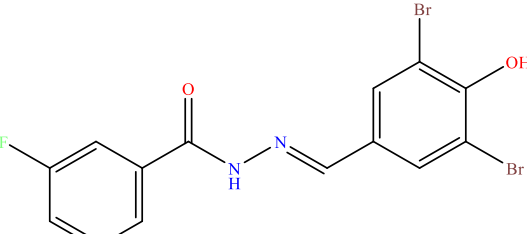
Figure 4.4: Lineweaver-Burk plot of compound **4** vs. biotin. Initial velocity data was transformed to linear analysis to evaluate inhibitor type. The error bars represent \pm SD of 3 experiments.

By definition, a noncompetitive inhibition refers to a type of inhibitor that displays affinity for the free enzyme and enzyme-substrate complex.^{229, 252} As mentioned above, the series of lines intercept each other at a point above the x-axis. This suggests that the inhibitor displays a higher degree of affinity for the free enzyme. In the case the inhibitor exhibits equal affinity towards the free enzyme and the enzyme-substrate complex, the lines would intercept at the X-axis. Finally, if the inhibitor shows a greater affinity for the enzyme-substrate complex, the series of lines would intercept below the X-axis.^{229, 252} To determine the binding affinity of the inhibitor towards the free enzyme and the enzyme-substrate complex, isothermal titration calorimetry experiments are currently being performed. Just like uncompetitive inhibition, noncompetitive inhibition cannot be overcome by increasing the concentration of substrate. Thus, offering a physiologically relevant advantage. Also, it should be noted that all noncompetitive inhibitors are in fact

allosteric inhibitors. Allosteric inhibitors offer the possibility of a higher degree of selectivity when taking into account other enzymes that might utilize the same substrate or a similar reaction mechanism. This, in turn, might translate into a drug with a clinically advantageous lesser degree of toxicity given that the pocket where it binds is unique to the drug target.^{229, 252}

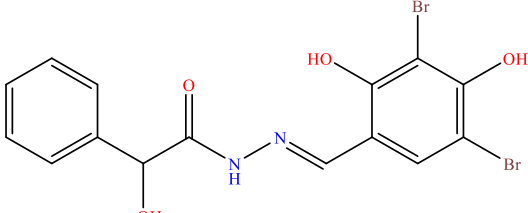
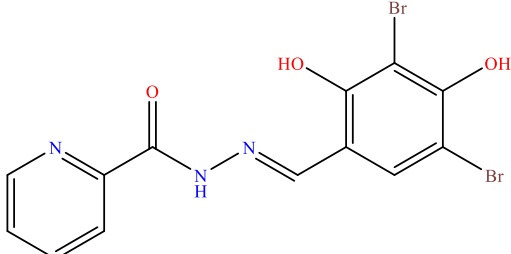
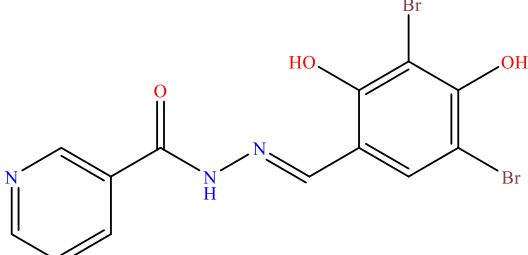
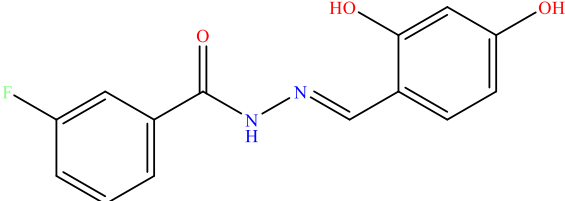
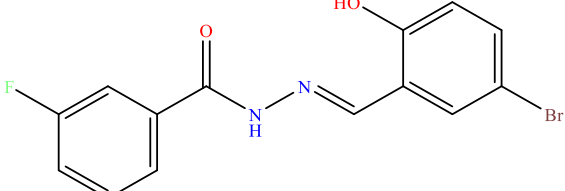
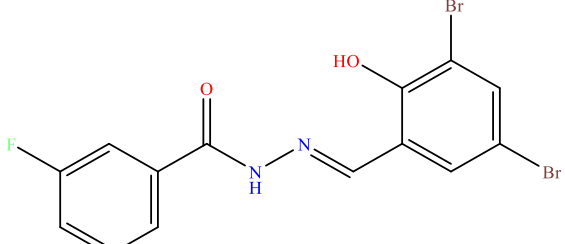
To further explore the chemical space surrounding the binding pocket of the novel noncompetitive inhibitors, we purchased several analogs of compound **4**. All of the compounds were assessed for binding via DSF and were also tested against the enzyme (Table 4.5).

Table 4.5: Binding and enzymatic characterization of analogs of compound **4**.

ID	IC ₅₀ (μM)	*T _m (°C)	Structure
5	2.3	57.0	
6	2.8	56.3	

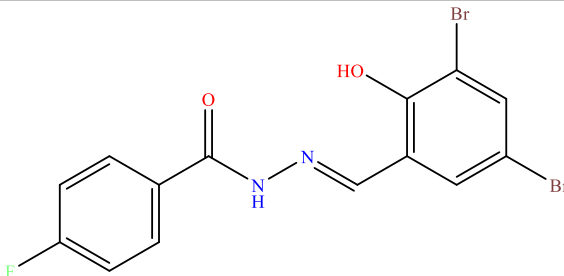
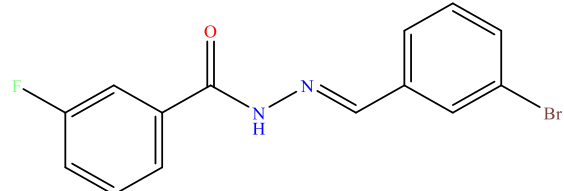
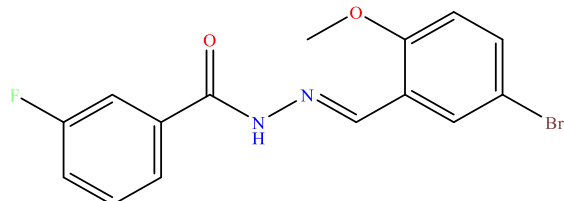
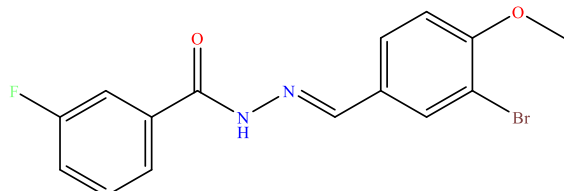
*T_m biotin control = 56.0 °C; T_m lead compound **1** = 56.7 °C; T_m compound **4** = 57.2 °C; T_m DMSO control = 54.3 °C

Table 4.5: Continued

ID	IC ₅₀ (μM)	*T _m (°C)	Structure
7	4.1	56.3	
8	5.8	56.0	
9	9.1	56.1	
10	14.8	55.9	
11	≥ 75.0	54.6	
12	≥ 75.0	55.9	

*T_m biotin control = 56.0 °C; T_m lead compound **1** = 56.7 °C; T_m compound **4** = 57.2 °C; T_m DMSO control = 54.3 °C

Table 4.5: Continued

ID	IC ₅₀ (μM)	*T _m (°C)	Structure
13	≥ 200.0	54.9	
14	≥ 200.0	54.3	
15	no inhibition	54.4	
16	no inhibition	54.9	

*T_m biotin control = 56.0 °C; T_m lead compound **1** = 56.7 °C; T_m compound **4** = 57.2 °C; T_m DMSO control = 54.3 °C

As observed in Table 4.5 there is almost a 1:1 relationship between binding, as measured by T_m shift when compared to controls, and potency. Compounds that displayed IC₅₀ values of ≤ 10.0 μM exhibited the highest change in T_m. In fact, the most potent analog, compound **5**, displayed a higher T_m (57.0 °C) than the biotin control itself (T_m = 56.0 °C). In comparison, the apo MtbBpL presented the lowest T_m of ~ 54.0 °C. Although we observed a 1:1 relationship with these compounds, one must never assume that binding

equals potency. For example, lead compound **1** displayed a T_m of 56.7 °C with an $IC_{50} \sim 75.0 \mu\text{M}$ when tested against MtbBpL.

As in the case of compounds **1-4**, it is difficult to identify the true pharmacophoric properties of the compounds. At this point, we have not performed a systematic SAR through chemistry. Rather it has been through compound availability and similarity within commercially available compound libraries. Nevertheless, we can generally group the compounds in 3 categories, those that displayed potencies of $\sim 2-5 \mu\text{M}$ (compounds **5-8**), those that displayed potencies between $\sim 10-15 \mu\text{M}$ (compounds **9-10**) and those that displayed little to no potency (compounds **11-16**). One can also observe that the moiety that is most different across all the compounds is the benzylidene side. This suggests that the benzylidene part and the positions of the substitutions within the benzene ring dictate the observed potency. Although we cannot discard that the benzohydrazide moiety is involved in protein contacts. Another possibility is that under aqueous or acidic conditions, the compound dissociates into the corresponding benzohydrazide and benzaldehyde. Here, the small fragments can then behave as independent molecules thus interacting with the protein in unexpected ways and possibly binding in small and previously unidentified pockets. It should be noted, that preliminary crystallization trials with the enzyme-inhibitor and the enzyme-inhibitor-substrate complexes have yielded a greater amount of crystals within a pH range of 5-6.5 which might trigger dissociation of the compounds. Unfortunately, the crystals are suboptimal for data collection. We are in the process of optimizing the hits for high-resolution x-ray diffraction data collection.

4.4 Conclusions and future work

In summary, HTS screening led to the identification series of benzylidene-benzohydrazides that act as inhibitors of MtbBpL. The preliminary SAR studies suggest that electronegative groups at position 3 and polar substations on the benzylidene moiety are favorable for inhibition. The antimycobacterial assay showed that the compounds are active in different carbon sources which might prove to be pharmacologically relevant. Also, the studies with HDF cells demonstrated a lack of cytotoxicity, a desirable characteristic from a drug discovery point of view. To our surprise, steady-state kinetic experiments showed that the compounds are noncompetitive inhibitors of the enzyme. This suggests the possibility of a previously unknown allosteric site within the essential Mtb protein that can be exploited through rational drug design. Our preliminary structural activity studies with several analogs of compound **4** suggest that the pharmacophoric properties of the compounds lie on the benzylidene moiety. With this in mind, crystallographic efforts are currently underway to determine the binary or ternary complexes and the location the potential allosteric site. Finally we are also in the process of performing isothermal titration calorimetry studies to characterize the different binding affinities that the compound might display for the free enzyme and the enzyme-substrate complex.

5. CONCLUSIONS

As conventional first and second-line anti-tubercular drugs become less effective due to the rapid emergence of MDR and XDR Mtb; there is a need for the development of more potent and specific drugs with new molecular targets and mode of actions. In this dissertation, we report the discovery and biochemical and biophysical characterization of novel inhibitors with different inhibition modalities against essential enzymes of Mtb.

In section 2 we utilized a structure-guided approach for the rational design of very potent compounds as competitive inhibitors of MtbAdoK. Here we utilized several preliminary structures, to guide the synthesis of a series of 6-substituted adenosine analogs. Enzymatic characterization showed that the compounds were specific to MtbAdoK when compared to the human counterpart. *In cellulo* studies revealed that the majority of the compounds displayed some activity against the mc²7000 Mtb strain with little to no activity against HDF cells. Also, further crystallization trials with the very potent compounds showed that the high potency and selectivity is predominantly attributed to the presence of unique chimney-like cavity within the MtbAdoK homodimer. This newly discovered compound-induced cavity can be utilized as a canvas for future structure-guided drug design efforts.

Section 3 of this dissertation describes the discovery, enzymatic and structural characterization a new series of dihydro spiro compounds that act as uncompetitive inhibitors of MtbAdoK. As opposed to section 2, where we utilized a structure-guided

approach, here we used an HTS approach to the identification of the inhibitors. Once the lead compound was identified, several other analogs were purchased and characterized enzymatically and *in cellulo*. These studies revealed that the compounds had low micromolar activity against the enzyme and sub-micromolar activity against our Mtb strain. In addition, steady-state kinetic experiments demonstrated that the novel dihydro spiro compounds acted as uncompetitive inhibitors of MtbAdoK. Thus, revealing a previously unknown family of non-nucleoside inhibitors and a novel inhibition modality of MtbAdoK. Although we have not been able to crystallize the enzyme-substrate complex successfully, we were able to crystallize most of the compounds in complex to the free enzyme. Further characterization through directed mutagenesis of the new binding pocket revealed that the location where the compounds bind is indeed the true dihydro spiro binding pocket. Taken together, this novel inhibitor type opens up a new route of structure-guided drug design. With this in mind, we are currently exploring the possibility of bridging the gap between the dihydro spiro binding pocket and the substrate binding site.

Lastly, in section 4 we explored the possibility of MtbBpL as a drug target. MtbBpL is the sole enzyme responsible for post-translational biotinylation of essential enzymes of Mtb; enzymes that are required in the *de novo* synthesis of lipids and for Mtb's survival under a lipid-based carbon source. As in the case of section 3, we utilized an HTS approach for the discovery of a series of benzylidene-benzohydrazides. Once the lead compound was identified, several analogs were purchased. Preliminary chemistry based SAR showed that polar substituents at the benzylidene moiety are optimal for inhibition. Whereas, electron withdrawing groups at position 3 of the benzohydrazide displayed

favorable inhibitory activity against the enzyme. Our whole-cell activity characterization showed that the compounds had no cytotoxic activity against HDF cells. In contrast, the compounds displayed inhibitory activity in dextrose and in acetate when utilized as unique carbon sources. Finally, our kinetic experiments showed that these inhibitors act as noncompetitive inhibitors against of the enzyme. Thus, suggesting the presence of previously unknown allosteric site within MtbBpL.

Taken together, the work presented in this dissertation focuses on the discovery and characterization of new drugs against two essential enzymes of *Mycobacterium tuberculosis*. Emerging evidence suggests that MtbAdoK might play a crucial role for tb during its latent phase of infection whereas MtbBpL might be one of the few enzymes that globally regulates lipid anabolism and catabolism. Here, we utilized a combination of biochemical and biophysical studies to identify unique inhibitors with novel mechanisms of action against the essential enzymes. The structural studies coupled to the novel inhibitors identified in this work pave the way for the design of more potent and specific inhibitors of the proteins.

REFERENCES

1. Hayman, J., *Mycobacterium ulcerans*: An infection from Jurassic time? *The Lancet* **1984**, 324 (8410), 1015-1016.
2. Kapur, V.; Whittam, T. S.; Musser, J. M., Is *Mycobacterium tuberculosis* 15,000 Years Old? *The Journal of Infectious Diseases* **1994**, 170 (5), 1348-1349.
3. Brosch, R.; Gordon, S. V.; Marmiesse, M.; Brodin, P.; Buchrieser, C.; Eiglmeier, K.; Garnier, T.; Gutierrez, C.; Hewinson, G.; Kremer, K.; Parsons, L. M.; Pym, A. S.; Samper, S.; van Soolingen, D.; Cole, S. T., A new evolutionary scenario for the *Mycobacterium tuberculosis* complex. *Proceedings of the National Academy of Sciences* **2002**, 99 (6), 3684-3689.
4. Cave, A. J. E.; Demonstrator, A., The evidence for the incidence of tuberculosis in ancient Egypt. *British Journal of Tuberculosis* **1939**, 33 (3), 142-152.
5. Freund, J., The story of clinical pulmonary tuberculosis. *American Journal of Public Health and the Nations Health* **1942**, 32 (1), 95-96.
6. Donoghue, H. D.; Lee, O. Y.-C.; Minnikin, D. E.; Besra, G. S.; Taylor, J. H.; Spigelman, M., Tuberculosis in Dr Granville's mummy: a molecular re-examination of the earliest known Egyptian mummy to be scientifically examined and given a medical diagnosis. *Proceedings of the Royal Society B: Biological Sciences* **2010**, 277 (1678), 51-56.

7. Hippocrates; Adams, F., *The genuine works of Hippocrates*. Sydenham Society: London, **1849**.
8. Murray, J. F.; Rieder, H. L.; Finley-Croswhite, A., The King's Evil and the Royal Touch: the medical history of scrofula. *The International Journal of Tuberculosis and Lung Disease* **2016**, *20* (6), 713-716.
9. Gurunluoglu, R.; Gurunluoglu, A., Paul of Aegina: Landmark in surgical progress. *World Journal of Surgery* **2003**, *27* (1), 18-25.
10. Barberis, I.; Bragazzi, N. L.; Galluzzo, L.; Martini, M., The history of tuberculosis: from the first historical records to the isolation of Koch's bacillus. *Journal of Preventive Medicine and Hygiene* **2017**, *58* (1), E9-E12.
11. Hardy, A., Captain of death: the story of tuberculosis. *Medical History* **1999**, *43* (1), 149-149.
12. Daniel, T. M., The history of tuberculosis. *Respiratory Medicine* **2006**, *100* (11), 1862-1870.
13. Spencer, D. R. C., The White Death—A history of tuberculosis. *Journal of Antimicrobial Chemotherapy*. **1999**, *44* (3), 423-423.
14. Wehmeyer, J. M., The dictionary of modern Medicine. *Bulletin of the Medical Library Association* **1992**, *80* (4), 389-390.
15. Kirby, S., 'Captain of all these men of death': The history of tuberculosis in nineteenth and twentieth century Ireland and No Charge — No undressing: Fronting up for good health. *Nursing Inquiry* **2006**, *13* (4), 304-305.

16. Knopf, S. A., *Hermann Brehmer*, and the semi-centennial celebration of Brehmer's sanatorium for the treatment of consumptives, the first institution of its kind July 2, 1904
17. Herzog, B. H., History of Tuberculosis. *Respiration* **1998**, 65 (1), 5-15.
18. Garrison, F. H., An introduction to the history of Medicine: with medical chronology, suggestions for study and bibliographic data. Philadelphia: W.B. Saunders, Fourth edition, **1929**.
19. Lakhtakia, R., The legacy of Robert Koch: surmise, search, substantiate. *Sultan Qaboos University Medical Journal* **2014**, 14 (1), e37-e41.
20. Sakula, A., Robert Koch: Centenary of the discovery of the tubercle bacillus, 1882. *The Canadian Veterinary Journal* **1983**, 24 (4), 127-131.
21. Boire, N. A.; Riedel, V. A. A.; Parrish, N. M.; Stefan, R., Tuberculosis: from an untreatable disease in antiquity to an untreatable disease in modern times? *Journal of Infectious Diseases & Preventive Medicine* **2013**, 1:106
22. Jakko van, I.; Zeaur, R.; Arnout, M.; Martin, J. B.; Roxane, S.; Roland, B.; Dick van, S., Characterization of *Mycobacterium orygis* as M. tuberculosis complex subspecies. *Emerging Infectious Disease journal* **2012**, 18 (4), 653.
23. Vasconcellos, S. E. G.; Huard, R. C.; Niemann, S.; Kremer, K.; Santos, A. R.; Suffys, P. N.; Ho, J. L., Distinct genotypic profiles of the two major clades of *Mycobacterium africanum*. *BMC Infectious Diseases* **2010**, 10 (1), 80.

24. Shi, R.; Sugawara, I., Pathophysiology of tuberculosis. In *Tuberculosis - Current Issues in Diagnosis and Management*, Mahboub, B. H.; Vats, M. G., Eds. InTech: Rijeka **2013**, p Ch. 07.
25. Ahmad, S., Pathogenesis, immunology, and diagnosis of latent *Mycobacterium tuberculosis* infection. *Clinical and Developmental Immunology* **2011**, 814943.
26. Bloom, B. R.; Murray, C. J. L., Tuberculosis: commentary on a reemergent killer. *Science* **1992**, 257 (5073), 1055-1064.
27. Guirado, E.; Mbawuike, U.; Keiser, T. L.; Arcos, J.; Azad, A. K.; Wang, S.-H.; Schlesinger, L. S., Characterization of host and microbial determinants in individuals with latent tuberculosis infection using a human granuloma model. *mBio* **2015**, 6 (1).
28. Jarvela, J. R.; Tuscano, L.; Lee, H.; Silver, R. F., Pulmonary responses to pathogen-specific antigens in latent *Mycobacterium tuberculosis* infection. *Tuberculosis* **2016**, 96, 158-164.
29. Paulson, T., Epidemiology: A mortal foe. *Nature* **2013**, 502 (7470), S2-S3.
30. WHO. Global Tuberculosis Report **2016**.
http://www.who.int/tb/publications/global_report/en/.
31. Crofton, J.; Mitchison, D. A., Streptomycin resistance in pulmonary tuberculosis. *British Medical Journal* **1948**, 2 (4588), 1009-1015.
32. Houghton, L.E., Treatment of pulmonary tuberculosis with streptomycin and para-amino-salicylic acid: A Medical Research Council investigation. *British Medical Journal* **1950**, 2 (4688), 1073-1085.

33. Keshavjee , S.; Farmer , P. E., Tuberculosis, drug resistance, and the history of modern Medicine. *New England Journal of Medicine* **2012**, *367* (10), 931-936.
34. Daniel, T. M., Rifampin — a major new chemotherapeutic agent for the treatment of tuberculosis. *New England Journal of Medicine* **1969**, *280* (11), 615-616.
35. Manten, A.; Van Wijngaarden, L. J., Development of Drug Resistance to Rifampicin. *Chemotherapy* **1969**, *14* (2), 93-100.
36. Fox, W.; Ellard, G. A.; Mitchison, D. A., Studies on the treatment of tuberculosis undertaken by the British Medical Research Council Tuberculosis Units, 1946 & 8211;1986, with relevant subsequent publications. *The International Journal of Tuberculosis and Lung Disease* **1999**, *3* (10), S231-S279.
37. Gillespie, S. H., Evolution of drug resistance in *Mycobacterium tuberculosis*: clinical and molecular perspective. *Antimicrobial Agents and Chemotherapy*. **2002**, *46* (2), 267-274.
38. Sun, G.; Luo, T.; Yang, C.; Dong, X.; Li, J.; Zhu, Y.; Zheng, H.; Tian, W.; Wang, S.; Barry, I. I. I. C. E.; Mei, J.; Gao, Q., Dynamic population changes in *Mycobacterium tuberculosis* during acquisition and fixation of drug resistance in Patients. *The Journal of Infectious Diseases* **2012**, *206* (11), 1724-1733.
39. Miller, J. H., Spontaneous mutators in bacteria: insights into pathways of mutagenesis and repair. *Annual Review of Microbiology* **1996**, *50* (1), 625-643.
40. Foster, P. L., Stress-induced mutagenesis in bacteria. *Critical Reviews in Biochemistry & Molecular Biology* **2007**, *42* (5), 373-397.

41. Saxowsky, T. T.; Doetsch, P. W., RNA Polymerase encounters with DNA damage: transcription-coupled repair or transcriptional mutagenesis? *Chemical Reviews* **2006**, *106* (2), 474-488.
42. Slupska, M. M.; Baikalov, C.; Lloyd, R.; Miller, J. H., Mutator tRNAs are encoded by the *Escherichia coli* mutator genes mutA and mutC: a novel pathway for mutagenesis. *Proceedings of the National Academy of Sciences of the United States of America* **1996**, *93* (9), 4380-4385.
43. McGrath, M.; Gey van Pittius, N. C.; van Helden, P. D.; Warren, R. M.; Warner, D. F., Mutation rate and the emergence of drug resistance in *Mycobacterium tuberculosis*. *Journal of Antimicrobial Chemotherapy*. **2014**, *69* (2), 292-302.
44. Kohanski, M. A.; DePristo, M. A.; Collins, J. J., Sublethal antibiotic treatment leads to multidrug resistance via radical-induced mutagenesis. *Molecular Cell* **2010**, *37* (3), 311-320.
45. Elliott, A. M.; Beming, S. E.; Iseman, M. D.; Peloquin, C. A., Failure of drug penetration and acquisition of drug resistance in chronic tuberculous empyema. *Tubercle and Lung Disease* **1995**, *76* (5), 463-467.
46. Malik, M.; Chavda, K.; Zhao, X.; Shah, N.; Hussain, S.; Kurepina, N.; Kreiswirth, B. N.; Kerns, R. J.; Drlica, K., Induction of mycobacterial resistance to quinolone class antimicrobials. *Antimicrobial Agents and Chemotherapy* **2012**, *56* (7), 3879-3887.
47. Boshoff, H. I. M.; Myers, T. G.; Copp, B. R.; McNeil, M. R.; Wilson, M. A.; Barry, C. E., The transcriptional responses of *Mycobacterium tuberculosis* to inhibitors

- of metabolism: novel insights into drug mechanisms of action. *Journal of Biological Chemistry* **2004**, 279 (38), 40174-40184.
48. Reves, R.; Blakey, D.; Snider, J. D. E.; Farer, L. S., Transmission of multiple drug-resistant tuberculosis: report of a school and community outbreak. *American Journal of Epidemiology* **1981**, 113 (4), 423-435.
49. WHO. WHO treatment guidelines for drug-resistant tuberculosis **2016**.
<http://www.who.int/tb/areas-of-work/drug-resistant-tb/MDRTBguidelines2016.pdf>.
50. CDC, Emergence of *Mycobacterium tuberculosis* with extensive resistance to second-line drugs — worldwide, 2000–2004. *Morbidity and Mortality Weekly Report* **2006**, (11), 301.
51. Eldholm, V.; Monteserin, J.; Rieux, A.; Lopez, B.; Sobkowiak, B.; Ritacco, V.; Balloux, F., Four decades of transmission of a multidrug-resistant *Mycobacterium tuberculosis* outbreak strain. *Nature Communications* **2015**, 6, 7119.
52. Migliori, G. B.; Loddenkemper, R.; Blasi, F.; Raviglione, M. C., 125 years after Robert Koch's discovery of the tubercle bacillus: the new XDR-TB threat. Is “science” enough to tackle the epidemic? *European Respiratory Journal* **2007**, 29 (3), 423-427.
53. Migliori, G. B., First tuberculosis cases in Italy resistant to all tested drugs. *Euro surveillance* **2007**, 12 (5).

54. Velayati, A. A.; Masjedi, M. R.; Farnia, P.; Tabarsi, P.; Ghanavi, J.; ZiaZarifi, A. H.; Hoffner, S. E., Emergence of new forms of totally drug-resistant tuberculosis Bacilli. *CHEST* **2009**, *136* (2), 420-425.
55. M., I. New, deadlier form of TB hits India **2012**.
<http://timesofindia.indiatimes.com/india/New-deadlier-form-of-TB-hits-India/articleshow/11396410.cms?referral=PM>.
56. Marisa, K.; Robin Mark, W.; Cindy, H.; Nicolaas Claudius Gey van, P.; Elizabeth Maria, S.; Borna, M.; Frederick Adriaan, S.; Mamisa, C.-N.; Ebrahim, H.; Gerrit, C.; Paul David van, H.; Thomas Caldo, V.; André Phillip, T., Emergence and spread of extensively and totally drug-resistant tuberculosis, South Africa. *Emerging Infectious Disease journal* **2013**, *19* (3), 449.
57. Mendoza, M., Mason, M. First U.S. case of extremely drug resistant strain of tuberculosis diagnosed **2009**. http://www.nbcnews.com/id/34516639/ns/health-infectious_diseases/t/danger-home-rare-form-tb-comes-us/#.WYPUmQw6t.
58. WHO. Drug-resistant TB: totally drug-resistant TB FAQ **2017**.
<http://www.who.int/tb/areas-of-work/drug-resistant-tb/totally-drug-resistant-tb-faq/en/>.
59. Tamma, P. D.; Cosgrove, S. E.; Maragakis, L. L., Combination therapy for treatment of infections with gram-negative bacteria. *Clinical Microbiology Reviews* **2012**, *25* (3), 450-470.
60. Lane, D., Designer combination therapy for cancer. *Nature Biotechnology* **2006**, *24* (2), 163-164.

61. Richman, D. D., HIV chemotherapy. *Nature* **2001**, *410* (6831), 995-1001.
62. Worthington, R. J.; Melander, C., Combination approaches to combat multidrug-resistant bacteria. *Trends in Biotechnology* **2013**, *31* (3), 177-184.
63. Kalle, A. M.; Rizvi, A., Inhibition of bacterial multidrug resistance by celecoxib, a cyclooxygenase-2 inhibitor. *Antimicrobial Agents and Chemotherapy*. **2011**, *55* (1), 439-442.
64. Fischbach, M. A., Combination therapies for combating antimicrobial resistance. *Current Opinion in Microbiology* **2011**, *14* (5), 519-523.
65. Suzanne, M. M.; Jennifer, F.; Barbara, S.; Yael, H.-M.; Lori, A.; Sundari, M.; Katya, S.; Peter, O.; Edward, A. G.; Paul, W. C.; Lisa, A.; Manuel, R.; Kathryn, S., Treatment practices, outcomes, and costs of multidrug-resistant and extensively drug-resistant tuberculosis, United States, 2005–2007. *Emerging Infectious Disease journal* **2014**, *20* (5), 812.
66. Dheda, K.; Gumbo, T.; Maartens, G.; Dooley, K. E.; McNerney, R.; Murray, M.; Furin, J.; Nardell, E. A.; London, L.; Lessem, E.; Theron, G.; van Helden, P.; Niemann, S.; Merker, M.; Dowdy, D.; Van Rie, A.; Siu, G. K. H.; Pasipanodya, J. G.; Rodrigues, C.; Clark, T. G.; Sirgel, F. A.; Esmail, A.; Lin, H.-H.; Atre, S. R.; Schaaf, H. S.; Chang, K. C.; Lange, C.; Nahid, P.; Udwadia, Z. F.; Horsburgh, C. R.; Churchyard, G. J.; Menzies, D.; Hesselning, A. C.; Nuermberger, E.; McIlleron, H.; Fennelly, K. P.; Goemaere, E.; Jaramillo, E.; Low, M.; Jara, C. M.; Padayatchi, N.; Warren, R. M., The epidemiology, pathogenesis, transmission, diagnosis, and

- management of multidrug-resistant, extensively drug-resistant, and incurable tuberculosis. *The Lancet Respiratory Medicine* **2017**, 5 (4), 291-360.
67. WHO. Guidelines for treatment of drug-susceptible tuberculosis and patient care. http://www.who.int/tb/publications/2017/dstb_guidance_2017/en/.
68. WHO. Guidelines for surveillance of drug resistance in tuberculosis **2015**. http://apps.who.int/iris/bitstream/10665/174897/1/9789241549134_eng.pdf.
69. CDC. Official American Thoracic Society/Centers for Disease Control and Prevention/Infectious Diseases Society of America Clinical Practice Guidelines: treatment of drug-susceptible tuberculosis **2016**. https://www.cdc.gov/tb/publications/guidelines/pdf/clin-infect-dis.-2016-nahid-cid_ciw376.pdf.
70. Unissa, A. N.; Subbian, S.; Hanna, L. E.; Selvakumar, N., Overview on mechanisms of isoniazid action and resistance in *Mycobacterium tuberculosis*. *Infection, Genetics and Evolution* **2016**, 45 (Supplement C), 474-492.
71. Carpena, X.; Loprasert, S.; Mongkolsuk, S.; Switala, J.; Loewen, P. C.; Fita, I., Catalase-peroxidase KatG of *Burkholderia pseudomallei* at 1.7Å resolution. *Journal of Molecular Biology*. **2003**, 327 (2), 475-489.
72. Zhang, Y.; Heym, B.; Allen, B.; Young, D.; Cole, S., The catalase-peroxidase gene and isoniazid resistance of *Mycobacterium tuberculosis*. *Nature* **1992**, 358 (6387), 591-593.
73. Vilchèze, C.; Jacobs, J. W. R., The mechanism of isoniazid killing: clarity through the scope of Genetics. *Annual Review of Microbiology* **2007**, 61 (1), 35-50.

74. Bulatovic, V. M.; Wengenack, N. L.; Uhl, J. R.; Hall, L.; Roberts, G. D.; Cockerill, F. R.; Rusnak, F., Oxidative stress increases susceptibility of *Mycobacterium tuberculosis* to isoniazid. *Antimicrobial Agents and Chemotherapy* **2002**, *46* (9), 2765-2771.
75. Zhao, X.; Yu, H.; Yu, S.; Wang, F.; Sacchettini, J. C.; Magliozzo, R. S., Hydrogen Peroxide-mediated isoniazid activation catalyzed by *Mycobacterium tuberculosis* catalase–peroxidase (KatG) and its S315T mutant. *Biochemistry* **2006**, *45* (13), 4131-4140.
76. Vilcheze, C.; Wang, F.; Arai, M.; Hazbon, M. H.; Colangeli, R.; Kremer, L.; Weisbrod, T. R.; Alland, D.; Sacchettini, J. C.; Jacobs, W. R., Transfer of a point mutation in *Mycobacterium tuberculosis inhA* resolves the target of isoniazid. *Nature Medicine* **2006**, *12* (9), 1027-1029.
77. Nusrath Unissa, A.; Hanna, L. E., Molecular mechanisms of action, resistance, detection to the first-line anti tuberculosis drugs: rifampicin and pyrazinamide in the post whole genome sequencing era. *Tuberculosis* **2017**, *105* (Supplement C), 96-107.
78. Grosset, J., The sterilizing value of rifampicin and pyrazinamide in experimental short course chemotherapy. *Tubercle* **1978**, *59* (4), 287-297.
79. Parsons Linda, M.; Somoskovi, A.; Salfinger, M., The molecular basis of resistance to isoniazid, rifampin, and pyrazinamide in *Mycobacterium tuberculosis*. *Respiratory Research*, **2001**, *2* (3), 164-168

80. Campbell, E. A.; Korzheva, N.; Mustaev, A.; Murakami, K.; Nair, S.; Goldfarb, A.; Darst, S. A., Structural mechanism for rifampicin inhibition of bacterial RNA polymerase. *Cell* **2017**, *104* (6), 901-912.
81. Ramaswamy, S.; Musser, J. M., Molecular genetic basis of antimicrobial agent resistance in *Mycobacterium tuberculosis*: 1998 update. *Tubercle and Lung Disease* **1998**, *79* (1), 3-29.
82. Lin, W.; Mandal, S.; Degen, D.; Liu, Y.; Ebright, Y. W.; Li, S.; Feng, Y.; Zhang, Y.; Mandal, S.; Jiang, Y.; Liu, S.; Gigliotti, M.; Talaue, M.; Connell, N.; Das, K.; Arnold, E.; Ebright, R. H., Structural basis of *Mycobacterium tuberculosis* transcription and transcription Inhibition. *Molecular Cell* **2017**, *66* (2), 169-179.
83. Zhang, Y.; Shi, W.; Zhang, W.; Mitchison, D., Mechanisms of pyrazinamide action and resistance. *Microbiology spectrum* **2013**, *2* (4), 1-12.
84. McCune, R. M.; Tompsett, R., Fate of *Mycobacterium tuberculosis* in mouse tissues as determined by the microbial enumeration technique. *The Journal of Experimental Medicine* **1956**, *104* (5), 737.
85. Zhang, Y.; Permar, S.; Sun, Z., Conditions that may affect the results of susceptibility testing of *Mycobacterium tuberculosis* to pyrazinamide. *Journal of Medical Microbiology* **2002**, *51* (1), 42-49.
86. Zhang, Y.; Mitchison, D., The curious characteristics of pyrazinamide: a review. *The International Journal of Tuberculosis and Lung Disease* **2003**, *7* (1), 6-21.

87. Scorpio, A.; Zhang, Y., Mutations in *pncA*, a gene encoding pyrazinamidase/nicotinamidase, cause resistance to the antituberculosis drug pyrazinamide in tubercle bacillus. *Nature Medicine* **1996**, 2 (6), 662-667.
88. Zhang, Y.; Scorpio, A.; Nikaido, H.; Sun, Z., Role of acid pH and deficient efflux of pyrazinoic acid in unique susceptibility of *Mycobacterium tuberculosis* to pyrazinamide. *Journal of Bacteriology* **1999**, 181 (7), 2044-2049.
89. Zhang, Y.; Wade, M. M.; Scorpio, A.; Zhang, H.; Sun, Z., Mode of action of pyrazinamide: disruption of *Mycobacterium tuberculosis* membrane transport and energetics by pyrazinoic acid. *Journal of Antimicrobial Chemotherapy* **2003**, 52 (5), 790-795.
90. Konno, K.; Feldmann, F. M.; McDermott, W., Pyrazinamide susceptibility and amidase activity of tubercle bacilli. *American Review of Respiratory Disease* **1967**, 95 (3), 461-469.
91. Scorpio, A.; Lindholm-Levy, P.; Heifets, L.; Gilman, R.; Siddiqi, S.; Cynamon, M.; Zhang, Y., Characterization of *pncA* mutations in pyrazinamide-resistant *Mycobacterium tuberculosis*. *Antimicrobial Agents and Chemotherapy* **1997**, 41 (3), 540-3.
92. Takayama, K.; Armstrong, E. L.; Kunugi, K. A.; Kilburn, J. O., Inhibition by ethambutol of mycolic acid transfer into the cell wall of *Mycobacterium smegmatis*. *Antimicrobial Agents and Chemotherapy* **1979**, 16 (2), 240-242.

93. Mikusová, K.; Slayden, R. A.; Besra, G. S.; Brennan, P. J., Biogenesis of the mycobacterial cell wall and the site of action of ethambutol. *Antimicrobial Agents and Chemotherapy*. **1995**, *39* (11), 2484-2489.
94. Telenti, A.; Philipp, W. J.; Sreevatsan, S.; Bernasconi, C.; Stockbauer, K. E.; Wieles, B.; Musser, J. M.; Jacobs, W. R., The *emb* operon, a gene cluster of *Mycobacterium tuberculosis* involved in resistance to ethambutol. *Nature Medicine* **1997**, *3* (5), 567-570.
95. Palomino, J. C.; Martin, A., Drug resistance mechanisms in *Mycobacterium tuberculosis*. *Antibiotics* **2014**, *3* (3), 317-340.
96. Johnson, R.; Jordaan, A. M.; Pretorius, L.; Engelke, E.; van der Spuy, G.; Kewley, C.; Bosman, M.; van Helden, P. D.; Warren, R.; Victor, T. C., Ethambutol resistance testing by mutation detection. *The International Journal of Tuberculosis and Lung Disease* **2006**, *10* (1), 68-73.
97. Safi, H.; Fleischmann, R. D.; Peterson, S. N.; Jones, M. B.; Jarrahi, B.; Alland, D., Allelic exchange and mutant selection demonstrate that common clinical *embCAB* gene mutations only modestly increase resistance to ethambutol in *Mycobacterium tuberculosis*. *Antimicrobial Agents and Chemotherapy*. **2010**, *54* (1), 103-108.
98. Safi, H.; Lingaraju, S.; Amin, A.; Kim, S.; Jones, M.; Holmes, M.; McNeil, M.; Peterson, S. N.; Chatterjee, D.; Fleischmann, R.; Alland, D., Evolution of high-level ethambutol-resistant tuberculosis through interacting mutations in decaprenylphosphoryl- $[\beta]$ -D-arabinose biosynthetic and utilization pathway genes. *Nature Genetics* **2013**, *45* (10), 1190-1197.

99. Finken, M.; Kirschner, P.; Meier, A.; Wrede, A.; Böttger, E. C., Molecular basis of streptomycin resistance in *Mycobacterium tuberculosis*: alterations of the ribosomal protein S12 gene and point mutations within a functional 16S ribosomal RNA pseudoknot. *Molecular Microbiology*. **1993**, 9 (6), 1239-1246.
100. Vilchèze, C.; Weisbrod, T. R.; Chen, B.; Kremer, L.; Hazbón, M. H.; Wang, F.; Alland, D.; Sacchetti, J. C.; Jacobs, W. R., Altered NADH/NAD⁺ ratio mediates co-resistance to isoniazid and ethionamide in mycobacteria. *Antimicrobial Agents and Chemotherapy* **2005**, 49 (2), 708-720.
101. Shean, K.; Streicher, E.; Pieterse, E.; Symons, G.; van Zyl Smit, R.; Theron, G.; Lehloenyane, R.; Padanilam, X.; Wilcox, P.; Victor, T. C.; van Helden, P.; Groubusch, M.; Warren, R.; Badri, M.; Dheda, K., Drug-associated adverse events and their relationship with outcomes in patients receiving treatment for extensively drug-resistant tuberculosis in South Africa. *PLOS ONE* **2013**, 8 (5), e63057.
102. WHO. Handbook for guideline development **2012**.
http://apps.who.int/iris/bitstream/10665/75146/1/9789241548441_eng.pdf.
103. WHO. The shorter MDR-TB regimen. **2016**.
104. King, D. E.; Malone, R.; Lilley, S. H., New classification and update on the quinolone antibiotics. *American Family Physician* **2000**, 61 (9), 2741-2748.
105. Stein, G. E.; Havlicek, D. H., Newer oral antimicrobials for resistant respiratory tract pathogens. *Postgraduate Medicine* **1998**, 103 (6), 67-76.
106. Aldred, K. J.; Kerns, R. J.; Osheroff, N., Mechanism of quinolone action and resistance. *Biochemistry* **2014**, 53 (10), 1565-1574.

107. Aubry, A.; Pan, X.-S.; Fisher, L. M.; Jarlier, V.; Cambau, E., Mycobacterium tuberculosis DNA Gyrase: Interaction with quinolones and correlation with antimycobacterial drug activity. *Antimicrobial Agents and Chemotherapy*. **2004**, *48* (4), 1281-1288.
108. Cheng, A. F. B.; Yew, W. W.; Chan, E. W. C.; Chin, M. L.; Hui, M. M. M.; Chan, R. C. Y., Multiplex PCR amplicon conformation analysis for rapid detection of *gyrA* mutations in fluoroquinolone-resistant *Mycobacterium tuberculosis* clinical isolates. *Antimicrobial Agents and Chemotherapy*. **2004**, *48* (2), 596-601.
109. Von Groll, A.; Martin, A.; Jureen, P.; Hoffner, S.; Vandamme, P.; Portaels, F.; Palomino, J. C.; da Silva, P. A., Fluoroquinolone resistance in *Mycobacterium tuberculosis* and mutations in *gyrA* and *gyrB*. *Antimicrobial Agents and Chemotherapy* **2009**, *53* (10), 4498-4500.
110. Aeschlimann, J. R., The role of multidrug efflux pumps in the antibiotic resistance of *Pseudomonas aeruginosa* and other Gram-negative bacteria. *Pharmacotherapy: The Journal of Human Pharmacology and Drug Therapy* **2003**, *23* (7), 916-924.
111. Jugheli, L.; Bzekalava, N.; de Rijk, P.; Fissette, K.; Portaels, F.; Rigouts, L., High level of cross-resistance between kanamycin, amikacin, and capreomycin among *Mycobacterium tuberculosis* isolates from Georgia and a close relation with mutations in the *rrs* gene. *Antimicrobial Agents and Chemotherapy*. **2009**, *53* (12), 5064-5068.

112. Krüüner, A.; Jureen, P.; Levina, K.; Ghebremichael, S.; Hoffner, S., Discordant resistance to kanamycin and amikacin in drug-resistant *Mycobacterium tuberculosis*. *Antimicrobial Agents and Chemotherapy*. **2003**, *47* (9), 2971-2973.
113. Zaunbrecher, M. A.; Sikes, R. D.; Metchock, B.; Shinnick, T. M.; Posey, J. E., Overexpression of the chromosomally encoded aminoglycoside acetyltransferase *eis* confers kanamycin resistance in *Mycobacterium tuberculosis*. *Proceedings of the National Academy of Sciences of the United States of America* **2009**, *106* (47), 20004-20009.
114. Stanley, R. E.; Blaha, G.; Grodzicki, R. L.; Strickler, M. D.; Steitz, T. A., The structures of the anti-tuberculosis antibiotics viomycin and capreomycin bound to the 70S ribosome. *Nature structural & molecular biology* **2010**, *17* (3), 289-293.
115. Johansen, S. K.; Maus, C. E.; Plikaytis, B. B.; Douthwaite, S., Capreomycin binds across the ribosomal subunit interface using *tlyA*-encoded-O-methylations in 16S and 23S rRNAs. *Molecular Cell* **2006**, *23* (2), 173-182.
116. DeBarber, A. E.; Mdluli, K.; Bosman, M.; Bekker, L.-G.; Barry, C. E., Ethionamide activation and sensitivity in multidrug-resistant *Mycobacterium tuberculosis*. *Proceedings of the National Academy of Sciences of the United States of America* **2000**, *97* (17), 9677-9682.
117. Wang, F.; Langley, R.; Gulten, G.; Dover, L. G.; Besra, G. S.; Jacobs, W. R.; Sacchettini, J. C., Mechanism of thioamide drug action against tuberculosis and leprosy. *The Journal of Experimental Medicine* **2007**, *204* (1), 73-78.

118. Vilchèze, C.; Jacobs JR., W. R., Resistance to isoniazid and ethionamide in *Mycobacterium tuberculosis*: genes, mutations, and causalities. *Microbiology Spectrum* **2014**, 2 (4).
119. Morlock, G. P.; Metchock, B.; Sikes, D.; Crawford, J. T.; Cooksey, R. C., *ethA*, *inhA*, and *katG* loci of ethionamide-resistant clinical *Mycobacterium tuberculosis* isolates. *Antimicrobial Agents and Chemotherapy*. **2003**, 47 (12), 3799-3805.
120. Hwang, T. J.; Wares, D. F.; Jafarov, A.; Jakubowiak, W.; Nunn, P.; Keshavjee, S., Safety of cycloserine and terizidone for the treatment of drug-resistant tuberculosis: a meta-analysis. *The International Journal of Tuberculosis and Lung Disease* **2013**, 17 (10), 1257-1266.
121. Chen, J. M.; Uplekar, S.; Gordon, S. V.; Cole, S. T., A point mutation in *cycA* partially contributes to the D-cycloserine resistance trait of *Mycobacterium bovis* BCG vaccine strains. *PLOS ONE* **2012**, 7 (8), e43467.
122. Leach, K. L.; Brickner, S. J.; Noe, M. C.; Miller, P. F., Linezolid, the first oxazolidinone antibacterial agent. *Annals of the New York Academy of Sciences* **2011**, 1222 (1), 49-54.
123. Reddy, V. M.; Einck, L.; Andries, K.; Nacy, C. A., *In vitro* interactions between new antitubercular drug candidates SQ109 and TMC207. *Antimicrobial Agents and Chemotherapy*. **2010**, 54 (7), 2840-2846.
124. Beckert, P.; Hillemann, D.; Kohl, T. A.; Kalinowski, J.; Richter, E.; Niemann, S.; Feuerriegel, S., *rplC* T460C identified as a dominant mutation in linezolid-

- resistant *Mycobacterium tuberculosis* strains. *Antimicrobial Agents and Chemotherapy*. **2012**, 56 (5), 2743-2745.
125. Lechartier, B.; Cole, S. T., Insight into the mode of action of clofazimine and combination therapy with benzothiazinones against *Mycobacterium tuberculosis*. *Antimicrobial Agents and Chemotherapy* **2015**, 59(8):4457-63
126. Sandhu, P.; Akhter, Y., The drug binding sites and transport mechanism of the RND pumps from *Mycobacterium tuberculosis*: insights from molecular dynamics simulations. *Archives of Biochemistry and Biophysics*. **2016**, 592 (Supplement C), 38-49.
127. Diacon , A. H.; Pym , A.; Grobusch , M.; Patientia , R.; Rustomjee , R.; Page-Shipp , L.; Pistorius , C.; Krause , R.; Bogoshi , M.; Churchyard , G.; Venter , A.; Allen , J.; Palomino , J. C.; De Marez , T.; van Heeswijk , R. P. G.; Lounis , N.; Meyvisch , P.; Verbeeck , J.; Parys , W.; de Beule , K.; Andries , K.; Neeley , D. F. M., The diarylquinoline TMC207 for multidrug-resistant tuberculosis. *New England Journal of Medicine* **2009**, 360 (23), 2397-2405.
128. Mahajan, R., Bedaquiline: First FDA-approved tuberculosis drug in 40 years. *International Journal of Applied and Basic Medical Research* **2013**, 3 (1), 1-2.
129. Matteelli, A.; Carvalho, A. C. C.; Dooley, K. E.; Kritski, A., TMC207: the first compound of a new class of potent anti-tuberculosis drugs. *Future microbiology* **2010**, 5 (6), 849-858.
130. Huitric, E.; Verhasselt, P.; Koul, A.; Andries, K.; Hoffner, S.; Andersson, D. I., rates and mechanisms of resistance development in *Mycobacterium tuberculosis*

- to a novel diarylquinoline ATP synthase inhibitor. *Antimicrobial Agents and Chemotherapy*. **2010**, 54 (3), 1022-1028.
131. Matsumoto, M.; Hashizume, H.; Tomishige, T.; Kawasaki, M.; Tsubouchi, H.; Sasaki, H.; Shimokawa, Y.; Komatsu, M., OPC-67683, a nitro-dihydroimidazooxazole derivative with promising action against tuberculosis *in vitro* and in mice. *PLOS Medicine* **2006**, 3 (11), e466.
132. Almeida Da Silva, P. E.; Palomino, J. C., Molecular basis and mechanisms of drug resistance in *Mycobacterium tuberculosis*: classical and new drugs. *Journal of Antimicrobial Chemotherapy*. **2011**, 66 (7), 1417-1430.
133. Rengarajan, J.; Sasseti, C. M.; Naroditskaya, V.; Sloutsky, A.; Bloom, B. R.; Rubin, E. J., The folate pathway is a target for resistance to the drug para-aminosalicylic acid (PAS) in mycobacteria. *Molecular Microbiology*. **2004**, 53 (1), 275-282.
134. Zheng, J.; Rubin, E. J.; Bifani, P.; Mathys, V.; Lim, V.; Au, M.; Jang, J.; Nam, J.; Dick, T.; Walker, J. R.; Pethe, K.; Camacho, L. R., Para-aminosalicylic acid is a prodrug targeting dihydrofolate reductase in *Mycobacterium tuberculosis*. *The Journal of Biological Chemistry* **2013**, 288 (32), 23447-23456.
135. Zhao, F.; Wang, X.-D.; Erber, L. N.; Luo, M.; Guo, A.-z.; Yang, S.-s.; Gu, J.; Turman, B. J.; Gao, Y.-r.; Li, D.-f.; Cui, Z.-q.; Zhang, Z.-p.; Bi, L.-j.; Baughn, A. D.; Zhang, X.-E.; Deng, J.-Y., Binding pocket alterations in dihydrofolate synthase confer resistance to para-aminosalicylic acid in clinical isolates of *Mycobacterium tuberculosis*. *Antimicrobial Agents and Chemotherapy*. **2014**, 58 (3), 1479-1487.

136. Nunn, P.; Porter, J.; Winstanley, P., Thiacetazone—avoid like poison or use with care? *Transactions of the Royal Society of Tropical Medicine and Hygiene* **1993**, *87* (5), 578-582.
137. Coxon, G. D.; Craig, D.; Corrales, R. M.; Vialla, E.; Gannoun-Zaki, L.; Kremer, L., Synthesis, Antitubercular activity and mechanism of resistance of highly effective thiacetazone analogues. *PLOS ONE* **2013**, *8* (1), e53162.
138. Brooks, B. D.; Brooks, A. E., Therapeutic strategies to combat antibiotic resistance. *Advanced Drug Delivery Reviews* **2014**, *78*, 14-27.
139. Pieters, J., Entry and survival of pathogenic mycobacteria in macrophages. *Microbes and Infection* **2001**, *3* (3), 249-255.
140. Gomez, J. E.; McKinney, J. D., M. Tuberculosis persistence, latency, and drug tolerance. *Tuberculosis* **2004**, *84* (1), 29-44.
141. Dick, T., How antibacterials really work: impact on drug discovery. *Future Microbiology* **2011**, *6* (6), 603-604.
142. Martinez, J. L.; Baquero, F., Mutation frequencies and antibiotic resistance. *Antimicrobial Agents and Chemotherapy*. **2000**, *44* (7), 1771-1777.
143. Boshoff, H. I. M.; Reed, M. B.; Barry Iii, C. E.; Mizrahi, V., DnaE2 polymerase contributes to *in vivo* survival and the emergence of drug resistance in *Mycobacterium tuberculosis*. *Cell* **2003**, *113* (2), 183-193.
144. Warner, D. F.; Ndwandwe, D. E.; Abrahams, G. L.; Kana, B. D.; Machowski, E. E.; Venclovas, Č.; Mizrahi, V., Essential roles for *imuA* and *imuB*-encoded accessory factors in DnaE2-dependent mutagenesis in *Mycobacterium*

- tuberculosis. Proceedings of the National Academy of Sciences* **2010**, *107* (29), 13093-13098.
145. Gashaw, I.; Ellinghaus, P.; Sommer, A.; Asadullah, K., What makes a good drug target? *Drug Discovery Today* **2011**, *16* (23), 1037-1043.
146. Esmail, H.; Barry, C. E.; Young, D. B.; Wilkinson, R. J., The ongoing challenge of latent tuberculosis. *Philosophical Transactions of the Royal Society B: Biological Sciences* **2014**, *369* (1645).
147. Segel, I. H., *Enzyme kinetics: behavior and analysis of rapid equilibrium and steady-state enzyme systems*. New York: Wiley, **1975**.
148. Lundstrom, K. H.; Chiu, M. L., *G protein-coupled receptors in drug discovery*. Boca Raton: Taylor & Francis, 2006.: **2006**.
149. Drews, J., Genomic sciences and the medicine of tomorrow. *Nature Biotechnology* **1996**, *14* (11), 1516-1518.
150. Hopkins, A. L.; Groom, C. R., The druggable genome. *Nature Reviews Drug Discovery* **2002**, *1* (9), 727-730.
151. Imming, P.; Sinning, C.; Meyer, A., Drugs, their targets and the nature and number of drug targets. *Nature Reviews Drug Discovery* **2006**, *5* (10), 821-834.
152. Diller, D. J., The synergy between combinatorial chemistry and high-throughput screening. *Current Opinion in Drug Discovery & Development* **2008**, *11* (3), 346-355.
153. Pereira, D. A.; Williams, J. A., Origin and evolution of high throughput screening. *British Journal of Pharmacology* **2007**, *152* (1), 53-61.

154. Takenaka, T., Classical vs reverse pharmacology in drug discovery. *BJU International* **2001**, *88*, 7-10.
155. Vogt, A.; Lazo, J. S., Chemical complementation: A definitive phenotypic strategy for identifying small molecule inhibitors of elusive cellular targets. *Pharmacology & Therapeutics* **2005**, *107* (2), 212-221.
156. Hughes, J. P.; Rees, S.; Kalindjian, S. B.; Philpott, K. L., Principles of early drug discovery. *British Journal of Pharmacology* **2011**, *162* (6), 1239-1249.
157. Rask-Andersen, M.; Almén, M. S.; Schiöth, H. B., Trends in the exploitation of novel drug targets. *Nature Reviews Drug Discovery* **2011**, *10* (8), 579-590.
158. Swinney, D. C.; Anthony, J., How were new medicines discovered? *Nature Reviews Drug Discovery* **2011**, *10* (7), 507-519.
159. Terstappen, G. C.; Schlupen, C.; Raggiaschi, R.; Gaviraghi, G., Target deconvolution strategies in drug discovery. *Nature Reviews Drug Discovery* **2007**, *6* (11), 891-903.
160. Zheng, W.; Thorne, N.; McKew, J. C., Phenotypic screens as a renewed approach for drug discovery. *Drug Discovery Today* **2013**, *18* (21), 1067-1073.
161. Sams-Dodd, F., Drug discovery: selecting the optimal approach. *Drug Discovery Today* **2006**, *11* (9), 465-472.
162. Singh, V.; Mizrahi, V., Identification and validation of novel drug targets in *Mycobacterium tuberculosis*. *Drug Discovery Today* **2017**, *22* (3), 503-509.
163. Lewis, K., Antibiotics: Recover the lost art of drug discovery. *Nature* **2012**, *485* (7399), 439-440.

164. Gregori-Puigjané, E.; Setola, V.; Hert, J.; Crews, B. A.; Irwin, J. J.; Lounkine, E.; Marnett, L.; Roth, B. L.; Shoichet, B. K., Identifying mechanism-of-action targets for drugs and probes. *Proceedings of the National Academy of Sciences* **2012**, *109* (28), 11178-11183.
165. Vane, J. R.; Botting, R. M., The mechanism of action of aspirin. *Thrombosis Research* **2003**, *110* (5), 255-258.
166. Triggle, D. J., Calcium antagonist's history and perspective. *Stroke* **1990**, *21* (12), IV-49-IV-58.
167. Triggle, D. J., Calcium channel antagonists: Clinical uses—past, present and future. *Biochemical Pharmacology*. **2007**, *74* (1), 1-9.
168. Van Heek, M.; France, C. F.; Compton, D. S.; McLeod, R. L.; Yumibe, N. P.; Alton, K. B.; Sybertz, E. J.; Davis, H. R., *In vivo* metabolism-based discovery of a potent cholesterol absorption inhibitor, SCH58235, in the rat and rhesus monkey through the identification of the active metabolites of SCH48461. *Journal of Pharmacology and Experimental Therapeutics*. **1997**, *283* (1), 157.
169. Rosenblum, S. B.; Huynh, T.; Afonso, A.; Davis, H. R.; Yumibe, N.; Clader, J. W.; Burnett, D. A., Discovery of 1-(4-fluorophenyl)-(3R)-[3-(4-fluorophenyl)-(3S)-hydroxypropyl]-(4S)-(4-hydroxyphenyl)-2-azetidinone (SCH 58235): a designed, potent, orally active inhibitor of cholesterol absorption. *Journal of Medicinal Chemistry*. **1998**, *41* (6), 973-980.
170. Chong, C. R.; Sullivan, D. J., New uses for old drugs. *Nature* **2007**, *448* (7154), 645-646.

171. Ejim, L.; Farha, M. A.; Falconer, S. B.; Wildenhain, J.; Coombes, B. K.; Tyers, M.; Brown, E. D.; Wright, G. D., Combinations of antibiotics and nonantibiotic drugs enhance antimicrobial efficacy. *Nature Chemical Biology* **2011**, 7 (6), 348-350.
172. Mazumdar, K.; Dastidar, S. G.; Park, J. H.; Dutta, N. K., The anti-inflammatory non-antibiotic helper compound diclofenac: an antibacterial drug target. *European Journal of Clinical Microbiology & Infectious Diseases* **2009**, 28 (8), 881.
173. Van Soolingen, D.; Hernandez-Pando, R.; Orozco, H.; Aguilar, D.; Magis-Escurra, C.; Amaral, L.; Van Ingen, J.; Boeree, M. J., The antipsychotic thioridazine shows promising therapeutic activity in a mouse model of multidrug-resistant tuberculosis. *PLOS ONE* **2010**, 5 (9), e12640.
174. Anderson, W. F., Structural genomics and drug discovery for infectious diseases. *Infectious disorders drug targets* **2009**, 9 (5), 507-517.
175. Manjasetty, B. A.; Turnbull, A. P.; Panjekar, S.; Büssow, K.; Chance, M. R., Automated technologies and novel techniques to accelerate protein crystallography for structural genomics. *Proteomics* **2008**, 8 (4), 612-625.
176. Jones, M. M.; Castle-Clarke, S.; Brooker, D.; Nason, E.; Huzair, F.; Chataway, J., The Structural Genomics Consortium: a knowledge platform for drug discovery: a summary. *Rand Health Quarterly* **2014**, 4 (3), 19.
177. Ioerger, T. R.; Sacchettini, J. C., Structural genomics approach to drug discovery for *Mycobacterium tuberculosis*. *Current Opinion in Microbiology* **2009**, 12 (3), 318-325.

178. Musa, T. L.; Ioerger, T. R.; Sacchettini, J. C., The tuberculosis Structural Genomics Consortium. *Advances in Protein Chemistry and Structural Biology* **2009**, *77*, 41-76.
179. Chim, N.; Habel, J. E.; Johnston, J. M.; Krieger, I.; Miallau, L.; Sankaranarayanan, R.; Morse, R. P.; Bruning, J.; Swanson, S.; Kim, H.; Kim, C.-Y.; Li, H.; Bulloch, E. M.; Payne, R. J.; Manos-Turvey, A.; Hung, L.-W.; Baker, E. N.; Lott, J. S.; James, M. N. G.; Terwilliger, T. C.; Eisenberg, D. S.; Sacchettini, J. C.; Goulding, C. W., The TB Structural Genomics Consortium: a decade of progress. *Tuberculosis* **2011**, *91* (2), 155-172.
180. Cole, S. T.; Brosch, R.; Parkhill, J.; Garnier, T.; Churcher, C.; Harris, D.; Gordon, S. V.; Eiglmeier, K.; Gas, S.; Barry, C. E.; Tekaiia, F.; Badcock, K.; Basham, D.; Brown, D.; Chillingworth, T.; Connor, R.; Davies, R.; Devlin, K.; Feltwell, T.; Gentles, S.; Hamlin, N.; Holroyd, S.; Hornsby, T.; Jagels, K.; Krogh, A.; McLean, J.; Moule, S.; Murphy, L.; Oliver, K.; Osborne, J.; Quail, M. A.; Rajandream, M. A.; Rogers, J.; Rutter, S.; Seeger, K.; Skelton, J.; Squares, R.; Squares, S.; Sulston, J. E.; Taylor, K.; Whitehead, S.; Barrell, B. G., Deciphering the biology of *Mycobacterium tuberculosis* from the complete genome sequence. *Nature* **1998**, *393* (6685), 537-544.
181. Bursey, E. H.; Kim, C.-Y.; Yu, M.; Terwilliger, T. C.; Hung, L.-W., An automated high-throughput screening method for the identification of high-yield, soluble protein variants using cell-free expression and systematic truncation. *Journal of Structural and Functional Genomics* **2006**, *7* (3), 139-147.

182. Griffin, J. E.; Gawronski, J. D.; DeJesus, M. A.; Ioerger, T. R.; Akerley, B. J.; Sasseti, C. M., High-resolution phenotypic profiling defines genes essential for mycobacterial growth and cholesterol catabolism. *PLOS Pathogens* **2011**, *7* (9), e1002251.
183. Zhang, Y. J.; Reddy, M. C.; Ioerger, T. R.; Rothchild, A. C.; Dartois, V.; Schuster, B. M.; Trauner, A.; Wallis, D.; Galaviz, S.; Huttenhower, C.; Sacchettini, J. C.; Behar, S. M.; Rubin, E. J., Tryptophan biosynthesis protects mycobacteria from CD4 T cell-mediated killing. *Cell* **2013**, *155* (6), 1296-1308.
184. Ducati, R. G.; Breda, A.; Basso, L. A.; Santos, D. S., Purine salvage pathway in *Mycobacterium tuberculosis*. *Current Medicinal Chemistry* **2011**, *18* (9), 1258-1275.
185. Villela, A. D.; Sanchez-Quitian, Z. A.; Ducati, R. G.; Santos, D. S.; Basso, L. A., Pyrimidine salvage pathway in *Mycobacterium tuberculosis*. *Current Medicinal Chemistry* **2011**, *18* (9), 1286-1298.
186. Long, M. C.; Escuyer, V.; Parker, W. B., Identification and characterization of a unique adenosine kinase from *Mycobacterium tuberculosis*. *Journal of Bacteriology*. **2003**, *185* (22), 6548-6555.
187. Reddy, M. C. M.; Palaninathan, S. K.; Shetty, N. D.; Owen, J. L.; Watson, M. D.; Sacchettini, J. C., High resolution crystal structures of *Mycobacterium tuberculosis* adenosine kinase: insights into the mechanism and specificity of this novel prokaryotic enzyme. *Journal of Biological Chemistry*. **2007**, *282* (37), 27334-27342.

188. Park, J.; Gupta, R. S., Adenosine kinase and ribokinase – the RK family of proteins. *Cellular and Molecular Life Sciences* **2008**, *65* (18), 2875-2896.
189. Schumacher, M. A.; Scott, D. M.; Mathews, I. I.; Ealick, S. E.; Roos, D. S.; Ullman, B.; Brennan, R. G., Crystal structures of *Toxoplasma gondii* adenosine kinase reveal a novel catalytic mechanism and prodrug binding. †This paper was incorrectly published in *Journal of Molecular Biology*. (2000) 296, 549-567 without the authors' corrections. The Publisher regrets any inconvenience caused to the authors. †Edited by I. A. Wilson. *Journal of Molecular Biology*. **2000**, 298 (5), 875-893.
190. Mathews, I. I.; Erion, M. D.; Ealick, S. E., Structure of human adenosine kinase at 1.5 Å resolution. *Biochemistry* **1998**, *37* (45), 15607-15620.
191. Romanello, L.; Bachega, J. F. R.; Cassago, A.; Brandao-Neto, J.; DeMarco, R.; Garratt, R. C.; Pereira, H. D. M., Adenosine kinase from *Schistosoma mansoni*: structural basis for the differential incorporation of nucleoside analogues. *Acta Crystallographica Section D* **2013**, *69* (1), 126-136.
192. Long, M. C.; Parker, W. B., Structure–activity relationship for nucleoside analogs as inhibitors or substrates of adenosine kinase from *Mycobacterium tuberculosis*: I. Modifications to the adenine moiety. *Biochemical Pharmacology* **2006**, *71* (12), 1671-1682.
193. Barrow, E. W.; Westbrook, L.; Bansal, N.; Suling, W. J.; Maddry, J. A.; Parker, W. B.; Barrow, W. W., Antimycobacterial activity of 2-methyl-adenosine. *Journal of Antimicrobial Chemotherapy* **2003**, *52* (5), 801-808.

194. Parker, W. B.; Barrow, E. W.; Allan, P. W.; Shaddix, S. C.; Long, M. C.; Barrow, W. W.; Bansal, N.; Maddry, J. A., Metabolism of 2-methyladenosine in *Mycobacterium tuberculosis*. *Tuberculosis* **2004**, *84* (5), 327-336.
195. Chen, C.-K.; Barrow, E. W.; Allan, P. W.; Bansal, N.; Maddry, J. A.; Suling, W. J.; Barrow, W. W.; Parker, W. B., The metabolism of 2-methyladenosine in *Mycobacterium smegmatis*. *Microbiology* **2002**, *148* (1), 289-295.
196. Blondin, C.; Serina, L.; Wiesmuller, L.; Gilles, A. M.; Barzu, O., Improved Spectrophotometric assay of nucleoside monophosphate kinase activity using the pyruvate kinase/lactate dehydrogenase coupling system. *Analytical Biochemistry* **1994**, *220* (1), 219-221.
197. Cer, R. Z.; Mudunuri, U.; Stephens, R.; Lebeda, F. J., IC₅₀ to K_i: a web-based tool for converting IC₅₀ to K_i values for inhibitors of enzyme activity and ligand binding. *Nucleic Acids Research*. **2009**, *37*, W441-W445.
198. Yung-Chi, C.; Prusoff, W. H., Relationship between the inhibition constant (K_i) and the concentration of inhibitor which causes 50 per cent inhibition (IC₅₀) of an enzymatic reaction. *Biochemical Pharmacology* **1973**, *22* (23), 3099-3108.
199. Otwinowski, Z.; Minor, W., Processing of X-ray diffraction data collected in oscillation mode. Elsevier: **1997**, Vol. 276, pp 307-326.
200. Collaborative, C. P., The CCP4 suite: programs for protein crystallography. *Acta crystallographica. Section D, Biological crystallography* **1994**, *50* (Pt 5), 760.
201. Adams, P. D.; Grosse-Kunstleve, R. W.; Hung, L.-W.; Ioerger, T. R.; McCoy, A. J.; Moriarty, N. W.; Read, R. J.; Sacchettini, J. C.; Sauter, N. K.; Terwilliger, T.

- C., PHENIX: building new software for automated crystallographic structure determination. *Acta Crystallographica Section D* **2002**, 58 (11), 1948-1954.
202. Emsley, P.; Lohkamp, B.; Scott, W. G.; Cowtan, K., Features and development of Coot. *Acta Crystallographica Section D* **2010**, 66 (4), 486-501.
203. Pettersen, E. F.; Goddard, T. D.; Huang, C. C.; Couch, G. S.; Greenblatt, D. M.; Meng, E. C.; Ferrin, T. E., UCSF Chimera—A visualization system for exploratory research and analysis. *Journal of Computational Chemistry* **2004**, 25 (13), 1605-1612.
204. PyMOL. The PyMOL Molecular Graphics System, Version 1.8 Schrödinger, LLC.
205. Abagyan, R.; Totrov, M.; Kuznetsov, D., ICM—A new method for protein modeling and design: Applications to docking and structure prediction from the distorted native conformation. *Journal of Computational Chemistry* **1994**, 15 (5), 488-506.
206. Franzblau, S. G.; Witzig, R. S.; McLaughlin, J. C.; Torres, P.; Madico, G.; Hernandez, A.; Degnan, M. T.; Cook, M. B.; Quenzer, V. K.; Ferguson, R. M.; Gilman, R. H., Rapid, low-technology MIC determination with clinical *Mycobacterium tuberculosis* isolates by using the microplate Alamar Blue assay. *Journal of Clinical Microbiology* **1998**, 36 (2), 362-366.
207. Krieger, Inna V.; Freundlich, Joel S.; Gawandi, Vijay B.; Roberts, Justin P.; Gawandi, Vidyadhar B.; Sun, Q.; Owen, Joshua L.; Fraile, Maria T.; Huss, Sofia I.; Lavandera, J.-L.; Ioerger, Thomas R.; Sacchettini, James C., Structure-

- guided discovery of phenyl-diketo acids as potent inhibitors of *M. tuberculosis* malate synthase. *Chemistry & Biology* **2012**, *19* (12), 1556-1567.
208. Long, M. C.; Shaddix, S. C.; Moukha-Chafiq, O.; Maddry, J. A.; Nagy, L.; Parker, W. B., Structure–activity relationship for adenosine kinase from *Mycobacterium tuberculosis*: II. modifications to the ribofuranosyl moiety. *Biocheical Pharmacology* **2008**, *75* (8), 1588-1600.
209. Snášel, J.; Nauš, P.; Dostál, J.; Hnízda, A.; Fanfrlík, J.; Brynda, J.; Bourderioux, A.; Dušek, M.; Dvořáková, H.; Stolaříková, J.; Zábranská, H.; Pohl, R.; Konečný, P.; Džubák, P.; Votruba, I.; Hajdúch, M.; Řezáčová, P.; Veverka, V.; Hocek, M.; Pichová, I., Structural basis for inhibition of mycobacterial and human adenosine kinase by 7-Substituted 7-(Het)aryl-7-deazaadenine ribonucleosides. *Journal of Medicinal Chemistry* **2014**, *57* (20), 8268-8279.
210. Massillon, D.; Stalmans, W.; van de Werve, G.; Bollen, M., Identification of the glycogenic compound 5-iodotubercidin as a general protein kinase inhibitor. *Biochemical Journal* **1994**, *299* (Pt 1), 123-128..
211. Ugarkar, B. G.; DaRe, J. M.; Kopcho, J. J.; Browne, C. E.; Schanzer, J. M.; Wiesner, J. B.; Erion, M. D., Adenosine Kinase Inhibitors. 1. Synthesis, Enzyme Inhibition, and Antiseizure Activity of 5-Iodotubercidin Analogues. *Journal of Medicinal Chemistry* **2000**, *43* (15), 2883-2893..
212. Loomis, C. R.; Bell, R. M., Sangivamycin, a nucleoside analogue, is a potent inhibitor of protein kinase C. *Journal of Biological Chemistry* **1988**, *263* (4), 1682-92.

213. Muchmore, S. W.; Smith, R. A.; Stewart, A. O.; Cowart, M. D.; Gomtsyan, A.; Matulenko, M. A.; Yu, H.; Severin, J. M.; Bhagwat, S. S.; Lee, C.-H.; Kowaluk, E. A.; Jarvis, M. F.; Jakob, C. L., Crystal structures of human adenosine kinase inhibitor complexes reveal two distinct binding modes. *Journal of Medicinal Chemistry* **2006**, *49* (23), 6726-6731..
214. Zemlicka, J.; Endo, T., O6-(4-Nitrophenyl)inosine and guanosine as chromogenic substrates for adenosine deaminase. *Nucleosides and Nucleotides* **1996**, *15* (1-3), 619-629.
215. Camp, D.; Li, Y.; McCluskey, A.; Moni, R. W.; Quinn, R. J., Diimidazo[1,2-4',5'-pyrimidines: N6-N1 conformationally restricted adenosines. *Bioorganic & Medicinal Chemistry Letters* **1998**, *8* (6), 695-698.
216. Katagiri, N.; Matsuhashi, Y.; Kokufuda, H.; Takebayashi, M.; Kaneko, C., A highly efficient synthesis of the antiviral agent (+)-cyclaradine involving the regioselective cleavage of epoxide by neighboring participation. *Tetrahedron Letters* **1997**, *38* (11), 1961-1964.
217. Itoh, T., Sugawara, T., Mizuno, Y, A Novel Synthesis of 1-deazaadenosine. *Heterocycles* **1982**, *17*, 305-309.
218. Malnuit, V.; Slavětínská, L. P.; Nauš, P.; Džubák, P.; Hajdúch, M.; Stolaříková, J.; Snášel, J.; Pichová, I.; Hocek, M., 2-Substituted 6-(Het)aryl-7-deazapurine ribonucleosides: synthesis, inhibition of adenosine kinases, and antimycobacterial activity. *ChemMedChem* **2015**, *10* (6), 1079-1093.

219. Park, J.; Singh, B.; Gupta, R. S., Mycobacterial adenosine kinase is not a typical adenosine kinase. *FEBS Lett.* **2009**, *583* (13), 2231-2236
220. Boshoff, H. I. M.; Barry, C. E., Tuberculosis metabolism and respiration in the absence of growth. *Nature Reviews Microbiology* **2005**, *3* (1), 70-80.
221. Long, M. C.; Allan, P. W.; Luo, M.-Z.; Liu, M.-C.; Sartorelli, A. C.; Parker, W. B., Evaluation of 3-deaza-adenosine analogues as ligands for adenosine kinase and inhibitors of *Mycobacterium tuberculosis* growth. *Journal of Antimicrobial Chemotherapy* **2007**, *59* (1), 118-121.
222. Niesen, F. H.; Berglund, H.; Vedadi, M., The use of differential scanning fluorimetry to detect ligand interactions that promote protein stability. *Nature Protocols* **2007**, *2* (9), 2212-2221.
223. Sambandamurthy, V. K.; Derrick, S. C.; Hsu, T.; Chen, B.; Larsen, M. H.; Jalapathy, K. V.; Chen, M.; Kim, J.; Porcelli, S. A.; Chan, J.; Morris, S. L.; Jacobs Jr, W. R., *Mycobacterium tuberculosis* $\Delta RD1 \Delta panCD$: a safe and limited replicating mutant strain that protects immunocompetent and immunocompromised mice against experimental tuberculosis. *Vaccine* **2006**, *24* (37-39), 6309-6320.
224. Chayen, N. E.; Shaw Stewart, P. D.; Blow, D. M., Microbatch crystallization under oil — a new technique allowing many small-volume crystallization trials. *Journal of Crystal Growth* **1992**, *122* (1), 176-180.

225. Heras, B.; Edeling, M. A.; Byriel, K. A.; Jones, A.; Raina, S.; Martin, J. L., Dehydration converts DsbG crystal diffraction from low to high resolution. *Structure* **2003**, *11* (2), 139-145
226. Huang, Q.; Szebenyi, D. M. E., Improving diffraction resolution using a new dehydration method. *Acta Crystallographica Section F* **2016**, *72* (2), 152-159.
227. Krauss, I. R.; Sica, F.; Mattia, C. A.; Merlino, A., Increasing the X-ray diffraction power of protein crystals by dehydration: the case of bovine serum albumin and a survey of literature data. *International Journal of Molecular Sciences* **2012**, *13* (3), 3782-3800.
228. Copeland, R. A., Reversible inhibitors. In *Enzymes*, John Wiley & Sons, Inc.: **2002**, pp 266-304.
229. Copeland, R. A., Reversible modes of inhibitor interactions with enzymes. In *Evaluation of Enzyme Inhibitors in Drug Discovery*, John Wiley & Sons, Inc.: **2013**, pp 57-121.
230. Cornish-Bowden, A., Why is uncompetitive inhibition so rare? *FEBS Letters* **1986**, *203* (1), 3-6..
231. Westley, A. M.; Westley, J., Enzyme inhibition in open systems: Superiority of uncompetitive agents. *Journal of Biological Chemistry* **1996**, *271* (10), 5347-5352
232. Hoepfner, A.; Schmitt, L.; Smits, S. H. J., Proteins and their Ligands: their importance and how to crystallize them. In *Advance Topics on Crystal Growth* **2013**.

233. Dougherty, D. A., The cation- π interaction. *Accounts of Chemical Research*. **2013**, 46 (4), 885-893
234. Gallivan, J. P.; Dougherty, D. A., Cation- π interactions in structural biology. *Proceedings of the National Academy of Sciences* **1999**, 96 (17), 9459-9464.
235. Zacharias, N.; Dougherty, D. A., Cation- π interactions in ligand recognition and catalysis. *Trends in Pharmacological Science* **2002**, 23 (6), 281-287.
236. Salaemae, W.; Azhar, A.; Booker, G. W.; Polyak, S. W., Biotin biosynthesis in *Mycobacterium tuberculosis*: physiology, biochemistry and molecular intervention. *Protein & Cell* **2011**, 2 (9), 691-695.
237. Joshi, S. M.; Pandey, A. K.; Capite, N.; Fortune, S. M.; Rubin, E. J.; Sasseti, C. M., Characterization of mycobacterial virulence genes through genetic interaction mapping. *Proceedings of the National Academy of Sciences of the United States of America* **2006**, 103 (31), 11760-11765.
238. Labedan, B.; Riley, M., Genetic inventory: *Escherichia coli* as a window on ancestral Proteins. In *Organization of the Prokaryotic Genome*, American Society of Microbiology: **1999**.
239. Cronan Jr, J. E.; Waldrop, G. L., Multi-subunit acetyl-CoA carboxylases. *Progress in Lipid Research*. **2002**, 41 (5), 407-435.
240. Portevin, D.; de Sousa-D'Auria, C.; Montrozier, H.; Houssin, C.; Stella, A.; Lan elle, M.-A.; Bardou, F.; Guilhot, C.; Daff e, M., The acyl-AMP ligase FadD32 and AccD4-containing acyl-CoA carboxylase are required for the synthesis of mycolic acids and essential for mycobacterial growth: identification of the

- carboxylation product and determination of the acyl-CoA-carboxylase components. *Journal of Biological Chemistry* **2005**, *280* (10), 8862-8874.
241. Soto-Ramirez, M. D.; Aguilar-Ayala, D. A.; Garcia-Morales, L.; Rodriguez-Peredo, S. M.; Badillo-Lopez, C.; Rios-Muñiz, D. E.; Meza-Segura, M. A.; Rivera-Morales, G. Y.; Leon-Solis, L.; Cerna-Cortes, J. F.; Rivera-Gutierrez, S.; Helguera-Repetto, A. C.; Gonzalez-y-Merchand, J. A., Cholesterol plays a larger role during *Mycobacterium tuberculosis in vitro* dormancy and reactivation than previously suspected. *Tuberculosis* **2017**, *103*, 1-9.
242. Lovewell, R. R.; Sasseti, C. M.; VanderVen, B. C., Chewing the fat: lipid metabolism and homeostasis during M. tuberculosis infection. *Current Opinion in Microbiology* **2016**, *29*, 30-36.
243. Dedieu, L.; Serveau-Avesque, C.; Kremer, L.; Canaan, S., Mycobacterial lipolytic enzymes: A gold mine for tuberculosis research. *Biochimie* **2013**, *95* (1), 66-73.
244. Marrero, J.; Rhee, K. Y.; Schnappinger, D.; Pethe, K.; Ehrt, S., Gluconeogenic carbon flow of tricarboxylic acid cycle intermediates is critical for *Mycobacterium tuberculosis* to establish and maintain infection. *Proceedings of the National Academy of Sciences* **2010**, *107* (21), 9819-9824.
245. Purushothaman, S.; Annamalai, K.; Tyagi, A. K.; Surolia, A., Diversity in functional organization of class I and class II biotin protein ligase. *PLOS ONE* **2011**, *6* (3), e16850.

246. Chapman-Smith, A.; Cronan, J. E., Jr., The enzymatic biotinylation of proteins: a post-translational modification of exceptional specificity. *Trends in Biochemical Sciences* **1999**, *24* (9), 359-363.
247. Duckworth, Benjamin P.; Geders, Todd W.; Tiwari, D.; Boshoff, Helena I.; Sibbald, Paul A.; Barry Iii, Clifton E.; Schnappinger, D.; Finzel, Barry C.; Aldrich, Courtney C., Bisubstrate adenylation inhibitors of biotin protein ligase from *Mycobacterium tuberculosis*. *Chemistry & Biology* **2011**, *18* (11), 1432-1441.
248. Ma, Q.; Akhter, Y.; Wilmanns, M.; Ehebauer, M. T., Active site conformational changes upon reaction intermediate biotinyl-5'-AMP binding in biotin protein ligase from *Mycobacterium tuberculosis*. *Protein Science*. **2014**, *23* (7), 932-939.
249. Gupta, V.; Gupta, R. K.; Khare, G.; Salunke, D. M.; Surolia, A.; Tyagi, A. K., Structural ordering of disordered ligand-binding loops of biotin protein ligase into active conformations as a consequence of dehydration. *PLoS ONE* **2010**, *5* (2), e9222.
250. Ashleigh, S. P.; Tatiana, P. S. d. C.; Min, Y. Y.; William, T.; Matthew, C. J. W.; Grant, W. B.; Andrew, D. A.; Steven, W. P., Structure guided design of biotin protein ligase inhibitors for antibiotic discovery. *Current Topics in Medicinal Chemistry* **2014**, *14* (1), 4-20.
251. Wilson, D. J.; Aldrich, C. C., A continuous kinetic assay for adenylation enzyme activity and inhibition. *Analytical Biochemistry* **2010**, *404* (1), 56-63.
252. Copeland, R. A., Reversible modes of interactions with enzymes. In *Evaluation of Enzyme Inhibitors in Drug Discovery*, John Wiley & Sons, Inc.: **2005**., pp 48-80.

APPENDIX A

SUPPLEMENTARY MATERIAL FOR SECTION 2

Close contacts of the MtbAdoK-2 complex ≤ 3.5 Å.

Atom	Residue	Distance
C2	Ser8.A CB	3.48
C2	Ser8.A OG	3.18
N3	Ser8.A OG	2.69
N3	Ser8.A CB	3.38
C4	Phe116.A CE1	3.49
C8	Phe102.A CD1	3.41
C3'	Asp12.A OD2	3.23
O4'	Val49.A CG1	3.45
C5'	Asp257.A OD2	3.34
O5'	Asp257.A OD2	2.55
O5'	Asp257.A CG	3.35
O3'	Asp12.A OD2	2.45
O3'	Gly48.A N	2.97
O3'	Asp12.A CG	3.23
O3'	Asn52.A ND2	3.10
O3'	Asp12.A OD1	3.26
O2'	Gly48.A N	2.83
O2'	Asp12.A OD1	2.65
O2'	Gly48.A CA	3.34
O2'	Ala10.A CB	3.35
N6	Gln173.A NE2	2.98

Crystal data collection and refinement statistics for MtbAdoK-2.

Statistic	MtbAdoK-2
Data collection	
Space Group	P41
Cell Dimensions	
a, b, c (Å)	49.0, 49.0, 262.2
α, β, γ (°)	90, 90, 90
Resolution (Å)	32.24-1.95 (2.02-1.95)
R_{merge}	0.071
$I/\sigma I$	22.2
Completeness %	94.5(98.2)
Redundancy	7.5
Refinement	
Resolution (Å)	1.95
No. of reflections	42508
$R_{\text{work}}/R_{\text{free}}$	0.18/0.22
No. of atoms	
Protein	4731
Ligand	90
Water	280
B factors	
Protein	52.2
Ligand/ion	58.7
Water	53.6
rmsd	
Bond lengths (Å)	0.007
Bond angles (°)	0.93

Close contacts of the MtbAdoK-3 complex ≤ 3.5 Å.

Atom	Residue	Distance
C2	Ser8.A OG	3.27
N3	Ser8.A OG	2.77
N3	Ser8.A CB	3.48
C4	Phe116.A CE1	3.44
C3'	Asp12.A OD2	3.36
O4'	Gln172.A NE2	3.10
O4'	Val49.A CG1	3.39
C5'	Asp257.A OD2	3.41
O5'	Asp257.A OD2	2.69
O5'	Gln172.A NE2	3.03
O5'	Asp12.A CG	3.39
O3'	Asp12.A OD2	2.42
O3'	Asp12.A CG	3.20
O3'	Gly48.A N	3.04
O3'	Asn52.A ND2	3.17
O3'	Asp12.A OD1	3.22
O2'	Asp12.A OD1	2.75
O2'	Gly48.A N	3.09
O2'	Gly48.A CA	3.43
O2'	Ala10.A CB	3.45
N6	Gln.173A OE1	3.26
N21	Ser36.B OG	2.82
N21	Ser36.B CB	3.49
N21	Phe102.A CE1	3.40
O22	Phe116.A CB	3.49

Crystal data collection and refinement statistics for MtbAdoK-3.

Statistic	MtbAdoK-3
Data collection	
Space Group	P41
Cell Dimensions	
a, b, c (Å)	48.9, 48.9, 262.0
α, β, γ (°)	90, 90, 90
Resolution (Å)	33.44-1.95(2.02-1.95)
R_{merge}	0.071
$I/\sigma I$	20.50
Completeness %	94.0(99.2)
Redundancy	7.3
Refinement	
Resolution (Å)	1.95
No. of reflections	41971
$R_{\text{work}}/R_{\text{free}}$	0.19/0.23
No. of atoms	
Protein	4727
Ligand	80
Water	233
B factors	
Protein	46.9
Ligand/ion	55.2
Water	47.3
rmsd	
Bond lengths (Å)	0.016
Bond angles (°)	1.4

Close contacts of the MtbAdoK-1 complex ≤ 3.5 Å. Analyzed from PDB ID 2PKM.

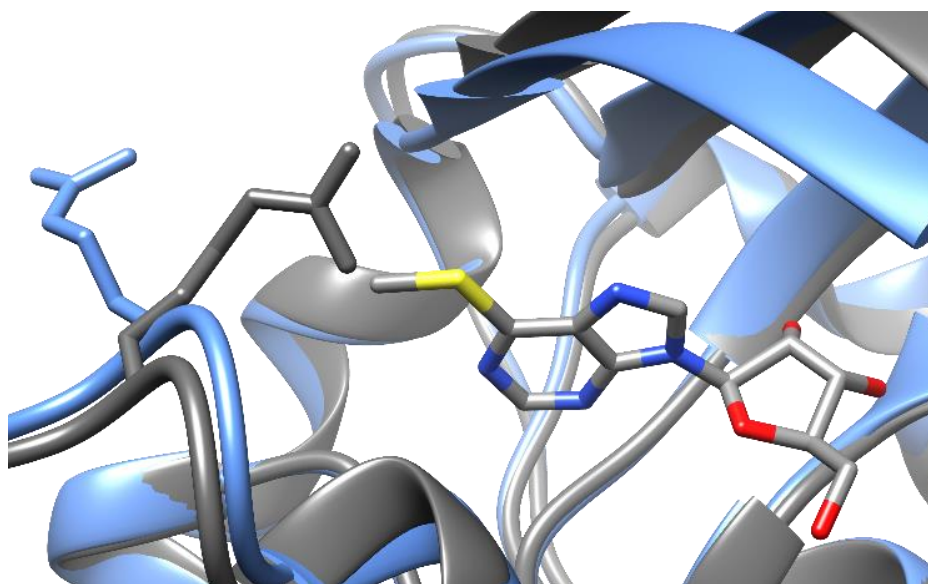
Atom	Residue	Distance
C2	Ser8.A OG	3.11
N3	Ser8.A OG	2.62
N3	Ser8.A CB	3.47
N3	Phe116.A CE1	3.42
C4	Phe116.A CE1	3.38
C4	Phe116.A CD1	3.39
C5	Gln172.A CB	3.46
C5	Phe116.A CD1	3.39
N1	Gln173.A NE2	2.99
N7	Ser36.B OG	2.65
C8	Phe102.A CE1	3.27
C8	Phe102.A CD1	3.48
C3'	Asp12.A OD2	3.35
C4'	Gln172.A NE2	3.49
O4'	Val49.A CG1	3.22
O4'	Gln172.A NE2	3.26
C5'	Asp257.A OD2	2.87
C5'	Asn52.A ND2	3.31
O5'	Gln172.A NE2	2.62
O5'	Asp257.A OD2	2.69
O5'	Asp257.A CG	3.32
O3'	Asp12.A OD2	2.70
O3'	Gly48.A N	2.99
O3'	Asn52.A ND2	3.01
O3'	Asp12.A CG	3.41
O2'	Gly48.A N	2.82
O2'	Asp12.A OD1	2.76
O2'	Gly48.A CA	3.28
N6	Gln173.A OE1	2.96
N6	Gln172.A O	3.26
N6	Ser36.B OG	3.43

Close contacts of the MtbAdoK-4 complex ≤ 3.5 Å.

Atom	Residue	Distance
C2	Ser8.A CB	3.49
C2	Ser8.A OG	3.45
N3	Ser8.A OG	2.88
N3	Ser8.A CB	3.40
C4	Phe116.A CE1	3.40
C5	Phe116.A CD1	3.38
N7	Phe116.A CD1	3.40
C8	Phe102.A CD1	3.28
C8	Phe102.A CE1	3.42
C2'	Asp12.A OD1	3.35
O4'	Val49.A CG1	3.27
O4'	Gln172.A NE2	3.20
C5'	Asp257.A OD2	3.30
O5'	Asp257.A OD2	2.48
O5'	Asp257.A CG	3.30
O5'	Gln172.A NE2	3.30
O3'	Asp12.A OD2	2.43
O3'	Gly48.A N	2.90
O3'	Asp12.A CG	3.16
O3'	Asn52.A ND2	3.23
O3'	Asp12.A OD1	3.17
O2'	Gly48.A N	2.80
O2'	Asp12.A OD1	2.59
O2'	Gly48.A CA	3.29
O2'	Asp12.A CG	3.45
S6	Arg176.A NH1	3.45
C20	Arg176.A NH1	3.41

Crystal data collection and refinement statistics for MtbAdoK-4.

Statistic	MtbAdoK-4
Data collection	
Space Group	P41
Cell Dimensions	
a, b, c (Å)	49.4, 49.4, 264.0
α, β, γ (°)	90, 90, 90
Resolution (Å)	33.8-1.99 (2.06-1.99)
R_{merge}	0.10
$I/\sigma I$	16.1
Completeness %	98.5(97.0)
Redundancy	7.0
Refinement	
Resolution (Å)	1.99
No. of reflections	42509
$R_{\text{work}}/R_{\text{free}}$	0.18/0.21
No. of atoms	
Protein	4714
Ligand	72
Water	303
B factors	
Protein	48.2
Ligand/ion	59.0
Water	49.3
rmsd	
Bond lengths (Å)	0.003
Bond angles (°)	0.66



Compound **4** induces movement of Arg176 towards active site. Superimposition of MtbAdoK-1 structure (blue, PDB ID 2PKM) with MtbAdoK-4 complex (grey). Arg176 and compound **4** are shown as sticks.

Close contacts of the MtbAdoK-5 complex ≤ 3.5 Å.

Atom	Residue	Distance
C2	Ser8.A OG	3.41
N3	Ser8.A OG	2.78
N3	Ser8.A CB	3.39
C4	Phe116.A CD2	3.39
C4	Phe116.A CE2	3.45
C5	Phe116.A CD2	3.38
N1	Gln173.A OE1	3.08
N7	Ser36.B OG	2.75
N7	Ser36.B CB	3.43
N7	Gln172.A NE2	3.33
C8	Gln172.A NE2	3.02
C8	Phe102.A CE1	3.22
C8	Phe102.A CD1	3.39
C8	Gln172.A CD	3.45
N9	Gln172.A NE2	3.33
C3'	Asp12.A OD2	3.30
O4'	Val49.A CG1	3.22
O4'	Gln172.A NE2	3.04
C5'	Asp257 OD2	3.30
N5'	Asp257.A OD2	2.69
N5'	Asp257.A CG	3.41
O3'	Asp12.A OD2	2.52
O3'	Gly48.A N	2.99
O3'	Asp12.A CG	3.28
O3'	Asn52.A ND2	3.11
O2'	Gly48.A N	2.92
O2'	Asp12.A OD1	2.75
O2'	Gly48.A CA	3.32
N6	Gln173.A NE2	3.41

Crystal data collection and refinement statistics for MtbAdoK-5.

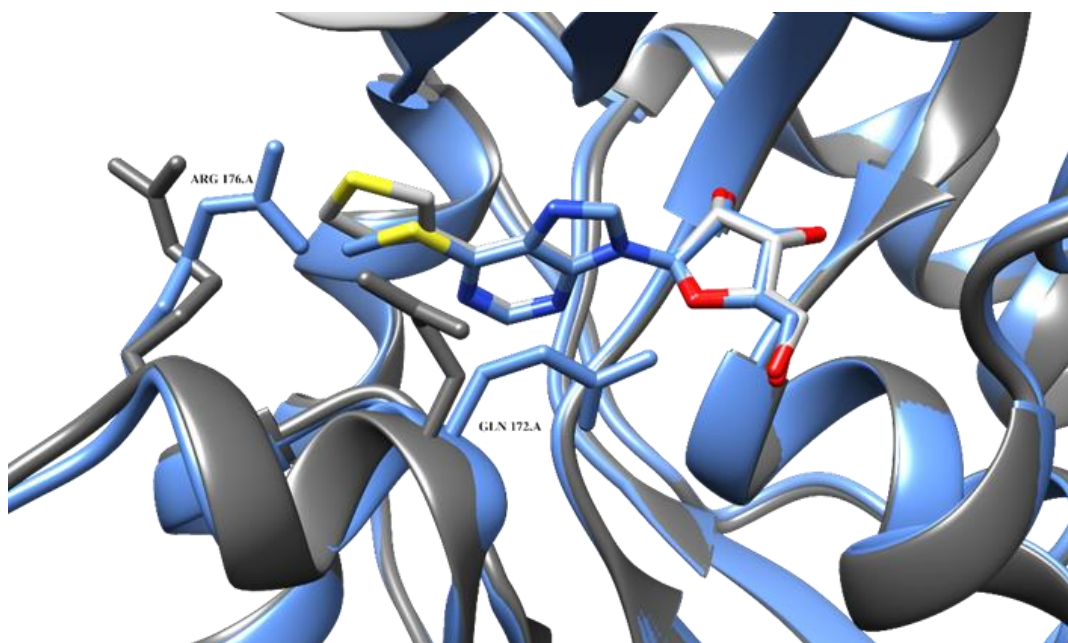
Statistic	MtbAdoK-5
Data collection	
Space Group	P3121
Cell Dimensions	
a, b, c (Å)	71.9, 71.9, 110.2
α , β , γ (°)	90, 90, 120
Resolution (Å)	41.28-1.75(1.81-1.75)
R_{merge}	0.06
$I/\sigma I$	32.6
Completeness %	99.9(100.0)
Redundancy	10.6
Refinement	
Resolution (Å)	1.75
No. of reflections	33869
$R_{\text{work}}/R_{\text{free}}$	0.19/0.22
No. of atoms	
Protein	2459
Ligand	31
Water	244
B factors	
Protein	35.4
Ligand/ion	33.4
Water	39.5
rmsd	
Bond lengths (Å)	0.006
Bond angles (°)	0.865

Close contacts of the MtbAdoK-6 complex ≤ 3.5 Å.

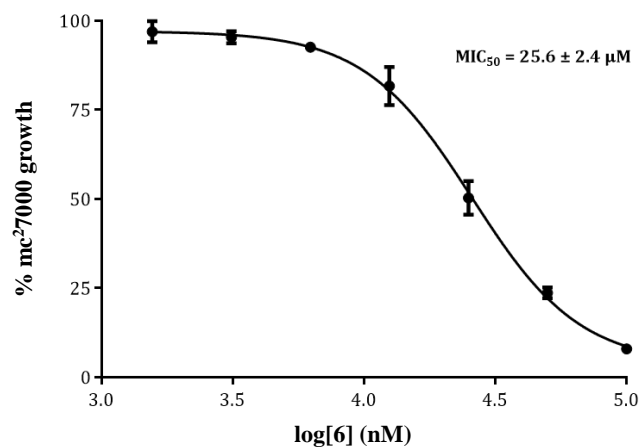
Atom	Residue	Distance
C2	Ser8.A OG	3.42
N3	Ser8.A OG	2.85
N4	Ser8.A CB	3.46
C4	Phe116.A CE1	3.44
C5	Phe116.A CD1	3.47
C8	Phe102.A CD1	3.44
C3'	Asp12.A OD2	3.37
C4'	Asn52.A ND2	3.39
O4'	Val49.A CG1	3.26
C5'	Asp257.A OD2	3.20
C5'	Asn52.A ND2	3.44
O5'	Asp257.A OD2	2.67
O3'	Asp257.A CG	3.49
O3	Asp12.A OD2	2.47
O3'	Gly48.A N	2.93
O3'	Asp12.A CG	3.27
O3'	Asn52.A ND2	3.17
O2'	Asp12.A OD1	2.85
O2'	Gly48.A N	3.12
O2'	Gly48.A CA	3.47
C20	Ser36.B OG	3.44
C22	Arg176.A CD	3.50

Crystal data collection and refinement statistics for MtbAdoK-6.

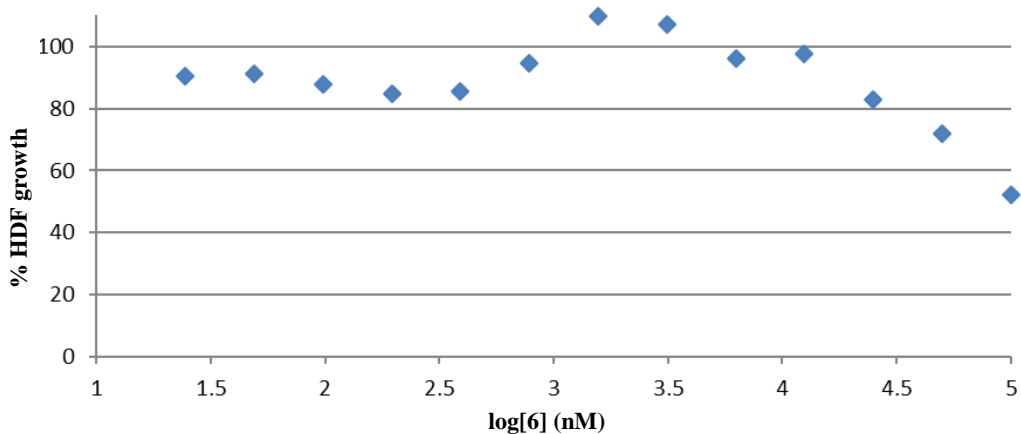
Statistic	MtbAdoK-6
Data collection	
Space Group	P212121
Cell Dimensions	
a, b, c (Å)	77.6, 82.0, 157.6
α, β, γ (°)	90, 90, 90
Resolution (Å)	45.88-2.36(2.44-2.36)
R_{merge}	0.12
$I/\sigma I$	20.21
Completeness %	99.5(99.4)
Redundancy	9.0
Refinement	
Resolution (Å)	2.36
No. of reflections	42046
$R_{\text{work}}/R_{\text{free}}$	0.18/0.21
No. of atoms	
Protein	5059
Ligand	80
Water	126
B factors	
Protein	57.8
Ligand/ion	63.8
Water	52.0
rmsd	
Bond lengths (Å)	0.006
Bond angles (°)	0.85



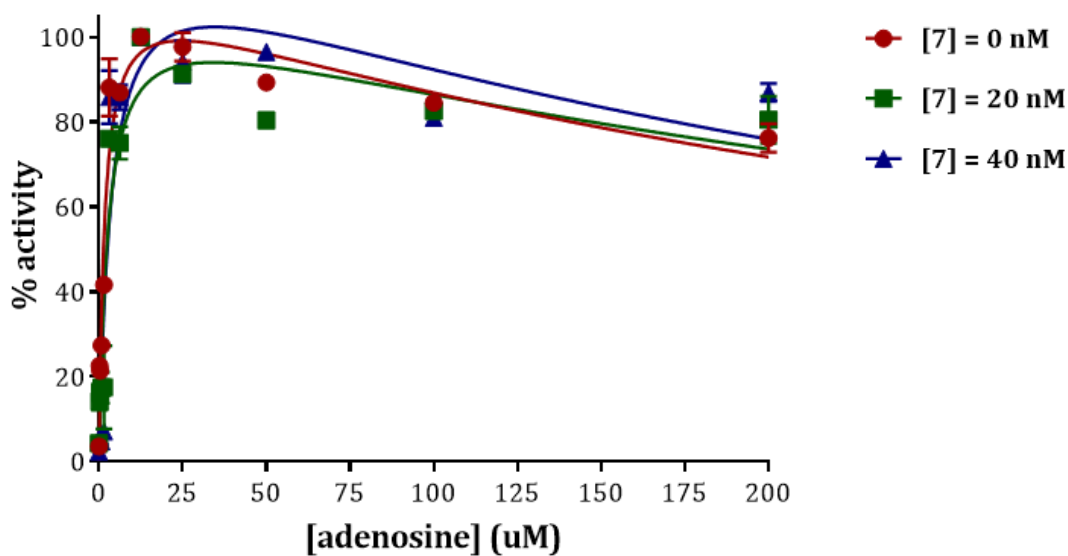
Superimposition of the crystal structure complexes of compounds **4** (blue) and **6** (gray). Residues Gln172 and Arg176 reorient themselves to accommodate the larger thiophene group. In both cases, residues are labeled by 3-letter code and chain identifier.



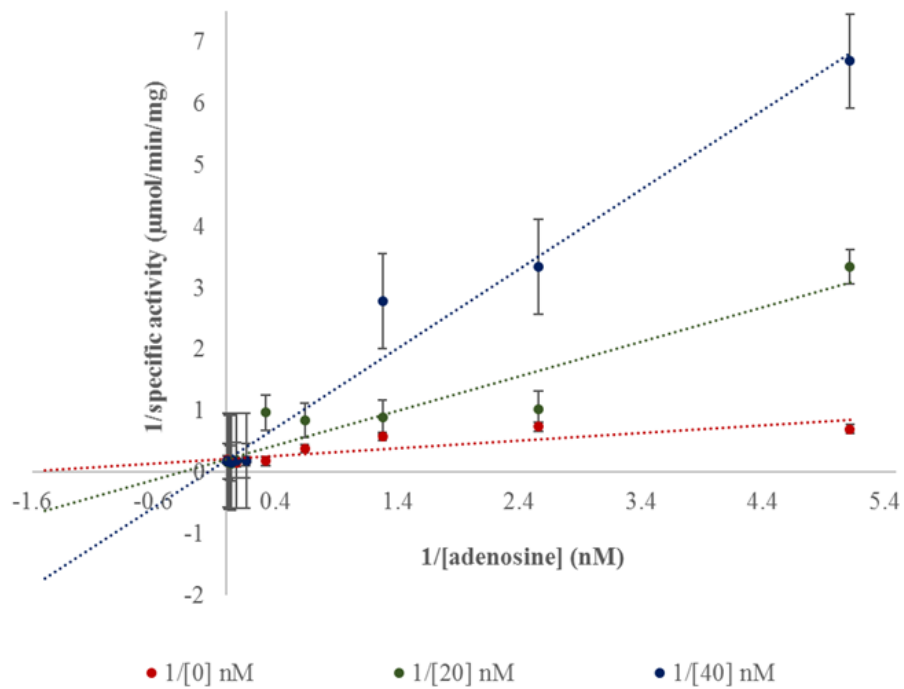
Dose-response curve of compound **6** when tested against mc²7000. Data is normalized to the 0 μ M (DMSO) control and the error reported represents the \pm SD of 3 experiments.



Dose-response curve of compound **6** when tested against HDF cells. Data is normalized to the 0 μM (DMSO) control.



Steady-state kinetics for compound **7**. The initial velocity of MtbAdoK was plotted against increasing concentrations of adenosine in the presence of 0.0 nM (DMSO-maroon), 20.0 nM (green) and 40.0 nM (blue) of **7**. The error bars represent \pm SD of 2 experiments.



Initial velocity data was transformed to linear analysis to evaluate inhibitor type. The error bars represent \pm SD of 2 experiments.

Close contacts of the MtbAdoK-7 complex ≤ 3.5 Å.

Atom	Residue	Distance
C2	Ser8.A OG	3.37
N3	Ser8.A OG	2.85
N3	Ser8.A CB	3.46
N7	Phe116.A CD1	2.87
C8	Phe102.A CD1	3.35
C2'	Asp12.A OD1	3.43
C3'	Asp12.A OD2	3.35
O2'	Asp12.A OD1	2.66
O2'	Gly48.A N	3.01
O2'	Gly48.A CA	3.40
O3'	Asp12.A OD2	2.50
O3'	Gly48.A N	2.98
O3'	Asp12.A CG	3.26
O3'	Asn52.A ND2	3.15
O4'	Gln172.A NE2	2.97
O4'	Val49.A CG1	3.44
O5'	Asp257.A OD2	2.56
O5'	Asp257.A CG	3.32
O5'	Gln172.A NE2	3.36
C21	Gln173.A OE1	3.30
C24	Ser36.B OG	3.49
C26	Ser36.B OG	3.50
C26	Ser36.B O	3.46
C27	Ser36.B O	3.28
C29	Gln172.A O	3.24
C30	Gln172.A O	3.13

Crystal data collection and refinement statistics for MtbAdoK-7.

Statistic	MtbAdoK-7
Data collection	
Space Group	P4 ₁
Cell Dimensions	
a, b, c (Å)	50.0, 50.0, 264.6
α, β, γ (°)	90, 90, 90
Resolution (Å)	50.08-1.65 (1.71-1.65)
R _{merge}	0.15
I/ σ I	9.50
Completeness %	99.8 (98.3)
Redundancy	6.6
Refinement	
Resolution (Å)	1.65
No. of reflections	76910
R _{work} /R _{free}	0.17/0.19
No. of atoms	
Protein	4672
Ligand	70
Water	588
B factors	
Protein	31.8
Ligand/ion	36.3
Water	42.1
rmsd	
Bond lengths (Å)	0.006
Bond angles (°)	0.86

Close contacts of the MtbAdoK-17 complex ≤ 3.5 Å.

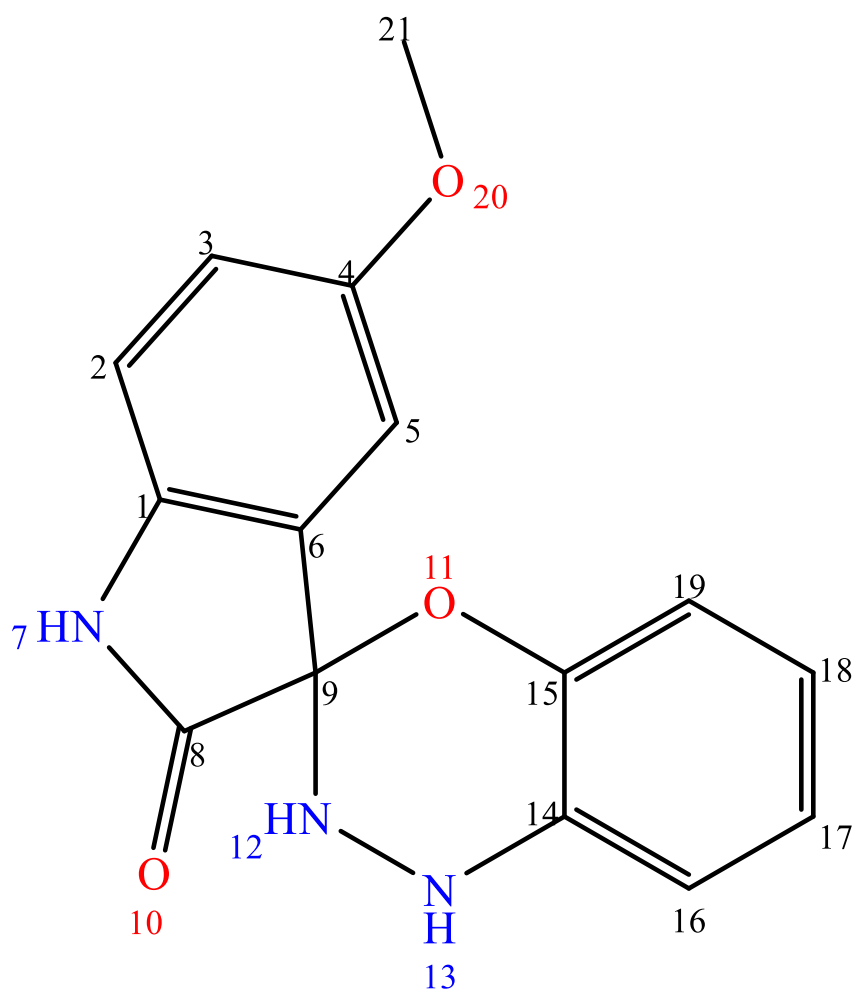
Atom	Residue	Distance
C2	Ser8.A CB	3.47
C2	Ala146.A CB	3.45
C2	Ser8.A OG	3.25
N3	Ser8.A OG	2.68
N3	Ser8.A CB	3.33
C4	Phe116.A CE1	3.44
C5	Phe116.A CD1	3.48
N1	Gln173.A NE2	3.11
N7	Phe116.A CD1	3.39
C8	Phe102.A CD1	3.35
C2'	Asp12.A OD1	3.35
C3'	Asp12.A OD2	3.28
O4'	Val49.A CG1	3.28
O4'	Gln172.A NE2	3.44
O5'	Asp257.A OD2	2.48
O5'	Asp257.A CG	3.40
O3'	Asp12.A OD2	2.39
O3'	Asp12.A CG	3.18
O3'	Gly48.A N	2.97
O3'	Asn52.A ND2	3.18
O3'	Asp12.A OD1	3.25
O2'	Gly48.A N	2.77
O2'	Asp12.A OD1	2.61
O2'	Gly48.A CA	3.19
O2'	Ala10.A CB	3.47
C19	Gln173.A NE2	3.47
C23	Leu38.B CD2	3.14
C23	Leu38.B CB	3.18
C24	Leu38.B CB	2.89
C25	Leu38.B CB	3.12
C25	Leu38.B N	3.04
C25	Leu38.B CA	3.50
C27	Leu38.B CB	3.40
C31	Phe17.B CE1	3.50
C32	Leu38.B CB	3.04
C32	Leu38.B N	3.32

Crystal data collection and refinement statistics for MtbAdoK-17.

Statistic	MtbAdoK-17
Data collection	
Space Group	P41
Cell Dimensions	
a, b, c (Å)	49.9, 49.9, 264.3
α, β, γ (°)	90, 90, 90
Resolution (Å)	35.29-2.35 (2.43-2.35)
R_{merge}	0.059
$I/\sigma I$	29.1
Completeness %	98.8(100.0)
Redundancy	6.9
Refinement	
Resolution (Å)	2.35
No. of reflections	26480
$R_{\text{work}}/R_{\text{free}}$	0.18/0.22
No. of atoms	
Protein	4720
Ligand	74
Water	230
B factors	
Protein	48.3
Ligand/ion	49.5
Water	40.0
rmsd	
Bond lengths (Å)	0.008
Bond angles (°)	1.04

APPENDIX B

SUPPLEMENTARY MATERIAL FOR SECTION 3



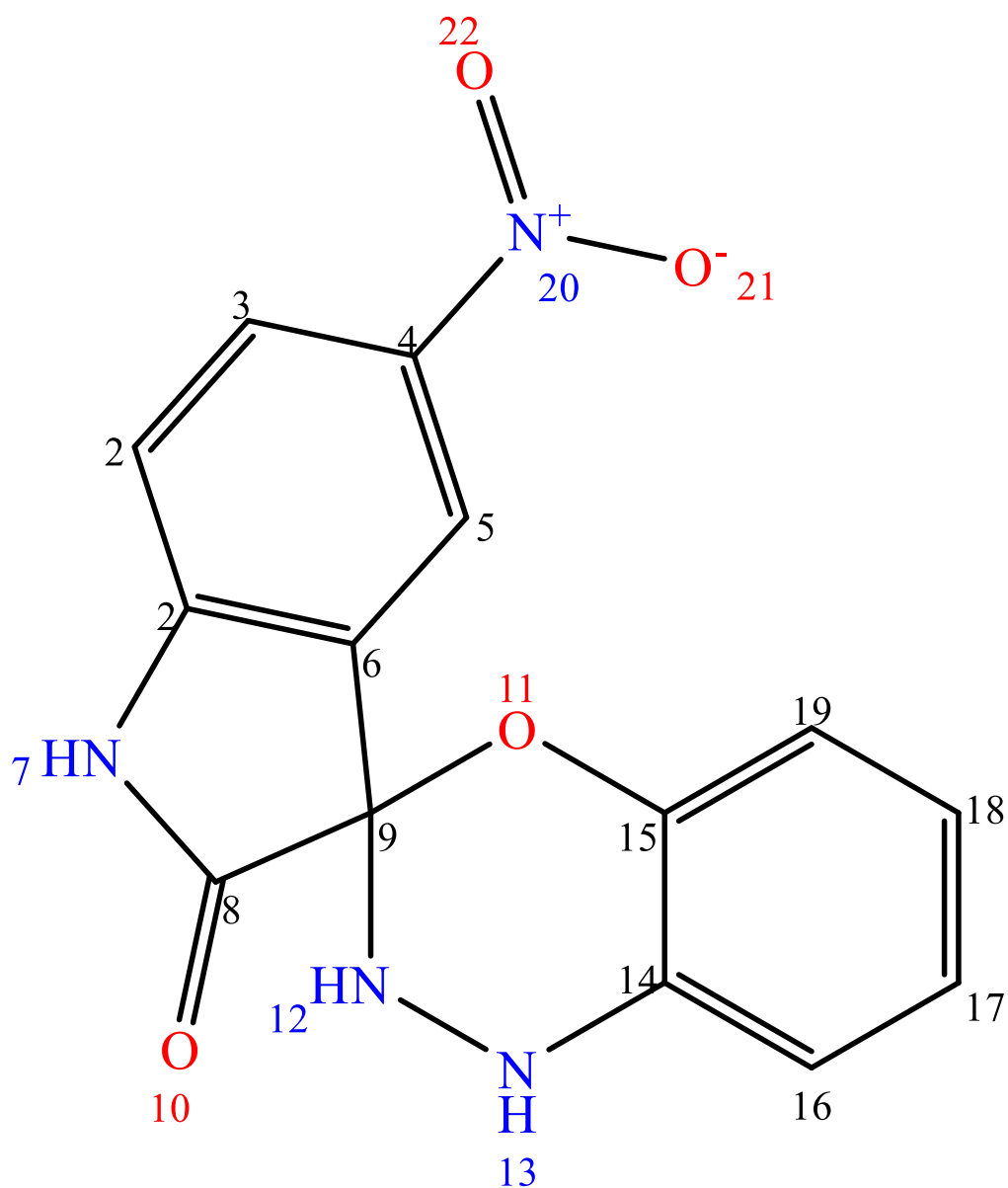
2

Structure and numbering convention for compound 2

215

Close contacts of the MtbAdoK-2 complex ≤ 3.5 Å.

Atom	Residue	Distance
C1	Arg176.A NH2	3.38
C2	Gln173.A OE1	3.19
C4	Gln172.A OE1	3.08
C5	Gln172.A OE1	3.12
C5	Arg176.A NH2	3.40
C6	Arg176.A CZ	3.30
C6	Arg176.A NH2	3.19
N7	Arg176.A CD	3.48
C8	Arg176.A CD	3.43
C8	Arg176.A NE	3.50
C9	Arg176.A NE	3.30
C9	Arg176.A CZ	3.31
O10	Leu38.B CD1	3.36
O11	Phe116.A CD2	2.89
O11	Phe116.A CB	3.29
O11	Phe116.A CG	3.03
N12	Arg176.A NE	2.80
N12	Arg176.A CD	3.32
N12	Arg176.A CZ	3.34
N13	Leu38.B CD1	3.49
C15	Phe116.A CB	3.21
C17	Ser36.B CB	3.50
C19	Phe116.A CB	3.07
O20	Gln172.A OE1	3.05
O20	Gln172.A CD	3.45
C21	Ser8.A OG	3.19

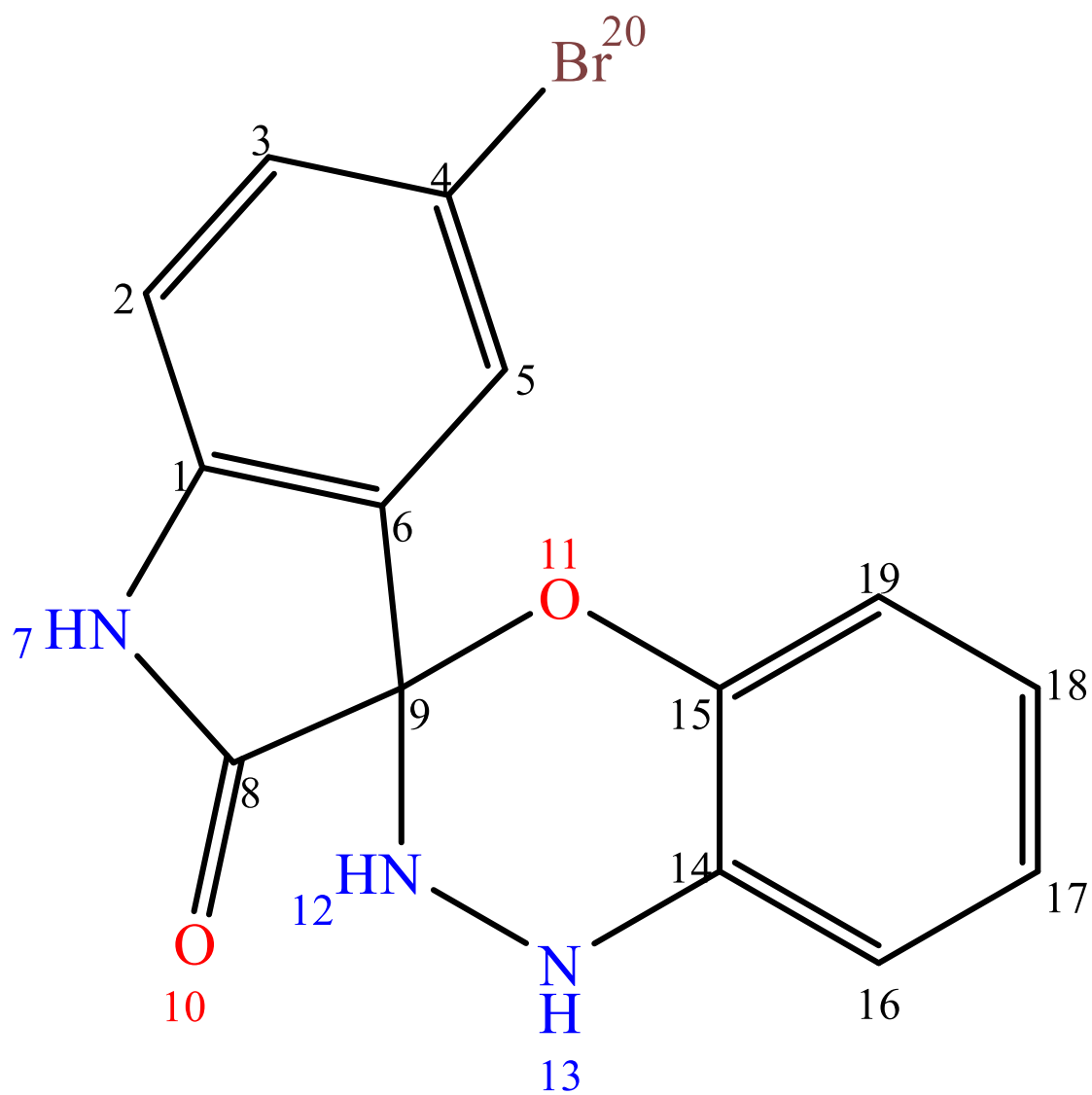


3

Structure and numbering convention for compound 3

Close contacts of the MtbAdoK-3 complex ≤ 3.5 Å.

Atom	Residue	Distance
C2	Gln173.A NE2	3.30
C3	Gln173.A NE2	2.93
C4	Arg176.A NH2	3.39
C5	Arg176.A NH2	3.14
C5	Phe116.A CE2	3.47
C5	Arg176.A CZ	3.35
C6	Arg176.A CZ	3.38
C6	Arg176.A NE	3.45
C6	Arg176.A NH2	3.50
C8	Leu38.B CD1	3.48
C9	Arg176.A NE	3.34
O10	Leu38.B CD1	3.39
O11	Phe116.A CD2	3.43
O11	Arg176.A NH1	3.37
C15	Phe116.A CB	3.42
C17	Ser36.B CB	3.47
C18	Phe102.A CE1	3.36
N20	Gln172.A OE1	3.43
O22	Gln172.A OE1	3.06



4

Structure and numbering convention for compound 4

Close contacts of the MtbAdoK-4 complex ≤ 3.5 Å.

Atom	Residue	Distance
C2	Gln173.A OE1	3.25
C3	Gln173.A OE1	3.21
C3	Gln173.A CD	3.41
C6	Phe116.A CE2	3.47
C9	Phe116.A CD2	3.37
O10	Leu38.B CD1	3.19
O11	Phe116.A CD2	3.46
O11	Arg176.A NH2	3.34
O11	Arg176.A CZ	3.32
N12	Arg176.A CD	3.13
N12	Arg176.A NH2	3.47
C19	Phe116.A CB	3.36
Br 20	Gln172.A OE1	3.45